NASA Technical Memorandum 88342

Summer School on Interstellar Processes: Abstracts of Contributed Papers

SUN

GC

n(H$_2$)

[cm^{-3}]

5
4
3
2
1
0

October 1986

Proceedings of a Workshop Held at
Grand Teton National Park, Wyoming
July 3 – 7, 1986

NASA

National Aeronautics and
Space Administration

Summer School on Interstellar Processes: Abstracts of Contributed Papers

Edited by
D. J. Hollenbach, Ames Research Center, Moffett Field, California
Harley A. Thronson, Jr., University of Wyoming, Laramie, Wyoming

October 1986

NASA

COVER: Face-on view of peak molecular hydrogen volume density for the first quadrant as viewed from the North Galactic Pole. Small white circles indicate HII region locations with known distances. (Abstract of paper by D. P. Clemens, D. B. Sanders, and N. Z. Scoville, see p. 99 of text.)

Preface

This volume contains the extended abstracts of the contributed papers given at the Summer School on Interstellar Processes which took place on July 3-7, 1986 in Grand Teton National Park, Wyoming. A separate publication from D. Reidel contains the invited papers given at this meeting; the program of these invited papers appears on the following two pages.
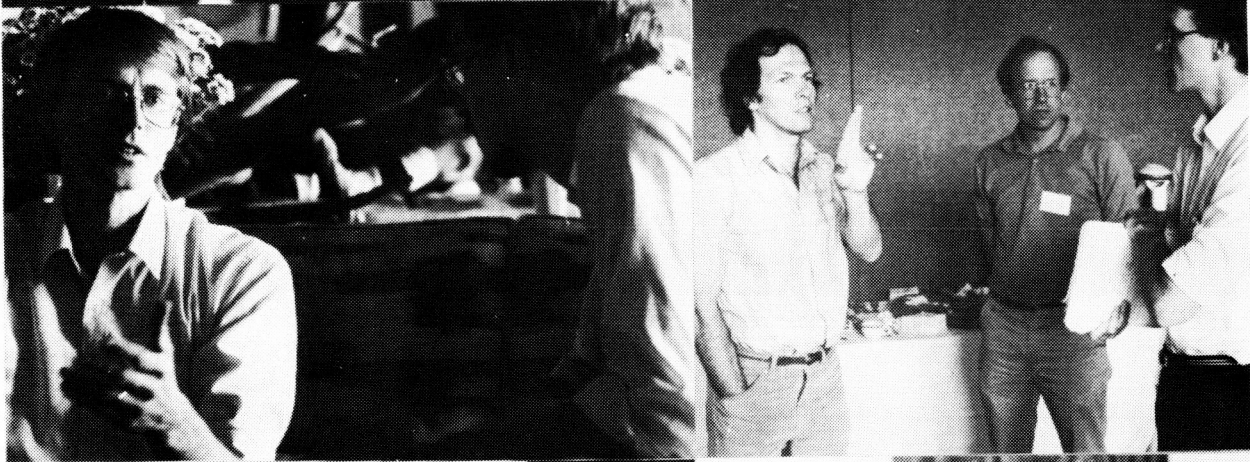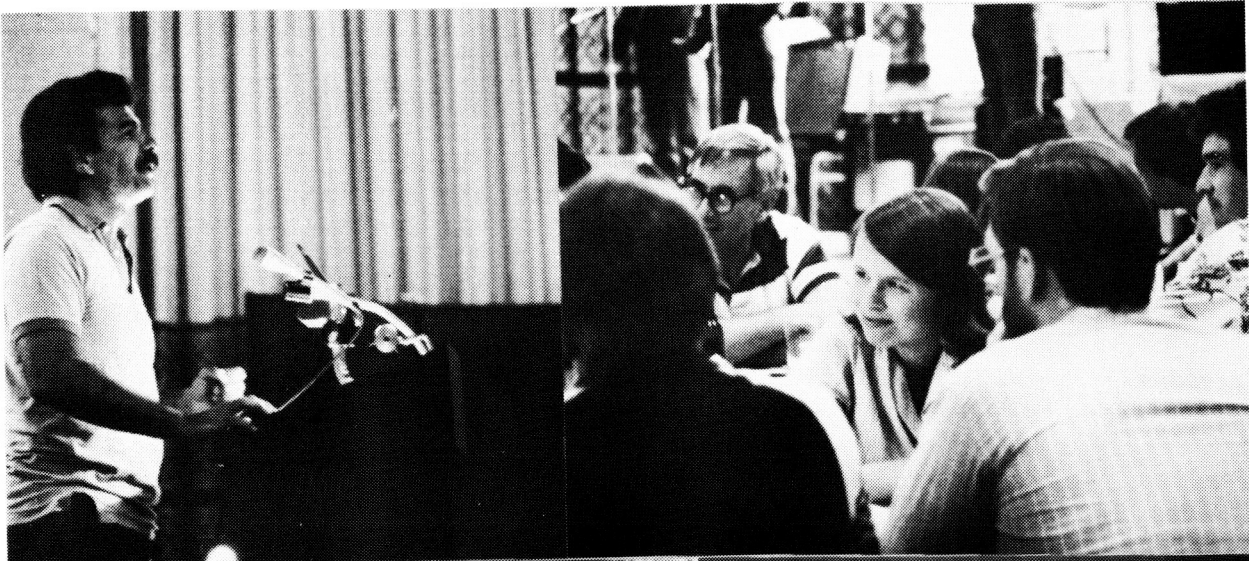
The purpose of the Summer School on Interstellar Processes was to present a summary of the current understanding of the interstellar medium and to discuss the basic physical processes which underlie interstellar phenomena. We were especially interested to attract an audience of graduate students and younger astronomers and to expose them to the wide variety of interesting processes operating in the interstellar medium. Although the invited talks were explicitly meant to be pedagogical reviews in line with the "summer school" tone of this meeting, the contributed papers in this volume are appropriate to typical symposia: they are generally reports on current research activities.

Approximately 200 astronomers attended the summer school and most of them appear as authors on one of the contributed papers in this volume. We would like to acknowledge their contributions, as well as the work of the Scientific Organizing Committee (J.M. Shull, L. Rodriguez, P. Martin, N. Scoville, C. Lada, D. Flower, T. de Jong, and J. Hackwell). We are also very grateful to the Local Organizing Committee (P. Johnson, M. Greenhouse, and T. Hayward), especially for attending to all the details which made the stay at Jackson Lake Lodge so enjoyable for the participants and their families. Finally, we would like to thank the Department of Physics and Astronomy, the Dean's Office of the College of Arts and Sciences, and the Research Office of the University of Wyoming for the financial support which, to a large degree, enabled many graduate students to attend the meeting.

David Hollenbach
NASA-Ames Research Center

Harley A. Thronson, Jr.
University of Wyoming

July 28, 1986

SUMMER SCHOOL ON INTERSTELLAR PROCESSES

Schedule of Invited Talks

FIRST DAY
Thursday July 2

900   Jura: "Overview: The Milky Way as a Galaxy"

1000   Torres-Peimbert: "Chemical Evolution of the Milky Way"

1100   Cowie: "Transfer of Energy and Mass in the ISM"

1300   Elmegreen: "The Formation and Destruction of
        Interstellar Clouds"

1400   Observational Constraints on the ISM
        Scoville: "The Molecular Component
        Kulkarni: "The Atomic Component"
        Savage: "The Hot Gas"
        Bloemen: "The High-energy Component"

SECOND DAY
Friday July 4

930   PANEL DISCUSSION ON PHASES OF THE INTERSTELLAR MEDIUM
                     Shull (moderator)
              McKee   Heiles
              McCray   Blitz   York

1300   Draine & Shull: "Shock Waves in Interstellar Space"

1400   Seab: "Grain Formation, Destruction, and Evolution"

1500   Tielens: "Grain Composition, Structure, and Chemistry"

1600   Allamandola: "The Spectroscopy of Dust and Large Molecules"

THIRD DAY
Saturday July 5

900   Myers: "Observations of Molecular Cloud Structure and
        Internal Motions"

1000   Scalo: "Theory of Fragmentation and Turbulence"

1100	Boss: "Theory of Collapse and Protostar Formation
1300	Elitzur: "Masers in the Interstellar Medium"
1400	Heiles: "Observations of the Interstellar Magnetic Field"
1500	Verschuur: "Discovery of a Distance Measure for HI Clouds and the Z Dependence of the Interstellar Magnetic Field"
1530	Zweibel: "Theory of the Interstellar Magnetic Field"

FOURTH DAY
Sunday July 6

900	Irvine, Goldsmith, & Hjalmarson: "Chemical Abundances in the Molecular Material"
945	Jenkins: "Chemical Abundances in the Atomic Material"
1030	Huntress: "Gas-phase Physical Processes"
1300	Prasad: "Chemical Evolution of Molecular Clouds"
1400	Brownlee: "Solar System/Interstellar Medium Connection: Grain Chemistry, Structure, and Isotopic Composition"
1500	Lutz: "The Solar System/Interstellar Medium Connection: Gas-phase Abundances"

FIFTH DAY
Monday July 7

830	Phillips: "Observations of the Cooling of the Interstellar Gas"
930	Flower: "Atomic and Molecular Physics of Interstellar Heating and Cooling"
1030	Black: "Heating and Cooling of Interstellar Gas"
1230	Dalgarno: Review and Closing Thoughts

CONTRIBUTED PAPERS
TABLE OF CONTENTS

B. HII Regions and Reflection Nebulae

C.   Planetary Nebulae and Mass Loss from Evolved Stars

D.   Supernova Remnants and Shock Regions

III. Interstellar Grains

A. Polycyclic Aromatic Hydrocarbons (PAHs)

B. Larger Grains and Grain Mantles

IV. Interstellar Chemistry and Elemental Abundances

A. Interstellar Chemistry

I. LOCAL STRUCTURE AND KINEMATICS OF ISM

A. Star Forming Regions and Molecular Clouds

FAR-INFRARED INVESTIGATION OF THE TAURUS STAR-FORMING REGION-- USING THE IRAS DATABASE.

Joanne D. Hughes,
Queen Mary College,
University of London,
Mile End Road,
London E1 4NS.

The Infrared Astronomical Satellite (IRAS) has given us the first completely unbiased sky-survey in the far-infrared with wavebands centred at 12, 25, 60 and 100 microns. Previous work on star-forming regions had involved preselection of likely sites for further study. The Taurus-Auriga complex was selected as the first molecular cloud to be investigated in this study firstly due to its relative proximity (160pc, Cohen and Kuhi (1979)), and secondly because it had already been the subject of several studies in recent years (Elias (1978), Cohen and Kuhi (1979), and Jones and Herbig (1979)) so that its contents are well catalogued. Once a working method has been developed for Taurus it can then be applied to molecular clouds with less well documented populations.

The Taurus clouds were defined as lying between 04h and 05h in R.A. and +16 to +31 degrees in Dec., then the IRAS point-source catalogue was searched for sources with good or moderate quality fluxes (see IRAS Explanatory Supplement) in all three of the shortest IRAS bands. The sources which were selected in this way were then classified into subgroups according to their IRAS colours (Emerson (1985)).

Taurus is generally believed to be an area of low-mass star formation (Herbig, Vrba and Rydgren (1986)), having no luminous O-B associations within or near to the cloud complex. Once field stars, galaxies and planetary nebulae had been removed from the sample only the molecular cloud "cores", T Tauri stars and a few emission-line A and B stars remained. The great majority of these objects are pre-main sequence in nature and, as stated by Chester (1985), main sequence stars without excess far-infrared emission would only be seen in Taurus if their spectral types were earlier than about A5 and then not beyond 25 microns.

By choosing our sample in this way we are naturally selecting the hotter and thus more evolved sources. To counteract this, the molecular cloud core-criterion was applied to sources with good or moderate quality fluxes at 25, 60 and 100 microns, increasing the "core" sample by about one third. The candidate protostar B335 (Gee et al. (1985)) is only detected by IRAS at 60 and 100 microns while Taurus is heavily contaminated by "cirrus" at 100 microns (see IRAS Explanatory Supplement). This means that detection at 25 microns is also required with those at 60 and 100 microns to avoid confusing a ridge of cirrus with a "genuine" protostar.

The far-infrared luminosity function of these sources is then calculated and converted to the visual band by a standard method (Mamon and Soneira (1982)) to compare with the field star luminosity function of

1

Miller and Scalo (1979) (noting that the field star luminosity function is defined for all stars, including giants).

The eventual aim of this work is to obtain the far-infrared luminosity functions for a number of molecular clouds which are known to be forming low-mass stars and to investigate how the slope is affected by changes in the density and turbulence of material.

Chester, T.J. 1985, Proceedings of the First International IRAS Conference (Noordwijk, Holland).
Cohen, M., and Kuhi, L.V. 1979, Ap. J. Suppl.,41,743.
Elias, J.H. 1978, Ap. J.,224,857.
Emerson, J.P. 1985, I.A.U. Symposium 115 on "Star Forming Regions" (in press).
Explanatory Supplement to the IRAS Catalogs and Atlases, U.S. Government Printing Office 1985.
Gee, G., Griffin, M.J:, Cunningham, C.T., Emerson, J.P., Ade, P.A.R., and Caroff, L.J. 1985, M.N.R.A.S.,215,15.
Herbig, G.H., Vrba, F.J., and Rydgren, A.E. 1986, Astron. J.,91,575.
Jones, B.F., and Herbig, G.H. 1979, Astron. J.,84 ,1872.
Mamon, G.A., and Soneira, R.M. 1982, Ap. J.,225,181.
Miller, G.E., and Scalo, J.E. 1979, Ap. J. Suppl.,41,513.

MM AND SUBMM MOLECULAR LINE OBSERVATIONS OF THE SOUTHWEST LOBE
OF L1551 - EVIDENCE OF A SHELL STRUCTURE.

Ruth Rainey[1], Glenn J. White[1], K. J. Richardson[1], M. J. Griffin[1], N. J. Cronin[2], J. Hilton[3], T. S. Monteiro[4].

1. Queen Mary College, University of London, England.
2. University of Bath, England.
3. Goldsmiths' College, University of London, England.
4. The University, Newcastle-upon-Tyne, England.

Observations have been made of the southwest outflow lobe of L1551 in several millimetre and submillimetre molecular lines. Maps have been made in the J=3-2 and J=2-1 transitions of CO over areas of 7.5 by 2.5 arc minutes and 5 by 5 arc minutes respectively at UKIRT. More detailed maps have also been made in the J=2-1 CO transition over an area of about 6 by 3.5 arc minutes at the NRAO 12m telescope. Additional observations of the J=4-3 transitions of HCN, HCO+ and H^{13}CO+ were made at selected positions.

The HCO+ J=4-3 transition was detected at several positions along the outflow axis and at the position of IRS 5. Similarly the HCN J=4-3 transition was detected at the position of IRS 5 and also at a position close to HH29. However, the J=4-3 transition of H^{13}CO+ was not detected at the position of IRS 5 even though it was observed at the position close to HH29 with a peak corrected antenna temperature of 0.23K at a V_{LSR} of 1 km s^{-1}. The detection of the J=4-3 transitions of both HCO+ and H^{13}CO+ close to the position of HH29 suggest the presence of very dense gas in this region.

LVG analysis of the various molecular lines observed give a kinetic temperature between 10 and 15K and a density from 10^5 to 10^6 cm^{-3} at the position of IRS 5 at the ambient cloud velocity. At the position close to HH29 LVG analysis of the CO observations gives a density between 10^3 and 10^4 cm^{-3} at a kinetic temperature of 25K for a V_{LSR} of 0 km s^{-1}. The density of the gas giving rise to the HCO+ emission could not be deduced by the LVG analysis. To the southwest of HH29 there is a large decrease in both the linewidth and intensity of CO emission. This may be due to the interaction between the outflow and a dense clump of gas which gives rise to HH29.

The maps of the CO J=3-2 and CO J=2-1 emission integrated in 3.25 km s intervals show the shell structure postulated by Snell and Schloerb (1985), particularly those maps made from the NRAO CO J=2-1 data shown in Figure 1. At 3.5 km s^{-1} the outline of the shell is clearly visible and the points A and B from the lunar occultation measurements of Snell and Schoerb (1985) lie on this shell. At velocities further from the ambient cloud velocity emission is from areas closer to the outflow axis. Red shifted emission from the northern edge of the shell may be a consequence of rotation of this shell.

References:-
Snell, R. L. and Schloerb, F. P. 1985, Ap. J., 295, 490.
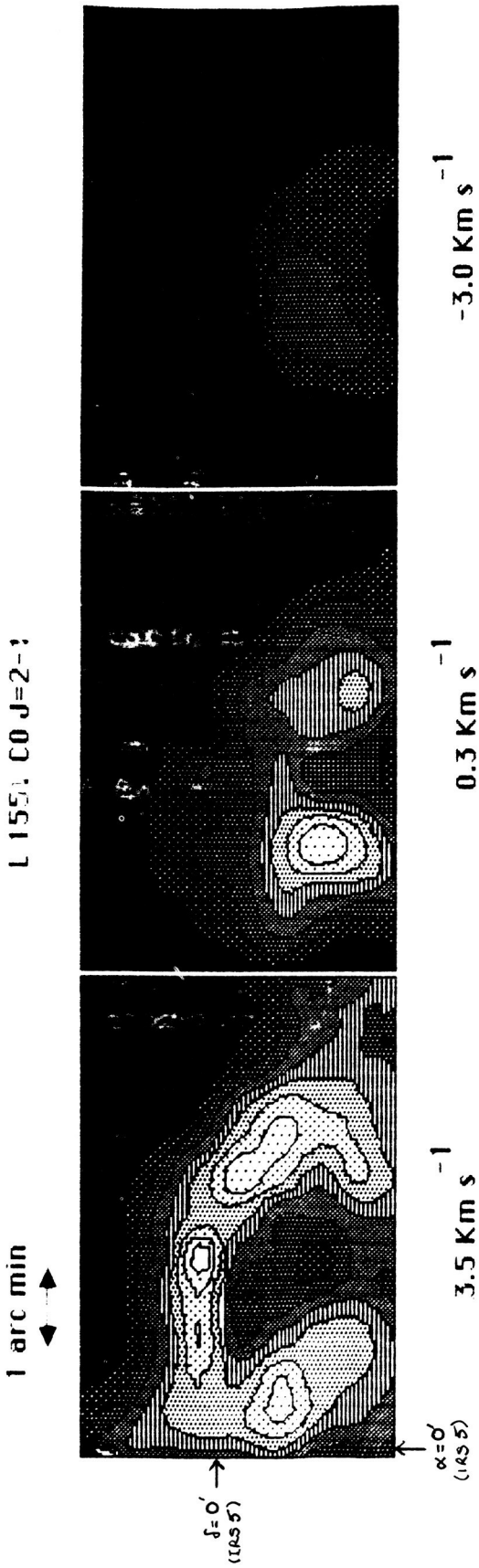
Figure 1

Figure 2. CO J=3-2 (solid line) and
CO J=2-1 (broken line) spectra
observed at the positions of
IRS 5 and 2'W2'S of IRS 5 at
UKIRT.

L 155% CO J=2-?

1 arc min

-3.0 Km s^{-1}

0.3 Km s^{-1}

3.5 Km s^{-1}

$\delta=0'$
(IRS 5)

$\alpha=0'$
(IRS 5)

4
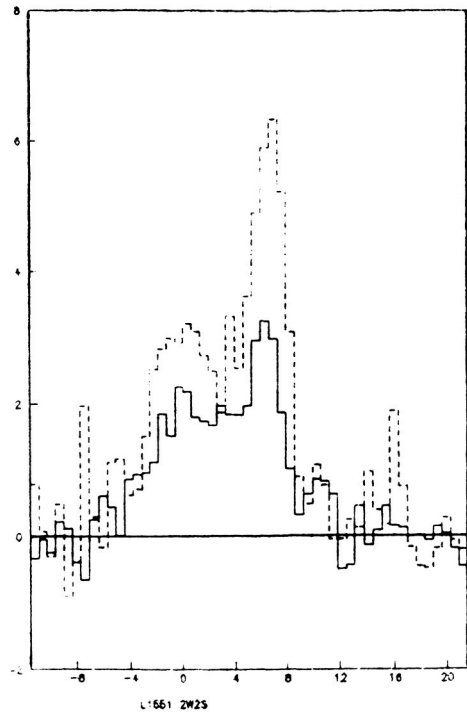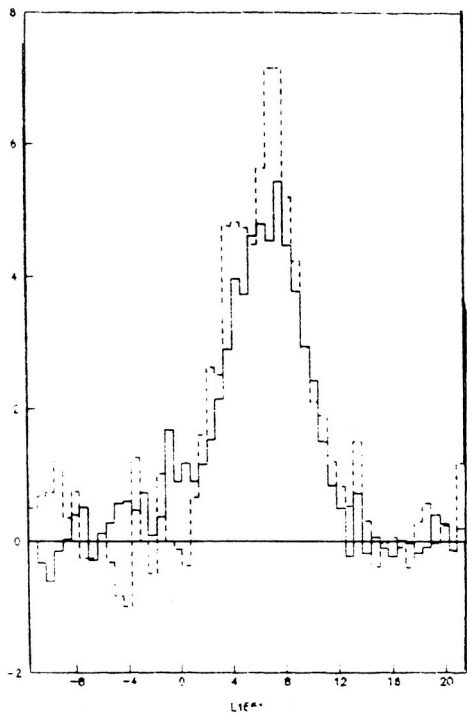
HIGH RESOLUTION OBSERVATIONS OF THE L1551 BIPOLAR OUTFLOW

Ronald Snell, Gerald Moriarty-Schieven, Stephen Strom,
Peter Schloerb, and Karen Strom
University of Masachusetts
and
Gary Grasdalen
University of Wyoming

ABSTRACT

The nearby dark cloud Lynds 1551 contains one of the closest examples of a well-collimated bipolar molecular outflow. This source has the largest angular size of any known outflow and was the first bipolar outflow to be detected (Snell, Loren, and Plambeck 1980). The outflow originates from a low-luminosity young stellar object, IRS-5, discovered by Strom, Strom, and Vrba (1976). Optical and radio continuum observations (Cohen, Bieging, and Schwartz 1982; Mundt and Fried (1983); Snell et al. 1985) show the presence of a highly collimated, ionized stellar wind orginating from close to IRS-5 and aligned with the molecular outflow. However, we have little information on the actual mechanism that generates the stellar wind and collimates it into opposed jets. The VLA observations indicate that the winds originate within 10^{15} cm of IRS-5, unfortunately at a size scale difficult to resolve. For these reasons, observations of the structure and dynamics of the hypersonic molecular gas may provide valuable information on the origin and evolution of these outflows. In addition, the study of the impact of the outflowing gas on the surrounding molecular material is essential to understand the consequences these outflows have on the evolution and star formation history of the entire cloud.

Though L1551 is the largest angular-sized outflow known, high angular resolution observations are still essential to fully resolve the complex dynamics that are present. The study by Snell and Schloerb (1985) provides some relevant insights into the structure of the molecular jets. This investigation utilized a lunar occulatation to obtain a high angular resolution (7 arcsec) CO observations of a cut though the blueshifted lobe of high velocity emission. Their single cut suggested that the lowest velocity outflowing gas was located at the periphery of the outflow, while the highest velocity gas was located at the center. Snell and Schloerb suggested that the data could be best modelled if the high velocity gas was confined to a expanding shell surrounding a cavity mostly evacuated of molecular material which may presently be filled with a low density stellar wind. The boundary of the shell was found to be coincident with the faint reflection nebulosity visible on the POSS photographs and interpreted by Snell et al. (1985) as scattered light from the stellar wind/molecular cloud interface.

The severe limitation in coverage of the outflow in the Snell and Schloerb observations begged for a more complete map at high angular resolution. Moriarty-Schieven et al. (1986) obtained a oversampled map of the CO emission of a portion of both the blueshifted and redshifted outflows in L1551 using Five College Radio Astronomy Observatory 14 m telescope. Data were obtained every 12 arcsec with a HPBW of 45 arcsec. The oversampled maps have been reconstructed to an effective angular resolution of 20 arcsec using a maximum entropy algorithm (Grasdalen, Hackwell, and Gehrz 1983). A portion of the blueshifted lobe of high velocity emission in L1551 is shown in the enclosed Figure for two

velocity intervals; on the right the highest velocity blueshifted emission (-5 to -2 km s^{-1}) and on the left the lowest velocity blueshifted emission (3 to 5 km s^{-1}). The bulk of the high velocity emission is found in the 3 to 5 km s^{-1}
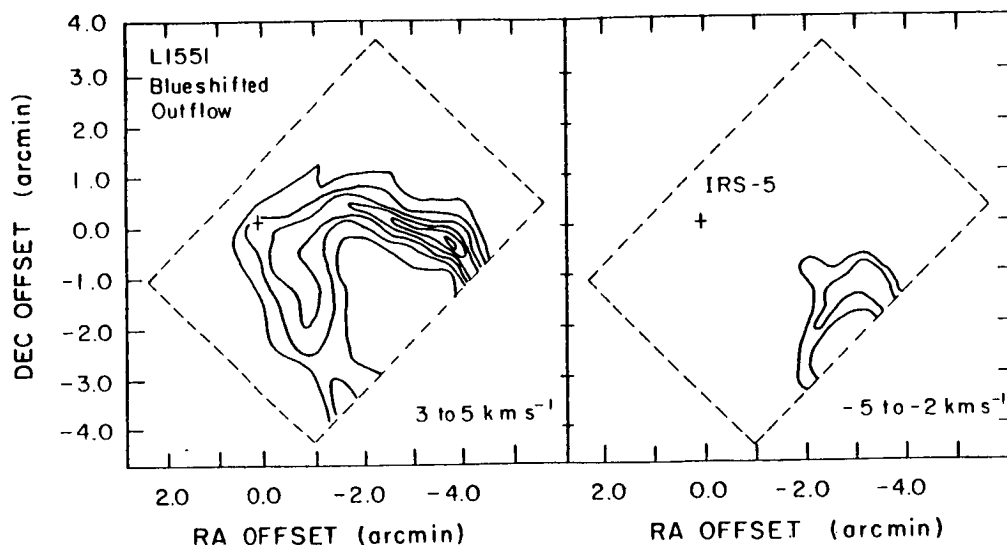
interval and delineates a shell-structure at the periphery of the outflow. The highest velocity gas is located at the center and is thought to represent gas on the front face of the shell expanding toward the observer. Similar kinematics and structure is also found for the redshifted outflow. The shell structure is found to be coincident with the arc of reflection nebulosity that presumably delineates the extent of the cavity and provides confirmation that such a shell model for the molecular outflow must be correct.

A continuation of the study of Moriarty-Schieven et al. will be presented at this meeting. The entire L1551 outflow has now been mapped at 12 arcsec sampling requiring roughly 4000 spectra. This data has been reconstructed to 20 arcsec resolution to provide the first high resolution picture of the entire L1551 outflow. This new data has shown that the blueshifted lobe is more extended than previously thought and has expanded downstream sufficiently to break out of the dense molecular cloud, but the redshifted outflow is still confined within the molecular cloud. Details of the structure and kinematics of the high velocity gas will be used to test the various models of the origin and evolution of outflows.

Cohen, M, Bieging, J.H., and Schwartz, P. 1982, Ap.J., 253, 707.
Grasdalen, G.L., Hackwell, J.A., and Gehrz, R.D. 1983, in Optical Society of America, Topical Meeting on Information Processing in Astronomy and Optics.
Moriarty-Schieven, G., Snell, R.L., Strom, S.E., Schloerb, P. Strom, K.M., and Grasdalen, G.L. 1986, in preparation.
Mundt, R., and Fried, J.W. 1983, Ap.J. (Letters), 274, L83.
Snell, R.L., Loren, R.B., and Plambeck, R.L. 1980, Ap.J. (Letters), 239, L17
Snell, R.L., Bally, J., Strom, S.E., and Strom, K.M. 1985, Ap.J., 290, 587.
Snell, R.L., and Schloerb, F.P. 1985, Ap.J., 295, 490.
Strom, K.M., Strom, S.E., and Vrba F.J. 1976, A.J., 81, 320.

A Compact Density Condensation Around L1551-IRS 5 - 2.7 mm Continuum Observations with 4" Resolution

Jocelyn Keene and Colin Masson
Downs Laboratory of Physics
Caltech
Pasadena CA 91125

The dark cloud L1551 contains the (arguably) best known example of bipolar molecular outflow (Snell, Loren and Plambeck 1980, *Ap. J. (Lett.)*, **239**, L17.) Such outflows are assumed to be driven by winds from young stars embedded in a cloud but the mechanism for collimation of the outflows is still in doubt, though it has been much debated. Among the possibilities put forth to date are intrinsically anisotropic stellar winds, isotropic stellar winds collimated by interstellar toroidal shaped clouds on the order of 10^{17} cm in size, or circumstellar disks of order 10^{15} cm in size. Because the outflow in L1551 as revealed by VLA cm continuum observations is collimated even at the arc second level (Bieging, Cohen and Schwartz 1984, *Ap. J.*, **282**, 699) it seems as though the stellar wind powering the outflow must either be initially anisotropic or be collimated by something very close to the star, such as a circumstellar disk.

We have observed L1551 in the continuum at 2.7 mm with the OVRO millimeter-wave interferometer in the winter of 1983-4 and again, more extensively, in 1985-6. The resulting map (Fig. 1) shows for the first time direct evidence for a density condensation capable of collimating an initially isotropic flow from IRS 5. This map was made from data taken in 1985-6 with projected baselines up to 100 m in length (37 kλ). It has been CLEANed and reconstructed with a 4" gaussian beam. It shows a nearly unresolved source with a suggestion of extension at the 3" level (assuming a gaussian source shape). The integrated flux density in this map is 170 mJy, in excellent agreement with lower resolution maps made during 1983-4. There is no suggestion that we are missing any flux in the interferometer maps; the source looks like a point source at all except the very longest baselines.

L1551   109171.085 MHZ

PEAK FLUX = 1.2387E-01 JY/BEAM
LEVS = 0.2000E-01 * (-1.00, 1.000, 2.000, 3.000, 4.000, 5.000, 6.000)
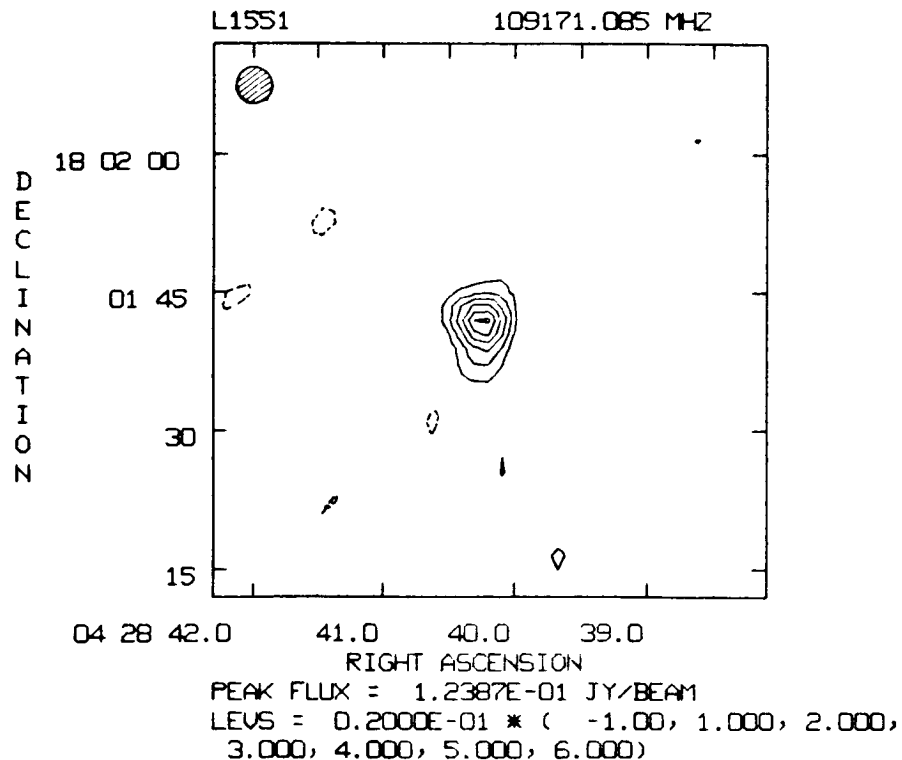
Figure 2 shows a composite spectrum of L1551 (taken from many sources). Through the points we have drawn a curve of the form $(1 - e^{-\tau})\, B(\nu,T)$ where τ is a function of the form ν^α. For $\lambda < 250\ \mu m\ \alpha_1 = 1$, while for $\lambda > 250\ \mu m\ \alpha_2$ was allowed to range from 1 to 2. It is obvious from this spectrum that the flux at 2.7 mm is due to the thermal radiation from dust that is also seen at shorter wavelengths. Very little of it can be due to the continuation of the nearly flat cm wavelength spectrum which is assumed to be from thermal bremsstrahlung radiation. The map in Figure 1 and spectrum in Figure 2 provide strong constraints on the size, $\Theta(\mathrm{FWHM}) \lesssim 3''$, temperature, and optical depth of the density condensation surrounding IRS 5. Given the size constraint of Figure 1, the product of the temperature, T, and optical depth, τ, at 2.7 mm must $\gtrsim 3$. The far-infrared spectral points put a strong constraint on T. Reasonable fits to this region of the spectrum were obtained for $55 < T < 70$ K and $2'' < \Theta \lesssim 3''$ with $1.7 \lesssim \alpha_2 \lesssim 2$. The implied opacity at 250 μm ranges from 3 to 12 for this range of parameters; thus this is an extremely optically thick source.

From our fit to the spectrum we deduce a mass of $\sim 0.8\ M_\odot$ for the circumstellar gas in agreement with Davidson and Jaffe (1984, *Ap. J.* (*Lett.*), **277**, L13). For a diameter of $3''$, the average gas density is $n_{H_2} \gtrsim 10^9$ cm^{-3} and the gravitational force on such an amount of material is more than sufficient to balance the pressure in the outflowing wind. The circumstellar material thus is capable of collimating the outflow from L1551 IRS 5.

The simple function shown in Figure 2 cannot reproduce the entire spectrum of L1551-IRS 5. Because of the bipolarity of the molecular flow it is obvious that any density condensation around IRS 5 must not be spherical. Although the opacity of the source is extremely high in some directions there must be a direction in which short wavelength radiation from an even smaller and hotter region can escape (along with the stellar wind).

L1551

$$T = 58\ \mathrm{K}$$
$$\alpha_2 = 1.7$$
$$\tau_{250} = 3$$
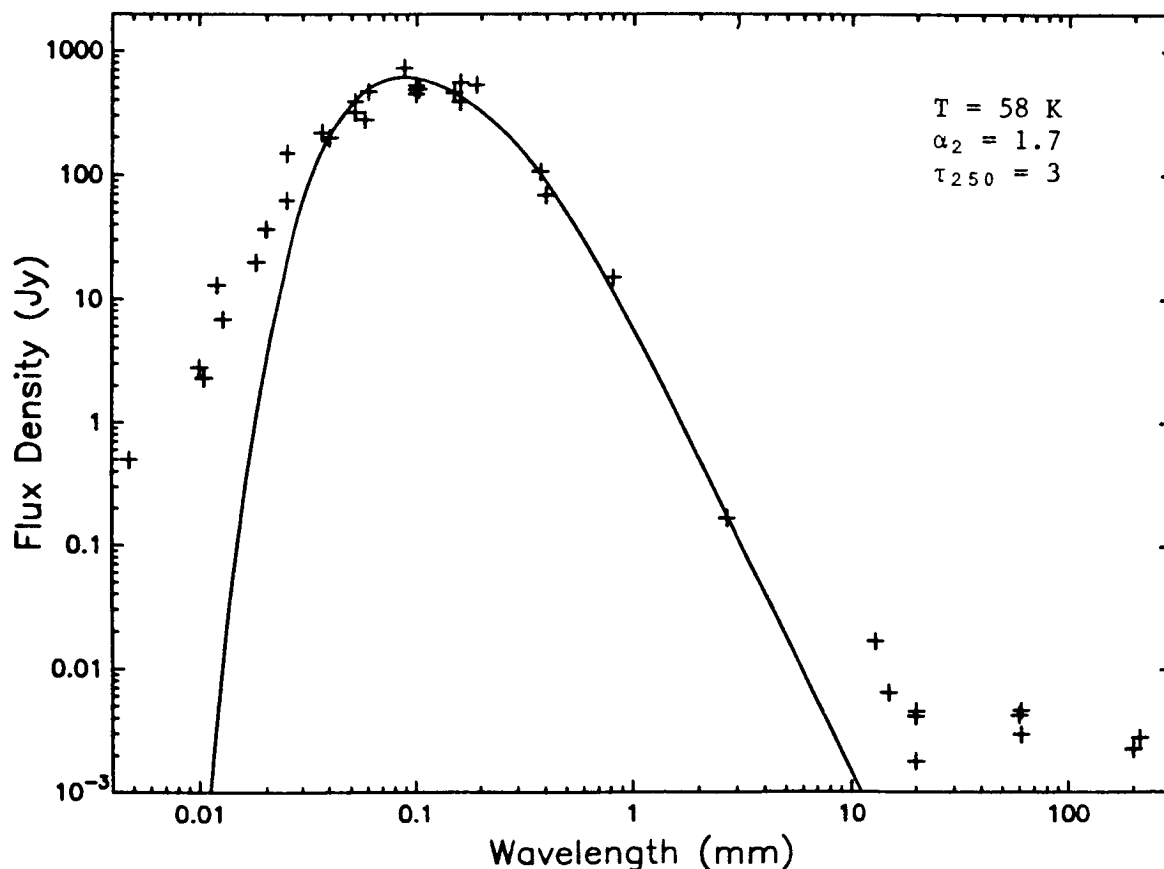
IMAGE RESTORATION AND SUPERRESOLUTION AS PROBES OF SMALL SCALE FAR-IR STRUCTURE IN STAR FORMING REGIONS

D. F. Lester, P. M. Harvey, M. Joy, H. B. Ellis Jr.
Department of Astronomy and McDonald Observatory, University of Texas
Austin, Texas 78712

This paper reports on far-infrared continuum studies from the Kuiper Airborne Observatory that are designed to fully exploit the small-scale spatial information that this facility can provide. This work gives us our clearest picture to date on the structure of galactic and extragalactic star forming regions in the far infrared. Our work is presently being done with slit scans taken simultaneously at 50 and 100μm, yielding one-dimensional data. Scans of sources in different directions have been used to get certain information on two dimensional structure. Planned work with linear arrays will allow us to generalize our techniques to two dimensional image restoration.

For faint sources, spatial information at the diffraction limit of the telescope ($\lambda/D \sim 23''$ at 100μm) is obtained, while for brighter sources, nonlinear deconvolution techniques have allowed us to improve over the diffraction limit by as much as a factor of four. Information on the details of the color temperature distribution is derived as well. This is made possible by the accuracy with which the instrumental point-source profile (PSP) is determined at both wavelengths. While these two PSPs are different, data at different wavelengths can be compared by proper spatial filtering as described below.

Our ability to do image restoration in the far-IR depends on having PSPs that are stable and well determined. Three effects can determine the shape and size of our PSPs; seeing, telescope tracking and scanning errors, and diffraction. The first may be considered to be $<2''$, assuming that the usual wavelength scaling law can be applied to the visual seeing. Using our technique of focal plane tracking with reflected stage motion, the second effect is held to this amount as well. Since the far infrared image profile on the KAO is therefore dominated by diffraction, and since the geometry of the telescope and photometer optics is invariant, it is not surprising that the PSPs are, in practice, extremely reproducible. Intercomparison of independent PSP data sets justifies the above discussion. On this spatial scale, the only sources in the sky that are justifiably good point sources in the far-IR are bare rocks in the solar system such as asteroids and moons, which subtend less than an arcsecond on the sky . We have used bright asteroids and Galilean satellites for this purpose with considerable success.

Scans at 50 and 100μm are compared using a beam matching procedure that is described in Lester *et al.* 1986 (Paper 4). This is based on a restoring function derived directly from the spatial transforms of the respective PSPs that, when convolved with the 50μm data, produces that 50μm profile that *would have been seen* had the 50μm data been taken in a beam with exactly the same shape as the 100μm beam. Effectively, this degrades the resolution of the diffraction limited 50μm profile to match that at 100μm, so the resulting ratio gives color temperature information on the scale of the 100μm beam. This analysis is of value not only for obtaining temperature information on a small scale, but for large scales as well, in which low flux levels surrounding a bright source would otherwise be confused by the wings of the beam. This latter point is well illustrated in Paper 4, in which a steep temperature rise near the ionization front in the S140 molecular cloud was clearly detected, even though the front is only 1 arcminute away from a cluster of compact sources (the protostellar cluster) that are factor of 20-50 brighter through our slits.

Considerable effort has been devoted to implementing deconvolution algorithms. Non-linear deconvolution methods offer the potential of superresolution -- that is, inference of power at spatial frequencies that exceed D/λ. This remarkable potential is made possible by the implicit

assumption by the algorithm of *positivity* of the deconvolved data, a universally justifiable constraint for photon processes. We have tested two nonlinear deconvolution algorithms on our data; the Richardson-Lucy (R-L) method and the Maximum Entropy Method (MEM). We have found MEM to be mathematically superior though R-L can be computationally more advantageous. A comparative discussion of these methods in the context of our data on M51 can be found in Lester, Harvey and Joy (1986, Paper 1).

What are the limits on the spatial resolution that can be achieved through image deconvolution? The answer is clearly a function of S/N on the object in question, but is also inextricably connected to the accuracy with which the PSP is known, and its stability between calibration objects. Even for infinitely bright objects, positional errors (in tracking and scanning) limit the resolution that can be achieved. While numerical image modelling experiments can give a general answer to this question that can be applied to different situations, our work on deconvolving independent PSPs with each other, and our work on the bright and (evidently) point-like object IRC+10216 (Lester, Harvey and Joy 1986, Paper 2) give similar limits that are derived in a more practical way. Our deconvolution of IRC+10216 at 50 and 100μm indicates a profile with FWHM<3" at 50μm and <6" at 100μm. *These limits are nearly a factor of four smaller than the FWHM of the diffraction spot of the telescope , approach that obtainable at other wavelengths , and are nearly a factor of five smaller than that previously achieved in the far -infrared.*

Our techniques have revealed the presence of a far-IR hole in the center of the spiral galaxy M51 (Paper 1) that indicates a deficit of star formation there. We have shown that the extended molecular outflow source IRC+10216 is remarkably compact compared with the molecular cloud that surrounds it. Substantial revision of the grain heating model for this source will be required to account for the invisibility of the surrounding cloud in the far-IR. In this same paper, we have shown that the distribution of cool dust in the planetary nebula NGC7027 is essentially identical to that of its ionized gas. While cold dust may surround this planetary, most of the luminosity arises from within the ionized region (Paper 2). Our observations of the extraordinary IRAS galaxy Arp 220 have been used to set limits on the size of the starburst there that are a factor of three smaller than those found from the IRAS data. When converted to optical depth, our size, flux and temperature information indicates that Av>25 towards the center of this source (Joy *et al.* 1986, Paper 3). Our measurements of the protostellar cluster in S140 (described in part above), whose three near-IR components are separated by 10-20", has resulted in total bolometric luminosities for each of the cluster members, as well as the temperature distribution of the cloud around them (Paper 4). Deconvolved slit scans parallel and perpendicular to the bipolar structure in the outflow region S106 show evidence for a doughnut-like structure with its axis oriented parallel to the outflow when the 50 and 100μm data are combined to give column density profiles. This is the first far infrared detection of such a disk (Harvey, Lester, and Joy 1986 ApJ, submitted).

Joy, M., Lester, D.F., Harvey, P.M., and Frueh, M. 1986 *Ap.J.*, in press Aug.1. (Paper 3)
Lester, D.F., Harvey, P.M. and Joy, M. 1986 *Ap.J.*, **302**, 280. (Paper 1)
Lester, D.F., Harvey, P.M. and Joy, M. 1986 *Ap.J.*, **304**, 623. (Paper 2)
Lester, D.F., Harvey, P.M., Joy, M., and Ellis, H.B. Jr. 1986 *Ap.J.*,
    in press Oct. 1. (Paper 4)

MODELING OF INFRARED FLUX SPECTRA FROM DISK-SHAPED INTERSTELLAR DUST CLOUDS.

GEORGE F. SPAGNA, JR. and CHUN MING LEUNG
Department of Physics, Rensselaer Polytechnic Institute
Troy, NY 12180-3590

Although there is growing observational and theoretical evidence for many disk-shaped objects of astrophysical interest, spherical geometry is assumed in most radiative transfer models. Recently we generalized the "quasi-diffusion" method developed by Leung (1975, 1976) for spherical geometry to solve the problem of scattering, absorption, and reemission by dust grains in a medium of disk geometry. The details of the numerical method and computational procedure are given elsewhere (Spagna and Leung 1986a). The method is applicable to a variety of astronomical sources whose dynamics are angular-momentum dominated and hence not accurately treated by spherical geometry, e.g., protoplanetary nebulae, circumstellar disks, bipolar-flow molecular clouds, accretion disks and disk galaxies.

Using this technique and realistic grain opacities we construct theoretical models to determine self-consistently the dust temperature distribution and infrared emission from disk-shaped, quiescent dark globules heated externally by the intersteller radiation field. The effects of the following parameters on the temperature structure and the emergent spectrum are studied: grain type (graphite and silicate), optical depth, density inhomogeneity, degree of disk flattening. Values for the grain opacities and the ambient interstellar radiation field are taken from the work of Mathis, Mezger, and Panagia (1983). The disk models are characterized by an aspect ratio (ratio of radius to half-thickness, R:Z) and an optical depth at 0.55 μm (measured from the cloud surface to the disk center in the midplane). For inhomogeneous models, a gaussian density distribution is assumed such that the ratio of central to surface density is 100.

To study the effects of source geometry, we also compare results for models with spherical and disk geometry. In this case both models have the same radius (taken to be 1 parsec) and central optical depth, the disk models having a 1:1 aspect ratio. While the dust temperature distributions in the two cases are very similar, the emergent flux for the disk model depends sensitively on the viewing angle. For clouds which are unresolved, one would naively expect, since the thermal emission is isotropic in the neighborhood of an emitting grain, and since the emission (in the far infrared) is optically thin, that the emergent flux spectrum should be characteristic only of the dust temperature, and independent of viewing angle. However, because of the lack of complete symmetry and the resulting radiation anisotropy, this is found *not* to be the case for the disk models. As an example, the figure shows the excess flux (emergent flux minus the ambient external flux at the cloud surface) spectrum for a disk model viewed at three different angles. The brightness of the disk clearly varies with viewing angle θ, being somewhat brighter seen edge-on than face on, and with both extremes brighter than when seen at an intermediate angle. The edge-on (θ = 90°) spectrum is identical in shape to that of the spherical model, but the flux is lower by about 30%. The flux at other viewing angles are even weaker and the longer wavelength side of the emission peak falls off faster, indicating that we are seeing less of the cooler interior dust.

An important consequence of this variation in emergent flux with viewing angle is that it implies a large uncertainty in estimating the radiating dust mass.

In particular, for disk-shaped clouds which are unresolved, one is likely to underestimate the mass of dust for obliquely viewed disks of all aspect ratios, and to grossly overestimate the the dust mass for flattened disks viewed edge-on. On the other hand, if spherical geometry is incorrectly assumed, the estimated dust mass may easily be off by over an order of magnitude. Other observational implications related to the interpretation of infrared observations of unresolved disked-shaped objects are discussed in Spagna and Leung (1986b).
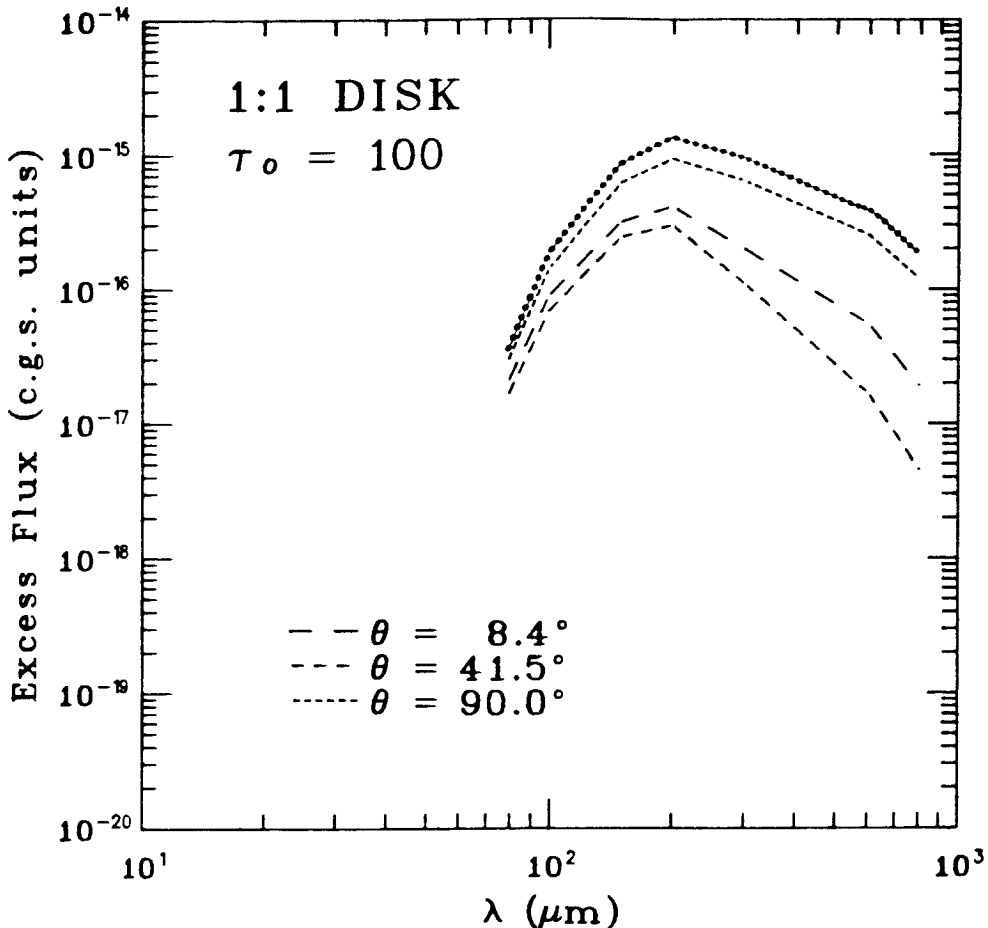
Comparison of excess flux spectra for graphite grains in centrally condensed spherical and disk models of the same optical depth. The dotted line is for the spherically symmetric model. For the disk model, the excess flux profile depends on the viewing angle θ and is strongest for edge-on viewing ($\theta = 90°$).

REFERENCES
Leung, C. M. 1975, *Ap. J.*, **199**, 340.
Leung, C. M. 1976, *J. Quant. Spectrosc. Rad. Transf.*, **16**, 559.
Mathis, J. S., Mezger, P. G., and Panagia, N. 1983, *Astr. Ap.*, **128**, 212.
Spagna, G. F., Jr., and Leung, C. M. 1986a, *J. Quant. Spectrosc. Rad. Transf.*, submitted.
Spagna, G. F., Jr., and Leung, C. M. 1986b, *Ap. J.*, submitted.

Models of Polarized Infrared Emission from Bipolar Nebulae

M. Shane Burns, Paul Johnson, & Harley A. Thronson, Jr.
Wyoming Infrared Observatory
University of Wyoming
Laramie, Wyoming 82071

Many stars with circumstellar dust shells show a high degree of linear polarization (Sato et al. 1985). We are developing a model which assumes that the polarization arises from scattering by circumstellar dust. This model is similar to those investigated by Heckert and Zellik (1985), Shawl (1975), and Elsasser and Staude (1978). Our model assumes a geometry in which the star is surrounded by an optically thin spherical dust shell and embedded within an optically thick disc. This geometry is consistent with that proposed for objects with bipolar molecular outflow. This is important because many bipolar flow objects have also been observed to be highly polarized (Sato et al. 1985).

The high degree of linear polarization is produced because the disc differentially attenuates the light from the star. The light incident from the point source is attenuated by a factor of $\exp(-\tau/\cos\theta)$ where θ is the angle between a ray from the point source to the scatterer and a ray normal to the disc; τ is the optical depth at the wavelength of interest. Hence, the light scattered from the regions directly above and below the disc give the largest contribution to the total flux. The scattering angle for light from these regions is near 90°, so the light is strongly polarized and, in the Rayleigh scattering regime, is polarized parallel to the disc.

The Stokes parameters for the scattered light from each particle in the shell are calculated by using the scattering matrix elements generated by a Mie scattering program. After the Stokes parameters for each particle are computed they are summed to give the Stokes parameters for the entire shell. The two graphs on the next page show the intensity and polarization spectrum generated by our model using the optical constants for "astronomical" silicates as defined by Draine and Lee (1984). A narrow ($\sigma=0.06\,\mu m$) log-normal particle size distribution was used with a mean size of 0.3 μm. The plane of polarization is parallel to the disc from 1.1 to 3.0 μm. The disc was assumed to be made up of the same material as the shell and to have an optical depth of 1.5 at 1.0 μm.

References:

Elsasser, H., & Staude, H. J. 1978, *Astr. Ap.* **70**, L3.

Draine, B. T., & Lee, H. M. 1984, *Ap. J.* **285**, 89.

Heckert, P. A., & Zeilik, M. 1985, *Astr. J.* **90**, 2291.

Sato, S., Nagata, T., Nakajima, T., Nishida, M., Tanaka, M., & Yamashita, Y. 1985, *Ap. J.* **291**, 708.

Shawl, S. J. 1975, *Astr. J.* **80**, 595.
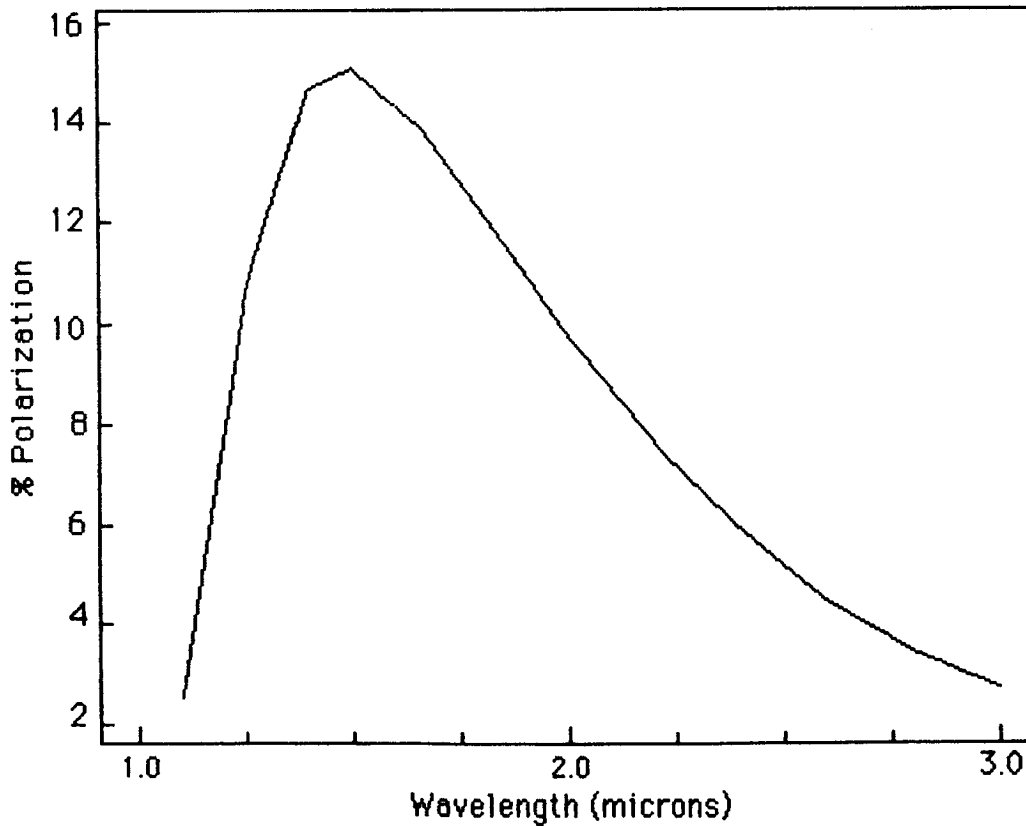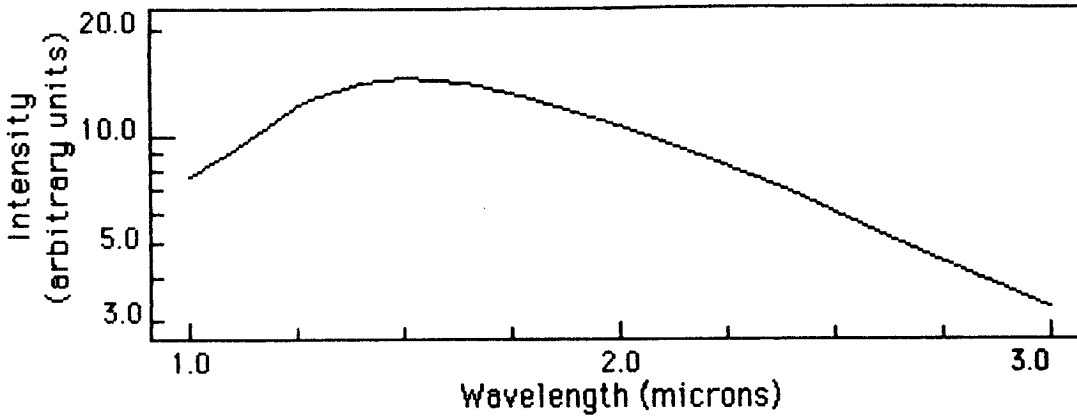
Are Young Stars Always Associated with Cold Massive Disks?
A CO and Millimeter Interferometric Continuum Survey

Mundy, L. G. (Caltech), Wilking, B. A. (U. of Missouri - St. Louis),
Myers. S. (Caltech), Howe, J. E. (U. of Texas, Austin),
Blackwell, J. H. (U. of Missouri - St. Louis), and Likkel, L. (UCLA)

We present the results of a combined millimeter-wave spectral-line and continuum survey of cold far-infrared sources selected to favor embedded young stars in the Galaxy. The spectral-line observations were performed with the 5 meter antenna of the University of Texas Millimeter-Wave Observatory. High resolution continuum observations were obtained with the Owens Valley (OVRO) Millimeter-Wave Interferometer. The goal of the survey was to gain insight into the mass, temperature, and distribution of cold dust which envelopes stars during the earliest stages of their evolution.

The sample for our survey was drawn from the IRAS point source catalog. Our selection criteria were: 1) the source color temperature as measured by the IRAS 25 μm and 60 μm bands was < 75 K, 2) the source lies between 2 and 25 degrees of the galactic plane at declinations north of -30 degrees, 3) the source has measured fluxes in at least 3 of the 4 IRAS bands, 4) the source was not identified as a main sequence or evolved star, a planetary nebulae, or extragalactic object in the IRAS catalog, and 5) the flux at 60 μm was >100 Jy. The initial sample consisted of 85 sources. Nearly one-half of these could be eliminated based upon identification with H II regions, reflection nebulae, planetary nebulae, externally heated clouds, and emission-line or reddened visible stars. The remaining 48 objects constitute our sample of potential young stellar objects and include some well-studied sources such as S140 and Cep A.

The first phase of our survey involved 1.2 arcmin resolution observations of ^{12}CO and ^{13}CO emission lines toward each source. All but two sources had detectable CO emission. We found that 40 % of the sources appear to be associated with star formation as evidenced by the presence of enhanced ^{12}CO line widths or broad wings (V = 20-50 km s^{-1}). At least five of these objects are associated with bipolar molecular outflows (IRAS 05338-0624, L1689N, IRAS 20126+4104, S140, and Cep A).

The second phase of our survey involves high resolution 2.7 mm continuum observations with 3 interferometer baselines ranging from 15 to 55 m in length. Preliminary results indicate that about 25 % of the sources in our sample have detectable continuum emission on scales less than 30 arcsec. The flux limit of the survey is roughly 100 mJy which corresponds to a gas and dust mass limit of 5 M$_\odot$ (50 K / T$_{dust}$) D$_{kpc}^{2}$ for a λ^{-1} dust emissivity law. The mass limit for a λ^{-2} emissivity law is a factor of 7 larger.

The high percentage of sources with enhanced ^{12}CO line widths or broad wings indicates that a significant fraction of our sample, ~40%, are likely to be young stars. The lower detection percentage in the continuum observations, ~25%, suggests that such objects not always surrounded by large concentrations of gas and dust. The continuum detection percentage for actual dust emission could be lower than that given above since emission from ionized gas could be responsible for the observed 2.7 mm emission in some objects.

To get an understanding of the type of object detected in our survey, a 4" x 6"

resolution map of one of the survey sources, L1689N, has been made using the OVRO mm interferometer. This object shows strong (0.6 Jy) 2.7 mm emission from a 13" x <6" (2100 x <1000 AU) region roughly centered on the IRAS point source position, IRAS 16293-2422. Based on a λ^{-1} emissivity law and a dust temperature of 38 K (Walker *et al.* 1986), the source contains ~1 $M_\odot$ of gas and dust. The position angle of the 2.7 mm emission is approximately 30° west of north which is perpendicular to the large scale magnetic field direction as defined by polarization measurements (Vrba, Strom, and Strom 1978) and roughly perpendicular to the CO outflow centered near this source (Wootten and Loren 1986; Walker *et al.* 1986). ^{13}CO line observations from the interferometer suggest that the structure may be rotating at ~2 km s^{-1} about an axis aligned with the magnetic field, perpendicular to the major axis of the observed continuum emission. Further observations will be need to confirm this possible rotation and thereby identify the dust structure as a circumstellar disk.

References

Vrba, F. J., Strom, S. E., and Strom, K. M. 1976, *A.J.*, **81**, 958.

Walker, C. K., Lada, C. J., Young, E. T., Maloney, P. R., and Wilking, B. A. 1986a, Ap.J.(Letters) *submitted.*

Walker, C. K., Lada, C. J., Young, E. T., Margulis, M., and Wilking, B. A. 1986b, Ap.J. *in preparation* .

Wootten, H. A., and Loren, R. B. 1986, NRAO Preprint.

THE ASYMMETRIC PROFILE OF THE H76α LINE
EMISSION FROM MWC349

L.F. Rodríguez and J. Cantó
Instituto de Astronomía, UNAM
Apdo. Postal 70-264, México, DF 04510, MEXICO

and

V. Escalante and J.M. Moran
Harvard-Smithsonian Center for Astrophysics
60 Garden St., Cambridge, MA 02138, USA

MWC349 is an emission-line star found by Merrill, Humason and Burwell (1932). Braes, Habing and Schoenmaker (1972) discovered that it is a strong radio source. The radio emission originates in a massive ionized wind that is expanding with a velocity of about 50 km s^{-1} (Hartmann, Jaffe and Huchra 1980). Its continuum spectrum fits well a $\nu^{0.6}$ power law from the cm wavelenghts to the far-IR (Dreher and Welch 1983). Radio recombination line emission from the envelope of MWC349 was first detected by Altenhoff, Strittmatter and Wendker (1981).

We have obtained good signal-to-noise ratio, Very Large Array observations of the H76α radio recombination line from the ionized wind of MWC349. Our data reveal that the profile is markedly asymmetric, with a steep rise on the "blue" side (see bottom of Figure). This asymmetry could be due to non-LTE effects in the formation and transfer of the line or to intrinsic asymmetries in the envelope. Our analysis suggests that most probably the peculiar profile is caused by a non-LTE enhancement of the line emission from the side of the envelope nearer to the observer. This asymmetry, reported for the first time here, has the opposite sense than that observed in optical and IR recombination lines, where a different effect (absorption of the stellar continuum by the gas in the wind between the star and the observer) is known to be dominant, leading to the classic P Cygni profile (see Figure).

We propose that the profiles of the radio recombination lines from ionized stellar winds will have this characteristic shape, while optical and IR recombination lines are characterized by P Cygni-like profiles. Unfortunately, at present the detection of radio recombination lines from ionized stellar winds is only feasible for MWC349 and a few other objects.

R E F E R E N C E S

Altenhoff, W.J., Strittmatter, P.A. and Wendker, H.J. 1981, Astr. Ap., 93, 48.

Braes, L.L.E., Habing, H.J. and Schoenmaker, A.A. 1972, Nature, 240, 230.

Dreher, J.W. and Welch, W.J. 1983, A.J., 88, 1014.

Hartmann, L., Jaffe, D. and Huchra, J.P.
1980, Ap. J., 239, 905.

Merrill, P.W., Humason, M.L. and Burwell,
C.G. 1932, Ap. J., 76, 156.

Tanaka, M., Yamashita, T., Sato, S.,
Nishida, M., Ukita, N. and Okuda,
H. 1985, P.A.S.P., 97, 1115.
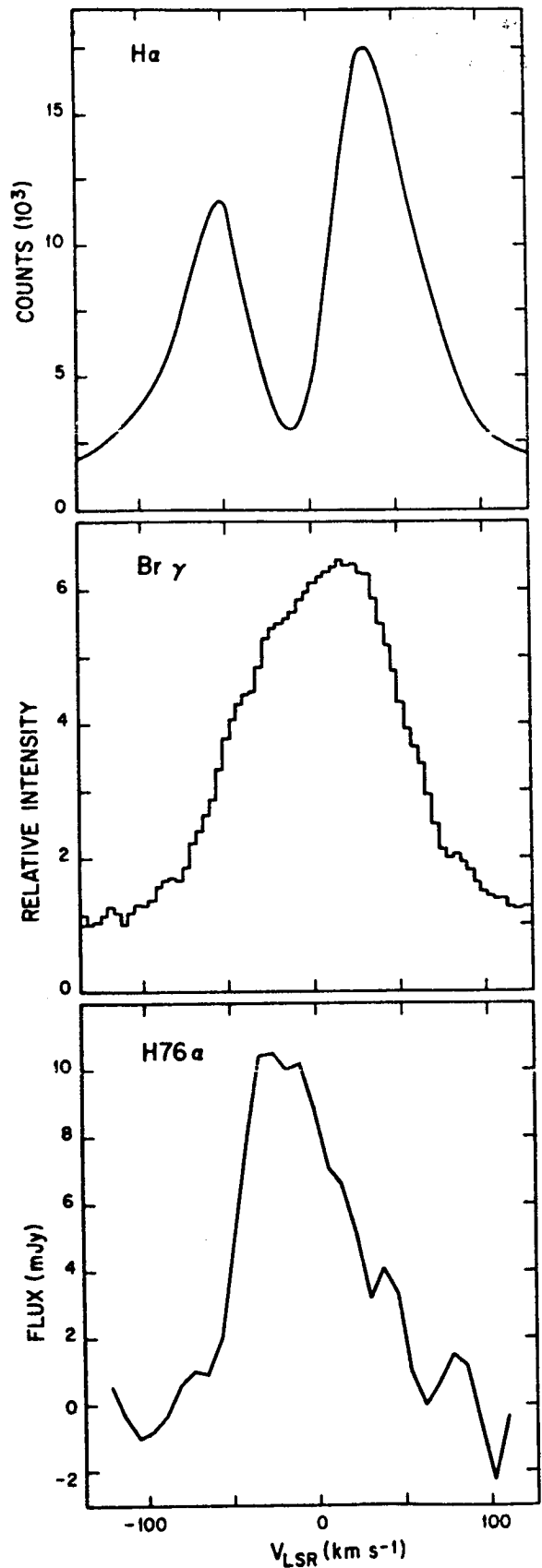
Figure. Spectra of Hα (top: Hartmann, et al. 1980), Br γ (middle: Tanaka et al. 1985), and H76α (bottom: this abstract). Note that the sense of the asymmetry in the Br γ line reverses in the H76α line.

C_3H_2 OBSERVATIONS AS A DIAGNOSTIC PROBE FOR MOLECULAR CLOUDS

L.W. Avery
Herzberg Institute of Astrophysics
Ottawa, Canada

Recently the three-membered ring molecule, cyclopropenylidene, C_3H_2, has been identified in the laboratory and detected in molecular clouds by Thaddeus, Vrtilek and Gottlieb (1985). This molecule is wide-spread throughout the Galaxy and has been detected by Matthews and Irvine (1985) in 25 separate sources including cold dust clouds, circumstellar envelopes, HII regions, and the spiral arms observed against the Cas A supernova remnant. In addition, Seaquist and Bell (1986) have detected C_3H_2 in the galaxy NGC5128.

A number of factors suggest that C_3H_2 may be an astrophysically important molecule. Its large dipole moment ($\approx 3.3D$) and widespread occurrence give rise to relatively strong lines in many sources. In addition, its relatively small moments of inertia and asymmetric top structure result in numerous spectral lines distributed throughout the cm and mm wavelength range.

In order to evaluate the potential of C_3H_2 as a diagnostic probe for molecular clouds, and to attempt to identify the most useful transitions, I have carried out statistical equilibrium calculations for the lowest 24 levels of the ortho species and the lowest 10 levels of the para species. Because collisional excitation rates for C_3H_2 are not yet available, the rates computed by Green (1980) for H_2O were used. Both H_2O and C_3H_2 have C_{2v} symmetry, with b-type transitions, so their quantum level structure is qualitatively similar, though the energy level separation in H_2O is larger because of its large moments of inertia. To compensate for this I have used Green's H_2O excitation rates for $T_K=200K$ to represent C_3H_2 at $T_K=10K$. (At 200K, the ratio of the average kinetic energy of H_2 molecules to typical H_2O energy level separations is comparable to the same ratio for H_2 and C_3H_2 at 10K). Also, the H_2O rates were scaled upward by an order of magnitude to reflect the significantly larger dipole moment and size of C_3H_2.

Many of the sources observed by Matthews and Irvine (1985) show evidence of being optically thick in the 1_{10}-1_{01} line. Consequently, the effects of radiative trapping should be incorporated into the equilibrium calculations. This was done using the Large Velocity Gradient approximation for a spherical cloud of uniform density as discussed by Goldreich and Kwan (1974).

Some results of the calculations for $T_K=10K$ are given in Figures 1-3. Each figure shows contours of the logarithm of the ratio of peak line brightness temperatures for ortho-para pairs of lines at similar frequencies. The background temperature was taken to be 2.8K. Such line-strength ratios should be relatively free of systematic errors due to effects such as differential beam dilution, telescope efficiencies, atmospheric transmission etc. In each figure n_{H_2} is the neutral hydrogen density, X the C_3H_2 abundance relative to H_2, and dV/dR the velocity gradient in the molecular cloud.

The 1_{10}-1_{01} and 2_{20}-2_{11} line pair of Figure 1 showd a marked density dependence. Over the central range of H_2 densities which are appropriate for molecular clouds the 1_{10}-1_{01} line is predicted to be in emission and the 2_{20}-2_{11} line in absorption against the microwave background. This has been observed in a number of dark clouds by Matthews et al. (1986). In addition, the predicted line strength ratio of this pair exhibits a strong dependence upon n_{H_2} which implies that it may be especially useful as a density probe of molecular clouds.
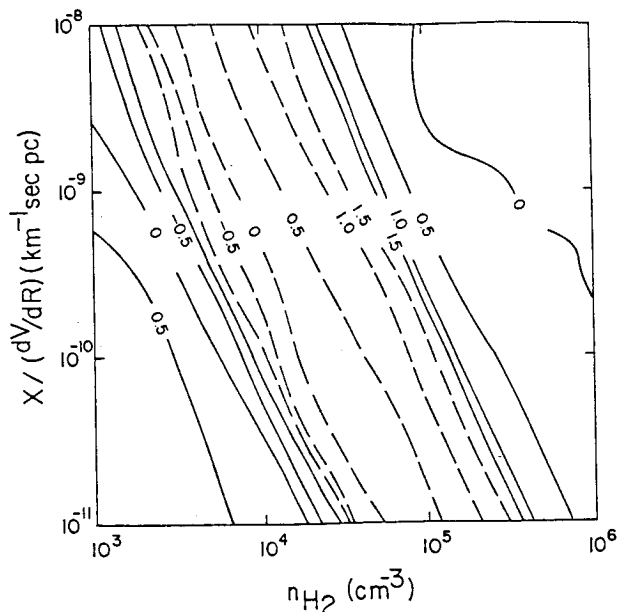
Figure 1.   Logarithm of $T_b(1_{10}-1_{01})$/ $T_b(2_{20}-2_{11})$.

The line frequencies are 18343 and 21587 MHz. Solid lines on the left represent both lines in absorption; on the right both lines in emission. In the area covered by dashed lines, the $1_{10}-1_{01}$ line is predicted to be in emission and the $2_{20}-2_{11}$ line in absorption.
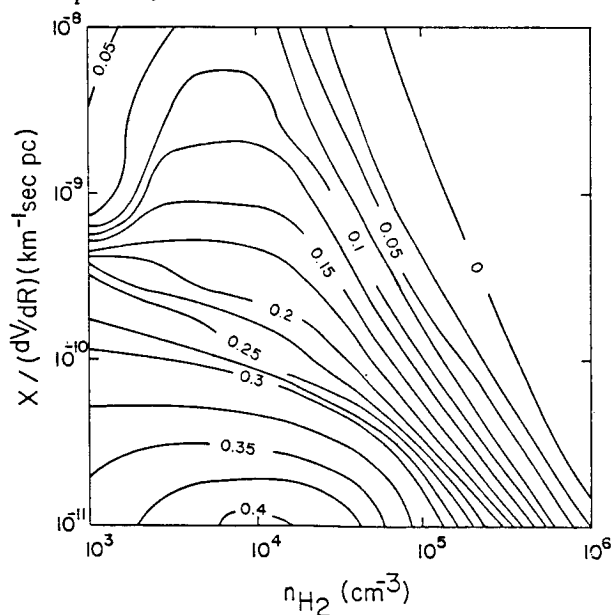
Figure 3.   Logarithm $T_b(2_{12}-1_{01})$/ $T_b(2_{02}-1_{11})$.

Both lines are in emission at frequencies of 85339 MHz and 82094 MHz.
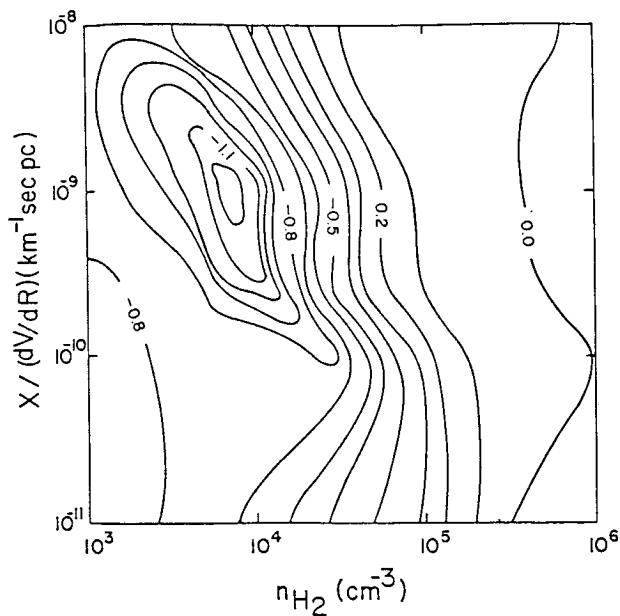
Figure 2.   Logarithm $T_b(3_{21}-3_{12})$/ $T_b(2_{11}-2_{02})$.

Both lines are in emission at frequencies of 44104 MHz and 46756 MHz.

Figure 2 suggests that the $3_{21}-3_{12}$ ortho line is likely to be quite weak relative to the $2_{11}-2_{02}$ para line at low-to-moderate H_2 densities. However, over certain parts of parameter space, information about both molecular abundance and n_{H_2} would be obtained from this pair.

The $2_{12}-1_{01}$, $2_{02}-1_{11}$ ratio in Figure 3 is relatively flat over density. (Note that different contour intervals are used in the three figures.) These lines appear to complement the K-band pair of Figure 1 very nicely in that their relative insensitivity to n_{H_2} yields information about $X/(dV/dR)$, which is necessary for a density determination from Figure 1.

In summary, it appears that the widespread nature of C_3H_2, the relatively large strength of its spectral lines, and their sensitivity to density and molecular abundance combine to make this a useful molecule for probing

20

physical conditions in molecular clouds. The $1_{10}-1_{01}$ and $2_{20}-2_{11}$ K-band lines may be especially useful in this regard because of the ease with which they are observed and their unusual density-dependent emission/absorption properties. These conclusions, however, are preliminary, and will need to be confirmed when better collisional rate coefficients are available.

REFERENCES

Goldreich, P. and Kwan, J. 1974, Ap.J., **189**, 441.
Green, S. 1980, Ap. J. Supp. **42**, 103.
Matthews, H.E., Madden, S.C., Avery, L.W., and Irvine, W.M. 1986, Ap.J. (Letters), in press.
Matthews, H.E. and Irvine, W.M. 1985, Ap.J. (Letters), **298**, L61.
Seaquist, E.R. and Bell, M.B. 1986, Ap.J. (Letters), **303**, L67.
Thaddeus, P., Vrtilek, J.M., and Gottlieb, C.A. 1985, Ap.J. (Letters), **299**, L63.

43 GHz VLBI Mapping of SiO Maser Emission Associated
with Orion-KL IRC-2

Lincoln J. Greenhill
James M. Moran
Harvard-Smithsonian Center for Astrophysics

We present a new milliarcsecond resolution spot map of the SiO maser emission associated with IRC-2 in Orion-KL. The two dominant groups of spectral features, near $V_{LSR} = -6$ and 16 km/s, were observed in the 43 GHz, $v=1$, $J=1\rightarrow0$ transition of SiO, using a Mark III VLBI system. The 74 km baseline ran from Haystack Observatory in Westford, Massachusetts to Five College Radio Astronomy Observatory (FCRAO) in New Salem, Massachusetts.

We observed five distinct maser features: -8.5 to -6.5 km/s; -5 to -1.5 km/s; 12 to 13.5 km/s; 16.5 to 19 km/s; and 20 to 21 km/s (stellar velocity $\approx$ 5 km/s). The relative positions were established, from an analysis of fringe phases, to an accuracy of about 5 milliarcseconds. All the features lay within an area of radius 0.08 arcseconds or 6×10^{14} cm, at a distance of 500 pc. Previous interferometric studies were only able to measure the gross separation between the red and the blue shifted groups (Lane 1982; Wright and Plambeck 1983). Our measurement of the separation between these two groups is consistent with those of the previous studies, indicating the persistence of these two centers of activity. The absolute positions of the masers with respect to IRC-2 are only known to an accuracy of about 1 arcsecond. We assume that IRC-2 is centered between the red shifted and the blue shifted maser features. The relative placement of these two groups of maser features agrees with observations of thermal emission from SO, which traces the outflow on a much larger scale (Plambeck *et al.* 1982). The SiO masers trace the neutral outflow from IRC-2 on the smallest scale yet observed.

References

Lane, A. P. 1982, Ph.D. Thesis, University of Massachusetts at Amherst.
Plambeck, M. C. H., Wright, R. L., Welch, W. J., Bieging, J. H., Baud, B.,
Ho, P. T. P., Vogel, S. N. 1982, *Ap J.*, **259**, 617.
Wright, M. C. H. and Plambeck, R. L. 1983, *Ap J. (Letters)*, **267**, L115.

PERVASIVE SMALL-SCALE STRUCTURE IN MOLECULAR CLOUDS

Buddy Martin
National Radio Astronomy Observatory

and

Elizabeth Lada
University of Texas

We have completed an unbiased CO survey of molecular cloud cores, and analyzed the profiles within the context of a model for emission from clumpy clouds. We find that all sources observed contain a significant amount of structure that is not resolved with our 2.3-arcmin beam, and that the parameters which describe the degree of clumping span a remarkably narrow range of the possible values.

We studied two separate samples of cloud cores: a large sample of warm cores comprising the 91 brightest points from the Massachusetts-Stony Brook 12CO survey of the first galactic quadrant (Sanders et al., 1986), and a sample of cool cores made up of 19 positions in the Taurus dark clouds chosen primarily on the basis of H2CO emission. We observed all sources in the 1-0 transition of 12CO and 13CO with the 5-m telescope of the Millimeter Wave Observatory, obtaining spectra with 0.65 and 0.16 km/s resolution.
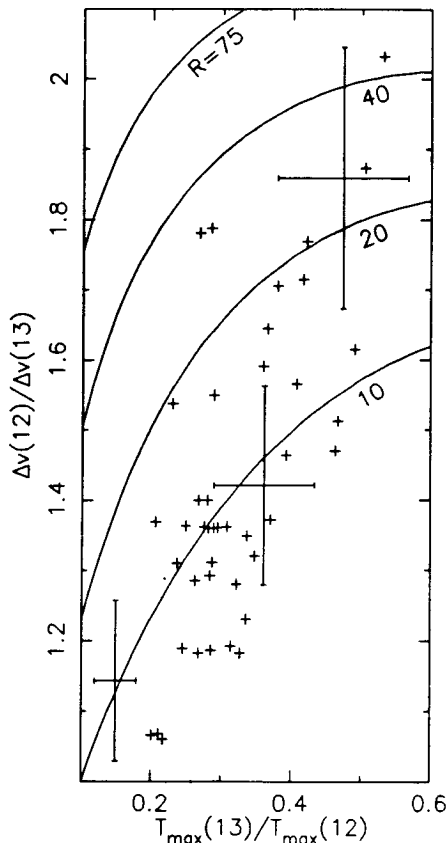
The first figure shows the ratio of peak intensities and ratio of linewidths between the two isotopes, for the sample of warm cores. Only about half of the sources are shown here, those with relatively simple profiles for which we could determine intensities and linewidths more accurately. Also shown are some representative error bars, and curves representing the predictions of a uniform-density microturbulent model for different values of the 12CO-to-13CO abundance ratio. For reasonable values of the abundance ratio ($R \cong 75$), this model predicts tremendous saturation-broadening of 12CO profiles, but most sources show only moderate enhancement of the 12CO linewidth.

These ratios can be explained if there is unresolved structure giving rise to significant variations of opacity across the beam. Our model cloud consists of a large number of identical clumps distributed randomly in the beam. These clumps have velocity widths v small compared to the width of the observed profile, which is determined by the relative motion of the clumps. The entire cloud is isothermal and in LTE.

With these assumptions the intensity and linewidth ratios depend on three parameters: the abundance ratio; the peak 13CO opacity through a single clump, τ_0; and the average number of clumps on a line of sight (counting only those clumps in a velocity range v at the line center), N. Small τ_0 and large N

(lots of transparent clumps on each line of sight) correspond to the microtur-
bulent limit, which is indistinguishable from a uniform gas distribution. In the
other extreme, large τ_0 and small N, at a given velocity at most one clump con-
tributes to the profile on each line of sight. Since each clump is opaque even in
13CO, the profile is determined largely by a variation of filling factor with
velocity, and profiles tend to be similar in the two isotopes. The observed
sources span the range between these two limits, but nearly all require a con-
siderable amount of unresolved structure to explain their intensity and linewidth
ratios.
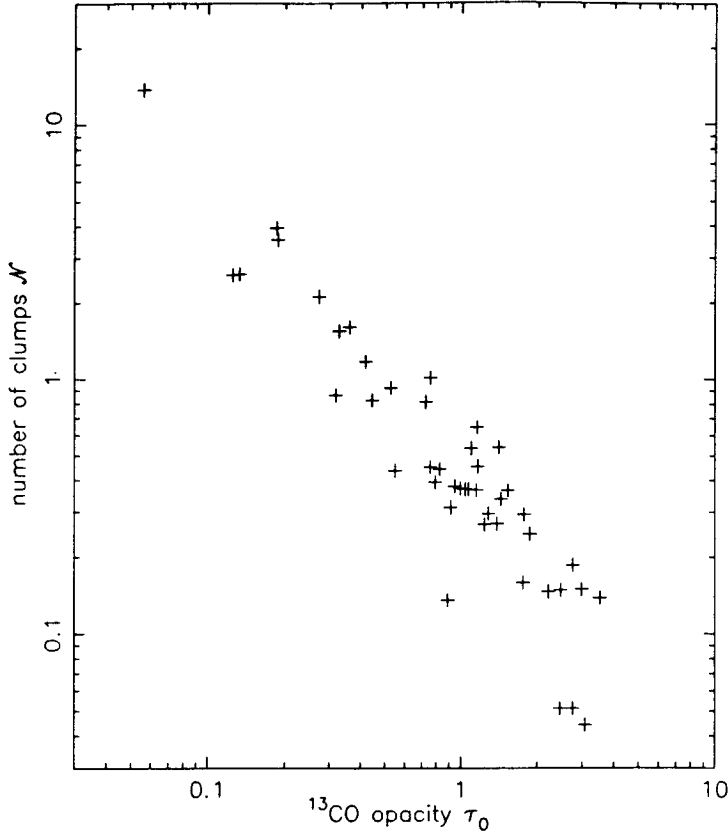
The second figure shows the model parameters which reproduce the measured
intensity and linewidth ratios for the sample of warm cores, assuming an abun-
dance ratio of 75. The sources in the upper left are close to the microturbulent
limit, while those to the lower right have the most clumpy structure. The
distribution of sources in the N-τ_0 plane is very similar for the cool cores.

A striking tendency toward constant $N\tau_0$ is present. The warm cores (left)
obey the relation
$$\log N = (-0.41 \pm 0.03) - (1.16 \pm 0.07)\log \tau_0,$$
while the cool cores (right) follow
$$\log N = (-0.03 \pm 0.03) - (0.97 \pm 0.06)\log \tau_0.$$
The boundary along the lower left of each distribution may represent an opacity
or column density threshold for the formation of a dense core, while that along
the upper right may correspond to a threshold for massive star formation (in
the case of the cool cores, for any star formation) resulting in disruption of
the core.

REFERENCES

Martin, H. M., Sanders, D. B., and Hills, R. E. 1984, MNRAS, 208, 35.
Sanders, D. B., Clemens, D. C., Scoville, N. Z., and Solomon, P. M. 1986,
    Ap. J. Supp., 60, 1.

HC$_3$N Maps of OMC1

Colin R. Masson and Lee G. Mundy
Caltech

We have made 3."8 resolution maps of HC$_3$N (J = 12-11) and 2.7 mm continuum emission in OMC1 using OVRO mm interferometer (Figure 1). The continuum map, which traces dust column density, shows that the Hot Core region consists of several clumps, the densest of which lies 3" SE of IRc2. HC$_3$N, which traces dense ($n_{H_2} \gtrsim 10^8$ cm^{-3}) gas, shows the velocity structure in the region. There is no simple pattern of rotation or expansion, nor does the emission resemble a disk centered on IRc2. Since the velocity difference between the Hot Core and IRc2 ($\sim$ 2 kms^{-1}) and the velocity dispersion in the hot core ($\sim$ 5 kms^{-1} HWHM) are comparable with the orbital velocity at a distance of 3" from a 20 M$_\odot$ object ($\sim$ 6 kms^{-1}), it is possible that the hot core material is bound to IRc2.

In the channel at 10.4 kms^{-1} V$_{LSR}$, we detect strong emission from the source 20" NE of IRc2, which confirms indications from continuum and CS (J = 2-1) maps (Mundy et al. 1986) that this is a very dense, possibly protostellar, object. This emission is clearly resolved from the hot core and is elongated north-south, along the direction of the ridge emission.

An additional interesting feature in these maps is a compact high velocity source located ~4" SW of IRc2. This source has a velocity dispersion of >20 km/s (FWHM) and is spatially coincident with the "zero-offset" source seen by Pauls et al. (1983) and a point source in the near IR images taken by Allen et al. (1984). The large localized velocity, dispersion and the highly obscured IR source suggest that this compact source is an outflow from a young stellar companion to IRc2.

References

Allen, D., Bailey, J., and Hyland, A. R., 1984, *Sky and Telescope*, **67**, 222.

Mundy, L. G., Scoville, N. Z., Baath, L. B., Masson, C. R., and Woody, D. P. 1986, *Ap.J.(Letters)*, **304**, L51.

Pauls, T. A., Wilson, T. L., Bieging, J. H., and Martin, R. N., 1983, *Astr. Ap.*, **124**, 23.

Figure Caption

Fig. 1: Contour maps of HC$_3$N and continuum emission in OMC1. The numbers in the corners of the maps denote V$_{LSR}$. The filled circle in IRc2 and the open circle is BN. The contour interval is 1 Jy/beam (6K) for the HC$_3$N maps and 0.1 Jy/beam for the continuum map.

HC₃N IN OMC1
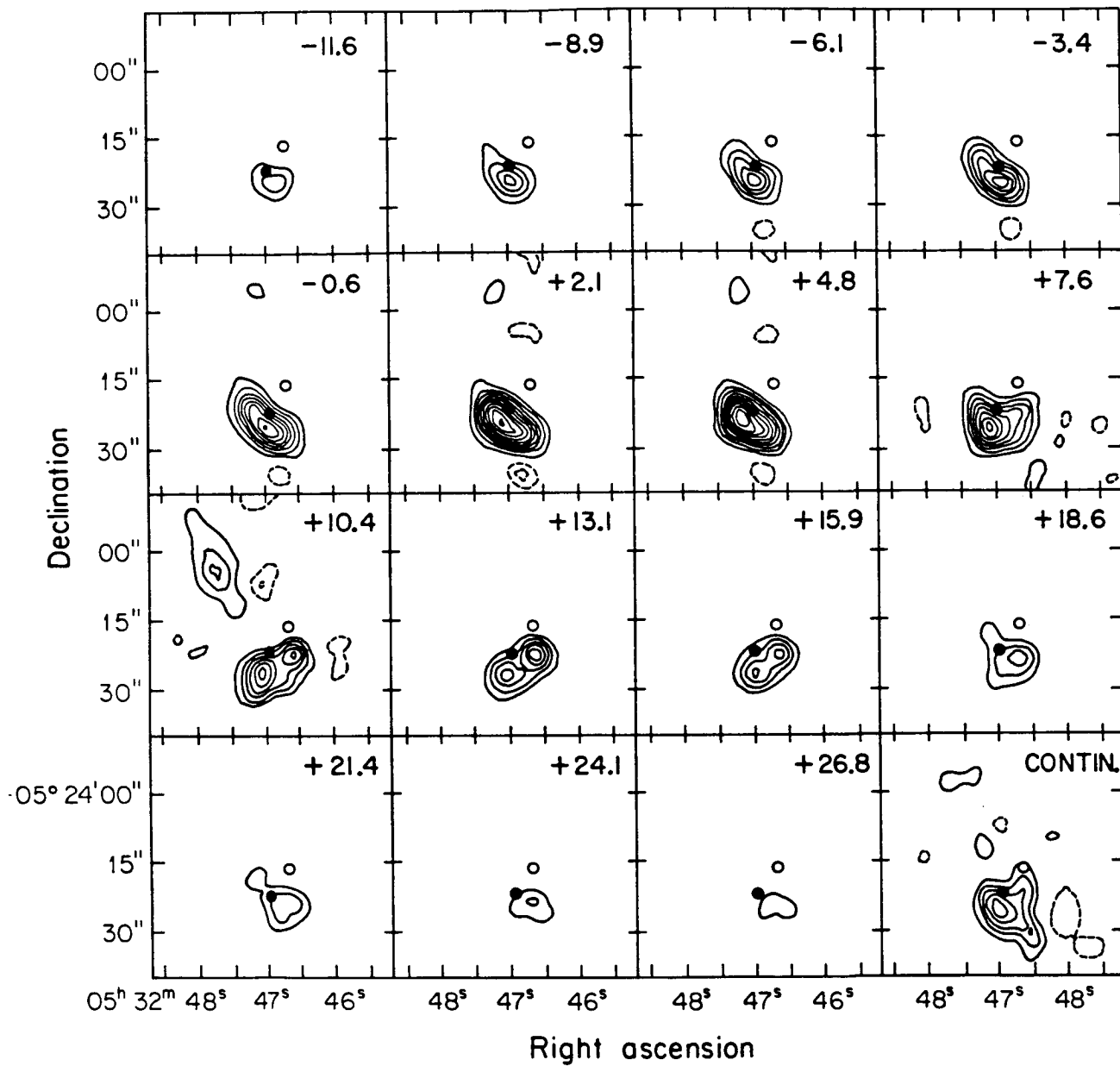
CO MAPPING OF THE ORION MOLECULAR CLOUD:
The Influence of Star Formation on Cloud Structure

F. Peter Schloerb, Ronald L. Snell, Paul F. Goldsmith, James A. Morgan
Five College Radio Astronomy Observatory
University of Massachusetts
Amherst, MA 01003

Regions of massive star formation have long been believed to have a profound influence on the structure of their surrounding molecular clouds. In this paper, we discuss the ways in which massive star formation has altered the structure and kinematics of the Orion Molecular Cloud.

The data to be discussed in this presentation consists of a large scale map of the CO J=1-0 emission from approximately 3 square degrees of OMC-1. During 1985, the Five College Radio Astronomy Observatory 14M antenna was used to map a $2° \times 1°$ region centered on $\alpha(1950) = 5^h33^m00^s$ $\delta(1950) = -5°30'00"$. The 1985 map, which is shown in Figure 1, is sampled at 45 arcsec spacing, which corresponds to the HPBW of the FCRAO antenna. Thus, the map contains some 12,800 individual spectra.

The region mapped in 1985 covers the well known HII regions M42, M43, and NGC1977, and the CO map contains abundant evidence of the interaction between these regions and the molecular cloud. Indeed, the global structure of the cloud appears to have been strongly influenced by the continuous formation of massive stars within the cloud. Individual instances of some of these interesting features will be discussed below, and it is interesting that there appear to be two classes of features which are indicative of this interaction: CO bright rims and CO holes.

<u>CO Bright Rims</u> – The region surrounding M42 contains several CO bright rim features which are the result of enhanced heating of the molecular gas at the boundary of the M42 HII region. We especially note the CO bright filaments which correspond well to the filaments and bright optical bar seen in [SII] images of M42. Other prominent examples of this morphology are the bright rim associated with NGC1977 and the local heating at the cloud edge adjacent to M43. The bright filamentary structure of the southern portion of the cloud in this map might also be due to these effects.

<u>CO Holes</u> – The expansion of the HII regions which accompany massive star formation can have a number of important effects on the structure of molecular clouds. Perhaps the simplest result of HII region formation is the removal of molecular gas from the vicinity of the HII region through either dissociation of the molecules or mass motion associated with the expansion of the HII region or stellar winds. The CO hole surrounding the M43 HII region offers the clearest example of such processes in action at the present time, but other examples (such as one occuring to the south of M42) suggest that previous epochs of star formation may have left their mark on the Orion Molecular Cloud.

During 1986, we have undertaken further mapping of OMC-1 to the south of the region covered by the map in Figure 1. This portion of the cloud contains significant regions of star formation, but O star formation has not occured and large HII regions have not developed to alter the appearance of the cloud. A detailed map of this region is thus an opportunity to view the structure of the

molecular cloud before it has been altered by massive star formation. Preliminary analysis of 1 square degree of data obtained in this region suggests that the structure and kinematics of the southern portion of the Orion cloud are indeed dramatically different from those of the region previously mapped. Comparison of the two regions thus supports models of the development of structure in molecular clouds through interaction with the HII regions formed within them.
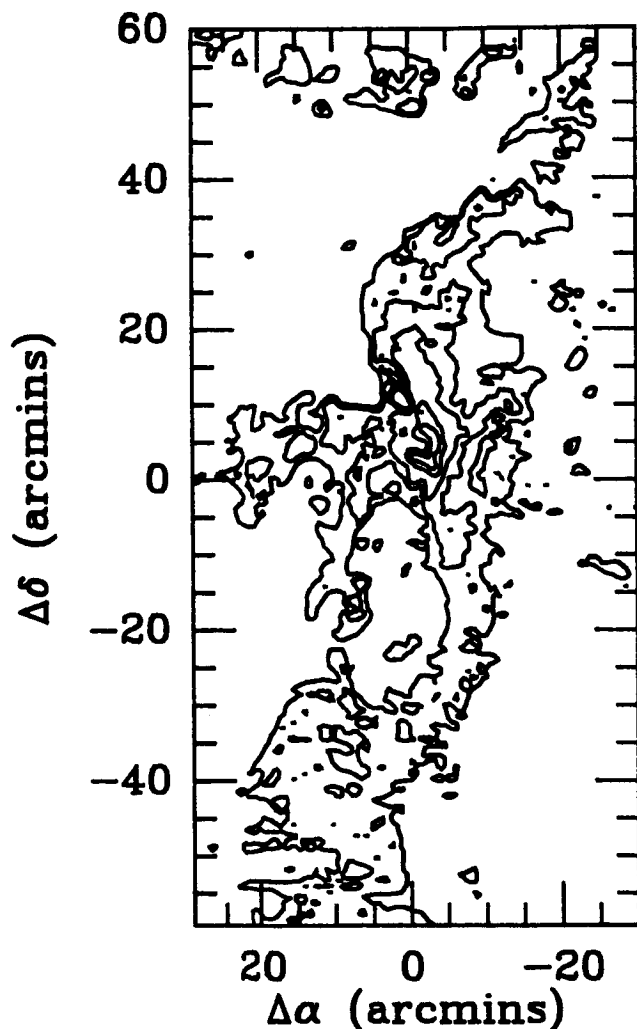
Figure 1 – Contour map of the peak antenna temperature of the CO J=1–0 emission from the Orion Molecular Cloud. Contour levels are 10K, 15K, 20K, 30K, and 40K. The map coordinates are referenced to $\alpha(1950)=5^h33^m00^s$ and $\delta(1950)=-5°30'00"$.

Filamentary Structure In The Orion Molecular Cloud

John Bally[1], Mark Dragovan[1], William D. Langer[2], Antony A. Stark[1], and Robert W. Wilson[1]

[1]AT&T Bell Laboratories, Crawford Hill
Holmdel, New Jersey

[2]Princeton University, Princeton N.J.

We present a large scale ^{13}CO map (containing 33,000 spectra) of the giant molecular cloud located in the southern part of Orion which contains the Orion Nebula, NGC1977, and the L1641 dark cloud complex. The overall structure of the cloud is filamentary, with individual features having a length up to 40 times their width. This morphology may result from the effects of star formation in the region or embedded magnetic fields in the cloud.

The Orion region contains the nearest giant molecular clouds (GMC's) to the Sun. Located at a distance of 500 pc, these clouds are situated 10 to 14 degrees below the galactic plane toward the outer galaxy, well away from potentially confusing background clouds. We picked the southern region of Orion for a detailed ^{13}CO survey of an entire GMC. The more abundant ^{12}CO species is optically thick along most lines of sight and is best suited as a probe of the kinetic temperature near the front surface of the cloud where the optical depth is unity. The rarer ^{13}CO species is optically thin in most directions as demonstrated by $C^{18}O$ observations; its brightness is a probe of the column density of molecular gas through the entire cloud.

The most intense feature in the map is a 13 pc elongated S-shaped filament located in the northern part of the cloud (Figure 1). This feature contains NGC1977 at its northern end, the Orion Nebula in the middle, and has an ill-defined southern end 20′ north of NGC1999. This filament is about 0.5 pc wide, has a total mass of $5 \times 10^3 M_\odot$, and shows a velocity gradient which peaks behind the Orion Nebula. The middle and lower portions of the map also exhibit fragmented and filamentary emission (Figure 2). Individual channel maps show about a dozen filaments. These filaments are straight, with little or no velocity gradient and are mostly aligned with the cloud. Some of these structures exhibit shapes reminiscent of the cometary globules seen in the Gum nebula.

Simple models of gravitational collapse of rotating or magnetized clouds produce flattened disc-like structures, however, the observed morphology of the Orion-A cloud requires a more sophisticated model of cloud formation or evolution. Filaments may be formed by several mechanisms including: 1) fragmentation of expanding shells associated with HII regions, stellar winds, or supernovae; 2) shadowing of the dissociating radiation from a localized source; and 3) magnetic fields.

If the observed velocity gradient in the major filament is interpreted as rotation about an East-West axis, then the filament can be supported against gravitational collapse along its length by centrifugal forces. For a rotation velocity of 1.75 km s^{-1} 4.5 pc from the center (implying a rotation period of 16 Myr), the computed dynamic mass (defined as the mass required to gravitationally bind the cloud) is $M_{dyn} = R(\Delta V)^2/G > 3 \times 10^3 M_\odot$, only slightly below the total mass derived from the ^{13}CO column densities. If a magnetic field threads the length of this structure, an upper bound on the strength of such a B-field can be obtained from the condition that the cylinder of gas is magnetically supported in the transverse direction. For a cylinder with major axis radius R and minor axis radius r, $B < M[8G/R^2 r^2]^{1/2} \approx 300 \mu G$. If turbulence plays a significant role in cloud support, the equilibrium B field value may be

considerably less.

We suggest a simple picture for the evolution of the Orion-A cloud and the formation of the major filament. A rotating proto-cloud (counter rotating with respect to the galaxy) contains a B-field aligned with the galactic plane. The northern portion of this cloud collapsed first, perhaps triggered by the pressure of the Ori I OB association. The magnetic field combined with the anisotropic pressure produced by the OB-association breaks the symmetry of the pancake instability, a filament rather than a disc is produced. The growth of instabilities in the filament formed sub-condensations which are recent sites of star formation.

Figure 1: A map showing the S-shaped, major filament in the northern part of the molecular cloud which contains OMC-1 and OMC-2. The contours show the ^{13}CO antenna temperature T_A^*, integrated from $V_{LSR}=7\,\mathrm{km\,s^{-1}}$ to $V_{LSR}=13\,\mathrm{km\,s^{-1}}$ in steps of 5 $\mathrm{K\,km\,s^{-1}}$.
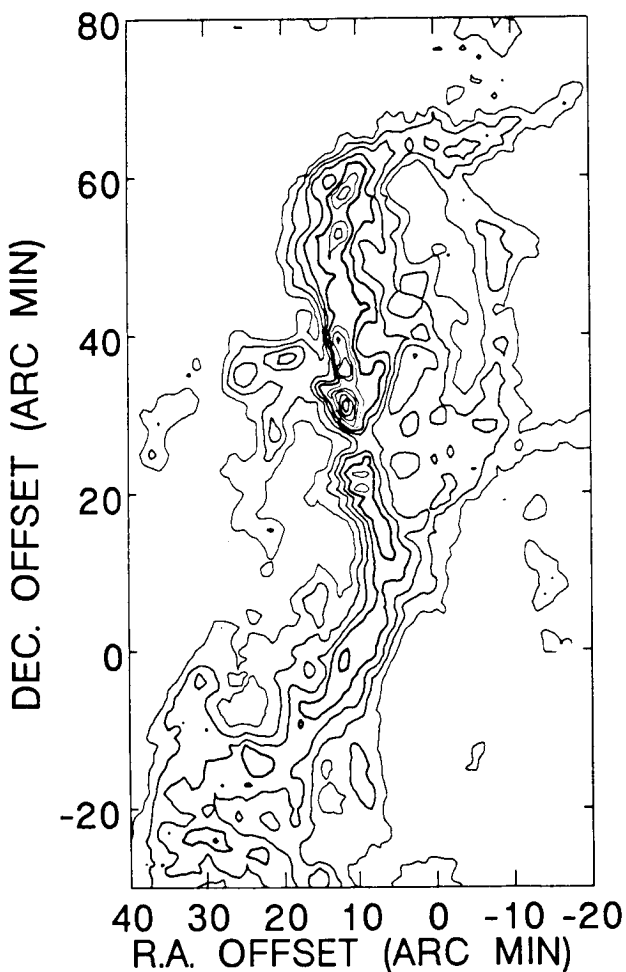
Figure 2: A map showing one of the "cometary" filaments located in the southern portion of the Orion-A molecular cloud. The contours show the ^{13}CO antenna temperature integrated from $V_{LSR}=5.5\,\mathrm{km\,s^{-1}}$ to $V_{LSR}=7.5\,\mathrm{km\,s^{-1}}$. Contours are in 2.5 $\mathrm{K\,km\,s^{-1}}$ steps.
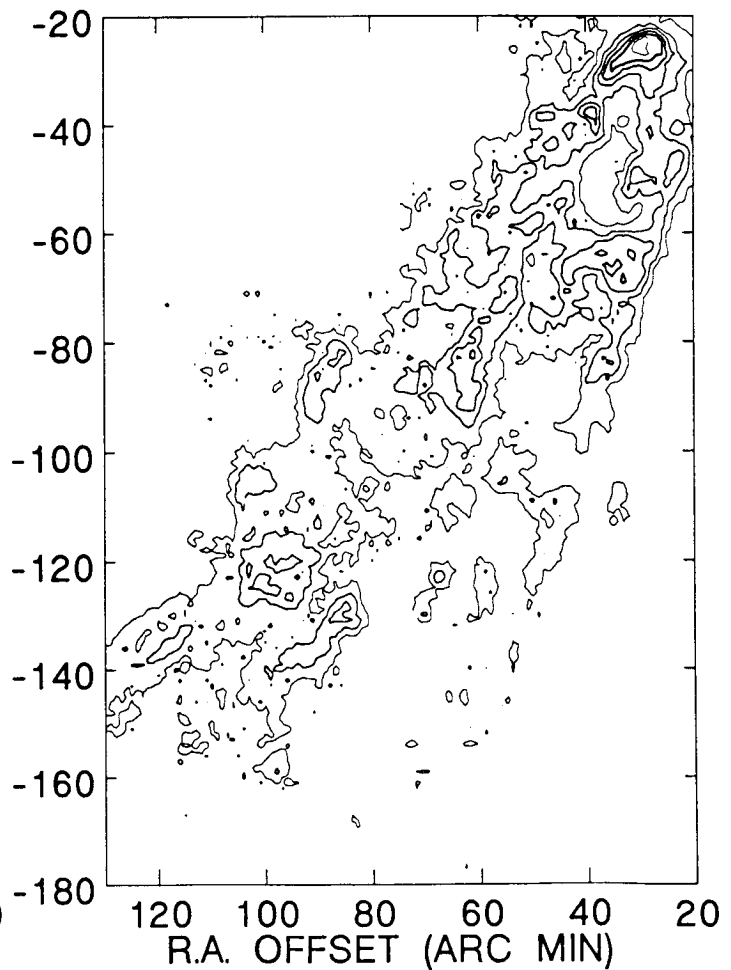
H AND K MAPS OF TWO STAR-FORMING REGIONS: S 140 AND CEP A OB3

Stephen J. Little, Bentley College

G. L. Grasdalen, J. A. Hackwell, and R. D. Gehrz, U. of Wyoming

The molecular clouds near S 140 and Cep A OB3 both contain regions that emit strongly in the infrared but which have relatively little or no emission in radio wavelengths. The lack of radio emission is usually interpreted to mean that little ionization has taken place, and that the IR emission comes from dust heated by a central pre-main sequence object (Blair et al, 1978, Beichman et al, 1979, Hughes and Wouterloot, 1984, among others). We have made high resolution maps of these two areas with H and K broadband filters with the 2.3m telescope of the Wyoming Infrared Observatory (WIRO). Our observations were made with an InSb detector using the standard WIRO mapping technique of multiple scanning to construct a series of 64"x64" pictures. Our scanning was made in one arcsec steps with a 7" aperture to produce a resolution of about 6" FWHM.

S 140

Observations of S 140 by Blair et al (1978) with moderate resolution (32" aperture) in J, H, and K, revealed a prominent IR source that they called S 140IR. We have scanned a 64"x124" box surrounding their S 140IR region and have obtained total IR fluxes which are in close agreement with Blair et al (see Table 1). Figure 1 shows that we

---

TABLE 1: OBSERVATIONS

S 140

	H(Jy)	K(Jy)	H(mag)	K(mag)	(H-K)
Blair et al (1978)	.82	4.26			
Present work:					
all of S 140IR	.78	4.13	7.76	5.46	2.30
Region A	.038	.242	11.05	8.54	2.51
Region B	.056	.266	10.64	8.44	2.20
Region C (central)	.38	2.09	8.54	6.19	2.35

Cep A OB3

	H(Jy)	K(Jy)	H(mag)	K(mag)	(H-K)
Present work:					
Region A	.078	.032	12.77	10.73	2.04
Region B	-	.035	-	10.63	>3
Region C	.069	.068	10.40	9.91	.49
Main Region (central)	.237	2.17	9.09	6.46	2.63

---

have been able to resolve additional detail in S 140IR. Our detail corresponds to that seen by Dinerstein et al (1979) at 0.9μm and Campbell (1986) at 1.0μm. The large (H-K) values for all components of S 140IR indicates that they are probably embedded in the parent molecular cloud with A_v = 25 mag and A_K = 2.2 mag (cf Elias, 1978). The separation of about 10" between components corresponds to approximately 9000 AU for a distance of 910 parsecs. FIR measurements by Harvey et al (1978) show a luminosity of 2×10^4 L_0, most of which is from the central object, but the two smaller sources must have about 1000 L_0 each if the FIR luminosity is apportioned in proportion to the K luminosities.

CEP A OB3

Recent radio studies of Cep A by Hughes and Wouterloot (1984) and FIR studies by Evans et al (1981) have shown the similarity of Cep A to S

140. There is, however, some emission detected from ionized regions by the radio observations, indicating a slightly more advanced stage of evolution for Cep A. We observed a 124"x124" area around the strongest source in Cep A in both H and K, and the K map is displayed in Figure 1. We have identified three sources (A,B, and C) separate from the main source, and information about these sources is shown in Table 1. The low value of (H-K) for source C indicates that it is probably a foreground star, but the remaining regions seem to be equally embedded in the molecular cloud. The main source also seems to show a definite bifurcation into two separate sources, although we have treated it as a single object in our measurements. All the objects can be enclosed in a circle of diameter 30" arc, which corresponds to 20,000 AU (or .1 pc) at a distance of 730 pc. This is small for a star cluster, but large for a binary system, and the fate of this system as it evolves is uncertain. The radio study by Hughes and Wouterloot (1984) is of very high resolution (1") and it shows 14 regions strung in a linear array across almost 60". The FIR luminosity is 2×10^4 L_0 for Cep A. The main source must be a single star or perhaps two stars of about this total luminosity. The fainter members A and B must have luminosities of the order of 150 L_0 if we can apportion the luminosity according to the K luminosity.

REFERENCES

Blair, G. N., Evans, N. J., Vanden Bout, P. A., and Peters, W. L., 1978, Ap. J., 219, 896.

Beichman, C. A., Becklin, E. E., and Wynn-Williams, C. G., 1979, Ap. J., 232, L47.

Campbell, B., 1986, Chapter in "Masers, Molecules, and Mass Outflows in Star-Forming Regions" ed. A. D. Haschick (Haystack Obs.).

Dinerstein, H. L., Lester, D. F., and Rank, D. M., 1979, Ap. J., 227, L41.

Elias, J. H., 1978, Ap. J., 224, 857.

Evans, N. J., et al, 1981, Ap. J., 244, 115.

Harvey, P. M., Campbell, M. F., and Hoffman, W. F., 1978, Ap. J., 219, 891.

Hughes, V. A., and Wouterloot, J. G. A., 1984, Ap. J., 276, 204.
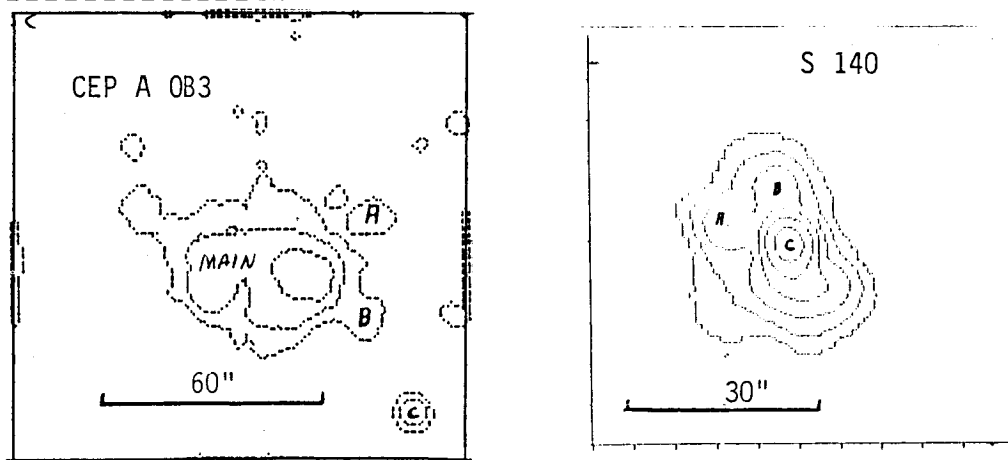
FIGURE 1. Contour plots of the K observations of S 140 and Cep A OB3. The Cep A levels are 200, 800, and 3200 μJy, and the S 140 levels are 100, 200, 400, 800, 1600, and 3200 $\times 10^{-5}$ Jy.

SUBMILLIMETRE MOLECULAR LINE OBSERVATIONS OF M17 - THE INTERACTION OF AN IONISATION FRONT AND MOLECULAR CLOUDS.

Ruth Rainey[1], Glenn J. White[1], Ian Gatley[2], S. S. Hayashi[3], N. Kaifu[3], M. J. Griffin[1], T. S. Monteiro[4], N. J. Cronin[5] and A. Scivetti[1].

1. Queen Mary College, University of London, England.
2. United Kingdom Infrared Telescope, Hawaii.
3. Nobeyama Radio Observatory, Japan.
4. The University, Newcastle-upon-Tyne, England.
5. University of Bath, England.

An area of about 9 by 10 arc minutes in the M17 molecular cloud has been mapped in the J=3-2 transition of CO. The strongest CO emission is observed to come from the two bars to the north and southwest, which lie just outside the areas of ionised gas seen in the radio continuum studies.

We are viewing the boundary between the ionised and molecular gas almost edge on. The most intense CO emission is from the area around the dense molecular cloud core M17SW in the southwest bar. To the east of M17SW there are signs of recent or continuing star formation including H_2O masers and an ultra-compact HII region (Genzel and Downes 1977, White and Macdonald 1979 and Felli, Churchwell and Massi 1984).

The CO J=3-2 spectra observed are complex with considerable variation in line shapes occuring over distances of less than one arc minute. We interpret the velocity structure of this region as arising from an ensemble of molecular cloud fragments in addition to extended emission. We have identified several cloud components at different velocities within both the northern and southwest bars of CO emission. In the northern bar the 23 km s^{-1} cloud reported by Lada (1976) is clearly identified. This lies behind the northern bar observed at radio and optical wavelengths. There is also some spatial correlation between the positions of individual cloud components we have identified and the peaks of H_2 v=1-0 S(1) emission observed by Gatley and Kaifu (1985), from which it appears that some cloud components may consist of post-shock molecular gas.

A simple kinematic model of the cloud components in the southwest bar in which they are considered to be clumps of post-shock gas lying close to the edge of the expanding HII region, with the shock being driven by Kleinmann's star, gives a velocity of $10.8^{+2.8}_{-1.0}$ km s^{-1} for the expansion velocity of the HII region, which is currently at a distance of $2.4^{+0.5}_{-0.6}$ pc from Kleinmann's star. The resulting shock is thought to be preceding the ionisation front and appears to have led to the fragmentation of the original cloud.

References:-
Felli, M., Churchwell, E. and Massi, M. 1984, Astr. Ap., 136, 53.
Gatley, I. and Kaifu, N. 1985, to appear in Proc. IAU Symposium 120.
Genzel, R. and Downes, D. 1977, Astr. Ap. Suppl., 30, 145.
Lada, C. J. 1976, Ap. J. Suppl., 32, 603.
White, G.J. and Macdonald, G. H. 1979, M. N. R. A. S., 188, 745.

Figure 1. Maps of the CO J=3-2 emission integrated in 2 km s^{-1} intervals. The central velocity of the relevant interval is given on each map. The positions at which spectra were obtained are marked with a dot on the 8 km s^{-1} map.
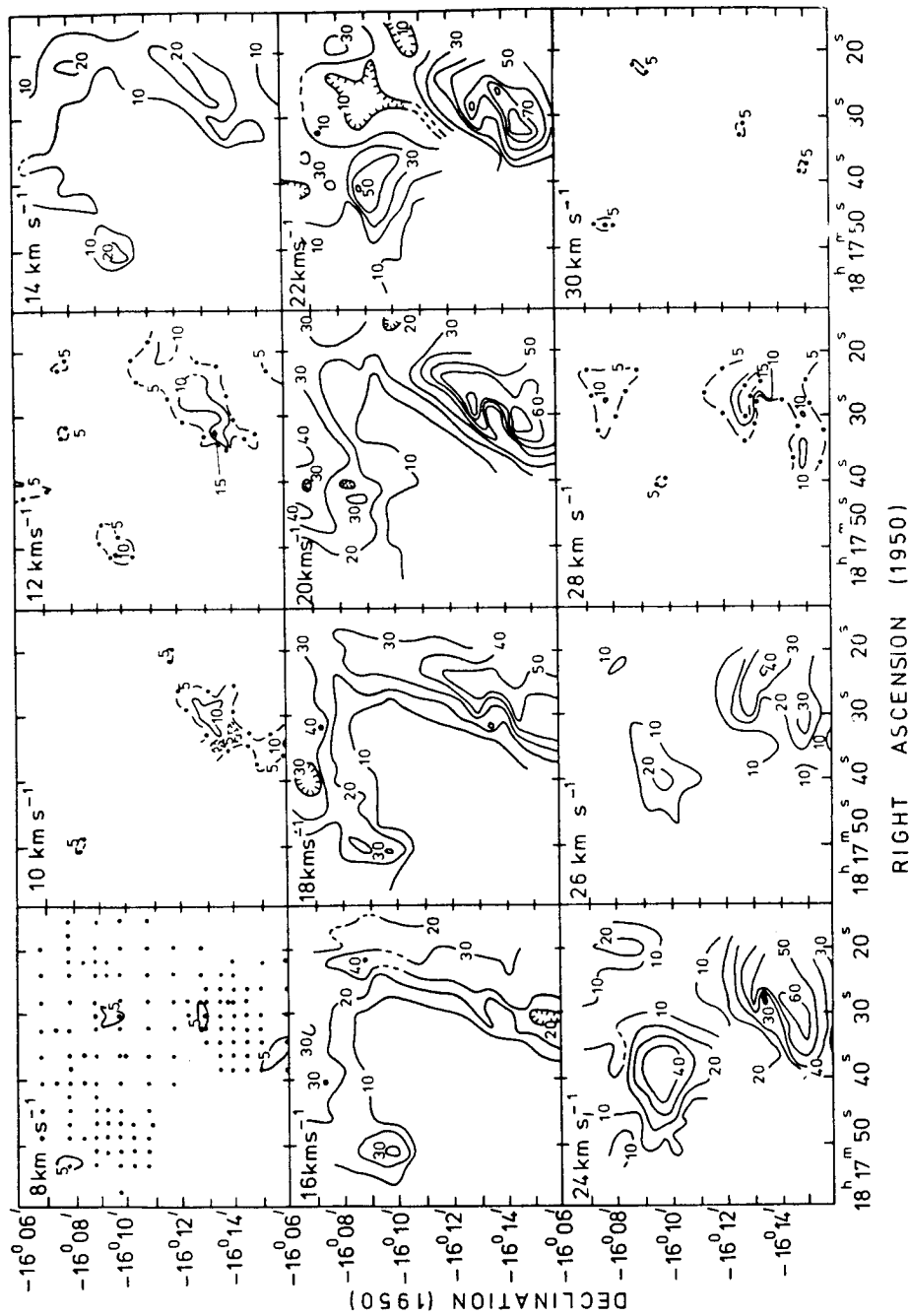
Near-Infrared Observations of IRAS Sources

In and Near Dense Cores

G.A. Fuller (U.C. Berkeley), P.C. Myers (CfA), R.D. Mathieu (CfA),

C.A. Beichman (IPAC), P.J. Benson (Wellesley) and R.E. Schild (CfA)

We report 0.4 to 20 μ m photometry of 27 IRAS point sources associated with dense cores in nearby dark clouds.

It is found that these objects have a bimodal distribution of spectral slopes. The objects in the group with steep spectral slopes (s= $\frac{log(S_\nu(25\mu m)/S_\nu(2.2\mu m))}{log(25/2.2)}$ $\sim$ 2) are typically within one half power radius of the core peak and are not visible on the POSS. The remainder of the objects are typically further from their cores, are optically visible and have shallow spectral slopes (s $\sim$ 0.6). Most of the sources in this group which have been previously identified are T Tauri stars. Both the groups of objects have essentially the same luminosity function with median luminosity of 1 - 2 $L_\odot$, which is similiar to the luminosity function for T Tauri stars.

The near-infrared (J,H,K,L) colors of the objects have been used to estimate the visual extinction to the stars. This indicates that the typical steep spectrum source has extinction A_v $\sim$ 30 magnitudes, which is larger by a factor of 3 to 4 than a uniform core can provide, thus the density must rise steeply in the vicinity of the star. For those objects where optical estimates of the extinction are available the optical estimates are typically smaller than our IR estimates by a factor of 1.6. For multiple scattering by grains that scatter primarily in the forward direction, this implies a grain albedo of ~0.4 at V, consistent with theoretical predictions for bare grains.

Using this derived extinction, the FIR emission from a spherical shell with an inverse power law density which contributes the correct amount of extinction has been modelled. It is shown that to be consistent with both the observations of the density of

the core at a scale of 1.5×10^{17}cm and the extinction derived from the near-IR colors there must be a circumstellar 'hole' of radius 10-100 A.U. for all density laws with exponents greater than 1.2.

It is also shown that a component in addition to the star and circumstellar shell is necessary to match the observed spectrum of steep spectrum sources. The additional component must contribute about 1/3 of the total luminosity of the source and have a sub-stellar temperature. It is suggested that the most likely source of this missing luminosity is a circumstellar disk.

From the number of sources observed in Taurus-Auriga and the number of known optically visible T Tauri stars in the same region, the time a young star remains in the highly obscured stage represented by our steep spectrum sources is estimated. This time is $3 - 8 \times 10^4$ years, which is shorter than the free-fall time for a typical dense core and is comparable to the dynamical time estimated for the CO outflows associated with many of the sources.

The Bird: A Pressure-Confined Explosion in the Interstellar Medium

Adair P. Lane (Boston University)
Antony A. Stark (AT&T Bell Laboratories)
David J. Helfand (Columbia University)

The non-thermal radio continuum source G5.3-1.0, mapped at 20 cm with the VLA by Becker and Helfand (1985, Nature **313**, 115), has an unusual bird-like shape (see figure below). In order to determine possible interaction of this source with adjacent cold gas, we have mapped this region in the J=1-0 line of CO using the AT&T Bell Laboratories 7m antenna and the FCRAO 14m antenna. The map shown below contains 1859 spectra sampled on a 1.5 arcminute grid; each spectrum has an rms noise of 0.2 K in 1 MHz channels. There are several molecular clouds at different velocities along the line of sight. The outer regions of a previously unknown Giant Molecular Cloud at l=4.7°, b=−0.85°, v=200 km s^{-1} appears to be interacting with G5.3-1.0: the molecular cloud has a bird-shaped hole at the position of the continuum source, except that the brightest continuum point (the bird's head) appears to be embedded in the cloud. The velocity of this GMC indicates it is within 2 kpc of the galactic center.

The morphology suggests that a supernova or other explosive event occurred near the outside of the GMC, in a region where $\langle n \rangle \sim 300$ cm^{-3}, and expanded into a region of lower density and pressure. The pressures, densities, and velocity gradients of molecular clouds near the galactic center are on average higher than those of clouds near the Sun. We therefore expect that Type II supernovae near the galactic center would be distorted by their interactions with their parent molecular clouds.
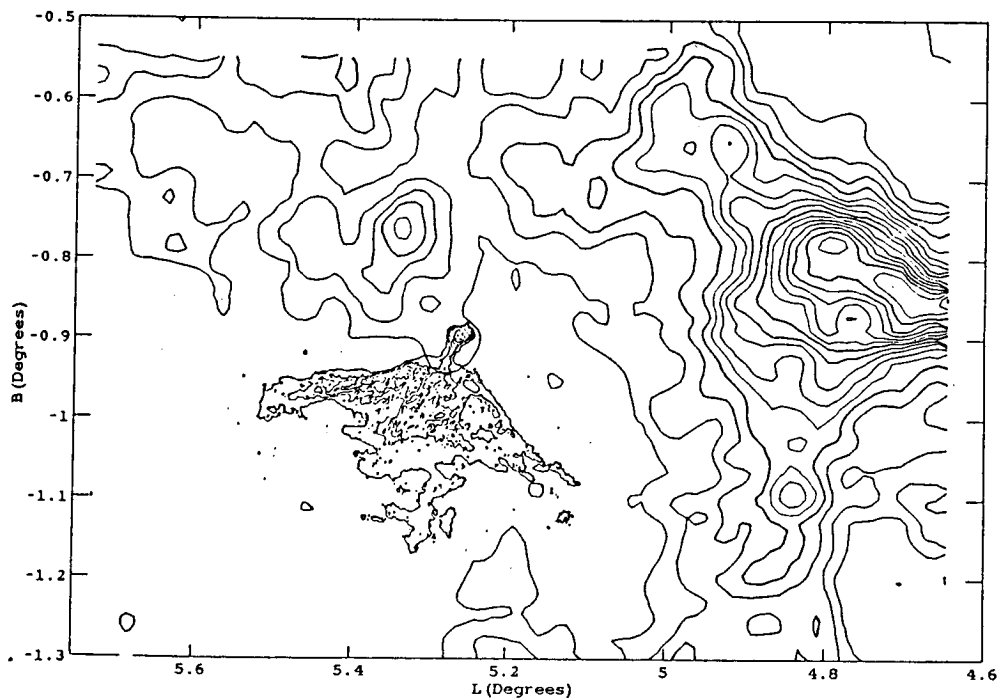
Contours of CO emissivity integrated over the velocity range 180–230 km s^{-1} superposed on the 20 cm VLA map of G5.3-1.0 from Becker and Helfand (1985). CO contours are at intervals of 20 K-km s^{-1}.

Mark G. Wolfire – NASA/Ames and Joseph P. Cassinelli – U. of Wisc.–Madison

Observational evidence suggests that stars greater than 100 $M_\odot$ exist in the Galaxy and LMC (Humphreys and Mc Elroy 1984, De Jager 1980), however classical star formation theory (Larson and Starrfield 1971, Kahn 1974) predict stellar mass limits of only $\sim$60 $M_\odot$. A protostellar accretion flow consists of inflowing gas and dust. Grains are destroyed as they near the central protostar creating a dust shell or cocoon. Radiation pressure acting on the grains can halt the inflow of material thereby limiting the amount of mass accumulated by the protostar. We first consider rather general constraints on the initial grain to gas ratio and mass accretion rates that permit inflow. We further constrain these results by constructing a numerical model. Radiative deceleration of grains and grain destruction prcesses are explicitly accounted for in an iterative solution of the radiation-hydrodynamic equations.

At the outer boundary grains see the infrared field emitted by warmer grains in the shell's interior. The outward radiative force must be less than the inward gravitational force

$$\Gamma = \left| \frac{\text{radiation}}{\text{gravity}} \right| = \frac{k_F L / 4\pi r^2 c}{GM/r^2} < 1 \tag{1}$$

where k_F is the flux mean of the dust opacity. We here approximate k_F by $k_B(T_{\text{rad}})$, the Planck mean of the radiation pressure coefficient, where T_{rad} is some characteristic temperature of the incident radiation field. The maximum of T_{rad} has been chosen to be 2000 °K since we believe that grains at the cocoon's inner edge will be destroyed before they can be heated to such a temperature. The opacity is calculated using an assumed grain model. As a standard we use the Mathis, Rumpl, Nordsieck (1977) (MRN) grain model which consists of graphite and silicate grains ranging in size between $a_- = 0.005~\mu m$ and $a_+ = 0.25~\mu m$ and is distributed in size as $a^{-3.5}$. Since the wavelength of the incident infrared light is generally larger than the grain size, the dominant source of opacity comes from the larger grains where most of the mass resides. We find infall onto a 100 $M_\odot$ core is allowed, for a wide range in T_{rad}, if the total grain number abundance is reduced by a factor of 4 relative to the standard MRN grain model and graphite grains larger than 0.2 times the MRN maximum size grains are depleted.

At the shell's inner edge, the outward radiation pressure must be less than the dynamic pressure of infalling material. If all of the stellar radiation field is absorbed in a thin region at the inner edge of the dust shell, r_1, then it is necessary that

$$\left| \frac{\text{radiation \quad pressure}}{\text{dynamic \quad pressure}} \right| = \frac{L/c}{\dot{M} v_{ff}(r_1)} < 1 \tag{2}$$

where $\dot{M}$ is the mass accretion rate and $v_{ff}(r_1)$ is the free-fall velocity at r_1. We estimate the dust destruction radius by equating radiative heating by the central star to radiative cooling at the grain sublimation temperature. We use the largest graphite grain size that satisfies the outer boundary condition, $a_+ = 0.05\mu$m, and assume here $T_{sub} = 1800$ °K. Since the free-fall velocity is the largest possible inflow velocity we get an estimate of the minimum rate of mass inflow necessary for accretion to continue. We find that inflow onto a 100 $M_\odot$ core requires a mass accretion rate of $> 10^{-3}$ $M_\odot$ yr^{-1}.

Proper estimates of limits on $\dot{M}$ and initial grain conditions require us to account for the deceleration of the flow between shell boundaries due to radiation pressure and to calculate grain destruction processes acting in the inflow. Processes of sublimation and vaporization by grain-grain collisions is considered for graphite and silicates plus surface reactions for graphites. We use the method of Wolfire and Cassinelli (1986) to calculate the grain temperatures and radiation field throughout the accretion flow. The rate of destruction depends on the grain composition, size, temperature, and inflow speed, therefore different grains are destroyed at different radial distances.

Accretion onto a 100 $M_\odot$ core was maintained for $\dot{M} = 5 \times 10^{-3}$ and a grain to gas ratio of 1/8 the standard Galactic value. This is a higher mass inflow and lower grain abundance than that estimated by the simple boundary conditions. The additional constraints are a result mainly of the deceleration of the inflow from the infrared radiation emitted by grains near the shell's inner edge that was not accounted for in the boundary conditions.

Silicate grains are destroyed by sublimation. About half of the mass of graphite grains are removed by surface reactions and half by sublimation. Vaporization by grain-grain collisions are found to be negligible.

These findings seem to suggest that star formation by spherical accretion requires rather extreme preconditioning of the grain and gas environment.

References

Humphreys, R. M. , and Mc Elroy, D. B. 1984, *Ap. J.*, **284**, 565.

De Jager, C. 1980, *The Brightest Stars*, (Dordrecht: D. Reidel).

Kahn, F D. 1974, *Astr. Ap.* , **37**, 149.

Larson, R. B. , and Starrfield, S. 1971, *Astr. Ap.* , **13**, 190.

Mathis, J. S. , Rumpl, W. , Nordsieck, K. H. 1977, *Ap. J.* , **217**, 425 (MRN).

Wolfire, M. G. and Cassinelli, J. P. 1986, to be published in Nov. 1 *Ap. J.*.

LOWER MASS LIMIT OF AN EVOLVING INTERSTELLAR CLOUD AND CHEMISTRY IN AN EVOLVING OSCILLATORY CLOUD

S.P. Tarafdar

Tata Institute of Fundamental Research
Homi Bhabha Road, Bombay 400 005
India

ABSTRACT

Simultaneous solution of equation of motion, equation of state and energy equation including heating and cooling processes for interstellar medium gives for a collapsing cloud a lower mass limit which is significantly smaller than the Jeans mass for the same initial density. The clouds with higher mass than this limiting mass collapses whereas clouds with smaller than critical mass passes through a maximum central density giving apparently similar clouds (i.e. same Av, size and central density) at two different phases of its evolution (i.e. with different life time). Preliminary results of chemistry in such an evolving oscillatory cloud show significant difference in abundances of some of the molecules in two physically similar clouds but with different life time. The problems of depletion and short life time of evolving clouds appear to be less severe in such an oscillatory cloud.

JEANS CRITERION IN A TURBULENT MEDIUM

Bonazzola S.[1], Falgarone E.[1,2], Heyvaerts J.[1], Pérault M.[1,2], Puget J.L.[1,2]

[1] Observatoire de Paris-Meudon, France
[2] Ecole Normale Supérieure, Paris, France

According to the classical Jeans analysis, all the molecular clouds of mass larger than a few $100 M_\odot$, size larger than about $1 pc$ and kinetic temperature $T_k < 30 K$ are gravitationally unstable.

We have shown that in clouds supported by internal supersonic motions, local gravitational instabilities may appear within molecular clouds which are globally stable.

The argument is threefold: i) when the turbulent kinetic energy is included into the internal energy term, the virial equilibrium condition shows that molecular clouds such as those observed, which are gravitationally unstable according to the Jeans criterion, are indeed globally stable if supported by a turbulent velocity field of power spectrum steeper than 3,

ii) $2D$ compressible hydrodynamical simulations show that a supersonic turbulent velocity field generates a turbulent pressure within clouds, the gradients of which stabilize the unstable scales (i.e. the largest scales and the cloud itself) against gravitational collapse,

iii) an analysis similar to the Jeans approach but including the turbulent pressure gradient term, gives basically the same results as those given in i).

Clouds of mean density lower than a critical value are found to be stable even though more massive than their Jeans mass. In clouds of mean density larger than that critical value, the gravitational instability appears only over a range of scales smaller than the cloud size, the largest scales being stable.

In practice, the observed mean densities are lower than this critical value: the observation of a small number of cores and stars of a few solar masses embedded in clouds of several hundred solar masses can only be understood in terms of small scale density fluctuations of large amplitude generated by the supersonic turbulence which would occasionally overtake the limit of gravitational stability.

This work has been submitted to Astronomy and Astrophysics.

SPECTRAL EVOLUTION OF YOUNG STELLAR OBJECTS

FRED C. ADAMS

U. C. Berkeley, Berkeley, CA 94720

We suggest an evolutionary sequence, from protostars to pre-main-sequence stars, for the classification of young stellar objects. This sequence is derived by comparing the predictions of the theoretical models of Adams and Shu with the morphological classification scheme of Lada and Wilking. We first define the spectral index in the near- and mid-infrared, $n \equiv d\log(\nu F_\nu)/d\log\nu$, and then interpret the class of sources with negative spectral indices as protostars. The inferred mass infall rates for these objects are generally consistent with the measured gas temperatures of ~ 35 K in Ophiuchus, and of ~ 10 K in Taurus. Fitting the data requires us to adopt cloud rotation rates in Ophiuchus which are typically an order of magnitude greater than in Taurus, and we speculate on the mechanistic origin for this difference. Next, we consider a subclass of T Tauri stars with near- and mid-infrared excesses and positive or zero spectral indices. We find that the objects with the steeper indices can be understood as the post-infall products from the collapse of rotating cloud cores, where the infrared excesses arise from the simple reprocessing of visible stellar photons in optically thick but spatially thin disks. The sources with flatter spectra may require massive accretion disks. Given the existence of protostars and naked star/disk systems, there is a natural interpretation of another subclass of T Tauri stars, those with two peaks in their emergent spectral energy distributions. These are readily explained as intermediate cases in which dust envelopes, optically thin in the infrared, still surround the stars and disks, perhaps because of residual infall. Finally, we find that the theory can be extended to explain the spectral energy distribution of FU Orionis, a famous outburst source. Our model suggests that FU Orionis has a disk, but it offers no discrimination between the competing ideas that the outburst took place on the star or in the disk.

Supershells and Propagating Star Formation

M.-M. Mac Low, R. McCray (Univ. Colo. - JILA),
and M. Kafatos (George Mason U.)

Correlated supernovae from an OB association can carve large cavities (>100 pc) in the ISM, and can punch holes completely through the disk of a spiral galaxy. SNR energy within such a cavity is thermalized before the shock reaches the supershell. Thus stellar wind theory may be used to model these superbubbles. We describe how the evolution of the superbubble depends on the density distribution of the galactic disk gas and the rate of supernovae in the OB association. At a radius of 100 - 300 pc, the supershell becomes gravitationally unstable, forming giant molecular clouds which are the sites for new star formation. This gravitational instability of the supershells provides a physical mechanism for propagating star formation and may account for the observation of bursts of star formation in galaxies.

SIZE-DENSITY RELATIONS IN DARK CLOUDS: NON-LTE EFFECTS

Philip Maloney

Dept. of Planetary Sciences, University of Arizona

One of the major goals of molecular astronomy has been to understand the physics and dynamics of dense interstellar clouds. Because the interpretation of observations of giant molecular clouds is complicated by their very complex structure and the dynamical effects of star formation, a number of studies have concentrated on dark clouds (Martin and Barrett 1978; Myers and Benson 1983; Arquilla and Goldsmith 1985). Leung, Kutner and Mead (1982) (hereafter LKM) and Myers (1983), in studies of CO and NH_3 emission, concluded that dark clouds exhibit significant correlations between linewidth and cloud radius of the form $\Delta v \propto R^{0.5}$ and between mean density and radius of the form $n \propto R^{-1}$, as originally suggested by Larson (1981). This result suggests that these objects are in virial equilibrium. However, the mean densities inferred from the CO data of LKM are based on an LTE analysis of their ^{13}CO data. At the very low mean densities inferred by LKM for the larger clouds in their sample, the assumption of LTE becomes very questionable. As most of the range in R in the density-size correlation comes from the clouds observed in CO, it seems worthwhile to examine how non-LTE effects will influence the derived densities.

The basis of the LTE analysis is the assumption that the excitation temperatures of the ^{12}CO and ^{13}CO J=1-0 transitions are identical. Then the difference in observed antenna temperatures T_R^* is due solely to the smaller optical depth of the ^{13}CO transition. The optical depth is then converted to a column density. To obtain mean densities, LKM used their LTE column densities to obtain cloud masses M, then defined the mean density as the volume-averaged density of a sphere of radius R and mass M.

For clouds with constant power-law density profiles of the form $n(r)=n_0(r/r_0)^\alpha$ the volume-averaged density depends only on the density at the cloud boundary, and for a fixed boundary density is independent of n_0 and r_0. Clouds which are not strongly centrally condensed will have densities which are everywhere similar to the mean density, while clouds with steep profiles may have central densities one or two orders of magnitude higher than the mean. For unresolved clouds, the mean density probably is an appropriate parameter to use in considering the excitation.

One way to assess the validity of LTE-derived densities is to construct cloud models and then to interpret them in the same way as the observed data. Figure 1 shows a plot of $n(H_2)$ versus cloud radius for homogeneous models of the dark clouds in the sample studied by LKM. The level populations were obtained assuming statistical equilibrium, using the Sobolev approximation for the radiative transfer. The kinetic temperature was derived by assuming that the ^{12}CO J=1-0 transition is thermalized in all the clouds. No correction has been made for the coupling between the beam and the source. The dark line is a least-squares best fit to the model density-radius relation; the slope is -0.51. This is considerably shallower than the slope of -1.3 derived by Myers using the data of LKM. The shallower slope is a direct result of non-LTE conditions in the cloud models: higher densities are required to increase the optical depth to compensate for the sub-thermal excitation of the ^{13}CO J=1-0 line. Microturbulent models of inhomogeneous clouds of varying central concentration with the linewidth-size and mean density-size relations found by Myers also show sub-thermal excitation of the ^{13}CO line in the larger clouds, with the result that LTE analysis considerably underestimates the actual column density.

A more general approach which doesn't require detailed modeling of the clouds is to consider whether the observed $T_R^*(^{13}CO)/T_R^*(^{12}CO)$ ratios in the clouds studied by LKM are in the range where the LTE-derived optical depths (and hence column densities) can be seriously in error due to sub-thermal excitation of the ^{13}CO molecule. Figure 2 shows the ratio of $T_R^*(^{13}CO)/T_R^*(^{12}CO)$ for the 1-0 transition as a function of ^{13}CO optical depth for varying values of the ratio of excitation temperatures of the two transitions, for $T_{EX}(^{12}CO) = 10$ K. The curves are labeled

with $T_{EX}(^{13}CO)/T_{EX}(^{12}CO)$. The ratio of antenna temperatures from LKM are in the range 0.2 - 0.8. It is clear from the figure that errors of ≈ an order of magnitude can be made by assuming LTE in situations where it is not appropriate.

The shallower relation between mean density and cloud size inferred from the non-LTE analysis has important implications for the structure and stability of dark clouds. In particular, the conclusion that they are in virial equilibrium may be incorrect. The mean densities in the larger clouds may be high enough to make them unstable to collapse.

REFERENCES

Arquilla, R., and Goldsmith, R.F. 1985, Ap. J. 294, 436.
Larson, R.B. 1981, M.N.R.A.S., 194, 809.
Leung, C.M., Kutner, M.L., and Mead, K.N. 1982, Ap. J., 262, 583 (LKM).
Martin, R.M., and Barrett, A.H. 1978, Ap. J. Suppl., 36, 1.
Myers, P.C., and Benson, P.J. 1983, Ap. J., 266, 309(MB).
Myers, P.C. 1983, Ap. J., 270, 105.

MODELS OF LKM DARK CLOUDS: DENSITY-SIZE RELATION
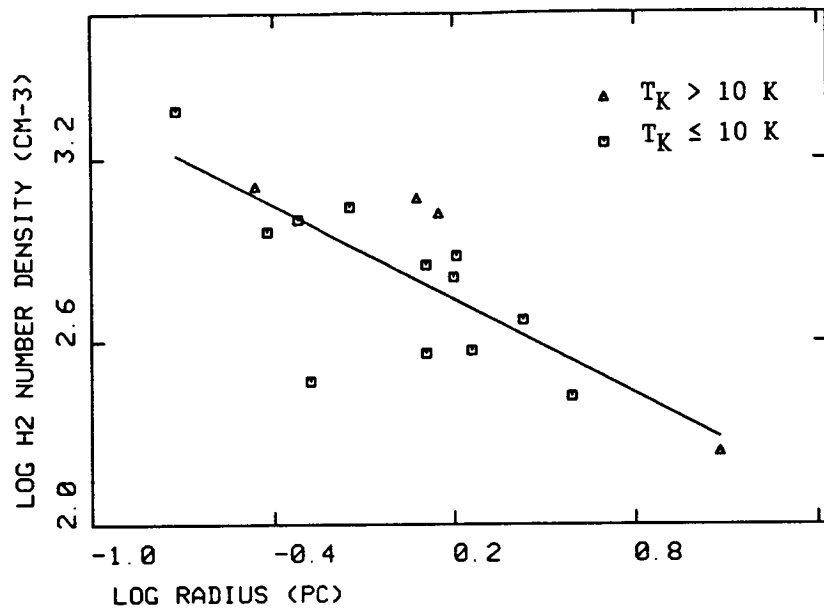
Figure 1.

Figure 2.
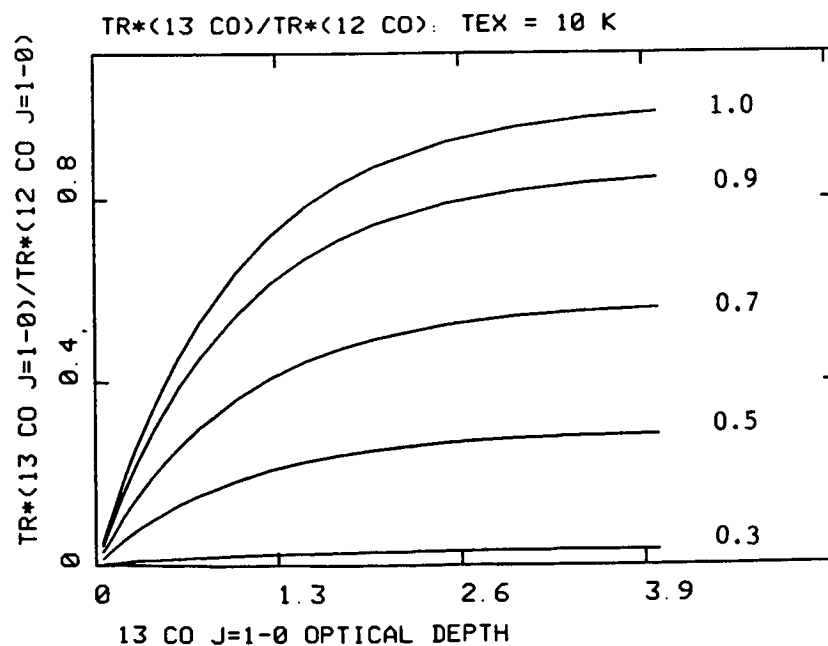
I. LOCAL STRUCTURE AND KINEMATICS OF ISM

B. HII Regions and Reflection Nebulae

THE UNSTABLE O6.5f?p STAR HD 148937 AND ITS INTERSTELLAR ENVIRONMENT

Claus Leitherer and Carlos Chavarria-K.
Landessternwarte Königstuhl
D-6900 Heidelberg
Germany

The massive, early-type star HD 148937 (spectral type O6.5?p) is surrounded by a unique set of nebulosities. A spherically symmetric Strömgren sphere (Radius $\simeq$ 25 pc), an ellipsoidal filamentary nebulosity (semimajor axis $\simeq$ 5 pc) interpreted as a stellar-wind-blown shell, and a bipolar nebular complex (semimajor axis $\simeq$ 1 pc) with HD 148937 located in the apparent center of symmetry. Here we report on observations of these nebulosities (narrow-band CCD imaging, IDS spectrophotometry, high resolution ($\Delta V \simeq$ 7 km sec^{-1}) spectroscopy) in an attempt to establish a consistent model of HD 148937 and its nebulosities.

The two bipolar nebulosities (known as NGC 6164/5 show striking resemblance. They are of similar extent and distance from HD 148937 implying a simultaneous origin due to an explosive event in HD 148937. A comparison of H_α- and H_β-images and IDS fluxes gives a rather homogeneous dust distribution all over the bipolar nebula with an extinction in agreement with E(B-V) of HD 148937. We conclude that the apparent morphology of NGC 6164/5 is not simulated by variable extinction but rather reflects the actual distribution of (excited) gas. Moreover, it is safe to assume that the distribution of H_α emission is identical with the total amount of gas in the inner nebulosities (i. e. NGC 6164/5 is density-bounded). The output of Lyman quanta of HD 148937 (log $N_L \simeq$ 49.15 sec^{-1}) even suffices to keep ionized the stellar-wind-blown shell and the Strömgren sphere. The ratio [O III]/H_β drastically decreases with increasing distance from HD 148937. This behavior is paralleled by a corresponding increase of [N II]/H_α indicating the transition from the high-ionization zone to the low-ionization zone. We stress the similarity to the structure of ejecta from novae (see Gallagher and Anderson 1976).

In establishing a geometrical model for the bipolar nebula we are led by its striking resemblance to ejecta from novae or symbiotic stars (e. g. Solf 1983). The high rotational velocity of HD 148937 ($v \cdot \sin i$ = 200 km sec^{-1}, Conti and Ebbets 1977) strongly implies axial symmetry for the system and thus giving rise to the ejection of matter preferentially along the two axes of symmetry. The detailed kinematic structure is derived from our highly-resolved line profiles. We find a double-cone structure nearly perpendicular to the line of sight with a kinematic age of 10^3 - 10^4 yr. The ejection of the nebulosities may be due to instabilities in this star close to the Of-WR transition phase. The high rotational velocity may play a crucial role in these instabilities.

The influence of rotation on the stellar wind of HD 148937 and the resulting non-isotropic mass flow could also account for the oval-shaped structure of the wind-blown shell. We underline that the spectral appearance of this shell is typical of wind-blown shells from e. g. WR-stars and clearly excludes an origin as due to a SN explosion.

The age of the bubble as determined from the luminosity of the wind is a few times 10^5 yr.

Since NGC 6164/5 is clearly ejected by the star and expands into space with virtually no contamination by ISM (the density in the stellar-wind cavity is $\sim 10^{-2}$ cm^{-3}) it provides the unique possibility of studying the chemical abundances of an evolved Of star. Our physical analysis gives an electron density of $1 \cdot 10^4$ cm^{-3} for NGC 6164 and $7 \cdot 10^3$ cm^{-3} for NGC 6165, respectively. The electron temperature is 6700 K. In these respects the nebulosities closely resemble normal H II regions. We find no evidence for shock excitation in the lines. The abundance analysis is treated in the usual way following Peimbert and Costero (1969). We find an overabundance of nitrogen relative to hydrogen by a factor of 6 relative to the sun for NGC 6164/5. On the other hand, the outer border of the Strömgren sphere (NGC 6188) shows abundances typical of normal H II regions. An overabundance of N by a factor of 6 is in good agreement with theoretical evolutionary modelling of stellar abundances by Maeder (1983). This provides strong support for the evolutionary state of Of stars as being intermediate between O- and WR-stars.

References:

Conti, P. S., Ebbets, D.: 1977, Astrophys. J. 213, 438
Gallagher, J. S., Anderson, C. M.: 1976, Astrophys. J. 203, 625
Maeder, A.: 1983, Astron. Astrophys. 120, 113
Peimbert, M., Costero, R.: 1969, Bol. Obs. Ton. Tac. 5, 3
Solf, J.: 1983, Astrophys. J. Lett. 266, L 113

TURBULENCE IN HII REGIONS

C. R. O'Dell
Rice University, Houston, Texas

It has been known for many decades that the Reynolds number in HII regions must be very high and that the corresponding fine scale flow must be turbulent. Even though the theoretical relation between turbulent element separation and random velocity ($v \sim r^{1/3}$) was derived by Kolmogoroff over forty years ago, there have been only a few attempts to test this theory and its corresponding assumptions. An attempt by Münch for M42 with marginal velocity resolution lead to ambiguous results, although more recent studies by Jean René Roy and his colleagues have been more credible. My collaborators and I have been systematically studying the internal velocities of a number of HII regions and are now able to test the theory with considerable certainty. The results should be important for the determination of the energy balance of HII regions and the relation of small scale motion to the process of star formation.

Our observations were made with two spectrograph systems. Detailed spectral maps of the entire nebulae were made in the $H\alpha$ line of NGC 7000 (□) NGC 1499 (o), and S252 (Δ) at an angular resolution of a few arcminutes using an echelle spectrograph, giving velocities accurate to a few km s^{-1}. The higher resolution coude feed system at K.P.N.O. was used to map the inner regions of NGC 6514 (T) and NGC 6523 in the intrinsically narrower [OIII] N1 line to an accuracy of about one km s^{-1} and an angular resolution of a few arcseconds. The data were analyzed by numerically fitting the digitized line profiles to Gaussian line profiles. This could be done for single or multiple line components, all of the above cited nebulae being single except for NGC 6523, which had two velocity systems (A and B). The resulting data for each spectral element was the radial velocity (V), the Full Width at Half Maximum (FWHM), and the intensity of each line. The resulting values are a unique data set of nebular velocities with accurately determined instrumental line widths and dispersions made over a wide dynamic range.

The data were analyzed using statistical methods. The first of these was to determine the r.m.s. dispersion of velocities in samples across the face of each nebula. The average dispersion was determined for that sample size (D) and from that, the most probably turbulent velocity (W). This process was then repeated for a larger sample size, until the entire area mapped was enclosed by a single sample. In its simplest form, where there is no averaging of velocity elements along a line of sight and optical depth effects are unimportant, Kolmogoroff theory would predict $W \sim D^{1/3}$. The results for the several nebulae are shown in the first figure, where a reference line of slope 1/3 is shown. The second method of analysis was to determine the structure function (B), which is $B(r) = \langle |V(r') - V(r'')|^2 \rangle$ where r is the distance between two points on the face of the HII region. Since B is calculated for all possible combinations of data points at each distance of separation, it gives a much more critical determination of the dependence of random motion upon velocity. The results for the structure function are shown in the second figure. The simplest model for the theory predicts that $B \sim r^{2/3}$ and a reference line of slope 2/3 is shown. Where error bars are not shown in either figure it means that the error was less than the symbol size.
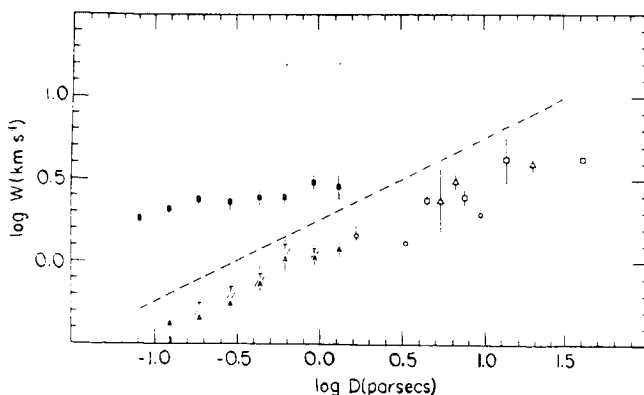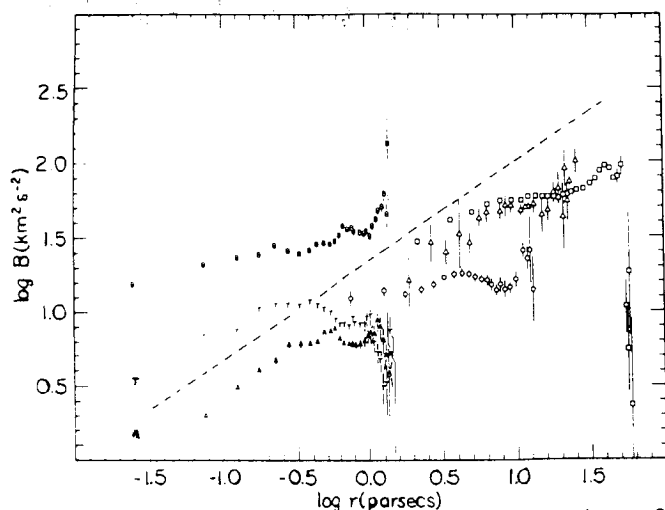
The vertical displacement of W and B for various nebulae is what is expected, as the absolute scale of the dispersion of velocities should depend upon the rate at which energy is fed into the system. If the ultimate source of this energy is photoionization, then W should scale as the 1/3 power of the local gas density, so that object to object variations in absolute scale are to be expected.

The slope in all objects does not agree with the expectations of the simplest theories except over only very small portions. In general it is always flatter. A deviation in this direction is difficult to explain, as the effects of compressibility and non-turbulent motion would both produce slopes that are much steeper than the reference values. The most realistic models for HII regions are those of von Hoerner (1951), who predicted FWHM and B for several realistic models. Again, the predicted slope for B was always greater than or equal to 2/3. Another important discrepancy is that the rate of increase of W is such that including the entire HII region would still not reach a velocity sufficient to explain the FWHM, a result similar to that drawn by Münch (1958) for M42. The only published idea for a flat slope is that of Fleck (1983) who argues that such a slope would result from the source of energy entering through the smallest scale velocity elements, rather than the largest, as commonly assumed.

More complete presentations of this work appear in a recent publication (O'Dell 1986a) or papers in press (O'Dell 1986b, O'Dell et al. 1986).

Fleck, R. C., Jr. 1983, Ap. J., 272, 645.

Münch , G. 1958, Rev. Mod. Phys., 30, 1035.

O'Dell, C. R. 1986a, Ap. J., 304, 767.

_____1986b, P.A.S.P., in press.

von Hoerner, S. 1951, Zeitschrift. für Astrophysik, 30, 17.

CO NEAR THE PLEIADES: ENCOUNTER OF A STAR CLUSTER WITH A SMALL MOLECULAR CLOUD

John Bally

AT&T Bell Laboratories, Crawford Hill, Holmdel, N.J.

and

Richard E. White

Five College Astronomy Department, Smith College, Northampton, MA.

Although there is a large amount of interstellar matter near the Pleiades star cluster, the observed dust and gas is not a remnant of the placental molecular cloud from which the star cluster was formed. Carbon monoxide (CO) associated with the visible reflection nebulae was discovered by Cohen (1975). Its radial velocity ($V_{LSR}=+10$ km s^{-1}) differs from that of the cluster ($V_{LSR}=-4$ km s^{-1}) by many times the cluster escape velocity, which implies that the cloud-cluster association is the result of a chance encounter. This circumstance and the proximity of the Pleiades to the sun creates an unique opportunity for study of interstellar processes at high spatial resolution. (At 125 pc, 1' corresponds to 0.036 pc.)

To study the molecular component of the gas, we mapped a 1.7 square degree field with the AT&T Bell Laboratories 7-meter antenna (1.7' beam) on a 1' grid in the J=1-0 ^{12}CO line, obtaining over 6,000 spectra with 50 kHz (0.13 km s^{-1}) resolution. The cloud core was mapped in the J=1-0 line of ^{13}CO. Further observations include an unsuccessful search for CS (J=2-1) at AT&T BL, and some ^{12}CO J=2-1 spectra obtained at the Millimeter Wave Observatory of the University of Texas.

Figure 1 shows a contour map of the ^{12}CO emission and the location of the 17 brightest cluster stars. Distinctive features of the Pleiades molecular cloud include the following.

1. The Pleiades molecular cloud resembles the small clouds detected at large galactic latitudes. There is no evidence for any ongoing star formation. The statistics of Magnani, Lada, and Blitz (1986) imply an *a posteriori* probability of order 10^{-3} for the observed encounter between the CO cloud and the cluster.

2. The cloud has a warm (T = 30 K), dense ($n_{H_2} \approx 1 \times 10^4$ cm^{-3}) core a few tenths of a parsec in diameter, containing 10 M$_\odot$ of gas. The total cloud mass is about 20 M$_\odot$. The absence of detectable CS emission from such a dense core suggests that self-shielding of CS against ultraviolet radiation is negligible .

3. The portion of the cloud nearest to the bright cluster stars η Tau (B8 III, 2600 L$_\odot$ at a projected separation of 30' or 1 pc from the cloud core) and 23 Tau (Merope, B6 IV, 1100 L$_\odot$, 15,' or 0.5 pc) exhibits a precipitous edge in its CO brightness, suggesting a dissociation front. The CO "cliff" coincides spatially with visible reflection nebulosity and the far infrared peak observed by IRAS.

4. The molecular cloud has a "wind-swept" or cometary morphology. The CO radial velocities and the "wings" located on either side of the cloud core suggests that the low density portions of the cloud have been decelerated as they approach the cluster. Possible acceleration mechanisms include ram pressure of a low density heated ambient medium, radiation pressure, and the rocket effect on the cloud created by the ablation of heated gas escaping from the cloud surface.

5. The wing of the cloud near 17 Tau (B6 III, 1600 $L_\odot$, 30' or 1 pc from the cloud core) clearly shows a bay in the CO emission contours, indicating the importance of photodissociation on the CO morphology.

6. The "tail" of the cloud presents a complex array of clumps and filaments. The clumps have radial velocities ranging from 7.5 to 10.5 km s^{-1} and masses less than 1 $M_\odot$. Clumps at the same velocity frequently lie along lines which point to the luminous stars, suggesting that mutual shielding by the clumps from the dissociating radiation effects the spatial structure of the molecular gas in the cloud tail.

References

Magnani, L., Lada, E. A., and Blitz, L. 1986, *Ap. J.*, *301*, 395.

Cohen, R. S. 1975, unpublished.

Figure 1: An ^{12}CO map showing the molecular cloud near the Pleiades. The contours show the antenna temperature (corrected to above the atmosphere) integrated from $V_{LSR}=7$kms to $V_{LSR}=12$km s^{-1}. Contour intervals are in steps of 1 Kkm s^{-1}. The positions of several of the brighter members of the Pleiades star cluster are indicated in the map. The (0,0) co-ordinates are $\alpha(1950)=03^h43^m21^s$ and $\delta(1950)=23°\,27'\,00''$.

CO NEAR THE PLEIADES
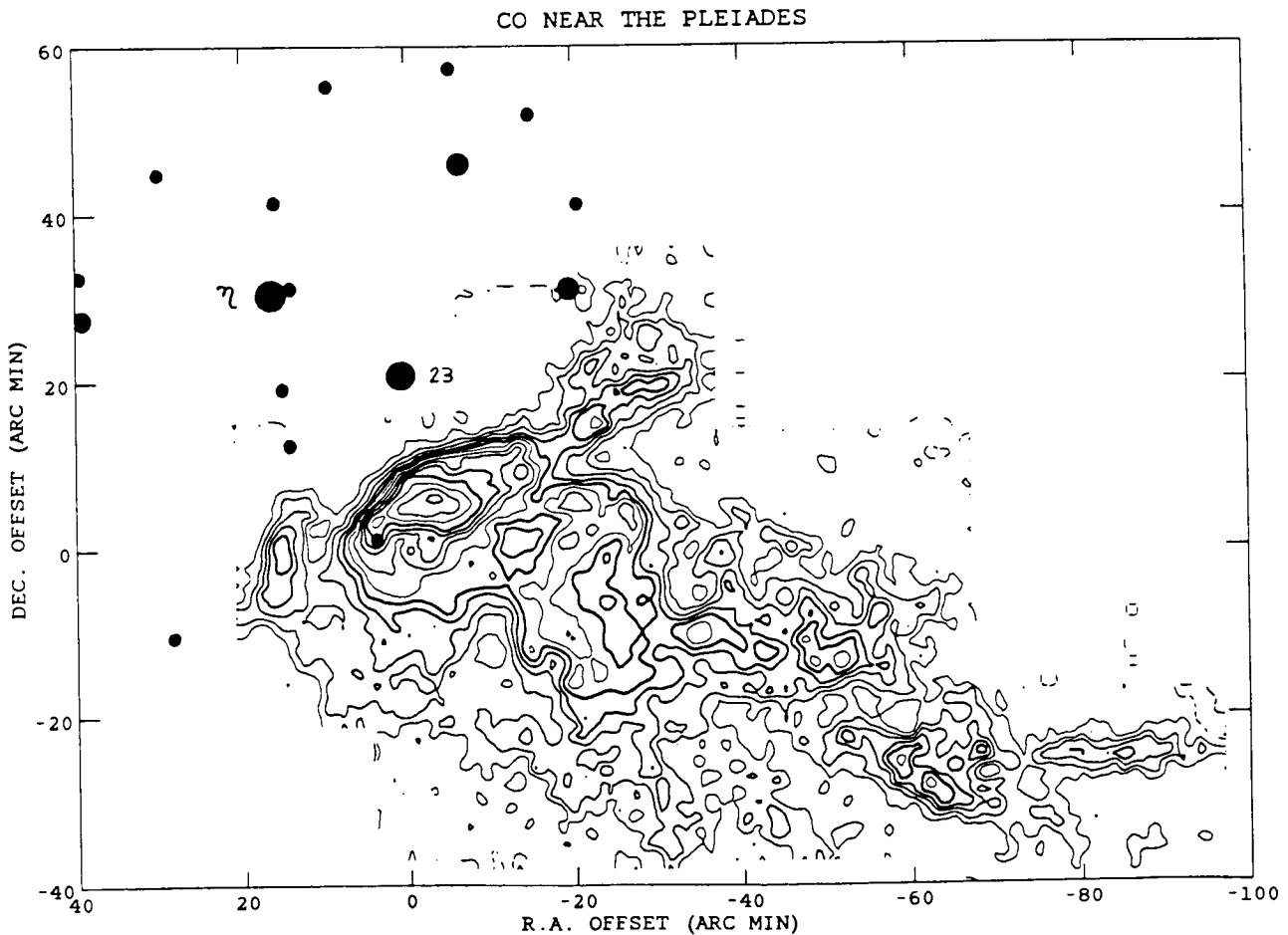
OPTICAL OBSERVATIONS OF VERY LOW IONIZATION H II REGIONS IN THE LARGE MAGELLANIC CLOUD

Miriam Peña
Instituto de Astronomía,
Universidad Nacional Autónoma de México

and

María T. Ruiz and Mónica Rubio
Departamento de Astronomía
Universidad de Chile

ABSTRACT

Several very low ionization isolated HII regions have been detected on a prism-objective plate of the Large Magellanic Cloud. Most of the objects show a very weak [OIII]λ5007 emission line and, on the other hand the [OII]λ3727 and [NII]λ6584 doublets are very intense. This kind of objects seem to be ideal in order to determine accurate N and O abundances, avoiding the use of large ionization correction factors in the N abundance determination.

Spectrophotometric observations of these regions have been carried out with the 4 m telescope and the 2-D Frutti spectrograph at Cerro Tololo, and with the 1.52 m and the Image Dissector Scanner (IDS) at La Silla, ESO. The wavelength range $\lambda\lambda$3700 - 7000 A was covered Calibrated fluxes of the emission lines detected have been measured, and from these data preliminar results of physical conditions of the gas as well as some ionic abundances have been derived.

Comparisons of the observations with ionization structure models show that the effective temperatures of the ionizing stars are less than 35 000 K.

Possible abundances gradients accross the LMC are discussed.

NON-EQUILIBRIUM IONIZATION AROUND CLOUDS

EVAPORATING IN THE INTERSTELLAR MEDIUM

J. BALLET
CEN-Saclay
Service d'Astrophysique - F91191 Gif Sur Yvette Cédex - FRANCE

J.F. LUCIANI   and   P. MORA
Ecole Polytechnique
Centre de Physique théorique - F91128 Palaiseau Cédex - FRANCE

It is of prime importance for global models of the interstellar medium to know whether dense clouds do or do not evaporate in the hot coronal gas. The rate of mass exchanges between phases depends very much on that. McKee and Ostriker's model (1977), for instance, assumes that evaporation is important enough to control the expansion of supernova remnants, and that mass loss obeys the law derived by Cowie and McKee (1977). In fact, the geometry of the magnetic field is nearly unknown, and it might totally inhibit evaporation, if the clouds are not regularly connected to the hot gas. Up to now, the only test of the theory is the U.V. observation (by the Copernicus and IUE satellites) of absorption lines of ions such as OVI or NV, that exist at temperatures of a few 10^5K, typical of transition layers around evaporating clouds.

As a first step Ballet et al.(1986) studied the effect of late ionization in evaporating flows, in the framework of Cowie and McKee's model (1977). A simple analysis predicts that, for a given ion, the delay depends only on the outer temperature T and the product N_eR, in which N_e is the outer electronic density and R is the cloud radius. For a given T, the delay is increasing as N_eR decreases, and for a given N_eR, it is maximum at the temperature corresponding to the onset of "saturation" of the electronic conduction (happening if the mean free path of electrons is of the same order as the cloud radius). Numerical calculations have confirmed that dependance. In typical interstellar conditions, the delay in the ionization of CIV, NV, OVI (to CV, NVI, OVII) is important. As a result, these ions survive much longer than inferred from equilibrium estimates, and reach layers further from the cloud surface. Their average density in the interstellar medium would be one or two orders of magnitude above the equilibrium predictions.

The numbers derived from U.V. observations (Jenkins, 1984) are way below predictions for all reasonable interstellar conditions. That suggests that evaporation is severely quenched. It is true if all OVI, NV and CIV present is observed. McKee and Ostriker (1977) had remarked that slightly subsonic turbulence would broaden the U.V. lines beyond detectability. If such turbulence takes place, only ions located close to cloud surfaces may appear in U.V. absorption lines surveys. Concerning OVI, NV and CIV, that would happen only in the case of a small delay in ionization. On the other hand, if the interstellar conditions imply a large delay, the flow could become turbulent before OVI and NV are reached. Such interstellar conditions would

allow a large amount of those ions to go unobserved in turbulent conditions. If N_e and T are typical of the hot gas, that would require $N_e RT < 10^{3.8}$ cm^{-3} pc K. U.V. lines of CIV would set somewhat tighter constraints if the abundance of gaseous interstellar carbon is more than $\frac{(C)}{(H)} = 1.5 \ 10^{-4}$,

corresponding to less than 2/3 of carbon in grains.

More recently, following a private suggestion by B. Lazareff, I investigated the effect on ionization of non-thermal electrons. The "saturation" effect occurs because the basic assumption of the analysis (that the electronic distribution is Maxwellian at each point with only a slight anisotropy leading to the heat flux) breaks down. The distribution function cannot be represented by a Maxwellian curve. Since the e-e collision rate goes down with energy, the existence of a hot tail in the cold layers is expected even before the onset of saturation. The ionization cross sections are zero below the ionization potential, 98 eV for NV and 138 eV for OVI, so that the ionization coefficients are sensitive only to electrons above that energy, corresponding to the bulk of the outer thermal electrons at 10^6K. It is obvious therefore that a better treatment of those hot electrons in the inner layers was necessary. Luciani et al. (1985) have suggested using an integral delocalization formula for computing the heat flux. They obtained a similar approximate formula for computing the isotropic part of the distribution function itself, and adapted it to the spherical case for my purpose. Because finding a self consistent solution would be too time consuming, I applied this delocalization formula directly to McKee and Cowie's model. It is also justified by the fact that the effect on ionization is expected to be more drastic than on the heat flux. After the distribution function is estimated at one point, the ionization coefficient is obtained by integrating the ionization cross section (from Arnaud and Rothenflug, 1985) over energy.

That effect increases the coefficients for ionization, and therefore speeds it up, reducing the previous delay in ionization and therefore the discrepancy between predictions and observations. However, as long as the flow is not altered, the ion quantity cannot be reduced below a lower limit proportional to $\dot{m}$ and the minimum time spent in the form of OVI or NV, that is usually $t_{min} = 1/N_e \ C_i(T)$ where the ionization coefficient is calculated at the outer temperature. That is still true if delocalization is taken into account, because at high energies the distribution function is always less than the outer Maxwellian.

References

Arnaud, M., Rothenflug, R., 1985, Astr. and Ap. Sup. 60, 425
Ballet, J., Arnaud, M., Rothenflug, R., 1986, Astr. and Ap. (in press)
Cowie, L.L., McKee, C.F., 1977, ApJ. 211, 135
Jenkins, E.B., 1984, The local interstellar medium, IAU colloquium 81, NASA conf. pub. 2345
Luciani, J.F., Mora, P., Pellat, R., 1985, Phys. Fluids, 28, 835
McKee, C.F., Ostriker, J.P., 1977, ApJ. 218, 148

I. LOCAL STRUCTURE AND KINEMATICS OF ISM

C. Planetary Nebulae and Mass-Loss from Evolved Stars

NEAR-INFRARED SPECTROSCOPY OF PLANETARY NEBULAE: HOW STRONG IS THE H_2 EMISSION?

H.L. Dinerstein, J. Carr, P.M. Harvey, and D.F. Lester
Astronomy Department and McDonald Observatory
University of Texas at Austin

Excited molecular hydrogen emission in a planetary nebula was first detected ten years ago in NGC 7027 (1). In NGC 7027, which is known to have an extensive molecular envelope, the presence of H_2 at the interface between the ionized and neutral zones seems natural. However, in view of the lack of previous evidence for neutral matter around most other planetary nebulae, the high detection rate of H_2 emission near 2 μm found by later searches (2,3,4) is something of a surprise. Any pattern in the incidence of H_2 in planetaries is not yet clear, however, since detections have been reported both for extended, presumably evolved objects (e.g.the Ring), and for compact, presumably young nebulae. If H_2 is indeed present in a large fraction of all planetaries, this implies that most planetaries have not yet evolved into fully-ionized, matter-bounded regions and that they may have substantial amounts of associated mass in neutral form.

In an effort to understand the systematics of the H_2 emission from planetary nebulae, we have undertaken a program of near-infrared spectroscopy using the University of Texas infrared reticon spectrometer. This instrument has a 1x32 element InSb photodiode array as a detector. All of the observations reported here were made on the McDonald Observatory 2.7 m telescope, with spectral resolving power $\lambda/\Delta\lambda = 600$. Our spectral coverage allows us to measure simultaneously the strengths of Brackett γ, He I 2.113 μm, He II 2.189 μm, and the v = 1-0 S(1) line of H_2 at 2.122 μm. One of the most important advantages of this instrument is that we are able to resolve H_2 from the adjacent He I line. Most previous observations of planetaries have been made at spectral resolving powers of about 100, which blend these lines. The contribution of the He I line has generally been dismissed as being unimportant (3), but we show that this may not be valid. Our higher resolving power also improves the line-to-continuum contrast; in some cases, the continuum is the limiting factor in detecting faint lines.

We have observed a central position on about 12 planetary nebulae in a 3" diameter beam. In most cases, we see He I 2.113 μm emission as well as Br γ. The He I line is typically of the order of 4 % the strength of Br γ, which we assume is due to nebular recombination emission; this is comparable to the reported strength of H_2 S(1) in several planetaries observed at low resolution. Failure to account for He I emission could therefore lead to overestimating the strength of H_2, or even mistaking He I for H_2 emission. In two nebulae, BD+30 3639 and SwSt 1, we see a stronger (relative to Br γ), apparently broad line at 2.113 μm. We note that the central stars of these two nebulae are both Wolf-Rayet (WC 9) stars, and suggest that the additional strength of the observed line is due to a stellar contribution. These results emphasize the importance of using sufficiently high spectral resolution when measuring the S(1) line to verify its identification and resolve it from He I. The S(1) line is intrinsically one of the strongest H_2 lines, and its strength relative those of other transitions is the chief means for probing the excitation mechanism responsible for the emission (5).

We find evidence for H_2 emission in roughly half the sample observed to date,which includes both nebulae previously claimed to contain H_2 and new candidates. In particular, the S(1) line

appears to be present in several of the most compact objects, including IC 5117 and Vy 2-2, but we do not detect it (to levels of < 1-2 % of Br γ) in the similarly compact nebulae IC4997 and Hb 12. However, Hb 12 had previously been shown to exhibit H_2, and was one of the few objects observed at high enough spectral resolution (2) that confusion with He I was not a problem. We suggest that this is a beam-size effect, and that the reason for this discrepancy lies in the spatial distribution of the H_2 emission. Several extended planetary nebulae including NGC 7027 and the Ring have been mapped in H_2 and it has been found that the H_2 intensity peaks outside the optical nebula, as if the molecular gas is distributed in a shell around the ionized region (2,4,6). We find the same effect in BD+30 3639, in which the ratio of H_2/Br γ increases dramatically toward the edge of the nebula.

In summary, emission from hydrogen molecules does appear to be quite common in planetary nebulae. However, care must be taken to allow for two potentially serious observational effects which can influence the conclusions of such studies. Future work must proceed with the following caveats in mind: (1) Sufficiently high spectral resolution is needed to resolve the S(1) line, often relied upon because it is relatively strong, from He I 2.113 μm, especially in view of possible stellar as well as nebular contributions to the helium line. (2) It appears to be generally the case that the H_2 is distributed in a shell outside the ionized region, so that mapping will be necessary in order to provide a realistic and complete picture of the molecular emission from planetary nebulae.

(1) Treffers, R.R., Fink, U., Larson, H. P., and Gautier, T.N. III 1976, *Ap. J.*, **209**, 793.
(2) Beckwith, S., Persson, S.E., and Gatley, I. 1978, *Ap. J. (Lett.)*, **219**, L33.
(3) Isaacman, R. 1984, *Astr. Ap.*, **130**, 151.
(4) Storey, J.W.V. 1984, *M.N.R.A.S.*, **206**, 521.
(5) Smith, H.A., Larson, H.P., and Fink, U. 1981, *Ap. J.*, **244**, 835.
(6) Beckwith, S., Neugebauer, G., Becklin, E.E., Matthews, K., and Persson, S.E. 1980, *A. J.*, **85**, 886.

Infrared Spectra of WC10 Planetary Nebulae Nuclei

D. H. Wooden, M. Cohen, J. D. Bregman, F. C. Witteborn,
D. M. Rank, L. J. Allamandola, and A. G. G. M. Tielens

The 5.2 – 8.0 micron spectra are presented for two planetary nebulae nuclei Hen1044 (He2–113) and CPD–56 8032 (Figure 1).   The unidentified infrared (UIR) emission bands at 6.2 microns, 6.9 microns, 7.7 microns are present in the spectra of Hen1044 and in CPD–56 8032, and the 8.6 micron band is present in the long wavelength shoulder of the 7.7 micron band in the spectrum of CPD –56 8032.   The 8–13 micron spectra of these two stars by Aitken et. al. (1980) (Figure 1 – dots) clearly show the presence of the 8.6 micron band in He2–113 while weakly resolving this feature in the spectra of CPD–56 8032.   In their spectra the 11.3 micron band is also clearly detected in both objects.   (The observation of the 2.8–3.6 micron region in these two objects has been made using the Australian National University's infrared spectrometer at the 2.3 meter telescope at Siding Spring Observatory.   The broad 3.3 micron feature is seen along with fainter emission features longward of 3.3 microns in both objects and this data will be presented later.)

The 6.2 micron and 7.7 micron bands are characteristic of the infrared active C–C stretching modes in polycyclic aromatic hydrocarbons (hereafter PAHs); the 3.3 micron, 8.6 micron, and 11.3 micron bands are respectively assigned to the in-plane stretching mode, the in-plane bending mode, and the out-of-plane bending mode of the aromatic CH bond (Leger and Puget 1984). The weak 6.9 micron emission feature is attributed to the UIR spectrum by Bregman et. al. (1983).

The IRAS LRS spectra of He2–113 (IRAS 14562–5406) and CPD–56 8032 (IRAS 17047–5650) are presented (Figure 2).   Cohen et. al. (1985) identify the broad plateau from 11.3 to 13.0 microns in the spectrum of He2–113 with increased hydrogenation of PAHs (Figure 3). This broad plateau is not seen in the LRS spectrum of CPD–56 8032.   Also, He2–113 has greater infrared excess emission in the 17–22 micron region than does CPD–56 8032.

The optical spectra of He2–113 have been reported by Carlson (1968), Webster and Glass (1974), and Carlson and Henize (1979) to be dominated by the strong emission lines of H, CII and [NII] on an underlying continuum, with fainter emission lines of HeI, CIII, OII, [SII] and [OII].   P Cygni line profiles yield a velocity difference between emission and absorption of about 200 km/s.   The dominance of the CII lines in the low excitation surrounding nebulae have led to a spectral classification of WC10 (and WC11 by van der Hucht and Conti 1981).   Cowley and Hiltner (1969) discussed the optical spectrum of CPD–56 8032 and consider it to be hydrogen poor. Webster and Glass (1984) also report on the optical spectrum of CPD–56 8032 and remark that spectroscopically "–56 8032 and He2–113 are essentially identical except for the H line strength, which suggests that excitation may not be solely responsible for the hydrogen line behavior." CPD–56 8032 is also assigned to the very late type Wolf-Rayet WC10 class.   The ultraviolet spectrum of CPD–56 8032 is reported by Houziaux and Heck (1982) and a carbon abundance is derived using $N(C)/N(H)=2.46 \times 10^{-3}$ to be $\log[C]=9.39$ compared to $\log[C]=8.55$ for the Sun.

In support of the assignment of the UIR bands to PAH emission we note that while the 6.2 micron and 7.7 micron bands attributed to the C–C stretching modes are very similar, the greater strengths of both the 8.6 and 11.3 micron features and the presence of the 11.3–13.0 micron plateau in He2–113 as compared with CPD–56 8032 indicates that the PAHs in He2–113 maybe more hydrogenated than those in CPD–56 8032, possibly reflecting a difference in hydrogen abundance in the zone in which the UIR emission arises.

Aitken, D.K., Barlow, M.J., Roche, P.F., and Spenser, P.M. 1980, M.N.R.A.S., 192, 679.
Bregman, J.D., Dinerstein, H.L., Goebel, J.H., Lester, D.E., Witteborn, F.C., and Rank, D.M. 1983, Ap. J., 274, 666.
Carlson, E.D. 1968, Unpublished Ph. D. dissertation, Northwestern University.
Carlson, E.D., and Henize, K.G. 1979, Vistas in Astronomy, 23, 213.
Cohen, M., Tielens, A.G.G.M., and Allamandola, L.J. 1985, Ap. J., 299, L93.
Cowley, A.P., and Hiltner, W.A. 1969, Astr. Ap., 3, 372.
Leger, A., and Puget, J.L. 1984, Astr. Ap., 137, L5.
Houziaux, L., and Heck, A. 1982, Wolf-Rayet Stars: Observations, Physics, Evolution.   IAU Symposium No. 99, Cozumal, Mexico, Sept. 18–22, 1981, p. 139.
van der Hucht, K.A., and Conti, P.S. 1981, Space Sci. Rev., 28, 273.
Webster, B.L., and Glass, I.S. 1974, M.N.R.A.S., 166, 491.

FIGURE 1

CPD-56° 8032

$\lambda(\mu)$

FLUX $(10^{-16} W/cm^2-\mu)$

He 2-113

$\lambda(\mu)$

FLUX $(10^{-16} W/cm^2-\mu)$

FIGURE 2

IRAS Name:
17047-5650

peak flux density –
8.4860E-12 W/m**2-micron
x-axis – 4 to 28 microns

IRAS Name:
14562-5406

peak flux density –
4.4899E-12 W/m**2-micron
x-axis – 4 to 28 microns

FIGURE 3

COHEN, TIELENS, AND ALLAMANDOLA

AVERAGE OF 20 SOURCES

FLUX × 10⁻¹²

PAHS

ABSORPTION

WAVELENGTH, microns

60
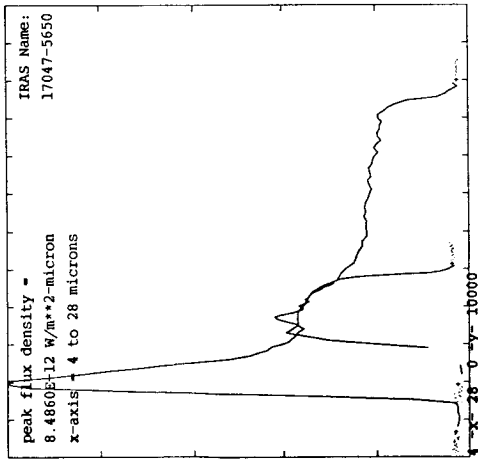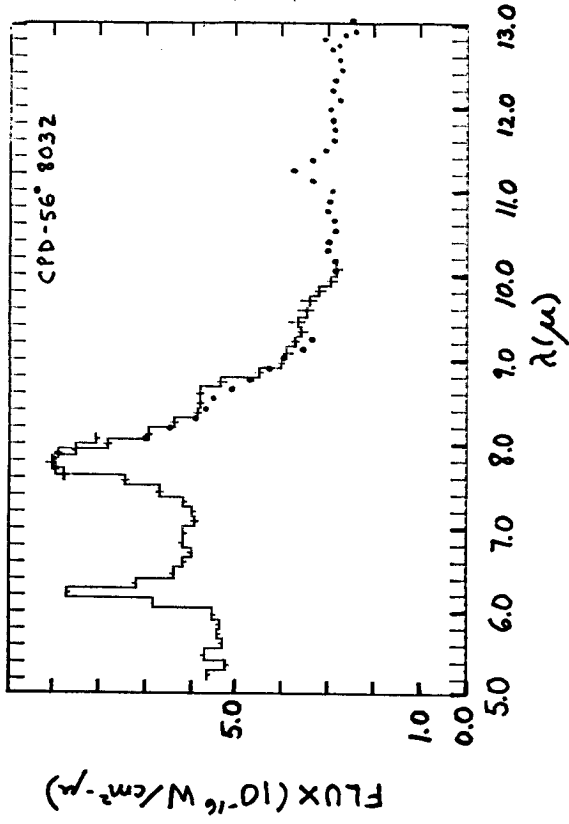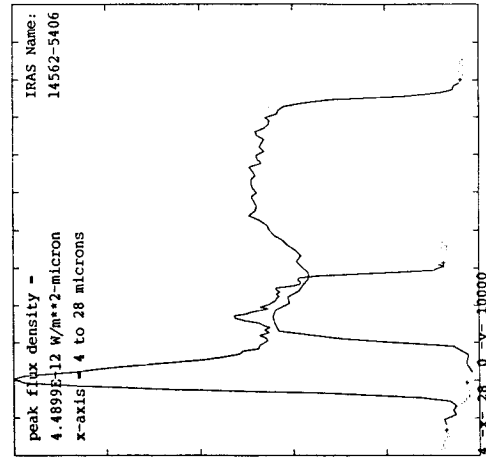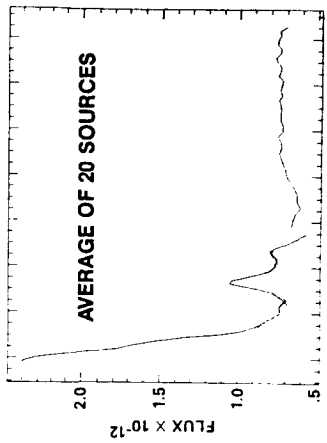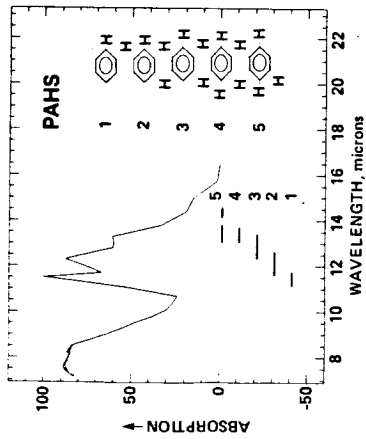
PLANETARY NEBULAE AND THE INTERSTELLAR MEDIUM

Lawrence H. Aller
University of California, Los Angeles, CA 90024

Planetary nebulae (PN) are recognized sources of enrichment of He and heavier elements in the interstellar medium (ISM). It has long been known that PN differ in chemical composition from the Sun and similar stars (see reviews by Peimbert 1978, Aller 1984, and by Kaler 1985 and references therein cited). Zuckerman and Aller (1986) find 62% of their sample of 68 PN with reasonably determined C/O ratios to have C/O > 1, as compared with 61% of the sample used in the present study wherein all determinations based on C II $\lambda4267$ are excluded. PN may be copious sources of interstellar C, soot, and silicate grains. In their sample of 41 PN, Aller and Czyzak (1983) noted that N also tends to be more abundant than in the Sun. Torres-Peimbert (1986) concludes that PN constitute an important N source for the ISM. On the other hand, many workers have noted that O is less abundant than in the Sun. If fluctuations, ΔT_ε, in electron temperature, T_ε, are significant, traditionally derived ionic abundances found from collisionally excited lines will have to be increased (Peimbert 1967; Dinerstein et al. 1985; Zuckerman and Aller 1986). Application of corrections required knowledge of ΔT_ε. It is generally believed that stars in the mass range range 2 to 5 M(sun) manufacture C and N in the CNO cycle and C-burning, but that Ne and heavier elements are not affected by nuclear processes occurring in PN progenitors.

Our objective here is to examine a larger sample of PN. In addition to available published data, we include some 40 objects largely concentrated towards the galactic center and anticenter regions. All were observed with the Lick 3^m telescope and image tube scanner (Aller and Keyes in preparation). Abundances of C, N, O, Ne, $C\ell$, and Ar are determined by a procedure in which theoretical models are used to obtain ionization correction factors (ICF). Of the 106 PN here discussed, 66 are N-rich and 40 are N-poor, N-rich being defined as objects wherein A(N) = log N(N) > 7.99 on the scale log N(H) = 12.00. The C-sample, which is dependent on IUE observations, is much smaller. Table 1 lists the mean abundances for C, N, and O and their ranges defined as log[< N(el)> ± σ] and the ratios Ne/O, etc., both for the entire galactic volume surveyed and the "solar neighborhood," here defined as containing those objects for which 8.0 < R < 9.0 kpc. R is the galactocentric distance; we adopt R(sun) = 8.5 kpc. There appear to be no significant differences between the average compositions in our neighborhood and the average taken over the entire observable portion of the galaxy.

Plots of Ne/H and O/H ratios with R suggest a gradual decline as R increases but the effect is largely smothered under a huge scatter. Some of the spread is certainly due to errors of observation, inadequacies of the models, uncertainties in the ICF factors, and inaccuracies in atomic parameters for the $3p^n$ configurations. Much of the dispersion must come from the intrinsic spread between "high Z" and "low Z" objects. The PN must be separated into population types for a more refined treatment. In both the Ne and O plots, the points most widely scattered with respect to the mean trend tend to pertain to N-rich objects. The overall means show an engaging comparison with solar values. See Table 2.
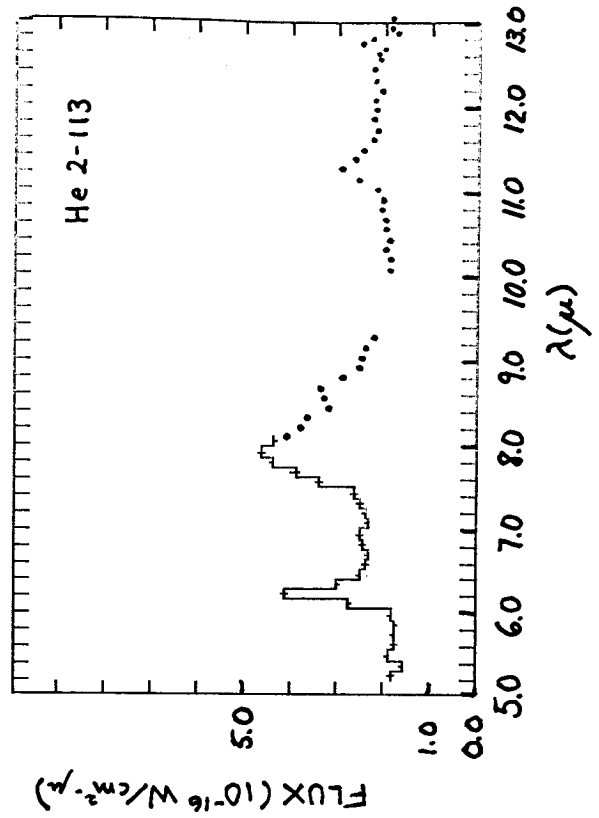
Conclusion. If we allow for uncertainties in solar abundances of Ne, S, Ar, and especially $C\ell$, there is a reasonable fit between solar and PN abundances. In the PN, however, the O abundance is "too low," while N and C are enhanced. If agreement for O is forced by choosing an appropriate ΔT_ε fluctuation, then Ne, S, $C\ell$, and Ar are all "overabundant" in the PN. Is it possible that O is often destroyed to form C and N, as appears to have happened in NGC 6537?

Table 1. Elemental Abundances for C, N, O, Ne, S, Cℓ, and Ar
A(element) = log{N(element)/N(H)} + 12.00

| | Entire Galaxy | | | 8.0 < R < 9.0 kpc | | |
	Range	n		Range	n
A(C) = 8.71	(8.26-8.93)	(26)	8.89	(8.3 -9.2)	(8)
A(N) = 8.26	(7.36-8.53)	(106)	8.22	(7.72-8.42)	(19)
A(O) = 8.65	(8.40-8.80)	(106)	8.71	(8.59-8.83)	(18)
Ne/O = 0.223 ± 0.066		(100)	0.24 ± 0.07 (18)		(18)
S/O = 0.0224 ± 0.012		(91)	0.024 ± 0.017 (14)		(14)
Cℓ/O = [0.44 ± 0.25] × 10^{-3}		(61)	[0.48 ± 0.25] × 10^{-3}		(8)
Ar/O = [0.68 ± 0.37] × 10^{-2}		(96)	[0.53 ± 0.18] × 10^{-2}		(15)

n = number of objects in each sample.

Table 2. Comparison of Solar and PN Logarithmic Abundances

Element	C	N	O	Ne	S	Cℓ	Ar
Sun	8.67[*]	7.99[*]	8.92[*]	8.05[+]	7.23[+]	5.5 ± 0.4	6.57[+]
PN	8.71	8.26	8.65	8.00	7.00	5.3	6.48

[*]Lambert, D.L., 1978, M.N.R.A.S., 182, 249; [+] Aller, L.H., 1986, in press.

References

Aller, L.H. 1984, Physics of Thermal Gaseous Nebulae (Dordrecht: Reidel).
Aller, L.H., and Czyzak, S.J. 1983, Ap. J. Suppl., 51, 211.
Dinerstein, H.L., Lester, D.F., and Werner, M.W. 1985, Ap. J., 291, 561.
Kaler, J.B. 1985, Ann. Rev. Astr. Ap., 23, 89.
Peimbert, M. 1967, Ap. J., 150, 825.
Peimbert, M. 1978, in IAU Symposium 76, Planetary Nebulae, ed. Y. Terzian
    (Dordrecht: Reidel), p. 215.
Torres-Peimbert, S. 1986, Pub. A.S.P. (in press).
Zuckerman,B., Aller, L.H. 1986, Ap. J., 301, 772.

High-Resolution Mapping of Mass Loss from Highly Evolved Carbon Stars

Roger Ball

Owens Valley Radio Observatory

California Institute of Technology

Summary. Interferometric observations of a pair of carbon stars which are evolving toward the planetary nebula stage have revealed evidence of episodic, non-spherically symmetric mass loss, and may lead to a fuller understanding of shielding properties of the dust grains involved in these flows.

Mass loss by stellar winds from red giants is an important source of recycled material to the interstellar medium. The precise evolutionary tracks of the stars involved are poorly known (see the review by Iben and Renzini 1983), but this process and the subsequent formation of planetary nebulae apparently can allow stars of initial masses up to $\sim 5\,M_\odot$ to reach stable end states as white dwarfs. The material-returned to the ISM is likely to be enriched to various degrees in CNO and other elements, depending on the previous history of the star. In order better to understand the physics of the mass loss process itself, Lee Mundy and I have mapped the molecular component of the mass outflow at high resolution with the Owens Valley Millimeter-Wave Interferometer in two well-known objects, CRL 2688 and CIT 6.

These carbon-rich objects are in a rapid mass loss phase, and are thought to be evolving from the asymptotic giant branch to planetary nebulae. We observed emission in 3 mm rotational lines of the molecules CS and CN. In the usual spherical models of mass outflow in these sources, one would expect to find CN distributed in a shell centered on the star; at the inner radius of the shell CN is formed from photodissociation of HCN, and is then dissociated itself at the outer radius. Therefore, by mapping the shell one can determine shielding properties of the grains in the flow. It is important to understand the grains better, because a large class of models – which has had limited success to date – explains the mass loss as being driven by radiation pressure on the dust near the stellar surface. The CS molecule, which traces the presence of rather dense gas ($\sim 10^5\,\mathrm{cm}^{-3}$ and greater) was observed in addition to CN so that departures from the expected symmetry in the flow itself would not confuse the issue.

However, interesting structure is seen in the flows which may complicate the interpretation of the results in terms of the photodissociation picture. Both objects have been resolved by the CS observations. The source sizes are some $21''$ by $12''$ for CRL 2688, and about 20 percent larger for CIT 6. The largest extent of the objects would then be $\sim 3 \times 10^{17}$ cm and 8×10^{16} cm, respectively, if the very uncertain "standard" distances from the literature are assumed. More interestingly, the two sources show a similar structure, consisting of a resolved, bright core with irregular extended emission. This extended structure is broken up into a number of unresolved, dense clumps with no regular velocity pattern. The dynamical ages of the clumps are in the range 200 to 600 years for CIT 6, and 900 to 2100 years for CRL 2688. The mass loss from these stars is clearly asymmetric and also is apparently rather episodic. An example of the irregular asymmetries is shown in the single velocity channel ($3\ \mathrm{km\ s}^{-1}$) map of CRL 2688 below.

CRL 2688, the Egg Nebula, shows features of particular interest. In the CS maps there is a velocity gradient of 9 km s^{-1} across the core, aligned along the major axis of the reflection nebula seen optically. This reflection nebula (Ney *et al.* 1975; Yusef-Zadeh, Morris, and White 1984) has two symmetric halves cut by a dark lane which is presumed to obscure the star. The dense molecular disk that should be associated with this lane is definitely not seen in the CS data, contrary to expectations. The CN, on the other hand, is extended in the disk direction as one might expect if the denser outflow there shields the gas from interstellar UV to greater radii. An explanation of the CS observations as a chemical abundance effect is being sought.

The CN maps of single velocity channels are, like the CS maps, centrally peaked. This observation rules out a simple shell distribution for the molecule, as predicted by the simplest photodissociation models, but the emission regions tend to have sharp edges and central plateaus. Thus, models featuring a sharp outer CN cutoff by photodissociation, with a nonzero abundance of the molecule at the outflow source, seem promising. In other words, not all of the CN is a daughter molecule formed by photodissociation of HCN.

Iben, I., Jr., and Renzini, A. 1983, *Ann. Rev. Astr. Ap.*, **21**, 271.

Ney, E. P., Merrill, K. M., Becklin, E. E., Neugebauer, G., and Wynn-Williams, C. G. 1975, *Ap. J. (Letters)*, **198**, L129.

Yusef-Zadeh, F., Morris, M., and White, R. L. 1984, *Ap. J.*, **278**, 186.

CRL2688   IPOL   97996.776 MHZ   CRL2688.ICLN.112

PEAK FLUX =   2.0903E+00 JY/BEAM
LEVS =   0.1900E+00 * (-3.00, -2.00, 2.000,
   3.000, 4.000, 5.000, 6.000, 7.000, 8.000,
   9.000, 10.00, 12.00, 14.00, 16.00, 18.00,
   20.00, 25.00, 30.00)
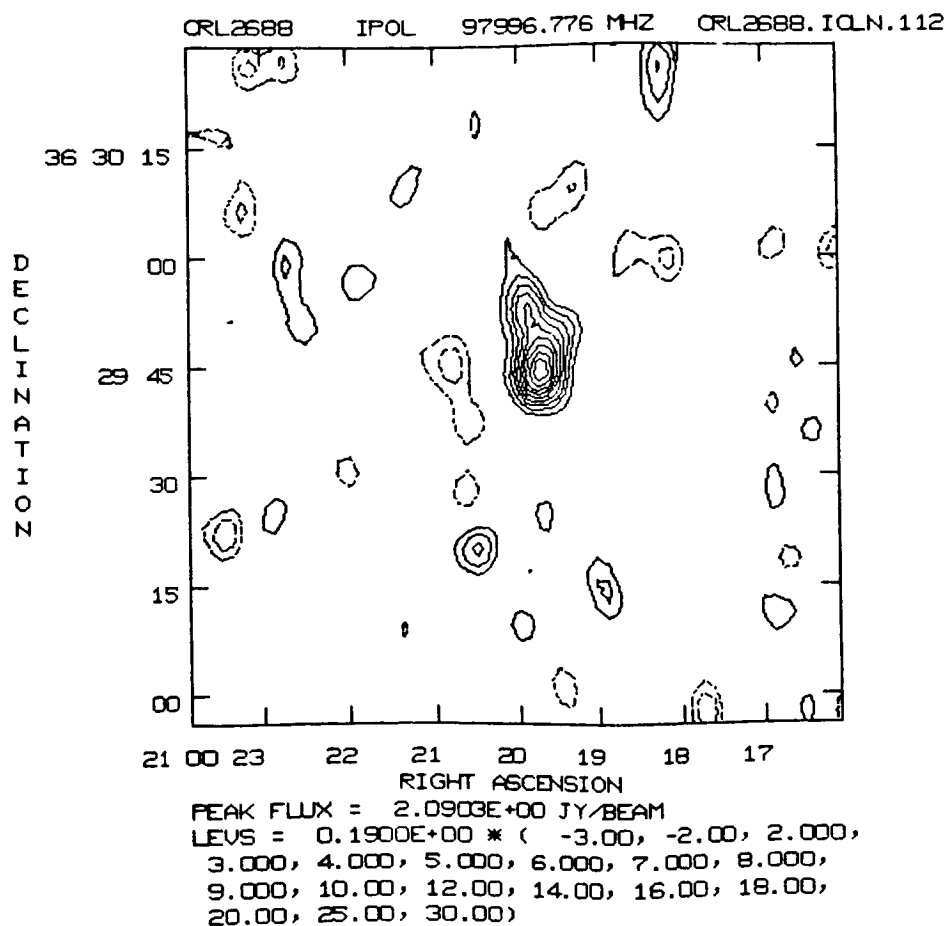
MASS RETURN TO THE INTERSTELLAR MEDIUM FROM HIGHLY-EVOLVED CARBON STARS

W. B. Latter (Steward Obs.), Harley A. Thronson, Jr. (WIRO),
Perry Hacking (IPAC), J. Bally (Bell Labs),
& J. Black (Steward Obs.)

1. INTRODUCTION

Carbon stars play a central role in the evolution of the interstellar medium, returning highly-processed material during a period of extensive mass loss. In addition, they represent a major period in the advanced evolution of moderate-mass stars. Since these stars are often very bright at mid- and far-infrared wavelengths, an extensive survey for them is possible using the data produced by the Infrared Astronomical Satellite.

2. SELECTION CRITERIA

We began our study by plotting visually-identified carbon stars in the 12 µm/25 µm/60 µm color-color diagram, along with the location of a number of mass-losing stars that lie near the location of the carbon stars, but are not carbon rich. Carbon stars were found to be heavily concentrated in one part of the diagram (e.g., Hacking et al. 1985, Zuckerman and Dyck 1986, Thronson et al. 1986), while oxygen stars are more widely distributed. Models show that this part of the color-color diagram is populated largely by circumstellar emission from amorphous carbon. Our first selection was to search through the IRAS Point Source Catalog (PSC) for objects that fell within the central box in the figure. Only objects were included in our sample that had high-quality detections by the satellite. About half of this sample had either a good IRAS Low Resolution Spectrum or a reliable visual spectral classification, which allowed us to both remove non-carbon-rich objects and to estimate the contamination in our final sample. This final sample consists of 619 objects, which we estimate is contaminated by 7% non-carbon-rich objects.

To estimate the mass return rate for all evolved circumstellar envelopes, both oxygen- and carbon-rich, we also searched the PSC for the entire class of stars with excess emission (in particular, $4.57 > F_\nu(12\ \mu m)/F_\nu(25\ \mu m) > 2.4$, $4.79 > F_\nu(25\ \mu m)/F_\nu(60\ \mu m) > 1$, while excluding hot photospheres).

3. THE DISTRIBUTION OF CARBON-RICH SHELLS IN THE MILKY WAY

Plotted on the plane of the sky, we find that the number of carbon-rich objects appears to decline toward the center of the Galaxy. Some of this decrease is due to incompleteness in our sample as a consequence of source confusion in the PSC.

We have constructed a statistical distribution of these objects in the galactic plane by adopting an average 12 μm "luminosity", L (12 μm) $= 4 \pi R^2 F_\nu$ (12 μm) $= 3 \times 10^9$ Jy-pc^2, for all the objects in our sample. This value was found by combining the data in Knapp and Morris (1985) for many well-studied objects with the PSC flux densities. This value is accurate to a factor of 4. We applied it to our sample to calculate average distances and found that the distribution of objects in the plane of the Galaxy is extremely uniform, with a surface density of about 6.5 kpc^{-2}. There is no clear concentration toward the center. This is in sharp contrast with reported distributions of oxygen-rich stars, but is in general agreement with that reported for visually-identified carbon stars.

For a uniform distribution in the Galaxy, we estimate a total number of infrared-emitting carbon-rich stars of 4600 $\times$ [$R^2/15$], where R is the radius of the Galaxy in units of kpc.

4. MASS-LOSS RATES, LIFETIMES, AND BIRTHRATES FOR EVOLVED STARS

Data in Knapp and Morris (1985) and in the PSC shows that the mass-loss rate for both carbon and oxygen stars may be estimated from the ratio [S] of the 12 μm to 60 μm IRAS flux densities, $\log[\dot{M} (M_\odot \text{ yr}^{-1})] = -4 - 0.112 \times \log[S]$. Applied to the carbon-rich envelopes in our sample, the mass-return rate for the galaxy is 0.04 $M_\odot$ yr^{-1}. For our sample of all circumstellar envelopes, the mass return rate is 0.3 $M_\odot$ yr^{-1}. Both calculations assume a radius of the Milky Way of 15 kpc.

An approximate average lifetime for the carbon-rich objects may be estimated from $(M_a-1.4)/\dot{M}$, where M_a is the average stellar mass (about 3 $M_\odot$ for this sample) and $\dot{M}$ is the average mass-loss rate (1.4 $\times 10^{-5}$ $M_\odot$ yr^{-1}). Our average calculated lifetime is 10^5 yrs.

The birthrate may likewise be estimated by dividing the mean lifetime into our estimated total number, giving 0.05 star yr^{-1}.

REFERENCES

Hacking, P. 1985, Pub. A. S. P., 97, 616.

Knapp, G. R., and Morris, M. 1985, Ap. J., 292, 640.

Thronson, H. A. et al., paper presented at the Workshop on the Late Stages of Stellar Evolution, Calgary, Canada, June 2 - 5, 1986.

Zuckerman, B., and Dyck, H. M. 1986, Ap. J., submitted.

I. LOCAL STRUCTURE AND KINEMATICS OF ISM

D. Supernova Remnants and Shock Regions

THE CLUMPY CIRCUMSTELLAR MEDIUM AROUND YOUNG SUPERNOVA REMNANTS

John R. Dickel
University of Illinois and Los Alamos National Laboratory

Eric M. Jones
Los Alamos National Laboratory

and

Jean A. Eilek
New Mexico Institute of Mining and Technology

Each of the youngest supernova remnants known in the Milky Way, Cas A, Kepler's SNR, and Tycho's SNR, shows a different morphological structure caused by different conditions in the progenitor stars and their surroundings. In all three cases, however, the observed shells have a thickness of about 1/4 the radius, a sharp outer edge, and significant brightness irregularities. These features require that the circumstellar medium be highly clumped.

To investigate the phenomenon, models of the expansion have been constructed using a one-dimensional spherical hydrodynamic code. As a supernova shock moves down the external density gradient of the star, material behind the shock begins to go into free expansion. Then as surrounding material is encountered a reverse shock moving back into the ejectum will be formed. Until the expansion has swept up about eight times the ejected mass when the situation can be considered as a point explosion in its surroundings, the dynamics are controlled by conditions between the shocks. This region is also where the synchrotron radio emission from relativistic electrons trapped in magnetic fields arises. Initial particles and fields are accelerated and amplified by eddy motion at the interface between the ejected and swept-up material and at the boundaries of clumps. Polarimetry shows that these SNR have a net radial orientation of their magnetic fields apparently from stretching by Rayleigh-Taylor instabilities at the contact surfaces. Without clumps the observed shell is much too narrow and steep on the inside.

To simulate true three-dimensional structure with the one-dimensional model, random contributions from several runs with varying parameters for the clumps were summed along the line of sight. The results shown in the figure were made from different summations of four runs having random spacings of the clumps with a mean separation of 5×10^{17} cm. Their Gaussian sizes were 1×10^{17} cm $\pm 10\%$ and their peak densities were $3.6+10^{24}$ gm cm^3 $\pm 10\%$. The latter was typically 10 times the mean density between clumps. These conditions were able to reproduce the varying brightness distributions of both the type I remnants, Kepler and Tycho. Whether the clumpiness is a result of presupernova mass loss or a general property of the interstellar medium is not known.

The remnant of the type II SN, Cas A, with its larger mass and greater brightness, requires correspondingly more massive clouds but the same type of phenomenon prevails. In this case, the material presumably came from the star as indicated by its observed composition.
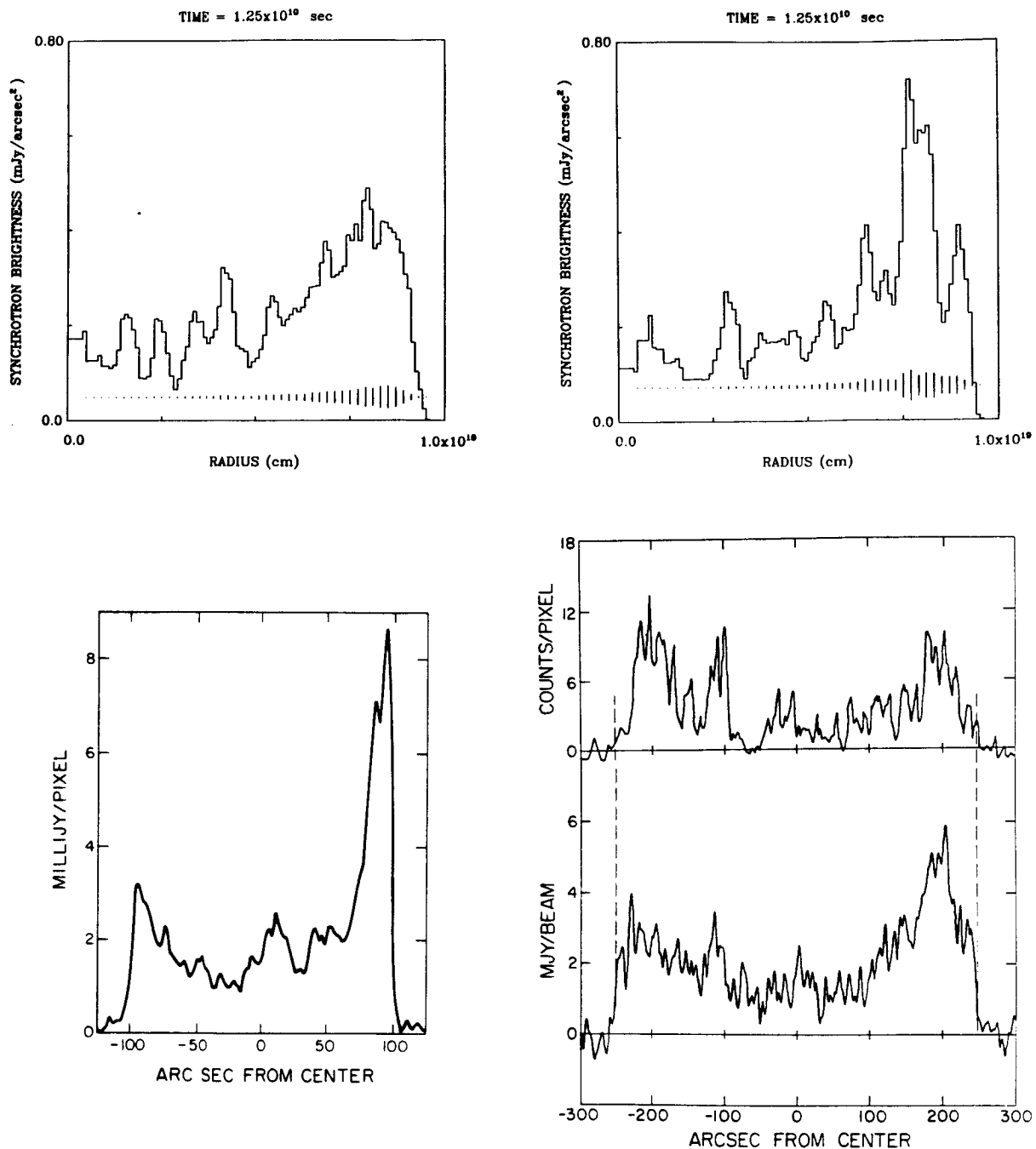
Figure:
Upper - Radial slices of the predicted radio synchrotron emission at a wavelength of 20 cm from two different summations of the four runs of the model type I SNR expanding into the clumpy medium described in the text. The time is 400 years after the explosion. The vertical vectors near the bottom represent the polarized power in a direction corresponding to a radial magnetic field.
Lower Left - South-north slice through the 20 cm radio emission from Kepler's SNR. A pixel represents a 1".75 by 2".75 Gaussian beam. The left side can be compared with the figure above.
Lower Right - South-north slices through the 11-cm radio and soft x-ray emissions from Tycho's SNR. The resolution was 4". The rim on the right can be compared with the modeled emission above.

68

THE MOLECULAR GAS IN THE SUPERNOVA REMNANT IC 443

Y.-L. Huang, R. L. Dickman, and R. L. Snell
Five College Radio Astronomy Observatory,
University of Massachusetts

ABSTRACT

Although a few highly perturbed regions characterized by gas motions with velocities larger than 20 km s^{-1} have been discovered during the last several years in the supernova remnant (SNR) IC 443, the nature of these perturbed clumps and their relationship to the quiescent molecular gas near the SNR remains unknown. In part, this is due to a lack of large-scale, high angular resolution observations. We have therefore carried out a systematic survey of this SNR in the CO (J=1→0) line, covering a roughly 50' × 50' region spaced by 2'. The observations were made with the 14 m telescope of the Five College Radio Astronomy Observatory (FCRAO), which has a resolution of 45" and a single sideband receiver temperature of 200 K at 2.6 mm wavelength.

Five new clumps were discovered, bringing the total number of known perturbed regions to eight [Figure 1; Huang, Dickman, and Snell 1986, *Ap. J. (Letters)*, **302**, L63]. To study the physical structure of these clumps in more detail, we have made more complete maps of the clumps in both the CO (J=1→0) and (J=2→1) transitions with the FCRAO telescope. These maps show that the extent of perturbed gas in a typical clump is several arcmin, or a few pc at a distance of 1.5 kpc.

We have also obtained the first detection of highly perturbed ^{13}CO (J=1→0) emission toward clump B ($\alpha = 6^h\ 14^m\ 15^s$, $\delta = 22°\ 27'\ 50"$; epoch 1950). Spectra of the ^{13}CO and CO (J=1→0) emission are shown in Figure 2. Our data suggest an average CO/^{13}CO intensity ratio of ~ 60 for the perturbed gas, which implies relatively optically thin CO emission. This value is consistent with the intensity ratio of the CO (J=2→1) and (J=1→0) lines in clump B. If the gas is optically thin in all perturbed clumps, they contain no more than a few solar masses, a value several orders of magnitude smaller than that of the quiescent cloud.

Speculation on the origin and fate of the clumps and their relationship to the quiescent cloud will be discussed in the workshop. This work was supported by NSF grant AST-8512903.
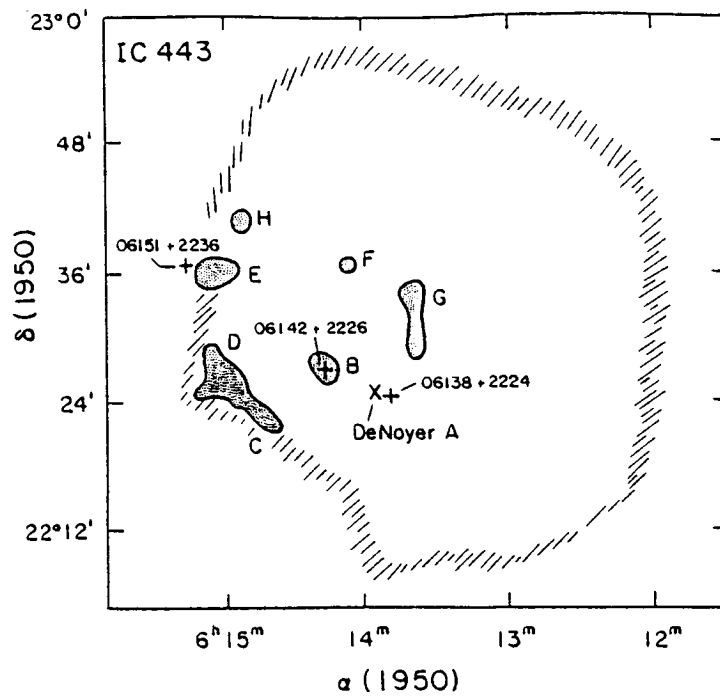
Figure 1: Schematic representation of the location of shocked clumps toward the SNR IC 443, as revealed by CO spectra obtained with the FCRAO 14 m telescope. The stippled region surrounding each clump corresponds to the area over which highly perturbed CO could be identified in our spectra. Also shown are the outline of the optical SNR and three bright IRAS point sources which may be associated with the clumps (Huang, Dickman, and Snell 1986).
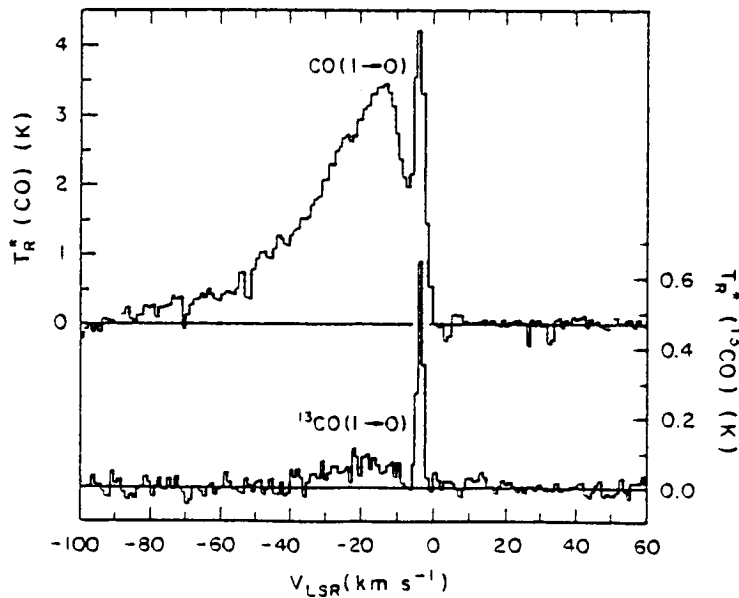
Figure 2: CO and ^{13}CO (J=1→0) spectra toward clump B ($\alpha = 6^h \ 14^m \ 15^s$, $\delta = 22°$ 27' 50"; epoch 1950). For clarity, the ^{13}CO spectrum has been blown up five time.

70

Observational discrimination between modes of shock propagation in interstellar clouds: predictions of CH^+ and SH^+ column densities in diffuse clouds

D. R. Flower
Physics Department
The University
Durham DH1 3LE (U.K.)

G. Pineau des Forets and E. Roueff
DAPHE
Observatoire de Paris
F-92195 Meudon Principal (France)

T.W. Hartquist
MPI fur extraterrestrische Physik
D-8046 Garching bei Munchen (F.R.G.)

Considerable effort in recent years has been devoted to the study of shocks in the diffuse interstellar medium. This work has been motivated partly by the observations of rotationally excited states of H_2 (Spitzer et al. 1973; Spitzer and Cochran 1973), and partly by the realisation that species such as CH^+, OH and H_2O might be formed preferentially in hot, post-shock gas (Elitzur and Watson 1980). The problem of CH^+ and the difficulties encountered when trying to explain the high column densities, observed along lines of sight to certain hot stars, have been reviewed by Dalgarno (1976).

The importance of a transverse magnetic field on the structure of an interstellar shock was demonstrated by Draine (1980) and Draine, Roberge and Dalgarno (1983). Transverse magnetic fields above a critical strength give rise to an acceleration zone or precursor, in which the parameters of the flow vary continuously. Chemical reactions, which change the degree of ionisation of the gas, also modify the structure of the shock considerably (Flower, Pineau des Forets and Hartquist 1985; Draine and Katz 1986).

Very recent work by ourselves (Pineau des Forets et al. 1986) and by Draine (1986) has shown that large column densities of CH^+ can be produced in magnetohydrodynamic shock models. Shock speeds $u_s \approx 10$ km s^{-1} and initial magnetic field strengths of a few μG are sufficient to produce ion-neutral drift velocities which can drive the endothermic C^+ (H_2,H) CH^+ reaction. These authors have also shown that single-fluid hydrodynamic models do not generate sufficiently large column densities of CH^+ unless unacceptably high shock velocities

($u_s \approx 20$ km s^{-1}) are assumed in the models. Thus, the observed column densities of CH$^+$ provide a constraint on the mode of shock propagation in diffuse clouds. More precisely, they determine a lower limit to the ion-neutral drift velocity.

A similar study of the sulphur chemistry behind shocks in diffuse clouds (Pineau des Forets, Roueff and Flower 1986) has lead to similar conclusions regarding the column density of SH$^+$, which is produced through the endothermic S$^+$(H$_2$,H)SH$^+$ reaction. Column densities N(SH$^+$) > 10^{12} cm^{-2}, which should be observable in absorption in the near ultraviolet region, are produced only when the maximum ion-neutral drift velocity $|u_i - u_n|_{max}$ > 5 km s^{-1}. Detection of these lines, whose predicted equivalent widths are given in the Table, should provide valuable information on the transverse magnetic field strength in the vicinity of the shock.

Line	λ (Å)	f_{line}	W_λ (mÅ)				
			log N=9.18	11.79	12.76	12.99	13.11
R$_{11}$(0)	3363.49	6.2 10^{-4}	9 10^{-5}	0.04	0.35	0.60	0.80
^{R}Q$_{21}$(0)	3339.97	4.6 10^{-4}	7 10^{-5}	0.03	0.26	0.44	0.58
^{S}R$_{21}$(0)	3336.64	3.7 10^{-4}	6 10^{-5}	0.02	0.21	0.36	0.47

References
Dalgarno, A. 1976, in Atomic Processes and Applications, eds. P.G. Burke and B.L. Moiseiwitsch (Amsterdam: North Holland), p.109.
Draine, B.T. 1980, Ap. J., 241, 1021.
Draine, B.T. 1986, Ap. J., in press.
Draine, B.T., and Katz, N.S. 1986, Ap. J., in press.
Draine, B.T., Roberge, W.G., and Dalgarno, A. 1983, Ap. J., 264, 485.
Elitzur, M., and Watson, W.D. 1980, Ap. J., 236, 172.
Flower, D.R., Pineau des Forets, G., and Hartquist, T.W. 1985, M.N.R.A.S., 216, 775.
Pineau des Forets, G., Flower, D.R., Hartquist, T.W., and Dalgarno, A. 1986, M.N.R.A.S., in press.
Pineau des Forets, G., Roueff, E., and Flower, D.R. 1986, M.N.R.A.S., submitted.
Spitzer, L., Drake, J.F., Jenkins, E.B., Morton, D.C., Rogerson, J.B., and York, D.G. 1973, Ap. J., 181, L116.
Spitzer, L., and Cochran, W.D. 1973, Ap. J., 186, L23.

II. GALACTIC-SCALE STRUCTURE AND KINEMATICS OF ISM

A. Galactic Nuclei

A CS J = 2 → 1 Survey of the Galactic Center Region

Antony A. Stark, John Bally, Mark Dragovan and Robert W. Wilson

AT&T Bell Laboratories, Crawford Hill
Holmdel, New Jersey

We present a CS map of the galactic center region consisting of 15,000 spectra covering $-1.°\!\!<\ell<3.°6$, $-0.°4<b<0.°4$, each having an rms noise of 0.15 K in 1 MHz filters. CS is a high-excitation molecule, meaning that it is excited into emission only when the ambient density $<n>\gtrsim 2\times10^4 cm^{-3}$. CS emission in the inner 2° of the galaxy is nearly as pervasive as CO emission, in stark contrast to the outer galaxy where CS emission is confined to cloud cores. Galactic center clouds are on average much more dense than outer Galaxy clouds. This can be understood as a necessary consequence of the strong tidal stresses in the inner galaxy.

In a roughly spherical cloud, of radius r_0, at a distance R_0 from the galactic center, consider the gravitational forces on a parcel of gas at a distance r_0 from the cloud center along a line towards the galactic center. If this parcel of gas is bound to the cloud, so that it follows a circular trajectory around the galactic center at a slower-than-orbital velocity, the cloud must exert a gravitational acceleration on it equal to Tr_0, where

$$T \equiv -\left.\frac{d}{dR}\left(\frac{v_{circular}^2}{R}\right)\right]_{R_0} + \frac{v_{circular0}^2}{R_0^2} \approx 2\frac{v_{circular}^2}{R_0^2}$$

(the rotation velocity $v_{circular}$ is approximately independent of R when $10pc \lesssim R \lesssim 20Kpc$). This acceleration is caused by the gravitational pull of the cloud, so that

$$\frac{GM_{cloud}}{r_0^2} \gtrsim Tr_0 \quad.$$

and

$$<\rho_{cloud}> \equiv \frac{M_{cloud}}{(4/3\ \pi r_0^3)} \gtrsim \frac{3T}{4\pi G} \approx \frac{3}{2\pi G}\frac{v_{circular}^2}{R_0^2} \approx 3.5\times10^3\ a.m.u.\ cm^{-3}\left[\frac{500\ pc}{R_0}\right]^2 \quad.$$

The minimum average density of a cloud is a strong function of galactic radius, and clouds near the galactic center must be many times more dense than clouds in the solar neighborhood. Gravitationally bound clouds within about 200 pc of the galactic center must be dense enough to excite the CS J=2→1 line.

The virial theorem relates cloud density to cloud size and to the internal pressure. The dominant pressure term is turbulent pressure characterized by a mean square velocity $<v^2>$. Define a mean gravitational radius $<r>$ such that the potential energy $W_{cloud} \equiv -GM_{cloud}^2/<r>$. For a spherical cloud where $\rho \propto r^\alpha$, with a sharp edge at r_0, the gravitational radius is related to the outer radius $\frac{r_0}{<r>}=\frac{\alpha+3}{2\alpha+5}$. The virial theorem can then be written as a requirement on the minimum internal velocity dispersion:

$$<v^2> \approx \frac{GM_{cloud}}{<r>} = \frac{4\pi G}{3}<\rho_{cloud}>\left(\frac{r_0}{<r>}\right)r_0^2 \gtrsim 2\ v_{circular}^2\left(\frac{r_0}{<r>}\right)\left(\frac{r_0}{R_0}\right)^2 \quad,$$

where for ρ_{cloud} we have substituted the tidal limit. This inequality does not impose a very

73

stringent limit on the random velocities internal to outer-galaxy clouds. Most clouds in the outer galaxy have velocities 2 or 3 times bigger than this minimum. For the dense, large clouds in the galactic center, however, it says that a 30 pc cloud 300 parsecs from the galactic center must have a FWHM linewidth of at least 37 km s^{-1} — a typical linewidth for a galactic center cloud. Clouds as large as those we find in the galactic center must have large linewidths, or they will not be in equilibrium and bound against the galactic tide.

Figure 1 — The CS Survey spectra, integrated over 100 km s^{-1} wide velocity ranges, and displayed as evenly spaced contours at 10 K·km s^{-1} intervals. The Sgr A cloud is at ℓ = 0.˚0, Sgr B2 is at ℓ = 0.˚66, and Clump 2 is at ℓ = 3.˚0, b = 0.˚4.
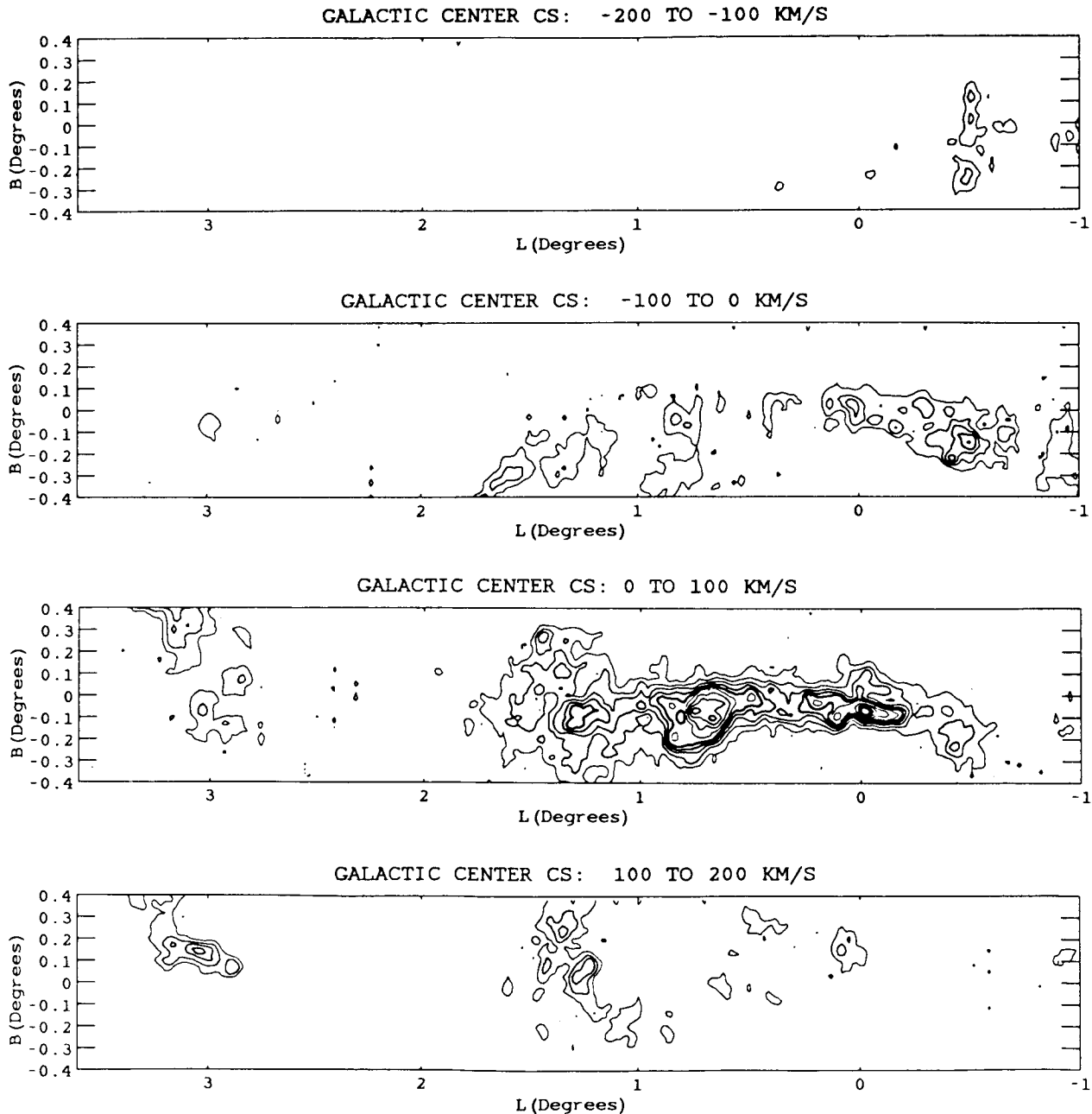
Aperture Synthesis Observations of the Molecular Ring in the Galactic Center

R. Güsten, R. Genzel, M.C.H. Wright, D.T. Jaffe, and J. Stutzki, Dept. of Physics and Dept. of Astronomy University of California, Berkeley

ABSTRACT

We report 88 GHz aperture synthesis observations of HCN $J=1\rightarrow0$ emission and absorption in the central 5 pc of the Galaxy. The data, taken at 5" to 10" spatial and 4 km s^{-1} spectral resolution with the Hat Creek mm-interferometer, show a complete, clumpy ring of molecular gas surrounding the ionized central 2 pc of the Galaxy. The ring is the inner edge of a larger disk extending to about 5 pc. Comparison with sub-mm (Harris et al., (1985) and FIR (Genzel et al., 1985) line data suggests that the HCN 1-0 line is slightly optically thick and originates in subthermally populated gas. The clumpy distribution of line emission reflects a combination of hydrogen volume and column density variations.

The new data clearly show a close physical relation between the molecular and the ionized gas in the central cavity. The "western arc" (Lo and Claussen, 1983; Serabyn and Lacy, 1985) appears to be the ionized inner surface of the molecular ring, and the "northern arm" and "bar" may be streamers of ionized gas falling from the ring toward the center.

The dominant large scale velocity pattern of the majority of the molecular gas in the inner 5 pc is rotation. No overall radial motion of the ring greater than about 20 km s^{-1} is apparent. The rotation is perturbed in several ways; 1) there is a very large local velocity dispersion, 2) the ring shows changes in position angle and inclination (warps), 3) there is a bright, redshifted cloud which appears to be located in the western part of the ring but does not participate in the rotation. These characteristics and the high degree of clumpiness indicate a non-equilibrium configuration of short ($<10^4$ to 10^5y) dynamical lifetime. The warping and tilting of the structure and the short dynamical lifetime make an accurate determination of "equilibrium" rotation velocity uncertain.

References
Genzel, R., Watson, D.M., Crawford, M.K. and Townes, C.H. 1985, Ap. J. 297, 766
Harris, A.I., Jaffe, D.T., Silber, M. and Genzel, R. 1985, Ap. J. (Letters) 294, L93
Lo, K.Y.and Claussen, M.J. 1983, Nature, 306, 647
Serabyn, E. and Lacy, J.H. 1985, Ap. J. 293, 445
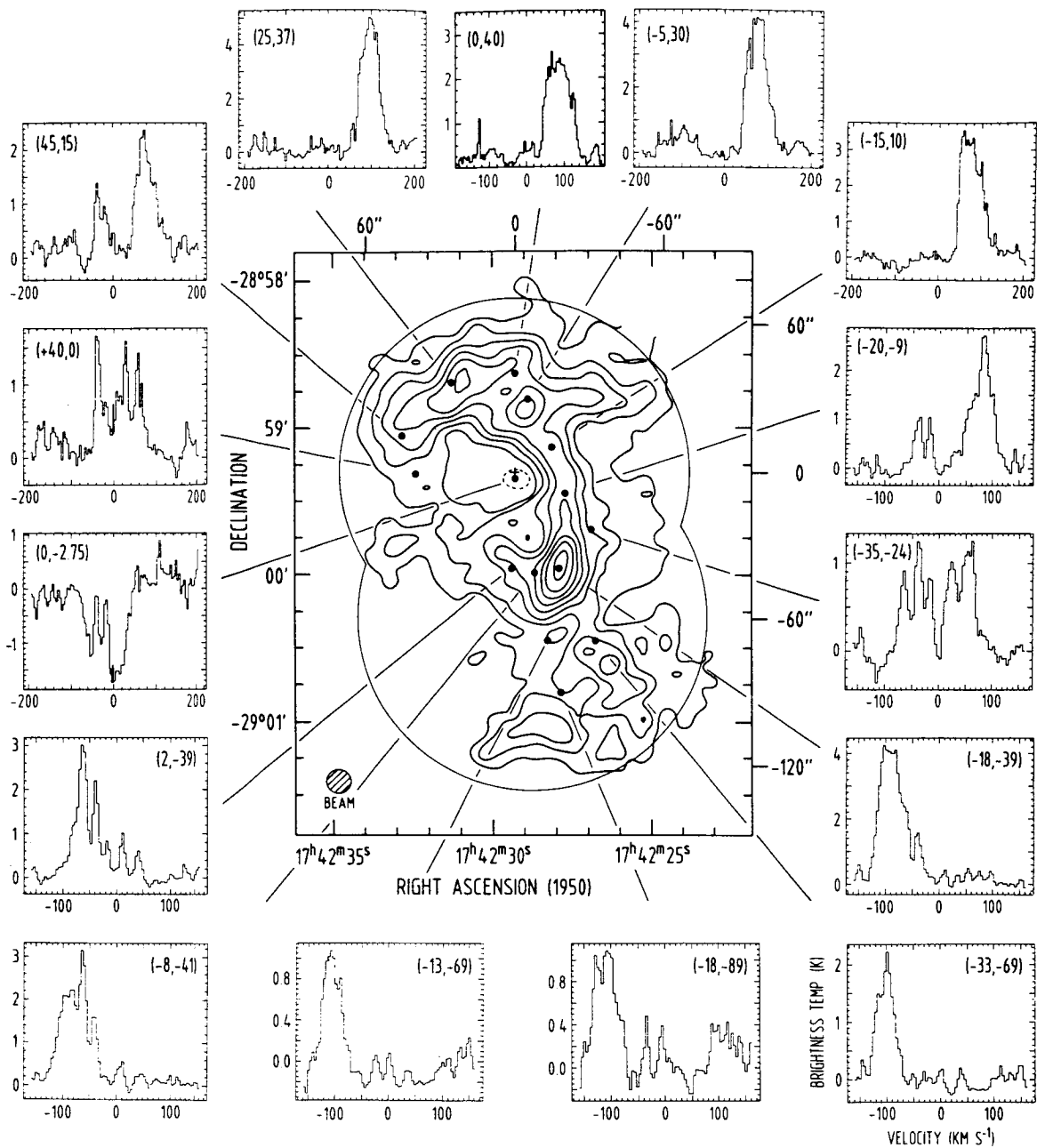
Fig. 1: Velocity integrated HCN 1-0 map (-150 km s^{-1} to 150 km s^{-1}, CLEAN ed) and selected spectra. The spatial resolution is 10.8" × 9" (FWHM, R.A. × Dec.), the spectral resolution is 4.23 km s^{-1}. Continuum emission has been subtracted. The contour units on the map are 0.2 K.

IUE ABSORPTION STUDIES OF BROAD- AND NARROW-LINE GAS IN SEYFERT GALAXIES

G. Mark Voit, J. Michael Shull, and Mitchell C. Begelman

Joint Institute for Laboratory Astrophysics
University of Colorado and National Bureau of Standards

The interstellar medium of a galaxy containing an active nucleus may be profoundly affected by the high energy (X-ray, EUV) continuum flux emanating from the central source. The energetic source may photoionize the interstellar medium out to several kiloparsecs, thereby creating a global H II region. With the International Ultraviolet Explorer (IUE) satellite we have attempted to observe in several Seyfert galaxies (NGC 3516, NGC 4151, NGC 1068, 3C 120) the narrow absorption lines expected from such global H II regions. Instead, in two of the galaxies (NGC 3516, NGC 4151) we found broad, variable absorption lines at C IV $\lambda1550$, N V $\lambda1240$, and Si IV $\lambda1400$ (Fig. 1), as well as weaker absorption features at O I $\lambda1302$ and C II $\lambda1335$. These features swamp any possible global H II region absorption.

Such broad absorption features have previously been observed in IUE data, but their origin is still not well understood. In this study we concentrate on the C IV $\lambda1550$ line in NGC 3516, an SB0 Seyfert I galaxy. The nineteen IUE short wavelength archive images of this object that are available at the University of Colorado Regional Data Analysis Facility (RDAF) constitute our data base. The broad C IV absorption component, which is superimposed on a broad emission feature, is blueshifted with respect to the narrow emission lines and the peaks of the broad emission lines. Both the broad emission-line region and the continuum emitting region must be at least partially covered by the absorbing region (Fig. 2). The absorption component appears to vary on time scales of less than ten days, and its equivalent width may be anti-correlated with the continuum flux at 1450 Å . Recombination-time arguments limit the density in the absorbing gas to greater than 10^5 cm^{-3}; C IV should be found at such high densities only within 10 pc of the central source. The blueshift of the absorption component suggests that the absorbing material is flowing outward from the galactic nucleus. Standard broad-line cloud models fail to account for the C IV absorption feature. The absorption may arise either in optically thin clouds in the broad-line region or in dense narrow-line clouds. We discuss the significance of UV resonance-line absorption in light of the partial X-ray absorption seen in this galaxy, and we present simple reverberation models for the absorbing region which give an anti-correlation of absorption with continuum flux. The absorption may also be related to optical spectroscopic evidence for outflows in NGC 3516.

Figure 1

Figure 2
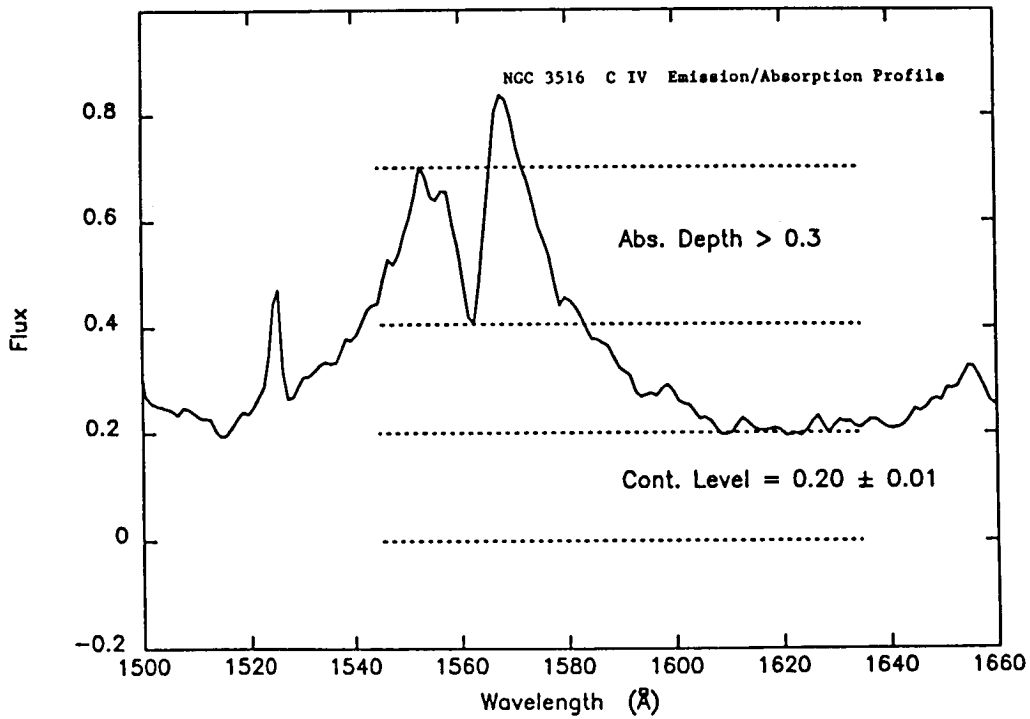
COLD ATOMIC HYDROGEN IN THE INNER GALAXY

John M. Dickey and R. W. Garwood, University of Minnesota
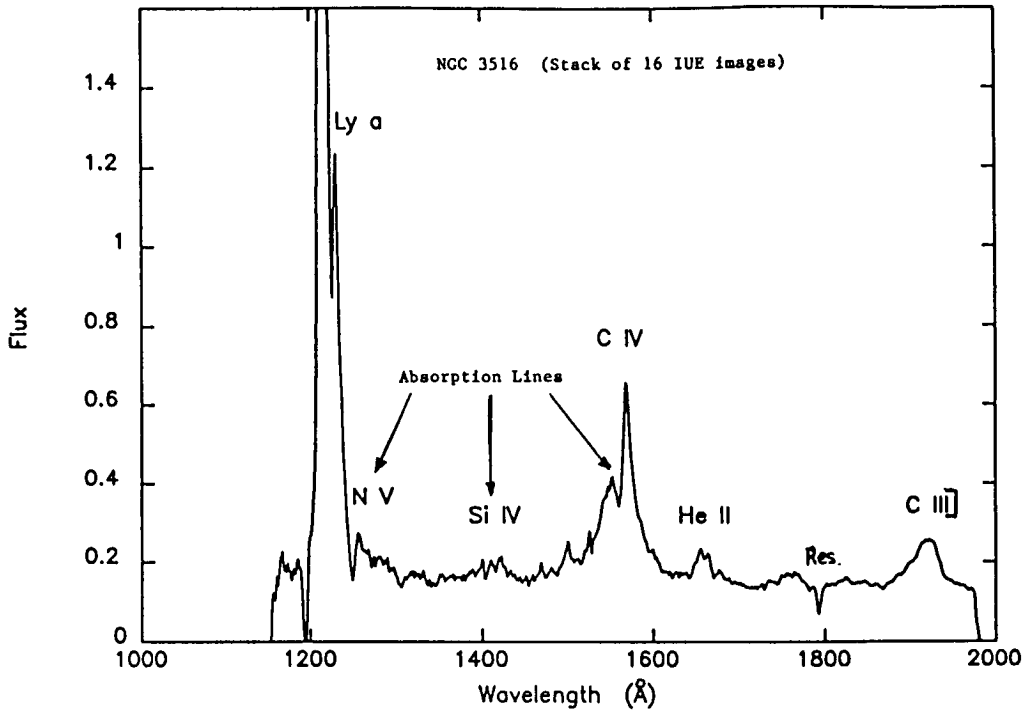
Abstract : We have used the VLA to measure 21 cm absorption in directions with $|b|<1°$, $|l|<25°$ to probe the cool atomic gas in the inner galaxy. We detect abundant H I absorption; typical lines are deep and narrow, sometimes blending in velocity with adjacent features. Unlike 21 cm emission not all allowed velocities are covered : large portions of the l-v diagram are optically thin. Although not similar to H I emission, the absorption shows a striking correspondance with CO emission in the inner galaxy : essentially every strong feature detected in one survey is seen in the other. Our provisional conclusion is that in the inner galaxy most cool atomic gas is associated with molecular cloud complexes. There are few or no cold atomic clouds devoid of molecules in the inner galaxy, although these are common in the outer galaxy.

Background : In spite of many low latitude surveys of 21cm emission our knowledge of the detailed distribution of atomic hydrogen in the inner galaxy is not complete. The problem is the blending of the two phases of atomic gas. The warm gas (10 to 20 km/s linewidths) fills in the emission spectra to cover all velocities allowed by galactic rotation, while the cool phase is often optically thick and selectively obscures background gas. The fundamental question of how the cool atomic phase is distributed in the inner galaxy has remained unanswered, in spite of our growing understanding of the distribution of cold molecular clouds through surveys of CO. In this project we are studying the cool phase directly through a 21 cm absorption survey of the galactic plane.

Observations : Unfortunately in absorption we cannot observe a regular lattice of points and construct a map as in emission surveys. We first had to survey in continuum with the VLA to find background sources. We have made a catalog complete to 50 mJy of compact (<30") continuum sources at low latitudes (Garwood et al, in preparation). From the hundreds of sources discovered we selected nine to study in absorption with the VLA in "phased-up" mode (Dickey et al 1984, Ap. J. Supp. 53, 591). The high resolution of the B array (4") avoids confusion due to emission structure. The spectra obtained cover -150 to +150 km/s with 2.6 km/s channels. The rms noise in optical depth ranges from 0.03 to 0.1.

Results : The figure shows a composite of the observed spectra arranged by longitude. Galactic coordinates (l,b) are given in the upper left of each spectrum. For comparison the longitude-velocity diagram of CO from Bania (1977, Ap. J. 216,381) and Clemens et al (1986 Ap. J. Supp. 60, 297) is shown. By tracing the longitudes of our sources horizontally across the l-v diagram one can see the correspondance between spectral features in CO and H I absorption, which is almost perfect. On the other hand, there is very little correspondance between absorption features and 21 cm emission lines; in emission the H I is largely saturated, and many clouds along the line of sight blend in velocity. In absorption there are narrow, distinct clouds, separated by velocities with no detected optical depth at all.

OPTICAL DEPTH
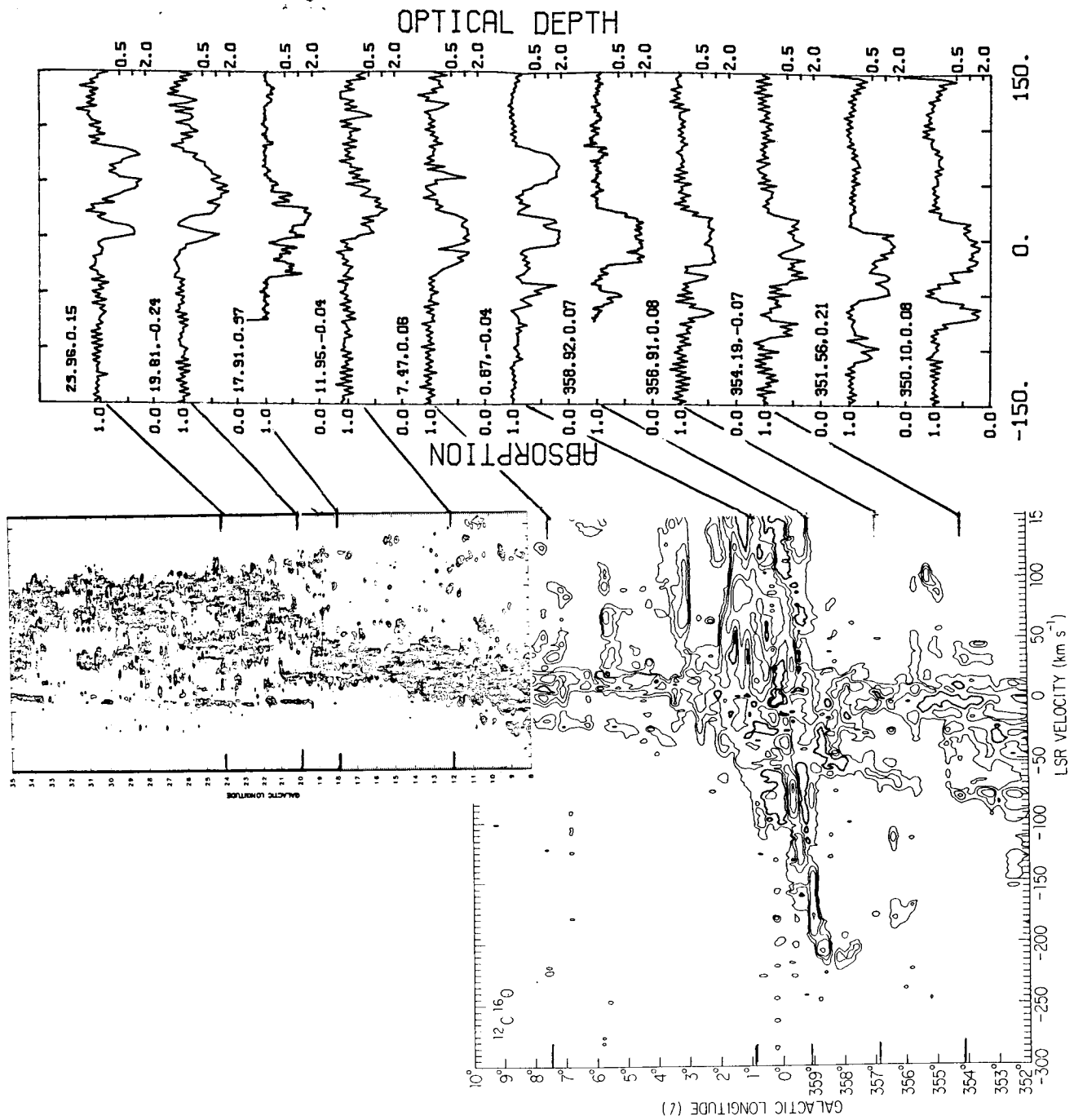
ABSORPTION

Conclusion : There is a one-to-one correspondance between features in the spectra of H I absorption, and the CO emission in the inner galaxy. This suggests that the cool diffuse phase of the interstellar medium is confined to the vicinity of molecular clouds. The atomic gas may be mixed with the molecules, or in a halo around and between molecular clumps. This situation is different from the solar neighborhood (observed at high latitudes) where many cool atomic clouds are seen with little or no molecular emission. The implication is that in the inner galaxy the role of the cool atomic phase is different from that in the outer galaxy. Whereas locally diffuse clouds are common (mean free path ~300pc) and giant molecular clouds are much less common, in the inner galaxy these two phases may be intimately associated.

II. GALACTIC-SCALE STRUCTURE AND KINEMATICS OF ISM

B. The Milky Way and External Galaxies

NEUTRAL HYDROGEN CLOUD DISTANCES AND THE STRENGTH OF THE
INTERSTELLAR MAGNETIC FIELD

Gerrit L. Verschuur
Unaffiliated

ABSTRACT. If HI clouds exist in pressure equilibrium in an environment
where gas pressure is a function of z-distance and if HI cloud density is a
function of z-distance, it can be shown that a quantity called the Virial
Measure is a function of z-distance. The Virial Measure is that distance at
which a cloud would be in gravitational equilibrium if its internal kinetic
temperature is indicated by profile linewidth. The Virial Measure is
derived from observed cloud parameters and has been calibrated for clouds
of known distance so that it can be used to determine the distance to other
HI clouds. The magnitude of various terms in the virial equation can thus
be derived for several hundred HI clouds. It is demonstrated that the
strength of the interstellar magnetic field is a function of z-distance.

1. THE DISTANCE TO HI CLOUDS

The distance at which an HI cloud would be in gravitational equilibrium is
very much greater than its real distance. This distance, to be called the
Virial Measure, D_V, has very different values for different populations of HI
clouds. Sufficient data exist for clouds of known distance—either local
clouds or others whose distances can be determined kinematically—to
allow D_V to be calibrated with respect to z-distance.

The Virial Measure is found by equating the gravitational energy
term, W, with $2T$ the thermal energy term, in the virial equation.
Neglecting other terms

$$W = 2T$$

or

$$\frac{3 G M^2}{5 R} = 3 N k T_k . \tag{1}$$

R - cloud radius, T_k =cloud kinetic temperature, G and k the usual constants, M the cloud mass, and N the total number of atoms in the cloud. It is assumed that the cloud contains only HI and that observed HI profile linewidths are indicative of cloud kinetic temperatures, T_k.

The published data on several hundred HI clouds give values for cloud mass (Mr^{-2}) in solar masses at the unknown distance (r, in kpc), the linewidth at half peak intensity (ΔV, in km/s) and angular diameter (θ, in degrees) at half peak intensity.

It can be shown (Verschuur, 1986a) that if D_V is the distance at which Equation 1 is satisfied, then

$$D_V = \frac{1.55\,(\Delta V)^2\,\theta}{(Mr^{-2})} \quad \text{Mpc.} \tag{2}$$
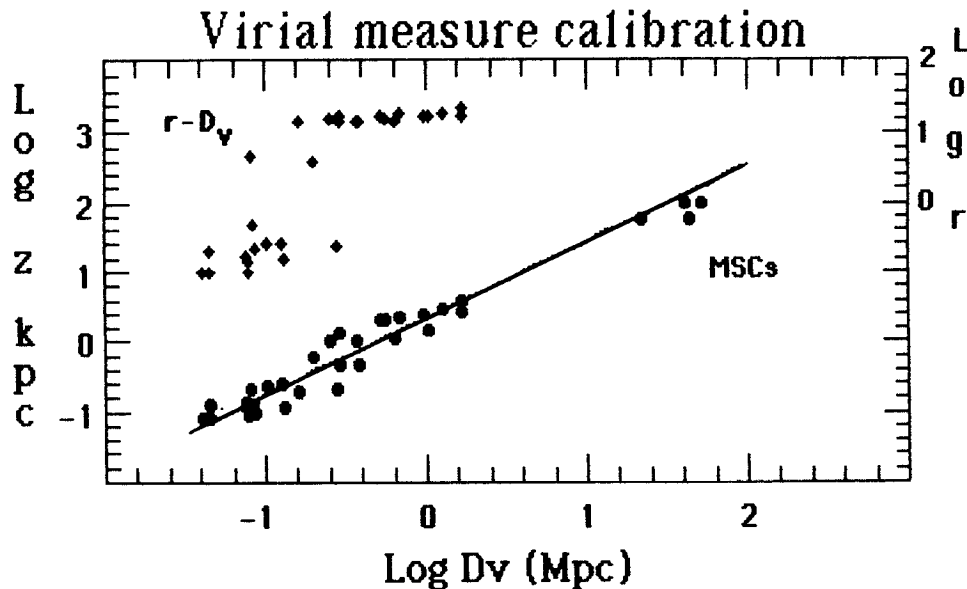
Figure 1. The calibration of the Virial Measure in terms of z-distance. Filled circles represent clouds, or averages for groups of up to 120 clouds, whose distances have been estimated by the original authors or were kinematically derived in the present work. Small plus signs indicate distance from the sun with the axis shifted 2 units. The Magellanic Stream Clouds are represented by four points at the right, but these were not used to determine the best-fit line.

Figure 1 shows the value of D_V plotted as a function of z-distance. Details of the calibration are given by Verschuur (1986a). A flat rotation

law and the newly agreed-upon solar location and motion (8.5 kpc, 220 km/s) were used to establish kinematic distances and these clouds are all at or beyond the solar circle.

The best-fit line drawn in Figure 1, derived without using the Magellanic Streams clouds at the upper right of the line, is defined by

$$\log z - 1.10 \log D_V - 2.95 \tag{3}$$

where z and D_V are in kpc. Thus it appears that if D_V can be derived for a cloud, the cloud's distance can be found from Equation 3.

In order to highlight the fact that D_V is a function of z-distance and not of distance from the sun, the Virial Measure values are also plotted with respect to r. These are shifted vertically by two decades in Figure 1. No direct relationship between D_V and r exists.

Something other than gravitational attraction is clearly acting to produce the relation shown in Figure 1. It is hypothesized that intercloud gas pressure, which may be a function of z in the halo, determines HI cloud stability. For the clouds of known distance, and for other HI clouds whose distances can now be derived using the relationship given in Equation 3, it is possible to find values of the internal gas pressure, nT, as a function of z-distance. This was done by first deriving the value for a quantity nTr directly from published cloud data. From Verschuur (1986a),

$$nTr - 0.32 \frac{\Delta V}{\theta} (Mr^{-2}) \quad cm^{-3} \, K \, kpc. \tag{4}$$

Once a cloud's distance is known a value for nT can be derived. In Figure 2 this quantity is plotted for all clouds in the data base. The best-fit line for the emission clouds in Figure 2 is found to be

$$\log nT = 3.62 - 0.72 \log z \tag{5}$$

with nT in $cm^{-3} K$ and z in kpc. Similar data for the Verschuur cold clouds, the Heiles cloudlets, and absorption clouds whose densities and diameters have been measured by independent means, are plotted as plus signs in Figure 2 and produce

$$\log nT = 2.45 - 0.78 \log z. \qquad (6)$$

nT versus z All clouds
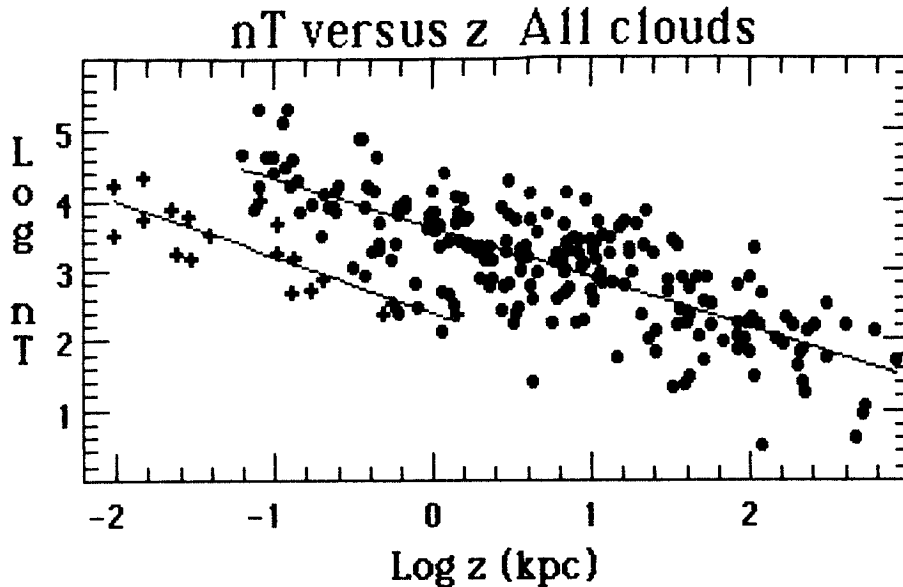
Figure 2. The gas pressure term, nT, as a function of distance from the galactic disk for clouds observed in emission (filled circles) and absorption (plus signs). The distances to the calibrators are independently known while the distance to all the clouds were found from Equation 3. The Verschuur cold clouds and a point representing the Heiles cloudlets have been included with this group. The best-fit lines to these two sets of data show clear and distinct differences as well as a common z-dependence.

Several important points emerge from a study of Figure 2:

1. The gas pressure in the emission features is clearly a function of z-distance.

2. If HI clouds exist in pressure equilibrium then we cannot have a condition where one group of clouds, those seen in emission, exist in a higher pressure regime than do the colder, absorption, clouds at the same z-distances. Examination of the initial assumptions reveals that emission profile linewidth is probably not a measure of cloud kinetic temperature. Some other cause for line broadening must be found, and whatever the reason it will have to account for the relationship found in Figure 1.

3. Several clouds are located at very great distances from the disk, more than 100 kpc away. However, the analysis implicitly assumes that nT is stratified parallel to the galactic disk. This assumption needs to be modified because at greater distances halo gas pressure—which must

utimately changes smoothly into to an intergalactic gas pressure—is more likely to be dependent on distance from the galactic center. The 'halo' gas pressure term is likely to drop to some ambient intergalactic value at distances of the order of several hundred kpc and the absolute value of derived distances beyond this are likely to be in error. The available data do indicate that the so-called very-high-velocity clouds and the Magellanic Stream clouds lie in intergalactic space.
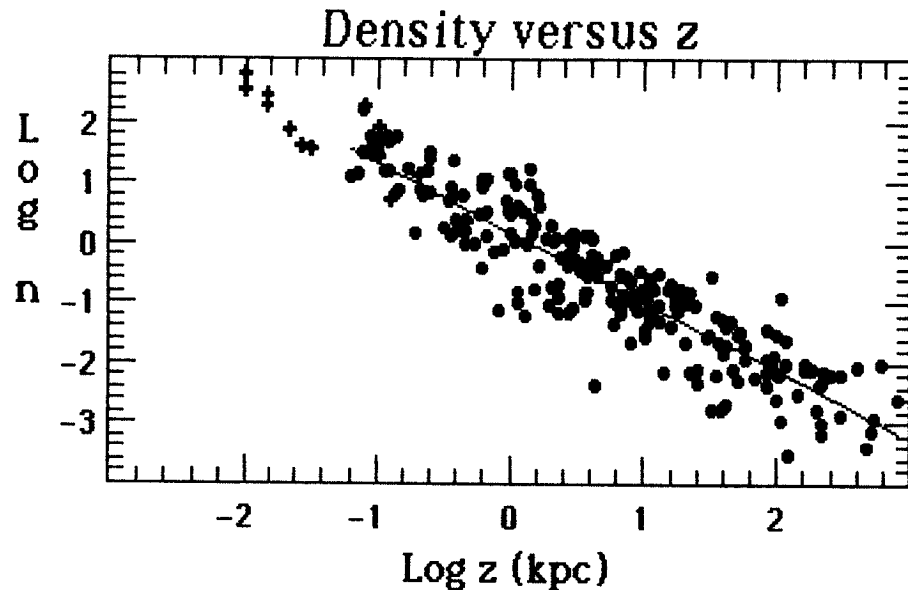
Figure 3. HI cloud density as a function of distance from the galactic disk. Filled circles refer to the emission clouds while the plus signs refer to the cold cloud and absorption line data. The line was fitted only to the emission clouds yet the absorption cloud information, determined in a completely independent manner, fits this line very well.

Next, the values for cloud densities can be determined from the data. This was done by taking the nT values and dividing by a temperature given by the linewidth, originally assumed to indicate T_k. Figure 3 plots the value of HI cloud density versus z-distance and shows that this is also z-dependent. The best-fit line is given by

$$\log n = 0.18 - 1.14 \log z. \qquad (7)$$

The absorption line and cold cloud data are plotted as small plus signs and lie on an extension of the line fit to the emission cloud data or

disappear into the jumble of these data. The densities for these two sets of clouds were determined by independent methods.

2. WHY VIRIAL MEASURE IS A FUNCTION OF Z–DISTANCE

It can be shown that if both the nT and n values are functions of z, then D_V must be a function of z as well.

Consider Equations 5 and 6 in the form

$$nT = A z^\alpha \tag{8}$$

and

$$n = B z^\beta. \tag{9}$$

If we ignore constant terms, we can consider the parameters applicable to a cloud of diameter θ at a height z kpc. Its mass, M, will be given by $n R^3$ where R is the cloud radius given by

$$R = \frac{\theta r}{2}.$$

Therefore, using Equation 9, we can write

$$M = B z^\beta \theta^3 r^3. \tag{10}$$

The left hand side of Equation 1 can then be written as

$$W = (B z^\beta)^2 \theta^5 r^5, \tag{11}$$

ignoring other constant terms.

For the right-hand side of Equation 1, we can write

$$2T = N k T_k = n T R^3$$

Using Equation 8, we obtain

$$2T = A z^\alpha \theta^3 r^3. \tag{12}$$

D_V, was originally defined by setting Equations 11 and 12 equal. Thus, solving for D_V, and evaluating the constants, we find that

$$D_V = \underline{1.13} \sqrt{\underline{A}} \times z^{\frac{(\alpha - 2\beta)}{2}} . \qquad (13)$$
$$\theta \quad B^2$$

From Figures 2 and 3 we derived Equations 5 and 7 and thus have values for A, B, α, and β. Equation 13 then becomes

$$D_V = \frac{47.46}{\theta} \times z^{0.785} . \qquad (14)$$

The Virial Measure is found to be a function of angular diameter as well as z-distance, in which case we may ask why such a dramatic relationship between D_V and z, as was revealed in Figure 1, became manifested? It turns out that the majority of the clouds have diameters in the range $0.4 < \theta < 1.2°$ with the median value of θ for the calibrators of 1°. Thus, to first order, we can assume that θ is a constant and, setting θ~1, Equation 14 becomes

$$\log z = 1.27 \log D_V - 2.14. \qquad (15)$$

Equation 15 has the same form as Equation 3—which was based on observations. The exponent is the same, within observational uncertainty, but the constant term is a little different. Uncertainties in the assumptions of a plane-parallel layered galaxy, cloud definition (assumption of cloud symmetry), observational scatter, and so on, may be acting to make the agreement less than perfect.

It appears that the D_V-z relation is the consequence of the hydrogen clouds being in pressure equilibrium in a medium in which nT and cloud HI density are both functions of z. The Virial Measure may be used to determine the distance to other HI clouds, provided they have approximately the same angular diameter as the calibrators.

3. CLOUD PROPERTIES AND THE STRENGTH OF THE INTERSTELLAR FIELD

During an early phase of this research an interesting 'coincidence' was noticed in connection to the gas pressure term, nT. If one could account for

line broadening in terms of an Alfvén velocity spread, the strength of the interstellar magnetic field could be simply related to nT. This idea had a short half-life but caused the author to look at the published 21-cm Zeeman effect data in order to determine whether the magnetic field in HI clouds might be a function of z-distance. Figure 4 shows the results of this work, summarized by Verschuur (1986b).

Field strength versus z-distance
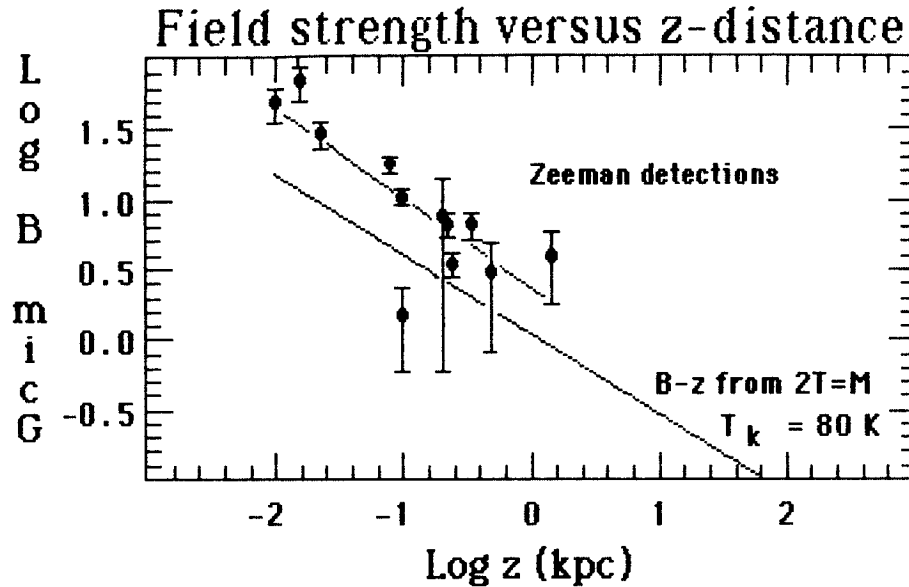
Figure 5. The strength of the interstellar magnetic field based on Zeeman effect measurements in HI clouds as a function of z-distance of the clouds. Error bars indicate two standard deviations. The upper line is the best-fit to the Zeeman data. The lower line is a field derived from equating the thermal energy content with magnetic energy in emission clouds believed to be in pressure equilibrium with their environment. Cloud kinetic temperature is assumed to be 80 K.

The important point that emerges from Figure 5 is that the interstellar magnetic field strength may, indeed, also be a function of z-distance. At z<100 pc it appears that the B > 10 μGauss, enough to align interstellar dust grains (Aanestad and Purcell, 1973).

The line fitted to the field detections, all line-of-sight components, is given by:

$$\log B = 0.38 - 0.64 \log z \qquad (16)$$

with B in μGauss and z in kpc.

An independent means for finding the value of the interstellar magnetic field is suggested by the distance analysis discussed in this paper. Once an HI cloud's distance is known we are able to derive all its properties, provided its kinetic temperature is known. Based on an examination of the n-z plot in Figure 3, and recognizing that the absorption cloud kinetic temperatures are well-known, and around 80 K, it is seen that the 'true' value for the cloud pressure may be found by adopting a value for the cloud kinetic temperature of about 80 K. Thus the values of the cloud gravitational energy content, W, the thermal content, $2\,T$ (Equation 1), and the magnetic energy content, M ($=B^2/8\pi \times$ Volume), can be derived, where B is assumed to be given by Equation 16.
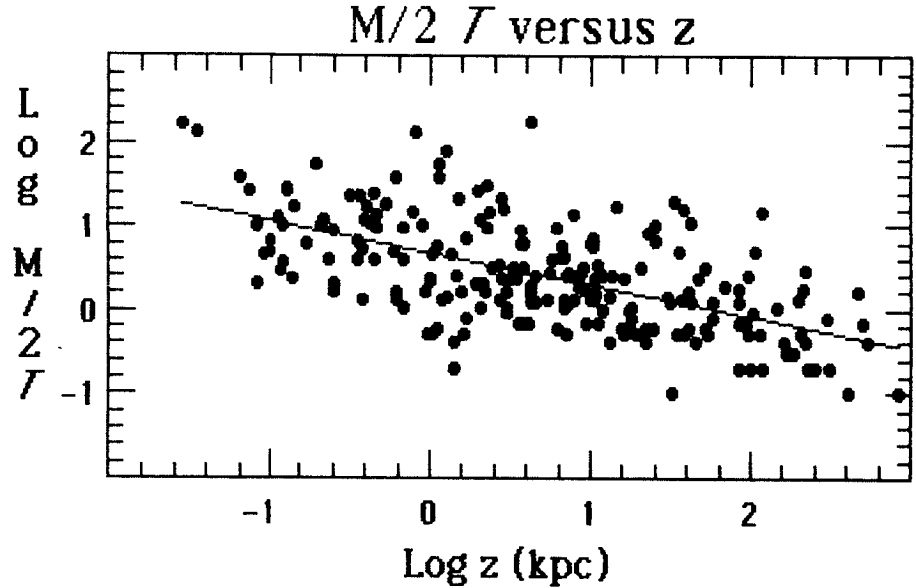
Figure 5. The ratio of magnetic energy content, M, to thermal energy content, $2\,T$ for all the emisson clouds in the data-base plotted as function of z-distance. The field strength, B, was derived from Equation 16 and the value of T_k was taken to be 80 K in all clouds.

The values of W, $2\,T$ and M were derived for several hundred clouds in the data base and Figure 5 shows the ratio of $M/2\,T$ as a function of z-distance. This ratio is z-dependence and given by

$$\log\ (M/2\,T) = 0.68 - 0.38\ \log z. \tag{16}$$

Figure 5 implies that at low z-distances either the field dominates the gas pressure—contrary to our original assumptions and interpretation of the data (above)—or the strength of the adopted field (based on the Zeeman data) is too large. Thus this approach was reversed. Under the assumption that the clouds are in pressure equilibrium and fields are frozen-in one may find the value of the field strength that would cause the two energy terms, $2\,T$ and M, to balance. Using Equation 16, the mean interstellar magnetic field strength is given by:

$$\log B = 0.05 - 0.57 \log z. \qquad (18)$$

The form of Equation 18 was sketched in Figure 4 as the lower line. The exponent is nearly the same as indicated by the Zeeman effect data—Equation 16. The field strength derived from equating magnetic and thermal energy densities would be more directly equal to that found from the Zeeman effect data if $T_k = 300$ K. However, the clouds in which the Zeeman measurements indicate the strongest fields are also found to have a gravitational energy content of the same order as the thermal content, suggesting that these clouds might be near to gravitational equilibrium. The fields in these clouds may be 'amplified' by gravitational contraction of these clouds, but if this is true the amplification must be considered with respect to ambient densities and fields indicated by the n-z and B-z plots rather than taken with respect to a mean density assumed for all of interstellar space, as was done in previous analyses. (Verschuur, 1970, Troland and Heiles, 1982).

4. CALIBRATION USING THE MAGELLANIC STREAM CLOUDS

The Magellanic Stream Cloud data originally drew this author's attention to the Dv-z relationship. According to Lin and Lynden-Bell (1982) the tail of the Stream, where most of these clouds are found, is about 60 kpc from the sun. If we take this to be approximately the same as their effective z-distance then the calibration presented in Figure 1 can be redone. This work gives

$$\log z = \log D_v - 2.71. \qquad (19)$$

Using this Equation, the nT-z and n-z dependences for the clouds were again determined and now found to be given by

and
$$\log nT = 3.63 - 0.69 \log z \qquad (20)$$

$$\log n = 0.17 - 1.15 \log z. \qquad (21)$$

When D_V is derived from Equations 20 and 21 (using Equation 13) we find that

$$\log z = 1.24 \log D_V - 2.11. \qquad (22)$$

The diferences between Equations 22 and 23 are smaller than were found between equations 15 and 3 which suggests that the distance calibration using the MSCs is a more valid way to approach these data. In other words, it may be possible to iterate using these parameters to find the best overall agreement. In future a far larger data base and/or a better model for the entire Magellanic Stream will allow a more accurate calibration of the Virial Measure in terms of z-distance and may even reveal second order terms. Verschuur (1986a) will recommend that in the meantime the MSCs be used to set the D_V calibration according to Equation 19.

4. REFERENCES

Aanestad, P. A. and Purcell, E. M. 1973, Ann. Rev. Astr. Ap. **11**, 309.
Lin, D. N. C and Lynden-Bell, D. 1982, M. N. R. A. S. **198**, 707.
Troland, T. H. and Heiles, C. 1982, Ap. J., **252**, 179.
Verschuur, G. L. 1970, IAU Symposium #34, "Interstellar Gas Dynamics",
             page 150. Editor H. J. Habing. (Reidel, Dordrecht)
Verschuur, G. L. 1986 a, b. Submitted to A. J.

Temporary mailing address: Box 995, Arecibo, P.R. 00613

91

THE MOLECULAR CONTENT OF THE NEARBY GALAXY
FROM IRAS AND HI OBSERVATIONS

David Bazell
Applied Research Corporation
8201 Corporate Drive
Landover, MD 20785

and

F. X. Desert
Goddard Space Flight Center
Greenbelt, MD 20771

Abstract: Because infrared emission is a very good tracer of mass at high latitudes, by combining it with HI observations it provides a convenient though indirect way of observing the spatial distribution of molecular material (Desert, Bazell, and Boulanger). Moreover, these observations will allow us to place limits on the fraction of total infrared luminosity emitted by dust associated with molecular and atomic hydrogen clouds.

We report a preliminary result from the study of the correlation between HI column density and 100 um infrared flux density as measured by the IRAS satellite. The ratio F100/W(HI) = R has an average value of roughly 17 KJy/sr/(K km/s) over the whole sky. Bright regions in the FIR such as the Galactic plane and HII regions have been excluded from our data.

The histogram of the number of pixels vs R (cf. fig.) has a strong peak near 17 (same units as before) and is asymmetric about this mean value, having a tail at higher values of R. We find that this basic shape is fairly independent of the region of the sky we observe. The peak confirms the general correlation between infrared emission and HI column density reported previously by Boulanger et al. (1985).

One way to explain the shape of the distribution is to assume a constant dust to gas mass ratio and a constant interstellar radiation field and associate points in the tail with molecular clouds. In this case the ratio R is higher for points in the tail because it does not account for the column density of molecular hydrogen.

As an initial test of our hypothesis we have created a histogram of F100/W(HI) for points corresponding to peak intensity of CO emission in the approximately 120 High Latitude Clouds (HLCs) discovered by Magnani, Blitz and Mundy (1985) (MBM). These points are clearly not a random selection of points from our all sky distribution, because they lie mainly in the tail of the distribution. By accounting for the total hydrogen column density we can move the points in the tail into the body of the distribution.

On the other hand, we want to estimate the proportion of points in the tail of the distribution which correspond to molecular clouds. For example, the four clouds A, B, C and D of Low et al. (1984) were examined by MBM and found to have no detectable CO emission. While three of these clouds lie within the main distribution, cloud A has a ratio R of approximately 30 (same units), which is somewhat out in the tail of the distribution.

Finally, by studying the distribution of R in regions containing only HI we can separate the contributions to the luminosity into atomic and molecular components.
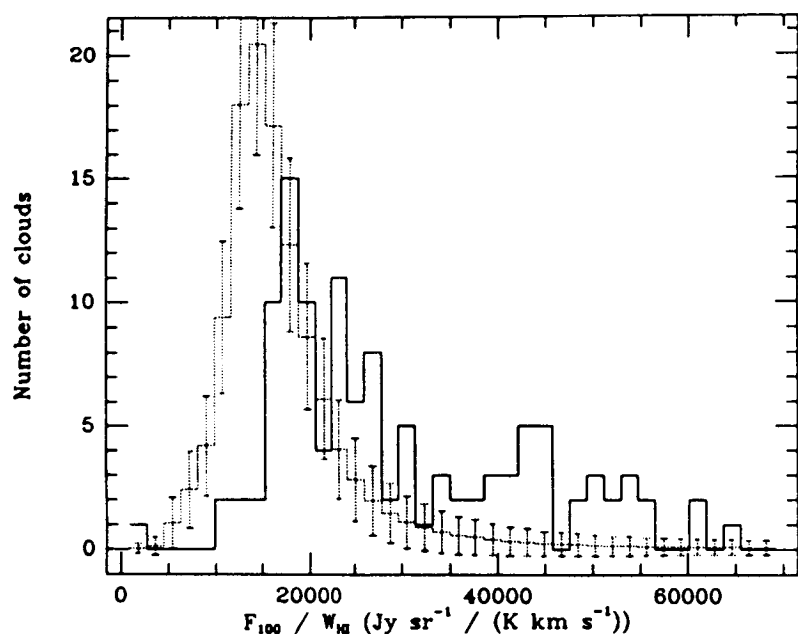
HISTOGRAM OF F100/W(HI)

Solid line: Number of clouds (MBM) with a given ratio of F100/W(HI). Dotted line: Number of pixels in the whole sky with a given ratio of F100/W(HI) normalized to total number of MBM clouds. Error bars indicate expected Poisson errors (square root of number of points). The high latitude molecular clouds lie mainly in the tail of the distribution of the whole sky.

Boulanger, F., Baud, B., van Albada, G. D., 1985, Astr. Ap., 144, L9.
Desert, F. X., Bazell, D., Boulanger, F., in preparation.
Low, F. J., et al., 1984, Ap. J. (Letters), 278, L19.
Magnani, L., Blitz, L., Mundy, L., 1985, Ap. J., 295, 402.

MILKY WAY HALO GAS KINEMATICS

Laura Danly

University of Wisconsin--Madison

Measurements of high resolution, short wavelength absorption data taken by IUE toward high latitude O and B stars are presented in a discussion of the large scale kinematic properties of Milky Way Halo gas. An analysis of these data demonstrates that: **(a)** the observed absorption widths (FWHM) of Si II are very large, ranging up to 150 Km/s for the most distant halo star; this is much larger than is generally appreciated from optical data; **(b)** the absorption is observed to be systematically negative in radial velocity, indicating that cool material is, on the whole, flowing toward the disk of the galaxy; **(c)** there is some evidence for asymmetry between the northern and southern galactic hemispheres, in accordance with the HI 21 cm data toward the galactic poles; **(d)** low column density gas with highly negative radial LSR velocity (V < -70 km/s) can be found toward stars beyond 1-3 kpc in the northern galactic hemisphere in all four quadrants of galactic longitude; and **(e)** only the profiles toward stars in the direction of known high velocity HI features show a clear two component structure. The figures below illustrate these results.

Figure 1 shows the measured full width at half intensity of Si II λ1260 for each star, shown in order of increasing distance from the galactic plane. The z-distance is *not shown to scale* Observations toward the north and south galactic poles are shown separately. In both hemispheres, the velocity of interstellar gas is shown to be systematically negative with respect to the local standard of rest, although this effect is much more evident toward the north galactic pole than toward the south galactic pole. In the northern galactic hemisphere, highly negative velocity interstellar material (V_{lsr} < -70 Km/s) is commonly found toward targets beyond about 1 Kpc. The southern hemisphere, however, shows little evidence for material with this velocity between 1 and 3 Kpc. Additional observations have been granted by IUE to permit a more conclusive comparison between the hemispheres. Figures 2a and b show the distribution on the sky of those stars in the northern galactic

figure 1

VELOCITY RANGE OF Si II 1260 ABSORPTION
TOWARD HIGH LATITUDE MILKY WAY HALO STARS

VELOCITY$_{lsr}$ (km/s)
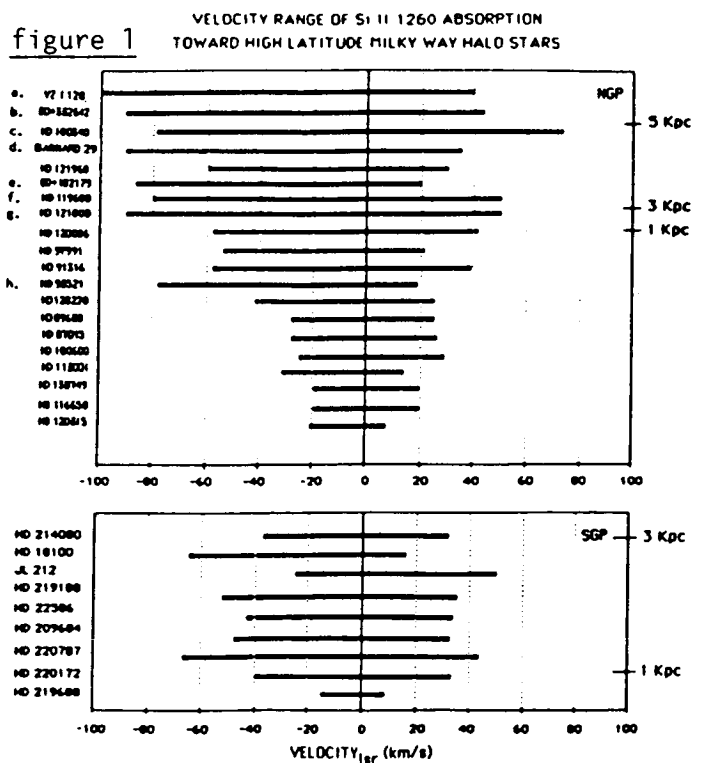
hemisphere which show absorption from highly negative material along the line of sight. The letters correspond to the lettered targets in Figure 1. The plotted positions are superimposed on a map of 21 cm emission from neutral Hydrogen detected by the Bell Laboratory horn survey (Stark, Bally, Linke and Heiles, 1986, in preparation). Contours of emission from material with a velocity in the range of -100 to -85 km/s and -85 to -70 km/s are shown. From these diagrams, it can be seen that targets showing highly negative velocity material in absorption can be found in all four galactic quadrants, with *no obvious correlation* between the widths and the features seen in 21 cm emission over the same velocity range. However, it is interesting that the profiles toward targets g and h do show an obvious two-component structure, while the profiles toward the other targets "grow" smoothly in width as lower column density material is sampled by lines with increasing f-values.

Figure 2a

2b

SBLH NH. -100<V<-85 KM/SEC

SBLH NH. -85<V<-70 KM/SEC
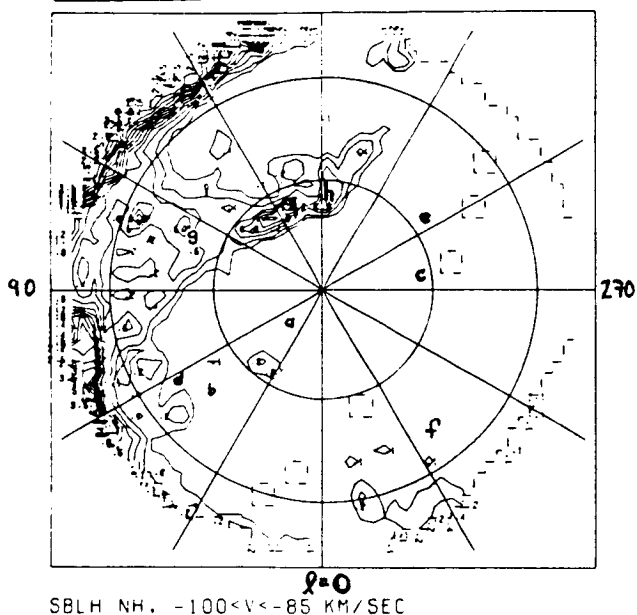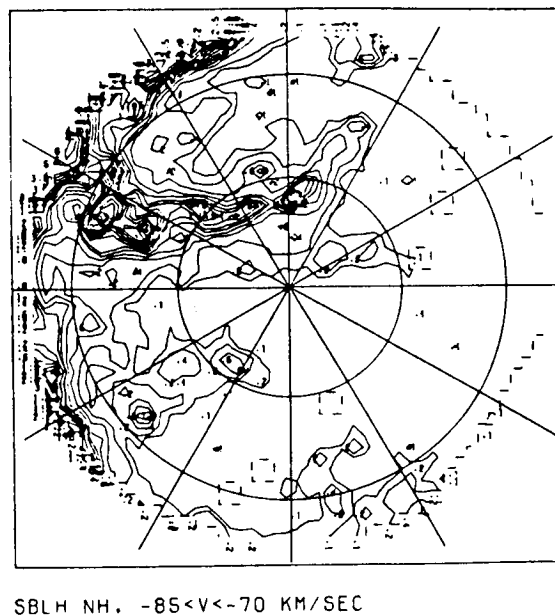
In conclusion, any complete description of halo gas must include gas with two distinctive types of absorbing characteristics:

(a) higher column density material in the form of condensed "clouds" seen over a range of velocities. Distance estimates based on these absorption data show that some of the gas in the emission feature in the second and third quadrants is within z=1.3 kpc, while clouds with more extreme velocities are distributed beyond this distance.

(b) low column density, possibly pervasive material which, in the solar neighborhood, is only encountered at distances beyond 1-3 kpc. This material has a column density that is too low to be detected previously with optical absorption studies.

IRAS OBSERVATIONS OF GIANT MOLECULAR CLOUDS IN THE MILKY WAY

David Mozurkewich
NRL-NRC Cooperative Research Fellow
E. O. Hulburt Center for Space Research
Naval Research Laboratory

and

Harley A. Thronson, Jr.
Wyoming Infrared Observatory
University of Wyoming

The IRAS data base has been used to study infrared radiation from molecular clouds in our galaxy. The sample of clouds was restricted to those with reliably determined molecular masses from large area, multi-isotope CO maps. They were normalized to $X(^{13}CO) = 2 \times 10^{-6}$. Flux densities at $60 \mu m$ and $100 \mu m$ were determined by integrating the flux density within rectangles drawn on the sky flux plates after subtracting a suitable background. The rectangles were chosen to be coextensive with the areas mapped in CO. Color corrections were made and luminosities calculated by assuming the optical depths were proportional to frequency. The flux densities were converted to dust masses with a value for $4a\rho/3Q = .04$ g/cm^2 at $100 \mu m$.

A plot of the infrared luminosity versus the molecular mass is shown in the upper panel. A linear fit to the data, excluding the Rosette (upper left point in both plots), is given by $\log(M_{H_2}) = (.71 + .22) \log(L_{IR}) + 0.53 + .14$ and has a correlation coefficient of 0.81. Formal 2σ uncertainties are quoted. We calculated the stellar mass in each cloud using the Salpeter initial mass function for young clusters with mass cutoffs at 0.1 and 100 $M_\odot$. The mean star formation efficiency in this sample is 0.0?. The efficiency of star formation will be larger if the upper mass limit is lower for some of the objects, particularly the lower mass clouds.

The cloud molecular mass is plotted versus dust mass in the lower panel. The data is fit by $\log(M_{H_2}) = (.70 + .22) \log(M_d) - 3.10 + 0.16$ with a correlation coefficient of 0.84. Again, the Rosette was not included in the fit. The mean gas to dust ratio is 420 with an uncertainty of a factor of two, rather than the commonly adopted value of 100. This supports the usual assertion that the $100 \mu m$ fluxes are only sensitive to the warm dust and hence trace star formation.

These relationships are in good agreement, quantitatively, with the results by Young et al. (1986, Ap. J. 304, 443) for galaxies, supporting the view that the far infrared emission they observed is associated with the molecular gas.
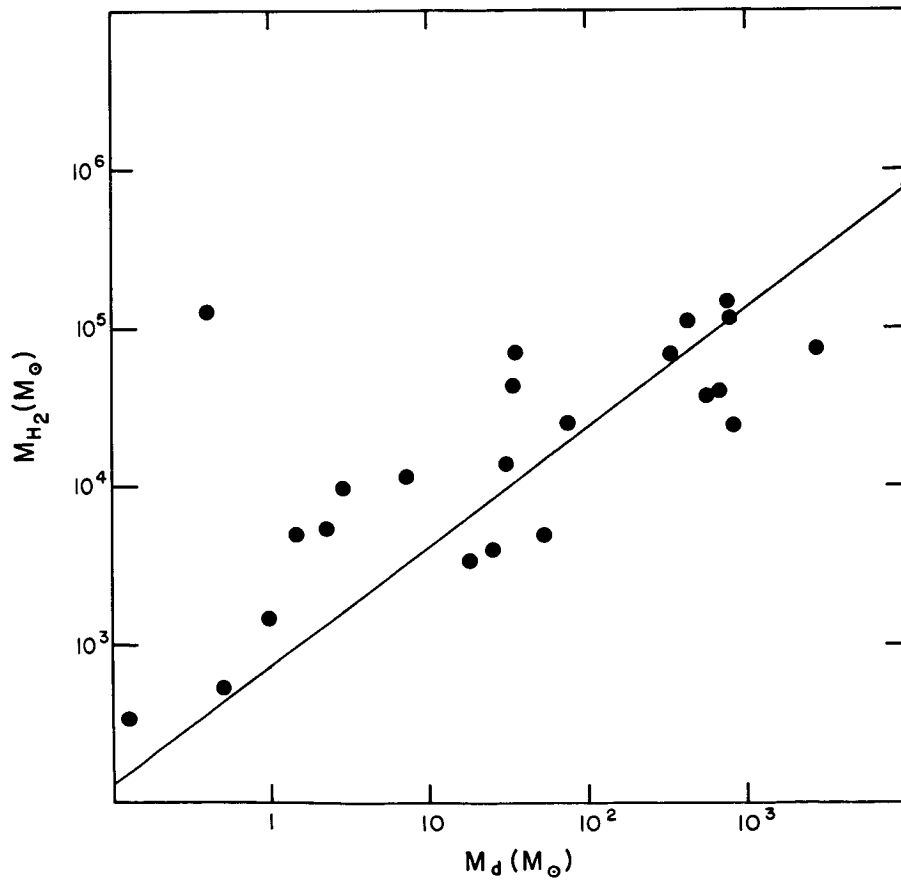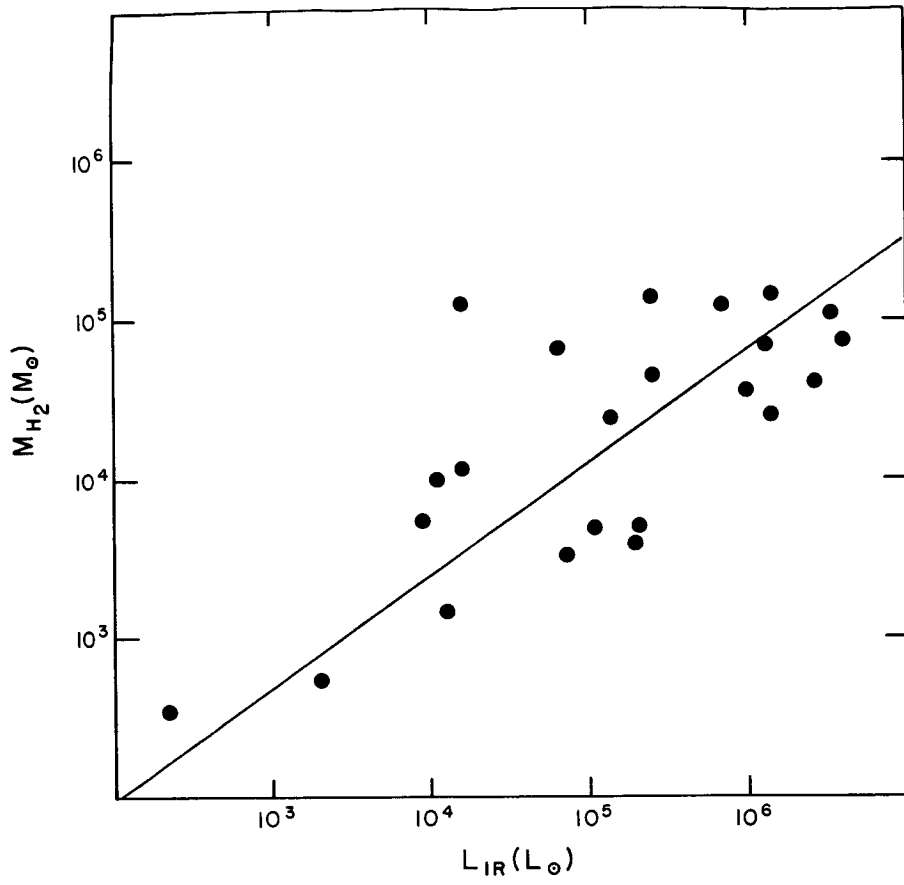
"Spiral Arms and Massive Star Formation: Analysis of the CO Face-on
Pictures of the Galaxy"

D. P. Clemens (Steward Observatory), D. B. Sanders (Caltech),
and N. Z. Scoville (Caltech)

The face-on distribution of molecular gas in the first Galactic
quadrant, derived from the Massachusetts-Stony Brook Galactic Plane CO
Survey (Clemens, Sanders, Scoville 1986), was compared to the Galactic
distribution of giant radio HII regions (see Figure 1 below). The HII
regions were found to preferentially select gas regions of higher than
average density (more than twice the mean) and showed a strong
correlation with the second power of the gas density. Systematic
effects were tested with a Monte Carlo simulated HII region
distribution and found to be negligible.

The 135 HII regions were selected from the radio catalogs of
Downes et al. (1980) and Wink et al. (1982). The HII regions were
required to be within the CO survey l and b limits, within the solar
circle, and not part of the 3 kpc expanding arm. The velocities of
the HII regions were tabulated by the catalog authors and obvious
associations with known objects and H_2CO absorptions were used by them
to assign distances. The distance assignments were here grouped into
two catagories; A) those HII regions with definite distance
assignments (85 objects); and B) those HII regions with less secure
distance assignments and those for which no near-far assignment was
possible (50 objects).

The mean H_2 gas density associated with each of the HII regions
was found by forming the average of the face-on gas properties within
a 300 pc x 300 pc box surrounding each HII region. The $\langle N(H_2) \rangle$, $\langle Z_o \rangle$,
and $\langle dZ \rangle$ values were combined to yield $\langle n(H_2;Z) \rangle$, where the Z used was
appropriate to the HII region.

Additionally, a sample of pseudo-HII region locations was
generated with a Monte Carlo routine. The Monte Carlo HII regions
were chosen to match the R and Z distributions of the real HII
regions, but to have random Galactic azimuth assignments. From this
sample a total of 840 pseudo-HII regions within the survey limits were
tabulated inside of R_o.

The mean molecular hydrogen density found (as averaged over 300
pc) for the (R,Z) Monte Carlo run was 1.21 ± 0.03 H_2 cm^{-3}. However, the
real HII regions gave a higher value of 1.72 ± 0.10 H_2 cm^{-3}. To quantify
the dependence of HII region density on molecular cloud density, the
HII regions were binned according to the value of their associated
molecular gas density. The number of HII regions reaches a peak
around 1-1.5 H_2 cm^{-3}. However, the volume of the Galaxy at each
density shows a strong decrease with increasing density. Thus, the
number of HII regions per unit volume associated with each density
rises from 0 to 4 H_2 cm^{-3}. If the number of HII regions per unit
volume N is assumed to obey a power law dependence with associated
molecular gas density as: $N = c \langle n(H_2;Z) \rangle^{alpha}$, then the slope of the
plot of ln(N) versus $ln(n(H_2;Z))$ (Figure 2, below) indicates the value
of the power index, alpha. The group A sample is characterized by an
alpha of 1.91 ± 0.16. The Monte Carlo value of 1.14 ± 0.05 shows that
although the proper (R,Z) HII region distributions will tend to select
high density gas, a random azimuth assignment selects both lower
density gas and a lower power law on gas density than the real HII

regions.

The power law index relates the star formation efficiency for massive OB stars (those forming giant radio HII regions) to the mean H_2 gas density. A power law index of zero would imply that star formation is uncorrelated with molecular hydrogen clouds; an index of unity (c.f., Young and Scoville 1982) implies that star formation rates depend on no properties other than the presence of molecular gas. However, an index of two (Schmidt 1959; Dopita 1985) implies that other factors, such as cooling or ambient pressure or cloud collisions (Scoville, Sanders, and Clemens 1986) play a role in triggering massive star formation.

References:

Clemens, D.P., Sanders, D.B., and Scoville, N.Z. 1986, Ap. J., submitted.

Dopita, M.A. 1985, Ap. J. (Letters), 295, L5.

Downes, D., Wilson, T.L., Beiging, J., and Wink, J. 1980, Astr.Ap. Suppl., 40, 379.

Schmidt, M. 1959, Ap. J., 129, 243.

Scoville, N.Z., Sanders, D.B., and Clemens, D.P. 1986, Ap. J. (Letters), submitted.

Wink, J.E., Altenhoff, W.J., and Mezger, P.G. 1982, Astr. Ap., 108, 227.

Young, J.S., and Scoville, N.Z. 1982, Ap. J. (Letters) 260, L11.
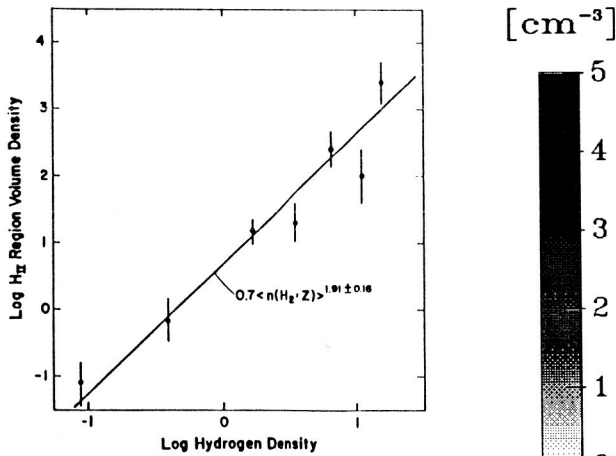
Figure 2: Log HII region volume density vs. molecular hydrogen gas density. Straight line has slope alpha = 1.91±0.16.
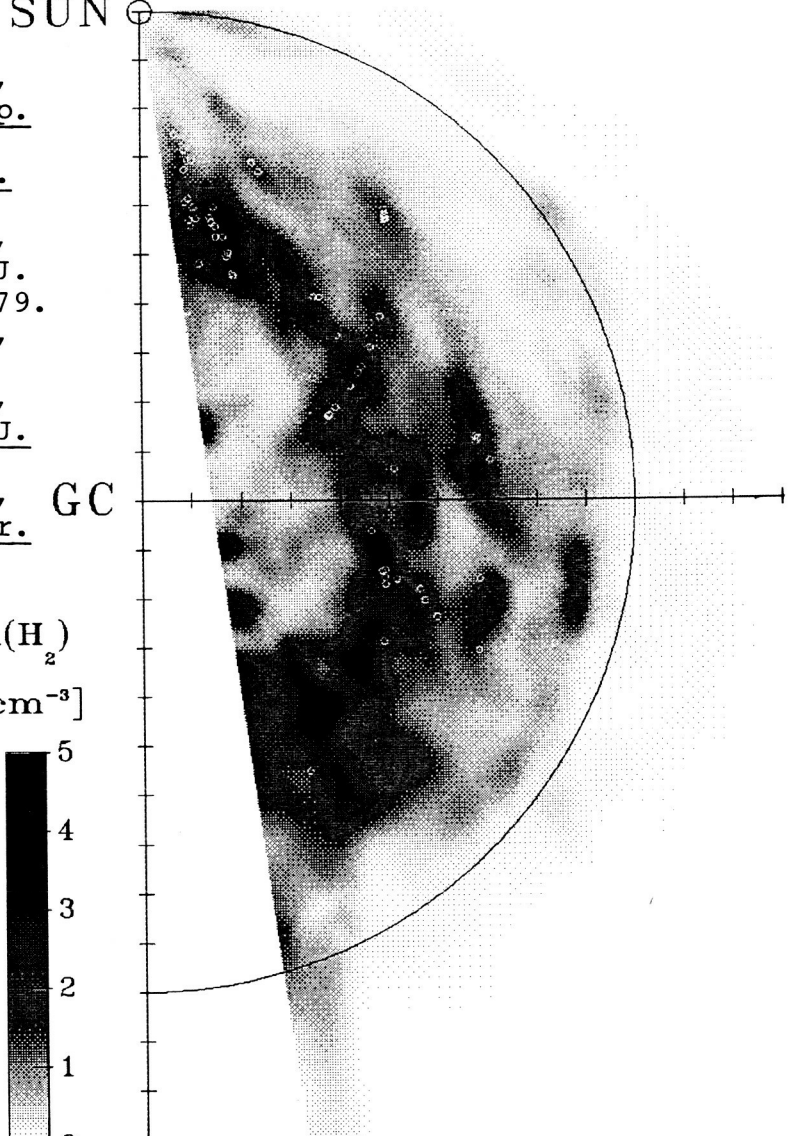
Figure 1: Face-on view of peak molecular hydrogen volume density for the first quadrant as viewed from the North Galactic Pole. Small white circles indicate group A HII region locations.

THE VELOCITY DISPERSION OF THE GIANT MOLECULAR CLOUDS: A VISCOUS ORIGIN

Chanda J. Jog (University of Virginia) and
Jeremiah P. Ostriker (Princeton University Observatory)

We propose the energy source and study the details of the acceleration mechanism for the random motion of the Giant Molecular Clouds (GMCs) in the Galaxy.

Introduction

The observations of interstellar cloud motion show that the cloud velocity dispersion is nearly constant, to within a factor of 2, for clouds covering at least three orders of magnitude in mass. For example, the GMCs with typical masses of ~ 5×10^5 $M_\odot$ have a one-dimensional, planar, cloud-cloud, random velocity dispersion of ~ 3-7 km s^{-1} (Clemens 1985; Stark 1984). The HI clouds, of ~ 400 $M_\odot$ each, on the other hand, have a typical one-dimensional velocity dispersion of ~ 6 km s^{-1} (Spitzer 1978). Clearly, the clouds are not in kinetic energy equipartition.

The spatial distribution of the GMCs in the galactic disk is not that of an isolated, 3-D system; rather, the GMCs exhibit a very thin disk (~ nearly a monolayer) distribution; with the ratio of the diameter of a typical GMC to the vertical scale-height of the GMC distribution being ~ 50 pc/150 pc = 0.3.

The supernova shocks, which can accelerate the low mass clouds, are extremely ineffective in accelerating the GMCs because of the much larger mass/area ratio for the GMCs.

The above points suggest that the GMCs do not constitute an isolated, 3-D system - rather, they indicate that the dynamics of the GMCs is mainly determined by the fact that they are located in a differentially rotating galactic disk, and that, as for particles in planetary rings, "viscosity" is the primary energy input.

Specifically, we propose that gravitational scattering of the massive clouds off each other in the differentially rotating galactic disk constitutes an effective gravitational viscosity; which causes an increase in the random kinetic energy of the GMCs at the expense of their ordered, rotational kinetic energy.

This mechanism is developed for the first time in this paper. In the problem of the planetary rings on the other hand, the gravitational interaction among the particles is negligible and in that case physical collisions account for the viscosity (see e.g., Goldreich and Tremaine, 1982).

Energy Input Due to the Gravitational Viscosity

We calculate the rate of increase, due to the gravitational viscosity, of the random kinetic energy of a test GMC with a non-zero initial random velocity. As long as this random velocity is much less than the rotational speed in the disk; the unperturbed motion in the galactic disk of such a test cloud is described by an epicycle, which can be represented as a coupled, two-dimensional harmonic oscillator.

Since an encounter between such a test cloud and a passing field cloud lasts for ~ an epicyclic time, one cannot evaluate the effects of the encounter under the

impulse approximation. Instead, we treat the encounter between the test cloud and a field cloud in the sheared disk as a perturbed, coupled, two-dimensional harmonic oscillator problem, with the gravitational interaction between the two clouds being the time-dependent perturbation force. In order to obtain the change in the energy of the test cloud per encounter, one has to evaluate the change in the total energy of the epicyclic motion of the test cloud. A major portion of this paper deals with this calculation. Assuming the subsequent encounters to be independent, one can then obtain the net rate of increase of the random kinetic energy of the test cloud.

The Steady-State Cloud Velocity Dispersion

In a steady-state, the rate of energy input from the viscosity due to gravitational and physical interactions among the GMCs in the differentially rotating galactic disk equals the rate of energy loss due to the inelastic physical collisions among the GMCs; this yields the value for the steady-state cloud velocity dispersion.

The main functional dependence of the resulting steady-state cloud velocity dispersion is $\sim [(Gm/r) \kappa H]^{1/3}$; where m and r are the cloud mass and cloud radius respectively, κ is the epicyclic frequency and H is the total vertical scale-height of the gas distribution. Note that this result is independent of the cloud number density and it depends only weakly (through κ) on the galactocentric radial distance of a cloud. Also note that the cloud velocity dispersion is an increasing function of (m/r) – this point clearly underlines the gravitational viscous nature of the cloud acceleration mechanism considered in this paper.

For the typical GMCs, each of mass $\sim 5 \times 10^5$ $M_\odot$, and located between the galactocentric radii 4 to 9 kpc in the Galaxy; the resulting one-dimensional cloud velocity dispersion is $\sim$ 4-6 km s^{-1}, in good agreement with the observed values of the same. The gravitational viscosity, therefore, provides the main energy input for the random motion of the GMCs in the Galaxy.

Discussion

In the viscous acceleration mechanism, the ultimate energy source is the rotational kinetic energy of the clouds in the disk. The fraction of the rotational kinetic energy lost in supporting inelastic cloud motions for $\sim$ ten billion years is small $\sim$ 0.1. Thus the rotational kinetic energy of the GMCs proves to be more than adequate for the long term support of their random motion.

As a result of the viscous interaction among the clouds, the clouds drift inwards with a local velocity of $\sim$ 0.3 km s^{-1}, thus depleting gas within the region of R $\leq$ 3 kpc in the Galaxy in $\sim$ ten billion years. This is in rough agreement with the observed minimum or the "hole" in the galactic CO distribution. The detailed analysis for this will be presented in a subsequent paper.

Thus, the dynamics as well as the radial distribution in the Galaxy of the GMCs is determined by their gravitational viscous interaction, which operates because of their location in the differentially rotating galactic disk.

References

Clemens, D.P.: 1985, Ap. J., 295, 422.
Goldreich, P. and Tremaine, S. D.: 1982, Ann. Rev. Astr. Ap., 20, 249.
Spitzer, L.: 1978, "Physical Processes in the Interstellar Medium," (New York: Wiley).
Stark, A.A.: 1984, Ap. J., 281, 624.

LOCAL INTERSTELLAR GASDYNAMICAL STABILITY IN SPIRAL ARM FLOW

Steven A. Balbus
Virginia Institute for Theoretical Astronomy

The stability of two-dimensional interstellar gas flow passing through a spiral potential has been investigated. The background flow is assumed to move in a tightly wound potential, which may be regarded as external or self-generated. The unperturbed flow, which may be time dependent, is self-gravitating and satisfies the Roberts (1969) equations of motion. A polytropic, single-fluid assumption has been used. Magnetic effects are not considered. The motivation behind this work is to try to understand how much of the diversity of spiral arm morphology can be understood by large scale gas dynamical processes alone. To this end, we suggest that "spurring and feathering", and forming molecular cloud complexes may be closely related in the sense of having dynamically similar origins.

The classic study of Goldreich and Lynden-Bell (1965; hereafter GLB) investigated the stability of a sheared infinite sheet (or slab) to general two-dimensional perturbations in the plane of the sheet. The motivation for this study was to better understand spiral arm formation in disk galaxies. In essence, the current investigation generalizes GLB to include arbitrary expansion and contraction of the sheet in such a way that specific angular momentum is conserved. These volume changes correspond physically to the compression and reexpansion of the fluid as it moves through the spiral arm region of the disk. The small wavelength perturbations are sensitive only to local flow conditions, and a fluid element behaves to leading order as though it were moving in an expanding (or contracting) sheared sheet. Thus, one asymptotic limit of our study is the GLB equation; another limit corresponds to the case studied by Balbus and Cowie (1985) in which the wavenumber points along the expansion velocity and is not sheared with the flow, but diminishes as the flow expands.

GLB found that perturbations which were stable to a Jeans type of gravitational collapse could nevertheless grow dramatically by the "swing amplification" mechanism (Toomre 1981). This amplifier works because the shear flow, which decreases outward in this problem, and the epicyclic motion, which is always retrograde, conspire to kinematically prolong the compressive phase of perturbative oscillation. This gives self-gravity an extended opportunity to amplify the compression. Therefore, in general nonaxisymmetric perturbations grow considerably more rapidly than their axisymmetric counterparts.

The situation is usually quite the opposite in the compressed gas regions of spiral arms. The reason is that locally the shear flow may be increasing outward. This is a simple consequence of angular momentum conservation in the compressed gas. In fact, in general it is not difficult to show that within the assumptions of the tight winding approximation,

$$\frac{d \ln \Omega}{d \ln r} = \frac{\kappa^2}{2\Omega^2} \left(\frac{\sigma}{2}\right) - 1 ,$$

where r is the radial location, Ω is the total angular velocity (including the small but rapidly changing piece induced by the spiral potential), κ is the epicyclic frequency, and σ is the density enhancement at r. For a flat rotation curve, if σ exceeds a modest factor of two, the shear flow will locally increase outward.

Now the swing amplification mechanism runs in reverse. The shear field and the retrograde epicyclic motion conspire to shorten the compressive phase of the oscillation, giving self-gravity <u>less</u> of a chance to amplify the perturbation. The result: wave numbers initially perpendicular to the arm (i.e. nearly radial) grow the fastest. This gives rise to extended structure preferentially along the arm. If the perturbation rapidly becomes non-linear and drops from the flow before the background shear flow draws it out from the arm, then regularly spaced structure along the arm is expected. The non-linear outcome of such large initial perturbations may be molecular complexes because of the rapid tendency to form molecules in cloud collisions (Smith 1980), of which there would be proportionately more compared with smaller initial amplitudes. (Such a model might fashionably be called "biased molecular cloud formation".) The smaller initial amplitude perturbations have smaller internal cloud collision rates, and plausibly less molecular gas. They take longer to become nonlinear and drop from the flow. Accordingly, they are more profoundly influenced by the reversed shear field near the arm. A trailing elongated perturbation would be drawn out away from the spiral arm on the convex side of the pattern. The downstream trailing portion of the perturbation would soon find itself in a region of normal (decreasing outward) shear flow, while the upstream leading portion of the perturbation would be in a region of reversed shear. The characteristic spur morphology would be shaped by such a flow environment. "Feathering" would result when the perturbation itself becomes nonlinear and repeats this process in the flow passing over it. In this manner, we suggest that molecular clouds and spiral arm features may be dynamically related.

The mathematical underpinnings of these ideas are presented in Balbus (1986).

REFERENCES

Balbus, S.A. 1986, preprint.
Balbus, S.A., and Cowie, L.L. 1985, <u>Ap. J.</u>, **297**, 61.
Goldreich P., and Lynden-Bell, D. 1965, <u>M.N.R.A.S.</u>, **130**, 125.
Roberts, W.W. 1969, <u>Ap. J.</u>, **158**, 123.
Smith, J. 1980, <u>Ap. J.</u>, **238**, 842.
Toomre, A. 1981, in <u>The Structure and Evolution of Normal Galaxies</u>, ed. S.M. Fall and D. Lynden-Bell (London: Cambridge University Press), p. 111.

The $^{32}S/^{33}S$ Abundance As A Function Of Galactocentric Radius In The Milky Way

Matthew A. Greenhouse and Harley A. Thronson, Jr.

Wyoming Infrared Observatory, University of Wyoming, Laramie, WY 82071_

Astration of heavy elements by the stars of the Milky Way form a fossil record which may preserve spacial distribution of the mass function for the stars in the galaxy. Sulfur is among the last common element for which the relative abundance of its various isotopes have yet to be completely measured within our galaxy. Explosive oxygen burning in massive stars is thought to be the process which dominates sulfur production within stars (Arnett et al. 1970; Woosley et al. 1973; Thielemann et al. 1985). These models predict that the various isotopes (^{32}S, ^{33}S, ^{34}S) are formed in relative abundance which depend strongly upon the mass of the parent star. This relative abundance is thought to be unaffected by subsequent stellar processing since all important sinks of sulfur destroy it without regard for isotopic form. Hence the spacial variation of the mass function (MF) can be studied by measuring the abundance variation of sulfur isotopes in the galaxy provided that the product yields for these isotopes are known accurately as a function of stellar mass.

Here we report the measurement of $[^{32}S]/[^{33}S]$ abundance ratio as a function of galactic radius. The $J = 2 \to 1$ lines of $^{13}C^{32}S$ and $^{12}C^{33}S$ at 92.49 and 97.17 GHz respectively were measured in eleven sources at various galactic radii during 1984 October and 1985 June using the cooled-Cassegrain Schottky diode mixer at the NRAO 12 m antenna on Kitt Peak, Arizona.[1] All data was taken with a 60" FWHM beam, position switching 15' in cross elevation. The spectra were dispersed in a 128 channel filter bank of 250 and 500 kHz resolution. In all cases the data from the same filter bank was used for both molecular species. For all sources except IRC +10°216, the two lines were observed sequentially at the same air mass on either side of the meridian transit. Furthermore, each object was observed at least on two separate nights. For the objects Sgr B2 and Sgr A the data in Table 1 and Fig. 1 is the weighted mean of the observations on different nights. Only the best nights data is presented for the other objects. The data for the evolved star IRC +10°216 was taken on separate nights and probably has an additional ±20% systematic uncertainty. Relative calibration was obtained by using a focal plane chopper wheel (Ulich and Haas 1976) while absolute calibration was found from periodic observations of Orion A taking T_R^* as 0.67 K and 0.39 K for $^{13}C^{32}S$ and $^{12}C^{33}S$ respectively. Peak antenna temperatures on this calibration object were repeatable to ±10% over the length of the observing run.

The results of the observation are presented in Table 1 along with the adopted values for $[^{12}C]/[^{13}C]$. Brightnesses for $^{13}C^{32}S$ were calculated by integrating over its seven fine structure lines. We assume that both these transitions are optically thin in all sources so that their corresponding molecular abundances are given by $\int \nu^{-2} T_R^*(CS) \, d\nu$.

Work is in progress to use this data to test current models of sulfur synthesis in high mass stars by requiring that their isotope product yields give physically reasonable MFs when compared to our measured abundances at each radius.

TABLE 1

Object	α(1950)	δ(1950)	R [kpc]	$\int T_R^*(^{13}CS)dv$ [K·km s^{-1}]	$\int T_R^*(C^{33}S)dv$ [K·km s^{-1}]	$\frac{[^{13}CS]}{[C^{33}S]}$	$\frac{[^{12}C]}{[^{13}C]}$	$\frac{[^{32}S]}{[^{33}S]}$
W3(OH)	2 23 17	61 39 00	12.2	1.4 ± 0.2	1.0 ± 0.2	1.4 ± 0.3	99 ± 17	137 ± 30
Ori A	5 32 47	-5 24 30	10.5	3.6 ± 0.2	3.1 ± 0.2	1.2 ± 0.1	50 ± 4	60 ± 7
Ori B	5 39 12	-1 55 42	11.0	1.6 ± 0.2	2.1 ± 0.2	0.8 ± 0.1	56 ± 8	45 ± 9
NGC 2264	6 38 25	9 32 29	11.1	1.6 ± 0.1	0.6 ± 0.1	2.8 ± 0.5	101 ± 22	283 ± 60
IRC+10°216	9 45 15	13 30 45	10.0	2.4 ± 0.3	0.1 ± 0.3	≥3.4 (2σ)		
Sgr A	17 42 42	-28 59 00	0	12.4 ± 0.5	4.6 ± 0.3	2.7 ± 0.2	26 ± 5	70 ± 14
Sgr B2	17 44 11	-28 22 30	0.1	16.8 ± 0.4	6.9 ± 0.4	2.4 ± 0.2	23 ± 3	55 ± 9
W33	18 11 19	-17 56 46	5.7	7.5 ± 0.3	4.9 ± 0.4	1.5 ± 0.1	42 ± 4	63 ± 7
M17	18 17 27	-16 14 54	8.0	4.5 ± 0.2	2.6 ± 0.3	1.7 ± 0.2	85 ± 14	145 ± 29
DR 21	20 37 13	42 08 51	9.9	1.4 ± 0.1	1.6 ± 0.2	0.9 ± 0.1	73 ± 11	66 ± 12
NGC 7538	23 11 37	61 12 00	12.7	1.6 ± 0.15	0.8 ± 0.2	2.0 ± 0.5	77 ± 21	154 ± 57

Notes: quoted uncertainties are ±1σ rms internal; systematic uncertainties are ±20%.

$$\frac{[^{13}CS]}{[C^{33}S]} = \frac{\int \nu^{-2}T_R^*(^{13}CS)dv}{\int \nu^{-2}T_R^*(C^{33}S)dv} , \qquad \frac{[^{32}S]}{[^{33}S]} : \frac{[^{13}CS]}{[C^{33}S]} \frac{[^{12}C]}{[^{13}C]}$$
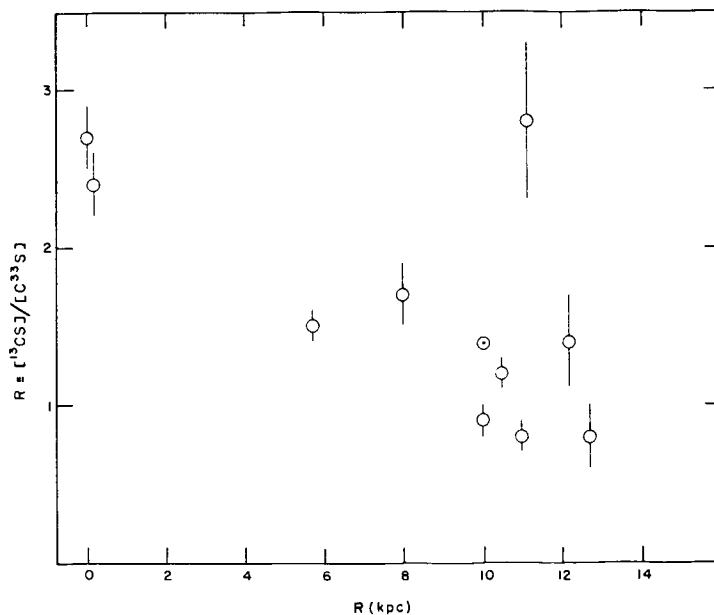
*Langer et al. 1984

Figure 1

REFERENCES

Arnett, W. D., and Clayton, D. D. 1970, Nature, 227, 780.
Langer, W. D. et al. 1984, Ap. J., 277, 581.
Ulich, B. L., and Haas, R. W. 1976, Ap. J. Suppl., 30, 247.
Woosley, S. E., Arnett, W. D., and Clayton, D. D. 1973, Ap. J. Suppl., 26, 231.

IS OH ABUNDANCE ENHANCED IN TIDALLY DISTORTED GALAXIES?

Joan T. Schmelz
Arecibo Observatory

An extensive survey of 240 galaxies for hydroxyl absorption has been completed using the Arecibo Observatory; the results can be found in Schmelz et al. (1986). These galaxies along with those observed by Rickard, Bania, and Turner (1982), and Baan et al. (1985) were used to compile a sample to test for statistical correlations between the optical depth of the 1667 MHz hydroxyl line and various parameters of the parent galaxy. To be included in the sample, the radio flux density of the galaxy at 1667 MHz had to be between 20 mJy and 1000 mJy and the galactic declination between 0° and 38°. Since this sample contains mainly non-detections, statistical methods for astronomical data with upper limits as described by Isobe, Feigelson, and Nelson (1986) were used to obtain correlation and regression information.

Preliminary studies indicate a strong correlation between OH optical depth and infrared to blue luminosity ratio (L_{IR}/L_B), where the infrared data were obtained from the Cataloged Galaxies and Quasars Observed in the IRAS Survey (Lonsdale et al. 1985). A second correlation is seen between the optical depth of the 1667 MHz line and galactic type, where a number from 1 to 15 (Elliptical to peculiar, distorted, or interacting) has been assigned to each galaxy. So, stable, isolated galaxies tend not to have detectable hydroxyl. On the other hand, galaxies with more gas and dust, galaxies with a more peculiar or distorted appearance, and galaxies which are more tidally interacting tend to have much more detectable OH.

These findings could indicate that these dusty, peculiar, distorted, and interacting galaxies could be the site of large amounts of shocked material where OH is likely to form. Hence, the hydroxyl abundance could be enhanced in these regions of shocked material making the detection of OH in these tidally distorted galaxies much more likely.

Baan, W.A., Haschick, A.D. Buckley, D., and Schmelz, J.T. 1985, Ap.J., 293, 394.

Isobe, T., Feigelson, E.D., and Nelson, P.I. 1986, Ap.J., in press.

Lonsdale, C.J., Helou, G., Good, J.C., and Rice, W. 1985, Catalogued Galaxies and Quasars Observed in the IRAS Survey.

Rickard, L.J, Bania, T.M., and Turner, B.E., 1982, Ap.J., 252, 147.

Schmelz, J.T., Baan, W.A., Haschick, A.D., and Eder, J., 1986, A.J., submitted.

6 CM OH ABSORPTION IN MEGAMASER GALAXIES

C. Henkel, R. Güsten
MPIfR, Auf dem Hügel 69
5300 Bonn 1, F.R.G.

and

W. Baan
Arecibo, P.O. Box 995
PR 00613
U.S.A.

Absorption in the $^2\Pi_{1/2}$ J = 1/2 Λ doublet transitions of OH, 182 K above the ground state, is detected in the megamaser galaxies IC 4553 (Arp 220), MK 231, MK 273, NGC 3690, and IRAS 17208-0014. The 4660, 4751, and 4766 MHz lines have intensity ratios moderately deviating from the LTE values (1:2:1). The OH rotational temperatures appear to be close to the temperature of the dust, ~60 K. The common characteristics of these galaxies (absence of 6 cm inversion, the optical depths, the infrared properties, the systematic trends in the line parameters, and the rotational temperatures) all suggest that the same pump process is responsible for the 18 cm line inversion in the five megamaser sources. The inversion is probably not due to an excitation mechanism involving collisions with HI or H_2. While excitation via photodissociation of H_2O cannot entirely be ruled out, we consider the most likely mechanism to be a combination of the intense FIR field (populating higher excited OH rotational states) and the non-thermal radiation from the nuclei of the parent galaxies (affecting the excitation within the Λ-doublets). According to an LVG model of the OH excitation of IC4553, the OH-cloud(s) have to be located close, within 200-300 pc, to the center of the galaxy. The excitation of the individual 18 cm lines depends critically on the effective background radiation field and hence on the galactocentric distance of the masing clump. With increasing distance first the 1720 MHz and then the 18 cm main line inversion is quenched, while 1612 MHz inversion is obtained up to ~600 pc. The 1612 MHz satellite line is predicted to be more intense than the 1720 MHz line. A critical test for our excitation model is to observe the $^2\Pi_{3/2}$ J = 5/2 Λ-doublet transitions which are predicted to be detectable in absorption.

A more detailed discussion of the data and their interpretation is given in Astron. Astr. (in press).

MOLECULAR HYDROGEN IN THE YOUNG STARBURST IN NGC 253

G. H. Rieke, M. J. Lebofsky, and C. E. Walker
Steward Observatory, University of Arizona

Abstract

We have observed shocked molecular hydrogen around the nucleus of the nearby galaxy, NGC 253. This galaxy has a relatively modest luminosity ($\sim 3 \times 10^{10}$ L$_\odot$) and appears to have no distortions or companions that would indicate a possible interaction. The energy of the galaxy appears to be derived primarily from a starburst (Rieke and Low 1975; Wynn-Williams et el. 1979; Rieke et al. 1980; Klein et al 1983; Beck and Beckwith 1984; Fabbiano and Trinchieri 1984). Thus, our observations have caused us to examine the starburst process in some detail to identify how the molecular hydrogen is excited.

We propose that the molecular hydrogen emission is produced by collisions of dense molecular clouds accelerated by supernovae explosions. Within the nucleus, this process occurs early in the life of the starburst. We suggest a sequence of nuclear starburst development; examples along this sequence from young to old would include NGC 253, M82, NGC 1097, and M31.

REFERENCES

Beck, S. C., and Beckwith, S. V. 1984, MNRAS, 207, 671.

Fabbiano, G., and Trinchieri, G. 1984, ApJ, 286, 491.

Klein, U., Urbanik, M., Beck, R., and Wielebinski, R. 1983, Astr. Ap., 127, 177.

Rieke, G. H., Cutri, R. M., Black, J. H., Kailey, W. F., McAlary, C. W., Lebofsky, M. J., and Elston, R. 1985, ApJ, 290, 116.

Rieke, G. H., and Low, F. J. 1975, ApJ, 197, 17.

WynnWilliams, C. G., Becklin, E. E., Mathews, K., and Neugebauer, G. 1979, MNRAS, 189, 163.

CHEMICAL EVOLUTION IN SPIRAL AND IRREGULAR GALAXIES

S. Torres-Peimbert
Instituto de Astronomía
Universidad Nacional Autónoma de México
Apartado Postal 70-264, México 04510 D. F., México

A brief review of models of chemical evolution of the interstellar medium in our galaxy and other galaxies is presented. These models predict the time variation and radial dependence of chemical composition in the gas as function of the input parameters: initial mass function, stellar birth rate, chemical composition of mass lost by stars during their evolution (yields), and the existence of large scale mass flows, like infall from the halo, outflow to the intergalactic medium or radial flows within a galaxy.

At present there is a considerable wealth of observational data on the composition of HII regions in spiral and irregular galaxies to constrain the models. Comparisons are made between theory and the observed physical conditions. In particular, studies of helium, carbon, nitrogen and oxygen abundances are reviewed.

In many molecular clouds the information we have on the amount of H_2 is derived from the observed CO column density, and a standard CO/H_2 ratio derived for the solar neighborhood. Chemical evolution models and the observed variations in O/H and N/O values, point out to the need to include these results in a CO/H_2 relation that should be, at least, a function of the O/H ratio. This aspect is also discussed.

III.   INTERSTELLAR GRAINS

A. Polycyclic Aromatic Hydrocarbons (PAHs)

IDENTIFICATION OF POLYCYCLIC AROMATIC HYDROCARBONS

A. Léger and L. d'Hendecourt
Groupe de Physique des Solides de l'Ecole Normale Supérieure
Université Paris 7, Tour 23 - 2 place Jussieu
75251 PARIS CEDEX 05 - FRANCE

ABSTRACT. The nature of the Very Small Grains evidenced by K. Sellgren (1985) is discussed. Their stability suggests that they are graphitic material and specifically Polycyclic Aromatic Hydrocarbons (PAHs). The expected IR emission of a typical PAH, coronene, gives an impressive spectroscopic agreement with the five observed "Unidentified IR Emission Features", leading to an unambiguous identification. Those PAHs are the most abundant organic molecules detected to this date ($f \sim 10^{-5}$).

1. NATURE OF VERY SMALL GRAINS

1.1. Refractory grains... which are large molecules

Sellgren (1984, 1985) has shown strong evidence for quantum heating of Very Small Grains. To survive heating up to temperatures about 1000 K these particles must be refractory. Léger and Puget (1984) have shown that ices and silicates would be sublimated whereas graphitic grains could resist. Graphite is made of weakly bound planes. Therefore frequently heated graphitic clusters are likely planar. In addition, the presence of ambient H atoms and dangling bonds on peripherical C atoms (Duley and Williams, 1981) suggest that they are large Polycyclic Aromatic Hydrocarbon (PAH) molecules.

2. SPECTROSCOPIC IDENTIFICATION

Léger and Puget (1984) derived the expected IR emission spectrum of such free molecules using the laboratory measured absorption of a typical large PAH: coronene. They found an impressive agreement with the so-called "Unidentified IR Emission Features" at 3.28 - 6.2 - 7.7 - 8.6 - 11.3 μm (Fig. 1), a similar agreement is obtained with other large pericondensed PAHs. This proposition can also solve the puzzle of the *high efficiency of the conversion - incoming UV/outcoming IR -* because when the energy is absorbed by a free flyer molecule and degraded into vibrational energy it is entirely re-radiated in the IR.

From the point of view of the Analytic Chemistry *the presence of some bands (3.28 - 6.2 and 11.3 µm) are highly characteristic of PAHs* (Bellamy, 1966) *and leaves little doubt on their identification* in the numerous objects where the bands are observed.

3. THE MOST ABUNDANT ORGANIC MOLECULES DETECTED IN SPACE

The abundance of PAHs can be derived from the relative emitted fluxes in FIR (large grains) and near-mid IR (transient heating of PAHs). One finds that few percent of the cosmic C is needed in those PAHs molecules. This brings PAHS to the level of *very abundant detected cosmic molecules, the most abundant organic ones* (see Table).

Figure 1 : Observed IR emission from HD 44179 (adapted from Russell et al. Ap. J. **220**, 568) and expected emission from coronene heated at 600 K.

These molecules have been unrecognized for a long time because they have no clear signature in the radiofrequency domain.

The presence of those PAHs may have many consequences: (1) if they are present in the Diffuse Interstellar Medium as well as in more irradiated regions where they have been detected, they can explain the strong unexpected 12 µm emission of the IRAS Cirrus. Spectroscopy of these clouds should give us the answer ; (2) they can play a role in the formation of H_2 as their geometrical cross section is larger than that of ordinary grains ; (3) they are attractive candidates for the Diffuse Interstellar Bands mystery in the Visible.

molecule	$f = $ atoms/n_H
H_2	~ 1
CO	10^{-4}
PAHs	10^{-5}
HCN H_2CO...	$\stackrel{<}{\sim} 10^{-7}$
$HC_{11}N$	10^{-10}

REFERENCES

- Bellamy L.J., 1966 : IR Spectra of Complex Molecules, Wiley.
- Duley W.W. and Williams D.A., 1981 : MNRAS **196**, 269.
- Léger A.; Puget J.L., 1984 : Astr. & Astrophys. **137**, L5.
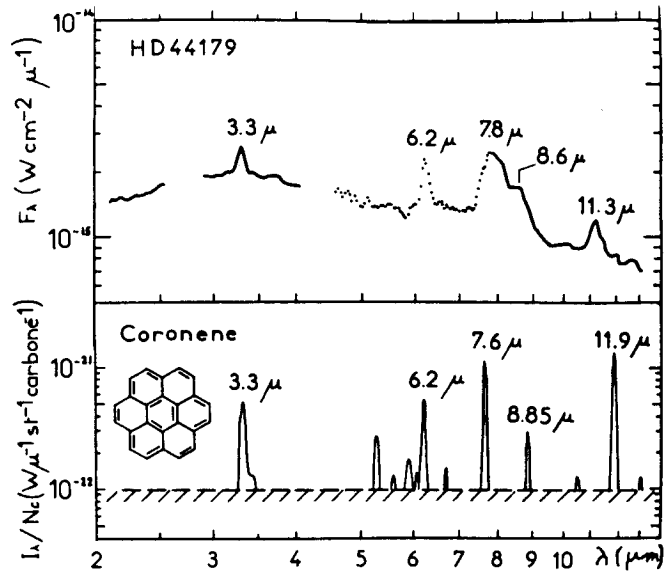- Sellgren K., 1984 : Ap. J. **277**, 623.

THE POSSIBLE EXISTENCE OF INTERSTELLAR POLYCYCLIC AROMATIC HYDROCARBONS (PAHs) IN COLLECTED INTERPLANETARY DUST PARTICLES

Scott A. Sandford
NASA/Ames Research Center
Moffett Field, California 94035

Extraterrestrial dust particles which are 3-50 microns in size are routinely collected in the stratosphere and are now available for general laboratory study (Brownlee et al., 1977; Walker, 1985). These grains represent true interplanetary dust particles (IDPs). The particles have been studied using a number of analytical techniques, including transmission and scanning electron microscopy, which provides morphological and mineralogical information down to scales on the order of 100 angstroms; noble gas and secondary ion mass spectrometry, which can be used to study elemental and isotopic abundances; and infrared transmission spectroscopy, which provides information about the molecular structures present. The study of IDPs is of great interest since they may contain "primitive" interstellar material that has been protected from alteration since the formation of the solar system.

IDPs are generally found to be of one of two varieties, either hydrous or anhydrous (Sandford and Walker, 1985; Bradley and Brownlee, 1986). Both types have "chondritic" elemental abundances and contain carbon as an important component. The hydrous IDPs tend to be compact objects that consist largely of layer-lattice silicate minerals like smectites and serpentines. The anhydrous particles tend to be more porous and appear to be mechanical mixtures of submicron silicate grains (mostly pyroxene and olivine) that are imbedded in an amorphous matrix. Both types of IDPs contain a wide variety of disequilibrated mineral components, implying that the particles have not been seriously altered since their formation.

This contribution will address issues associated with the carbon containing components of IDPs which occur in a variety of physical forms (Bradley et al., 1984), including amorphous mantles and matrix material. The amorphous material is not elemental carbon, but contains minor amounts of oxygen and nitrogen, suggesting the presence of more complex compounds, possibly in the form of hydrocarbons. The presence of hydrocarbons within the IDPs is suggested by the existence of a weak 3.4 micron absorption feature in the infrared spectra of some of these particles (Sandford and Walker, 1985), and the presence of weak bands in the 5-8 micron region of a spectrum taken from an IDP acid residue (Sandford, 1986). The exact form of the hydrocarbon phase(s) in IDPs is not presently known.

The amount of material in each IDP is small (about 1-10 ng), precluding the chemical techniques normally used to analyze carbonaceous samples. If the hydrocarbons in IDPs are similar to those found in meteorite acid residues, they consist of a complex polymer with a bridged aromatic structure and functional groups like COOH, OH, and CO (Hayatsu et al., 1977). Many of the meteorite acid residues also exhibit deuterium enrichments (Yang and Epstein, 1983) similar to those seen in the IDPs (McKeegan et al., 1985). In the IDPs, these deuterium enrichments are found to be correlated with the presence of isotopically normal carbon, implying a hydrocarbon carrier.

It is useful to compare the observed properties of the hydrocarbon phase in IDPs with those expected for polycyclic aromatic hydrocarbons (PAHs), since these molecules may be present in the interstellar medium (Leger and Puget, 1984; Allamandola et al., 1985) and may act as the "building blocks" from which the meteoritic polymer is formed. Despite the lack of knowledge of the

exact form of the hydrocarbons in IDPs, there are three areas where the consistency of this possibility can be checked.

First, the vibrational spectra of IDPs can be compared to those attributed to interstellar PAHs. Unfortunately, the infrared spectra of IDPs are dominated by silicate mineral bands and no strong evidence for the presence of PAHs in whole particle spectra has been seen (Sandford and Walker, 1985). The Raman spectra of IDPs, however, are dominated by features at 6.2 and 7.6 microns that are strikingly similar in position and profile to the most intense emission bands attributed to PAHs in the interstellar medium (Allamandola et al., 1985; B. Wopenka, private communication). The source of the bands in the IDPs is believed to be the amorphous, low-Z material that surrounds the particles' constituent mineral grains. In addition to the suggestive match of these two bands, many of the IDP Raman spectra show emission at longer wavelengths which could be due to fluorescence or phosphorescence. PAHs are known to behave in this manner (Berlman, 1965).

The carbon correlated deuterium enrichments seen in the IDPs are also consistent with a PAH origin. In the past, deuterium-rich material in meteorites has been taken as an indication that these objects contain molecules that formed in dense molecular clouds at temperatures of about 10K (Yang and Epstein, 1983). However, it has recently been pointed out that free PAHs made up of 25 carbon atoms or less would be expected to preferentially lose normal hydrogen over deuterium during photoexcitation (Allamandola et al., 1986). Thus, the carbon-correlated deuterium enrichment seen in some IDPs is not only consistent with the presence of modified interstellar PAHs, but may possibly provide a means of probing the identity of the smallest interstellar PAHs.

If PAHs do, in fact, exist in the interstellar medium then it would not be surprising to find similar material in the IDPs, since PAHs are known to be relatively robust molecules (Allamandola et al., 1985) and the IDPs do not appear to have been strongly altered since their formation.

In summary, there is a strong possibility that the IDPs presently being collected in the stratosphere, particles that are probably from comets, may contain PAH-like molecules. If this is the case, then the organic molecules in IDPs probably represent interstellar molecules that have undergone relatively little alteration since their incorporation into the solar system.

References:

Allamandola, L.S., Tielens, A.G.G.M., and Barker, J.R., 1985, Astrophys. J. Lett. 290, L25.

Allamandola, L.S., Tielens, A.G.G.M., and Barker, J.R., 1986, Astrophys. J., in preparation.

Berlman, I.B., 1965, Handbook of Fluorescence Spectra of Aromatic Molecules, (Academic Press, NY).

Bradley, J.P., Brownlee, D.E., and Fraundorf, P., 1984, Science 223, 56-58.

Brownlee, D.E., Tomandl, D.A., and Olszewski, E. 1977, Proc. 8th Lunar Sci. Conf., 149-160.

Hayatsu, R., Matsuoka, S., Scott, R.G., Studier, M.H., and Anders, E., 1977, Geochim. Cosmochim. Acta 41, 1325-1339.

Leger, A., and Puget, J.C., 1984, Astron. Astophys. 137, L5.

McKeegan, K.D., Walker, R.M., and Zinner, E., 1985, Geochim. Cosmochim. Acta 49, 1971-1987.

Sandford, S.A., 1986, Science 231, 1540-1541.

Sandford, S.A., and Walker, R.M., 1985, Astrophys. J. 291, 838-851.

Walker, R.M. 1985, NASA Conference Publication 2403, 55-69.

Yang, J., and Epstein, S., 1983, Geochim. Cosmochim. Acta 47, 2199-2216.

<u>More Interstellar Emission Features at 3.3-3.6 μm</u>! A.T. TOKUNAGA, T. NAGATA, K. SELLGREN, R.G. SMITH (Inst. for Astronomy, Univ. of Hawaii), T. ONAKA, Y. NAKADA (Dept. of Astronomy, Univ. of Tokyo), A. SAKATA, and S. WADA (Univ. of Electrocommunications, Tokyo). We have obtained 3.20-3.55 μm spectra of HD 44179, NGC 7027, BD +30 3639, and Elias 1 with a new cooled-grating array spectrometer (CGAS) at the NASA Infrared Telescope Facility. At a resolving power of 1500, these are the highest spectral resolution data obtained on the family of interstellar emission bands at 3.3-3.6 μm that are presently thought to originate from very small hydrocarbon grains (Allamandola et al. 1985; Geballe et al. 1985).

The present data set consists of observations of NGC 7027 and BD+30 3639 obtained in July 1985 with a 7-detector array, and observations of HD 44179 and Elias 1 obtained in January 1986 with a 32-detector array. A 300 line/mm grating blazed at 3.0 μm was used for these observations. The entrance aperture of the spectrometer was 3 arc-sec.

Our most complete data set was obtained on HD 44179; the other sources were observed only on the main emission feature at 3.29 μm. Our spectrum of HD 44179 is shown in the figure below. In addition to the 3.29 μm feature, broad emission features which must arise from particles are observed at 3.34, 3.40, 3.46, 3.51, and 3.52 μm. Curiously, these features appear to be nearly equally spaced in wavelength. The 3.40, 3.46, and 3.51/3.52 μm features appear to be present in the lower resolution spectrum of HD 44179 published by Geballe et al. (1985). These features and an additional one at 3.56 μm were also recently seen in sources IRAS 21282+5050 and AFGL 437 by de Muizon et al. (1986).

Our data set shows:

1. Confirmation of a new set of emission features in HD 44179, IRAS 21282+5050, and AFGL 437.

2. Yet another emission feature at 3.34 μm that may be a new member of the family of emission features in this spectral region.

3. The 3.515 μm feature observed by de Muizon et al. (1986) is seen to be two emission features in HD 44179 at our higher resolution.

4. Possible unresolved emission features at 3.37 and 3.45 μm were observed; these emission features requires confirmation.

5. A short-wavelength wing to the strong 3.29 μm feature is seen clearly for the first time in HD 44179. There appears to be no corresponding wing to the long-wavelength side of the 3.29 μm feature.

6. The central wavelength and width of the 3.29 μm feature is identical in HD 44179, NGC 7027, and BD+30 3639. The central wavelength of Elias 1 is the same as the others, but its width is narrower.

7. There appears to be structure in the 3.29 μm feature of NGC 7027 and BD+30 3639 which is different from each other and HD 44179. This may indicate additional emission features, similar in intensity to the 3.46 μm feature, superimposed onto the 3.29 μm feature.

Conclusions. High resolution spectra of the 3.20-3.55 μm region show new emission features and details of the emission feature profiles. While our spectra

show greater complexity than might have been expected, these spectra also offer a stringent test of any proposed identification. It is significant that the 3.29 μm feature has an invariant central wavelength, even at high resolution, and this strongly supports the case for a very specific substance or mixture of substances which is giving rise this feature. We do not have at present an identification for the other emission features.

REFERENCES.
Allamondola, L.J., Tielens, A.G.G.M., and Barker, J.R. 1985. Ap.J., 290, L25.
de Muizon, M., Geballe, T.R., d'Hendecourt, L.B., and Baas, F. 1986. Preprint.
Geballe, T.R., Lacy, J.H., Persson, S.E., McGregor, P.J., and Soifer, B.T. 1985. Ap.J., 292, 500.
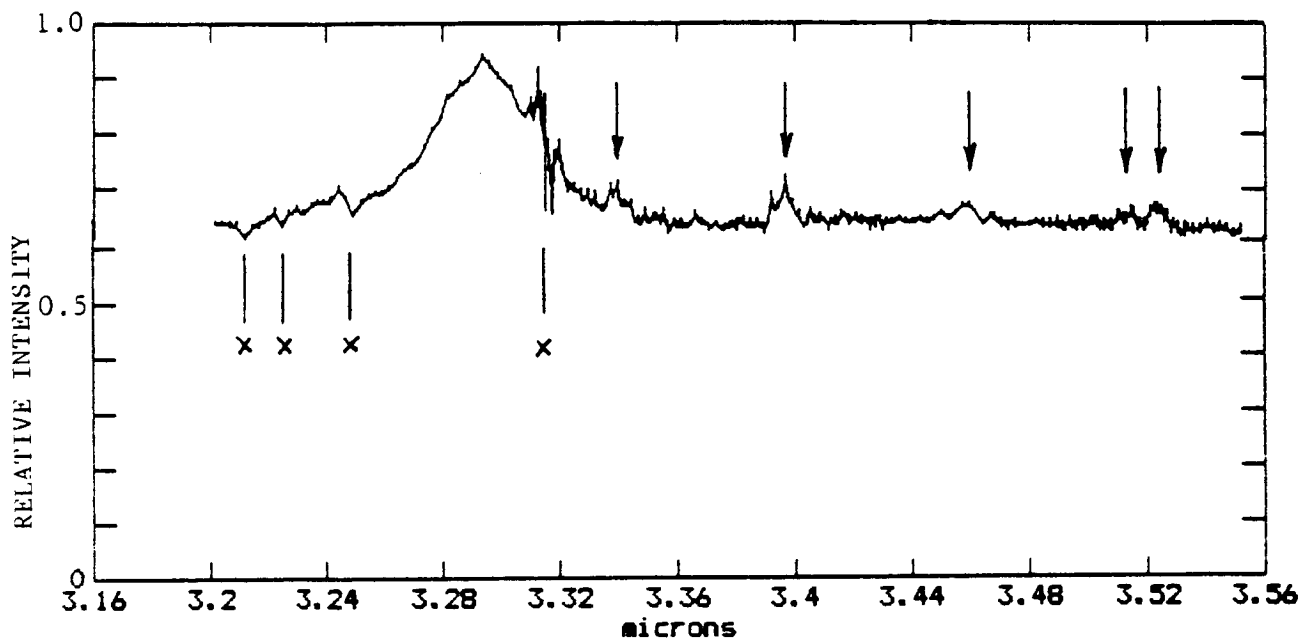
Spectrum of HD 44179. Emission features at 3.34, 3.40, 3.51, and 3.52 μm are indicated by " ". Regions of poor telluric correction are indicated by "x".

Resolution of the 7.7μm Emission Feature in NGC 7027

J.D. Bregman, L.J. Allamandola, A.G.G.M. Tielens, F.C. Witteborn
NASA Ames Research Center

D.M Rank, and D. Wooden
Lick Observatory and Board of Studies in Astronomy and Astrophysics,
University of California at Santa Cruz

The unidentified infrared (UIR) features are a group of emission bands observed in a variety of objects, which can be characterized as having moderate density gas (densities from 10^4 to 10^7 cm^{-3}) and a nearby uv source. The origin of the features is still uncertain, but the current evidence points to polycyclic aromatic hydrocarbons (PAH's) as the most likely candidates. There are a few problems with identifying PAH's as the source of the UIR features. First, each different PAH has bands at different wavelengths, so that from one source to another there would be a variation in some of the UIR features if the mixtures of PAH's varied, and there is no a-priori reason to expect one dominant PAH mixture. Figure 1 shows the positions and strengths of transitions for three different PAH molecules. The region around the UIR band at 7.7μm is particularly sensitive to the particular PAH species since the bands from the different molecules are well separated, unlike at 6.2μm where they are essentially superimposed. Secondly, there is no lab spectrum of any PAH that matches a UIR spectrum. This may be because the UIR spectrum is a combination of PAH emission from a mixture of molecules (discrete bands) and emission from small amorphous carbon particles (broad, continuous features).

Possible tests which would support the PAH hypothesis include observing variations of the UIR features among different objects, and observing sharp features (particularly in the 7-8μm region) that could be associated with individual molecules. Figure 2 shows a spectrum of NGC 7027 from 5.7-8.3μm (open diamonds) compared to a schematic spectrum (solid line) assembled by plotting the positions and relative strengths of bands observed in laboratory spectra of Pyrene, Chrysene, and Coronene, adding a sloping continuum, and assuming a line width of about 0.1μm for illustrative purposes (the natural line width for large PAH's should be about 2% at these wavelengths. Allamandola et al., 1985). All three PAH's contribute to the 6.2μm feature, while Chrysene is the primary source of the 7.0μm band. The most interesting and important part of the spectrum is the sharp feature that is observed at 7.6μm in NGC 7027. It is very narrow and is not coincident with an atomic emission line, but occurs at the same frequency as the strong 7.62μm band in Coronene. The sharpness of the feature and the coincidence with the Coronene band leads us to identify this feature with molecular emission, since solid state features would be resolved at this spectral resolution.

Variability of the 7.7μm feature is evident from the spectra in Figure 3. In all three objects, the rise towards 7.7μm starts at the same wavelength, but the width of the 7.7μm peak is quite different between objects. In M1-78 (and NGC 7027) the peak is nearly flat for three channels from 7.60-7.84μm, while at the opposite extreme is BD+30°3639, in which the peak is a single channel wide at 7.84μm. The reason for these differences must lie in the different mixtures of PAH molecules that contribute to this feature. Evidence for this interpretation are apparent in Figure 2, where the sharp feature at 7.60μm accounts for the short wavelength side of the

peak of the 7.7μm feature in NGC 7027 (and probably in M1-78 as well). The lack of this component could result in the spectrum observed for SAO 161375. The even later peak wavelength observed for BD+30°3639 is most likely due to a sharp molecular emission at 7.84μm superimposed on a broad feature similar to that observed in the other objects.

The lack of a significant variation in the 6.2μm feature among these objects is equally important since this is expected if the features arise from PAH's. The variation of the 7.7μm band combined with the lack of variation of the 6.2μm band and the observation of a very sharp (most likely molecular) feature in NGC 7027 combine to argue strongly in favor of PAH's as the material responsible for the UIR features.

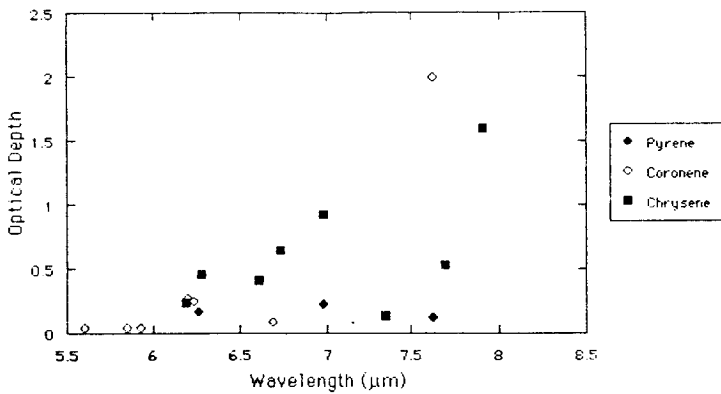Allamandola, L.J., Tielens, A.G.G.M., and Barker, J.R. 1985, Ap.J.Lett., 290, L25

Figure 1

Schematic diagram of band strengths
and wavelengths for 3 PAH molecules.
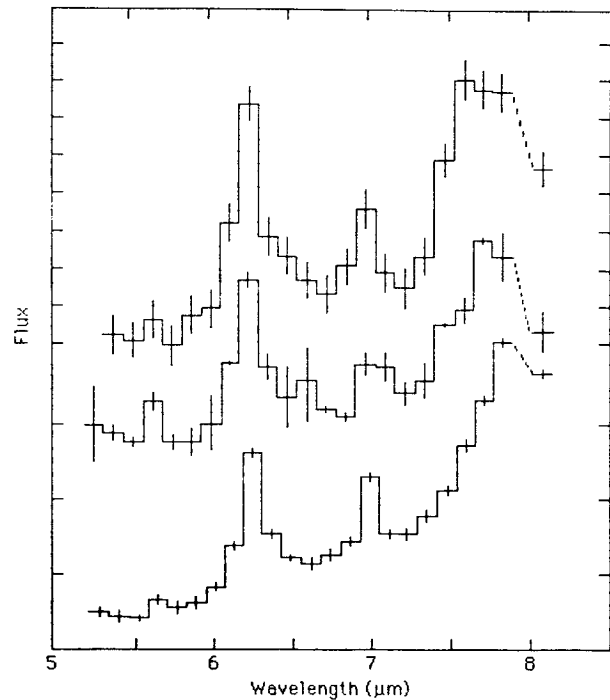

Figure 2

5.7-8.3μm spectrum of NGC 7027
(open diamonds) compared with a
schematic PAH spectrum (see text).

Figure 3

Spectra of (from top to bottom) M1-78,
SAO 161375, and BD+30°3639. Note
the variations in the 7.7μm feature.

SPECTROSCOPY AND CCD-PHOTOGRAPHY OF EXTENDED
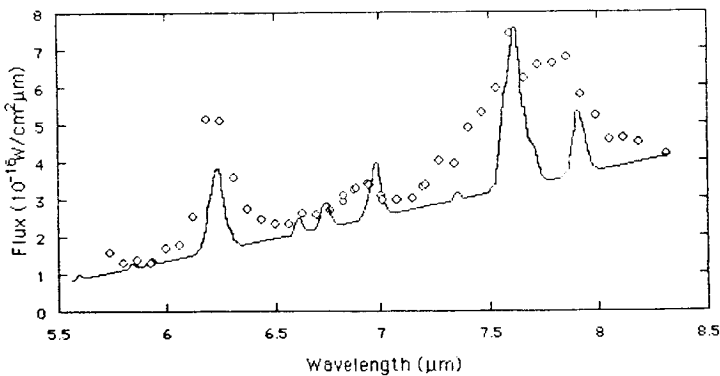# RED EMISSION IN REFLECTION NEBULAE

Adolf N. Witt
Ritter Observatory, The University of Toledo

and

Rudolph E. Schild
Harvard-Smithsonian Center for Astrophysics

Recent spectrographic studies of extended red emission (ERE) seen in the 0.6μ to 0.9μ spectral region in many reflection nebulae have shown fluorescence by amorphous hydrogenated carbon to be the most probable cause of the ERE. CCD imaging of reflection nebulae in the B, V, R, and I bands has revealed that the ERE, while generally diffuse and extended with an intensity distribution similar to that of the visual brightness profile, can be spectacularly enhanced in spatially well-defined filaments, visible in the R and I bands, but not in B or V.

Following our discovery of ERE in the sub-micron wavelength region in NGC 2023 (Witt, Schild, and Kraiman 1984), we showed that the ERE was present in other reflection nebulae as well and was most likely the result of an excitation process involving near-UV photons (Witt and Schild 1985). A more recent extensive CCD survey of 14 reflection nebulae (Witt and Schild 1986) shows ERE to be present in about 90% of the nebulae observed.

We have carried out spectrographic observations of the nebulae NGC 2023 and NGC 7023, using the intensified Reticon scanner (IRS) of Kitt Peak National Observatory on the No-2 0.9m telescope. The spectral region covered extends approximately from 0.61μ to 0.84μ, with a spectral resolution $\lambda/\Delta\lambda = 500$. Spectra were obtained for 12 locations in NGC 7023 (beam size 22".0) and for 8 locations in NGC 2023 (beam size 45".5). The nebular spectra, when divided by the energy distribution of the corresponding illuminating star, exhibit a broad emission band (FWHM ~ 1200 Å) with its peak's position ranging from 0.63μ to 0.69μ in wavelength for different fields in NGC 7023, from 0.67μ to 0.72μ for different fields in NGC 2023. The emission band is followed by a pronounced minimum near 0.8μ and strong indications of a renewed rise towards a further band at $\lambda > 0.8\mu$. The emission band provides about 30% of the total nebular intensity in R.

A common material expected to be present in interstellar space and exhibiting fluorescence with characteristics similar to those observed is hydrogenated amorphous carbon (a-C:H). Duley (1985) has suggested fluorescence by a-C:H as the cause of the red emission in the Red Rectangle. Watanabe, Hasegawa and Kurata (1982) have presented laboratory data, showing that the peak of the fluorescence band of a-C:H can be found anywhere between 0.625 and 0.75μ wavelength depending on the hydrogen concentration in the amorphous carbon. The results of Watanabe et al. (1982) applied to our findings suggest the existence of amorphous carbon particles with a hydrogen concentration of about $8 \times 10^{22} cm^{-3}$ within the solid material in NGC 7023 and about $6 \times 10^{22} cm^{-3}$ in NGC 2023.

CCD images of NGC 2023 and NGC 7023, obtained with the CfA CCD detector on the 0.6m telescope of the Whipple Observatory, reveal spectacular filaments in those nebular regions where the bandstrength of the R emission is enhanced. These regions have a projected offset distance from the respective illuminating star of

0.10 to 0.15 pc. In NGC 2023, in particular, these filaments are not visible in V or B., suggesting that they are not related to local density enhancements but rather to environmental factors favoring the particular grain material and excitation conditions required for the more efficient production of ERE.

References:

Duley, W. W. 1985, M.N.R.A.S. 215, 259.

Watanabe, I., Hasegawa, S., and Kurata, Y. 1982, Jap. J. Appl. Phys. 21, 856.

Witt, A. N., Schild, R. E. and Kraiman, J. B. 1984, Ap. J., 281, 708.

Witt, A. N. and Schild, R. E. 1985, Ap. J., 294, 225.

Witt, A. N. and Schild, R. E. 1986, Ap. J. Suppl., (Dec. 1, '86, in press).

IRAS SURFACE BRIGHTNESS MAPS OF VISIBLE REFLECTION NEBULAE: EVIDENCE FOR NON-EQUILIBRIUM INFRARED EMISSION

Michael W. Castelaz and M. W. Werner
NASA-Ames Research Center
Moffett Field, California 94035

and

K. Sellgren
Institute for Astronomy
University of Hawaii
2680 Woodlawn Drive
Honolulu, Hawaii 96822

Surface brightness maps at 12 μm ($\Delta\lambda$ = 6.5 μm), 25 μm ($\Delta\lambda$ = 11 μm), 60 μm ($\Delta\lambda$ = 33μm), and 100 μm ($\Delta\lambda$ = 34 μm) of 16 visible reflection nebulae were extracted from the IRAS (Infrared Astronomical Satellite; Neugebauer et al. 1985, Ap.J., 278, L1) database. The maps were produced by coadding IRAS survey scans over areas centered on the illuminating stars, and have spatial resolutions of 0.9' x 4' at 12 and 25 μm, 1.8' x 4.5' at 60 μm, and 3.6' x 5' at 100 μm. Extended emission in the four IRAS bandpasses was detected in fourteen of the reflection nebulae.

The IRAS data was used to measure the flux (νF_ν) of the infrared emission associated with each source. The energy distributions show that the 12 μm flux is greater than the 25 μm flux in 11 of the nebulae, and the peak flux occurs in the 60 or 100 μm bandpass in all 16 nebulae. The 60 and 100 μm flux can be approximated by blackbodies with temperatures between 30 and 50 K, consistent with temperatures expected from grains in thermal equilibrium. The IRAS 12 and 25 μm fluxes are orders of magnitude in excess of that expected from extrapolation of greybody fits to the 60 and 100 μm data.

The excess 12 and 25 μm emission is attributed to a non-equilibrium process such as emission from thermal fluctuations of very small grains (0.001 μm) excited by single ultraviolet photons (Sellgren 1984, Ap.J., 277, 623; Leger and Puget 1985, Astron. Ap., 137, L5), or emission from polycyclic aromatic hydrocarbons (PAHs) excited by ultraviolet radiation (Allamandola, Tielens, and Barker 1985, Ap.J. Letters, 290, L25). The common features of the energy distributions of the 16 reflection nebulae, also seen in the reflection nebulae associated with the Pleiades (Castelaz, Sellgren, and Werner 1986, submitted to Ap.J.), suggest that PAHs or very small grains may be found in most reflection nebulae.

INFRARED STUDIES OF SUPERNOVA REMNANTS WITH THE IRAS

E. Dwek, R. Petre, and A. Szymkowiak
NASA/Goddard Space Flight Center

Abstract: A comparative study of the infrared and X-ray fluxes and morphologies of supernova remnants (SNR) can yield valuable information on their evolution and on their interaction with the ambient interstellar medium (ISM).

Infrared observations of SNR: The infrared observations used in this study were obtained with the Infrared Astronomical Satellite (IRAS) which performed an all-sky survey at 12, 25, 60, and 100 microns. Galactic remnants detected in the IRAS survey include the historical remnants: Cas A, Tycho, Kepler; and the adiabatic remnants: IC 443, Puppis A, RCW 86, and the Cygnus Loop. Among those not detected are SN 1006 and RCW 103.

Infrared emission mechanisms: Mechanisms operating within a SNR that can contribute to the observed infrared (IR) emission are: synchrotron emission from accelerated electrons; infrared line and free-free emission from shocked optical nebulosities; and thermal emission from dust. Thermal dust emission can arise either from interstellar or circumstellar dust swept up by the expanding supernova (SN) shock, or from circumstellar or supernova dust that is swept up by the reverse shock that propagates through the ejecta.

Comparison of IR to X-ray cooling of SNR: Thermal dust emission is the dominant source of IR radiation in all the detected remnants listed above. A comparison of the IR and X-ray morphologies of the extended remnants shows that they are spatially well correlated, suggesting that the IR emission arises from collisionally heated dust that resides in the X-ray emitting plasma. For a given dust-to-gas mass ratio and dust model the ratio of infrared to X-ray cooling of a remnant (hereafter the IRX ratio) is then only a function of gas temperature. We calculated this ratio for all remnants listed above, and compared it with the theoretically predicted value (Figure 1). We found that: 1) the observed IRX ratio follows the general theoretical trend of decreasing IRX ratio with increasing remnant age; and 2) the IRX ratio is significantly larger than unity for all remnants, suggesting that gas-grain collisions are the dominant cooling mechanism of the shocked gas. The enhanced cooling resulting from gas-grain collisions will, however, have a negligible effect on the dynamical evolution of the remnants considered here.

Interaction with the ISM: Some remnants have IRX ratios that deviate significantly from the theoretical value. These deviations can be shown to result from varying conditions in the ambient ISM.

Nature of the emitting dust: A detailed analysis of the spectrum of Cas A (Dwek, Dinerstein, Gillett, Hauser, and Rice; submitted to Ap. J.; see Figure 2), and a preliminary study of that of Tycho and Kepler indicate that the IR spectrum from these remnants arises from an interstellar mixture of silicate and graphite dust. The excess 12 microns emission, over that expected from a standard MRN grain size distribution, suggests the presence of very small dust particles in the ISM which are stochastically heated by the shocked gas.

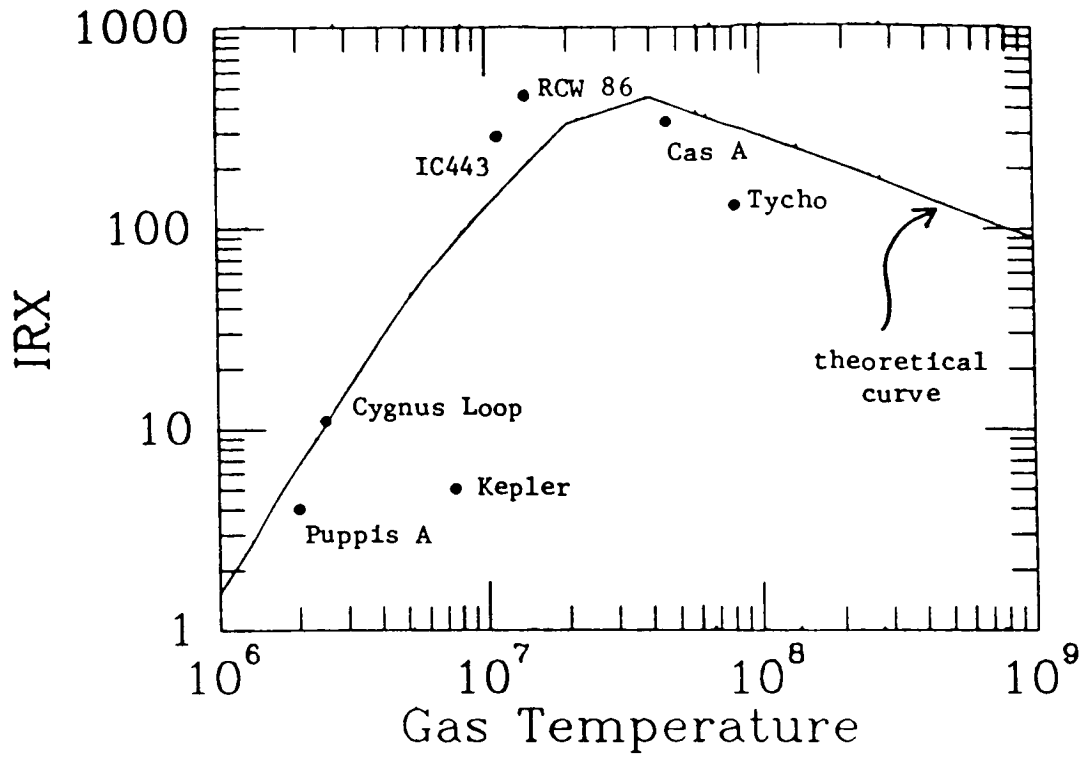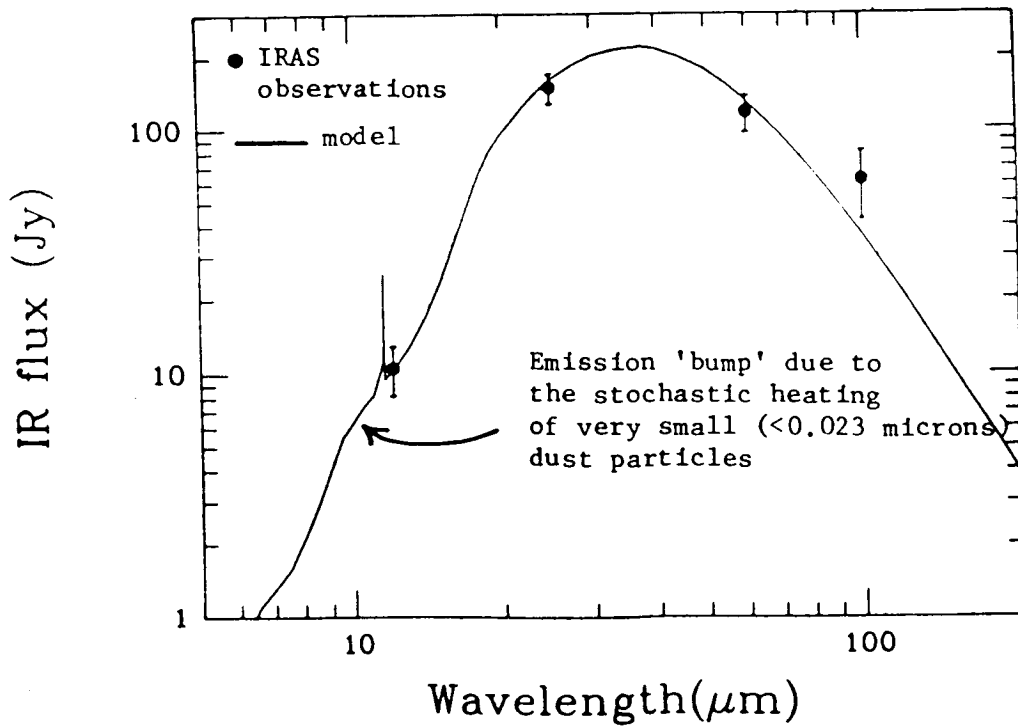**Figure 1:** The IRX ratio of selected SNR

Figure 2: The infrared spectrum of Cas A

Unusual Relative Strengths of the Diffuse Interstellar Bands in Some Interstellar Dust Clouds

J. Krełowski
N. Copernicus University
Torun, Poland

and

G.A.H. Walker
Geophysics & Astronomy Dept.
U.B.C., Vancouver, Canada

We find that some of the diffuse interstellar features (DIB) in the spectra of certain stars at high galactic latitudes (1 > 15°) are unusually weak or absent while others have the strength expected for their color excess. In some cases the stars are probably reddened by single interstellar clouds. There appear to be three families of DIB where:

(i)   4430, 4882 and 6180 are absent.

(ii)   5362, 5449, 5487, 5508, 5780, 6196, 6203, 6269, 6284 are about one third of their expected strength,

(iii) the 2200 feature and 4763, 4780, 5494, 5535, 5545, 5797, 5850, 6376, 6379, 6614 are of approximately normal strength for the color excess.

The effect for families (ii) and (iii) is demonstrated in Figure 1 for a number of lines. The high signal to noise Reticon spectrograms in the region 5760 to 5860A are of (A) HD 91316 E(B-V) = 0.03, (B) 40111 E(B-V) = 0.16 (C) 24398 E(B-V) = 0.29, (D) 2905 E(B-V) = 0.31, (E) 42087 E(B-V) = 0.34. The diffuse features are identified and, from more extensive observations we consider HD2905 to have normal relative DIB strengths. 5780 is obviously significantly weaker in C, the star at high galactic latitude.

In the galactic plane we find that 4430 is significantly weaker for stars which have values of E(15-18) > 0.2. This effect is also correlated with certain regions in galactic longitude. In Perseus for example 4430 is significantly weaker than in Cepheus where E(15-18) is < 0.2. This suggests that the behavior of family (i) is related to the presence or absence of the fine particle component or some other component of the interstellar dust which causes the enhanced UV extinction.

The existance of the three families implies that at least three agents cause the DIB and that the proportions of the agents or the physical conditions giving rise to the DIB can vary from cloud to cloud.
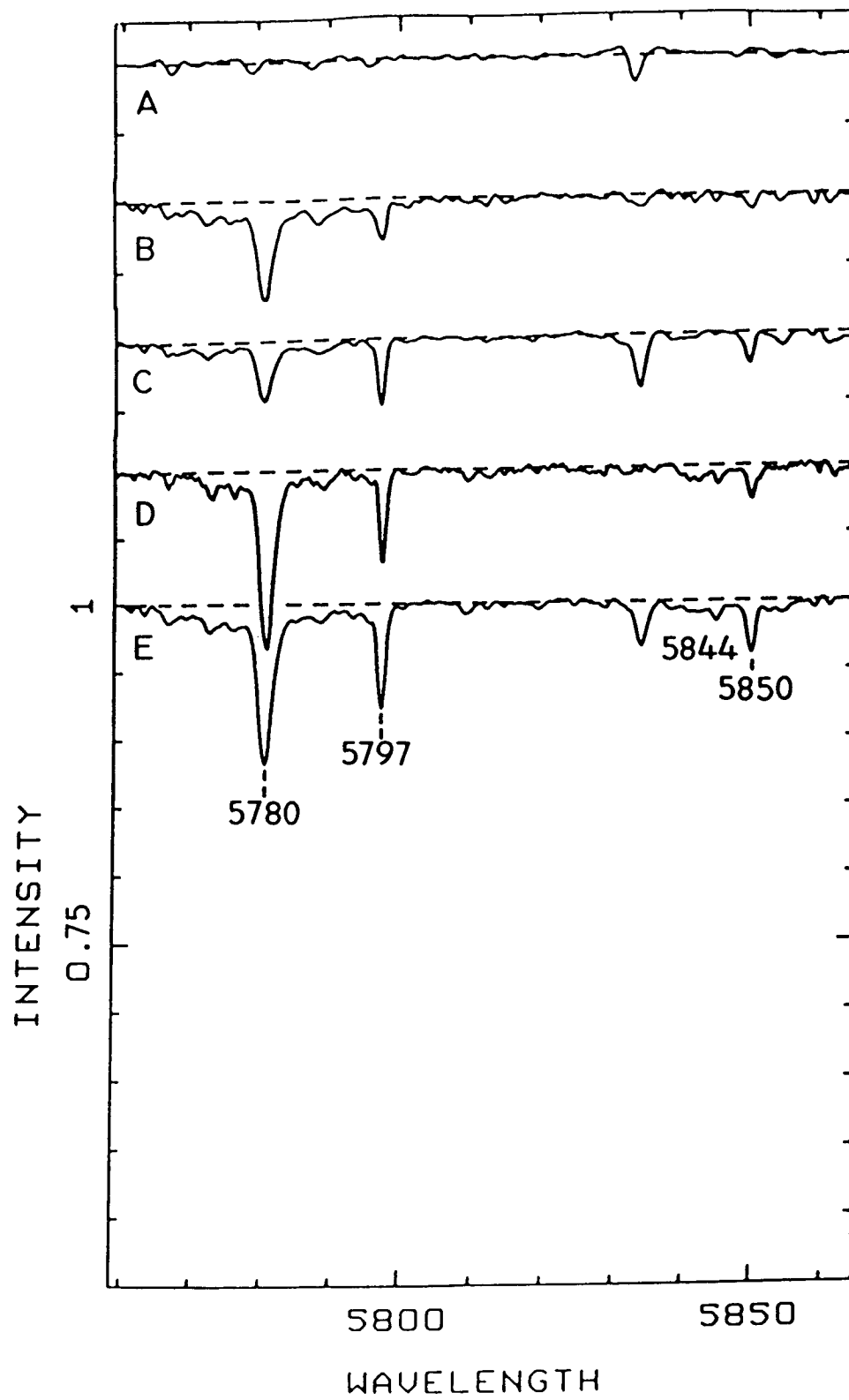
FIGURE 1.

III.   INTERSTELLAR GRAINS

B.   Larger Grains and Grain Mantles

MODERATE SPECTRAL RESOLUTION OBSERVATIONS OF 3 MICRON ABSORPTION FEATURES IN HIGHLY OBSCURED OBJECTS

Robert G. Smith, Kris Sellgren, and Alan T. Tokunaga
Institute for Astronomy, University of Hawaii

The 3μm absorption spectra of sources seen in or behind molecular clouds generally show a variety of absorption features which have been explained by three separate absorptions:

(1) A broad absorption feature at 3.08μm which is attributed to water ice particles.

(2) An absorption between 3.3 and 3.6μm which appears as a long wavelength wing to the 3.08μm ice band. This has been attributed to scattering by large water ice particles (Leger et al. 1983) and to absorption by $NH_3.H_2O$ complexes in the ice (Knacke et al. 1982).

(3) A narrower absorption at 3.4μm superimposed on the long wavelength wing. This feature is generally believed to be due to the stretching vibration of CH which occurs near 3.4μm, although the exact nature of the molecule is unknown.

Using the cooled-grating array spectrometer (CGAS) at the NASA Infrared Telescope Facility, we have begun a program aimed at providing high quality spectra at moderate resolution ($\lambda/\Delta\lambda \sim 200$ at 3.0μm) of a wide range of objects known to exhibit these features. We hope to provide a good sample of spectra for comparison with theoretical and experimental work on the constituents of grains in the interstellar medium.

As a representative sample of the spectra obtained so far, we present in Fig. 1, spectra of the late-type mass-loss star OH 0739-14 and the protostars Mon R2 IRS-2 and IRS-3 (solid circles). These spectra are in the form of optical depths, obtained by fitting a blackbody of the appropriate temperature between points of the spectrum which lie beyond the influence of any of the strong 3μm absorption features. As an illustration of the differences between the spectra, the solid line in each diagram shows the results of a calculation of the absorption profile of particles with a silicate core and ice mantle, using Mie theory. Following the work of Leger et al. 1983, the optical constants of amorphous water ice at 77K were used in the calculation with a grain-size distribution similar to that deduced by Mathis et al. 1977. Note that our current intent is not a rigorous modelling of the absorption profiles but rather an attempt to clearly show the distinct differences between the spectra. For example, the work of Hagen et al. 1981, 1983 and van de Bult et al. 1985 has shown that amorphous ice at 10K provides a better fit to the short wavelength side of the 3.08μm feature although alternate explanations may be NH_3 ice absorption (Knacke et al. 1982) or scattering by ice particles (Hanner 1984).

Several important points can be made regarding the spectra of Fig. 1:

(1) A simple amorphous ice model provides a reasonable fit to the spectrum of OH 0739-14 but cannot explain the short wavelength absorption of the Mon R2 sources without going to ice at a much lower temperature.

(2) Both the Mon R2 sources show a long wavelength wing to the 3.08μm ice feature and some indication of an absorption feature at 3.4μm although this may in fact be part of the long wavelength wing.

(3) Mon R2 IRS-3 appears to have another absorption feature at about 3.25μm.

These initial results provide an additional impetus to continue this study in an attempt to understand the considerable differences between these spectra. In

particular, it may be possible to relate the shape of some of these absorption features to physical conditions in protostellar clouds by observing a large sample of protostars.

REFERENCES:

van de Bult, C.E.P.M., Greenberg, J.M., and Whittet, D.C.B. 1985, M.N.R.A.S., 214, 289.
Knacke, R.F., McKorkle, S., Puetter, R.C., Erickson, E.F., and Kratschmer, W. 1982, Ap. J., 260, 141.
Hagen, W., Tielens, A.G.G.M., and Greenberg, J.M. 1983, Astr. Ap., 117, 132.
Hagen, W., Tielens, A.G.G.M., and Greenberg, J.M. 1981, Chem. Phys., 56, 367.
Hanner, M.S. 1984, Ap. J., 277, L75.
Leger, A., Gauthier, S., Defourneau, D., and Rouan, D. 1983, Astr. Ap., 117, 164.
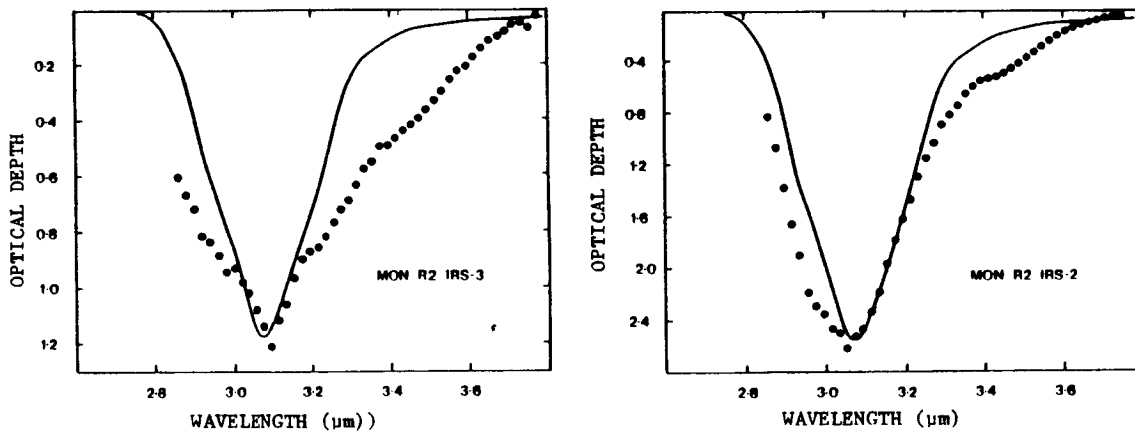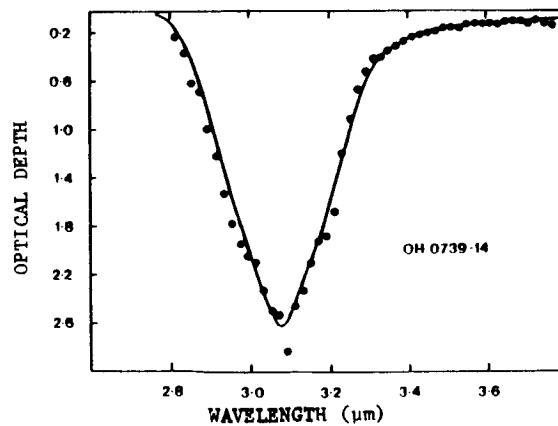Mathis, J.S., Rumpl, W., and Nordsieck, K.H. 1977, Ap. J., 217, 425.

FIGURE 1.

SOME RECENT INFRARED SPECTROSCOPY OF INTERSTELLAR PROCESSES

T. R. Geballe
U. K. Infrared Telescope; Hilo, Hawaii

I. Introduction

The intent of this paper is to demonstrate the potential which infrared spectroscopic techniques provide for studying interstellar processes. Several examples are given. The data were obtained at UKIRT, using its frequency-chopped Fabry-Perot spectrometer and its seven-channel cooled grating spectrometer.

II. Shocked Molecular Hydrogen

The emission from the V=1-0 S(1) line of H_2 has been mapped over a large portion of the supernova remnant IC443 by Burton et al. (1986, in preparation). A section of this map is shown in Fig. 1. The emission is clumped along a ridge where the expanding shell of the SNR has interacted with a molecular cloud. The clumps may be density enhancements in the molecular cloud or be the result of fragmentation caused by the shock. The observed intensity ratios of the 2μm lines imply that the H_2 is collisionally excited and that the extinction to the shocked gas is 2 mag at 2μm. The total luminosity from H_2 lines is about 1000 L_0, making IC443 one of the most luminous galactic H_2 line sources. The mass of hot, shocked gas is $\sim$0.2 M_0.
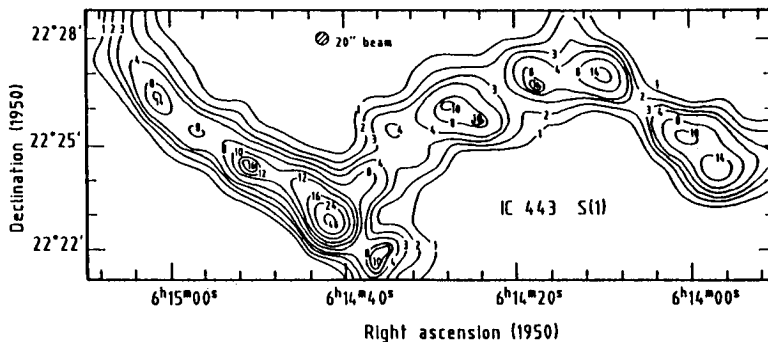

Fig. 1

Figure 2 shows a 3-4μm spectrum of Pk 1 in Orion (Wade and Geballe, 1986, in preparation). Numerous H_2 lines are easily seen. The most highly excited of these is the 0-0 S(17), whose upper level energy (T = 25,500 K) is the highest yet detected from H_2 in a shocked region. The even higher excitation S(21) line at 3.37μm may also be detected. Excitation temperatures derived from pairs of highly excited lines in this spectrum are typically 2700 K, considerably higher than those determined from the strong, but lower excitation 2μm lines. This result is expected for H_2 undergoing post-shock cooling. Accurately determined intensity ratios and velocity profiles of high and low excitation lines may yield important information concerning the shock physics and/or the presence of multiple shocks.

Fig. 2

Orion
Pk 1
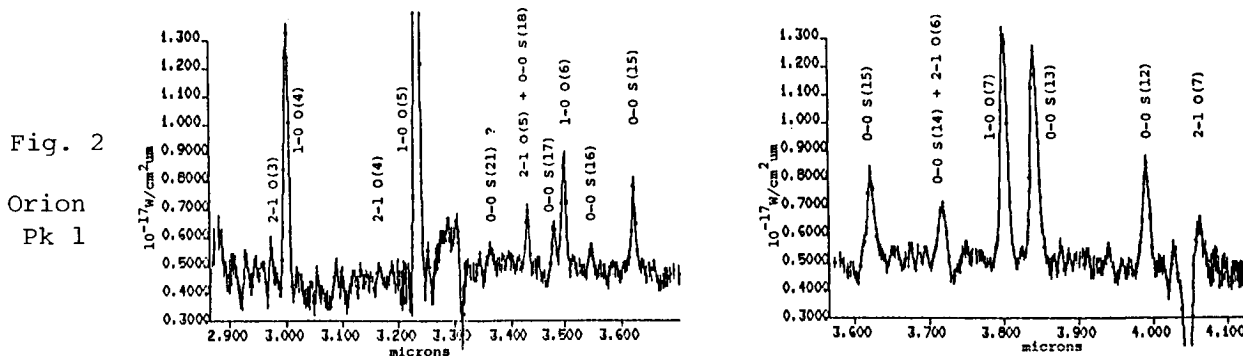
II. Molecules in Grain Mantles

Ice band spectra at resolving powers of 100 have been in existence for many years. The combination of observations from Mauna Kea and higher spectral resolution allow a significant increase in information. Figure 3 shows the ice band of GL2136

(Greenberg et al.; 1986, in preparation), obtained at a resolving power of ~350. For the most part the profile is smooth, but several distinctive structures are seen. These are: a narrow maximum in optical depth at 3.09µm, a shoulder at 3.25µm, and (possibly) a shallow feature at 3.4µm. All have been seen in spectra of other sources. No sharp features have been detected on the long wavelength wing.

Fig. 3

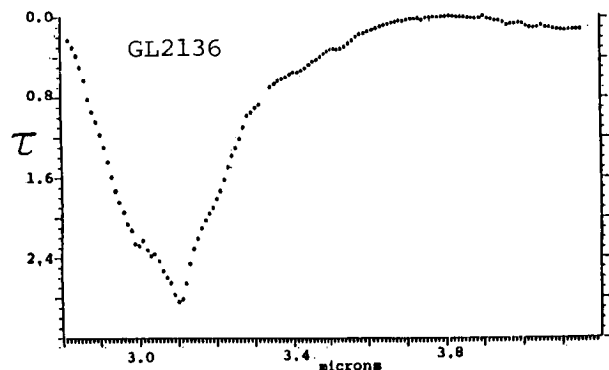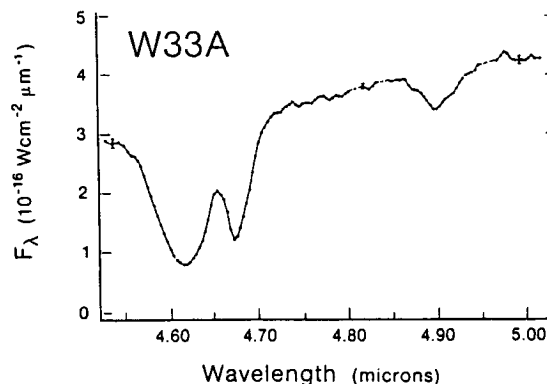Fig. 4

The infrared source W33A is perhaps the most important astronomical resource for the study of grain mantles. Its 4.5-5.0µm spectrum (Geballe et al., 1985, Astron. Ap., 146, L6) contains three strong absorptions (Fig. 4). The narrowest of these, at 4.67µm, due to solid CO, has been detected in many obscured sources. The others, at 4.62µm and 4.90µm, have not been clearly detected elsewhere. Work by the Laboratory Astrophysics group (Leiden Univ.) indicates that their carriers are, respectively, unidentified $C \equiv N$ - and sulfur - bearing molecules which are produced on the mantles by UV-photolysis.

III. Unidentified Emission Features

Recent spectroscopy of the well-known 3µm unidentified emission features has resulted in 1) accurate characterizations of their spectral shapes, 2) proof of the existence of source-to-source variations in their relative strengths, and 3) the discovery of several new emission features. Figures 5 and 6 are a good example of the range of phenomena which has been found. The planetary nebula BD +30 3639 exhibits a strong 3.3µm feature, a weak or absent 3.40µm peak, and a "plateau" of emission extending to 3.6µm (Geballe et al., 1985, Ap. J., 292, 500). In contrast the source IRAS 21282+5050 has, in addition to a strong 3.3µm feature and plateau, a strong 3.40µm feature and additional peaks at 3.46, 3.51, and 3.56µm (de Muizon et al., 1986, Ap. J. Letters, in press). The variety and wavelength range of the 3µm features appears to be consistent with their being emitted by PAHs (some with molecular subgroups attached), but specific identifications have not yet been made.
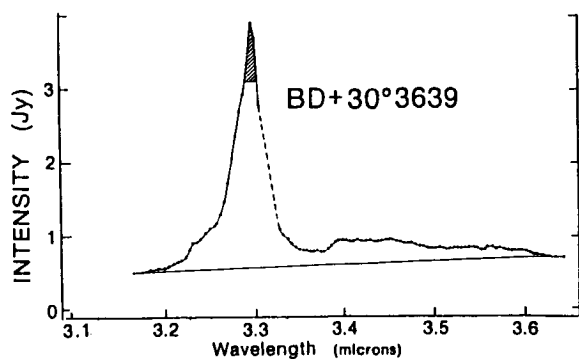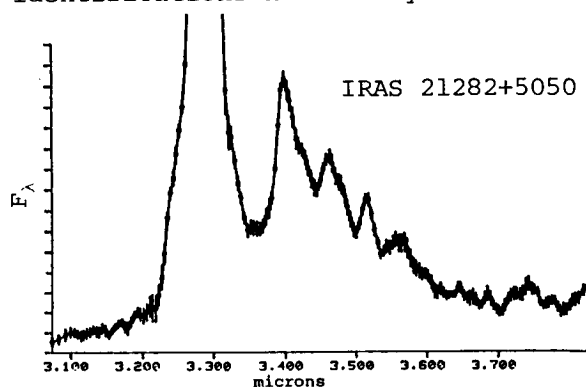
Fig. 5

Fig. 6

130

The 3.1 μm Ice Band in Infrared Reflection Nebulae

Y. Pendleton, M. Werner, and A.G.G.M. Tielens
NASA Ames Research Center

Recent observations show that infrared reflection nebulae are common phenomena in star forming regions. For instance, infrared reflection nebulae have been observed in the lobes of bipolar outflow sources where the geometry is such that the illuminating star is heavily obscured, possibly by a disk, but radiation escapes through the poles to illuminate the dust adjacent to the star. Near infrared scattered light can be used to probe the properties of the dust grains, the nature of the embedded source, and the geometry of the nebula. We have made extensive observations of two nearby infrared reflection nebulae, Orion Molecular Cloud 2 IRS1 (OMC-2/IRS1) (Pendleton et al, 1986 Ap.J., in press) and Cepheus A IRS6a (Cep-A/IRS6a). In the case of OMC-2/IRS1 we were able to constrain the properties of the illuminating source, IRS1, from a combination of far infrared and near infrared data. We found the luminosity and temperature of OMC-2/IRS1 to be ~500 $L_\odot$ and ~1000K, respectively. Both sources show deep absorption features in reflected light at 3.1 μm. The 3.1 μm feature, commonly attributed to water ice, appears in the spectrum taken along the line of sight to the illuminating source as well as toward the nebula in OMC-2/IRS1. The origin of the feature in the reflected light is unclear. It may be produced by the grains in the nebula or it may result from pure extinction, either in the circumstellar shell of the star or in foreground material. Figure 1 shows the observed 2.2-3.8 μm spectra of Cep-A/IRS6a.

We are using Mie scattering models of ice coated grains to study the constraints on the properties and location of grains that could produce a feature similar to that observed in OMC-2 and Cep-A. Mie scattering models of ice coated silicate grains with total grain radii $0.03 \le a \le 1.5$ μm were calculated over the wavelength range $2.2 \le \lambda \le 3.8$ μm. Figure 2 shows the differential scattering cross section, $dC_{sca}/d\Omega$, versus wavelength for several grain sizes and a scattering angle of 60 degrees. In all cases $dC_{sca}/d\Omega$ reaches a minimum at wavelengths shortward of 3.1 μm (~2.85 μm), in fact the scattering cross section appears to be quite large at the wavelength where the 3.1 μm feature is the most pronounced. We conclude that scattering by ice particles alone could not be responsible for the 3.1 μm feature observed in infrared reflection nebulae. However, when extinction and scattering by non-icy particles is included in the analysis it appears possible to reproduce a 3.1 μm band similar to the observations. We have calculated scattering by graphite and silicate grains. The results suggest for a Mathis, Rumpl, and Nordsieck (Mathis et al, 1977, Ap.J., 217, 425) grain distribution that graphite is the dominant contributor to the near infrared continuum scattering.

Cep A IRS6a 4" beam
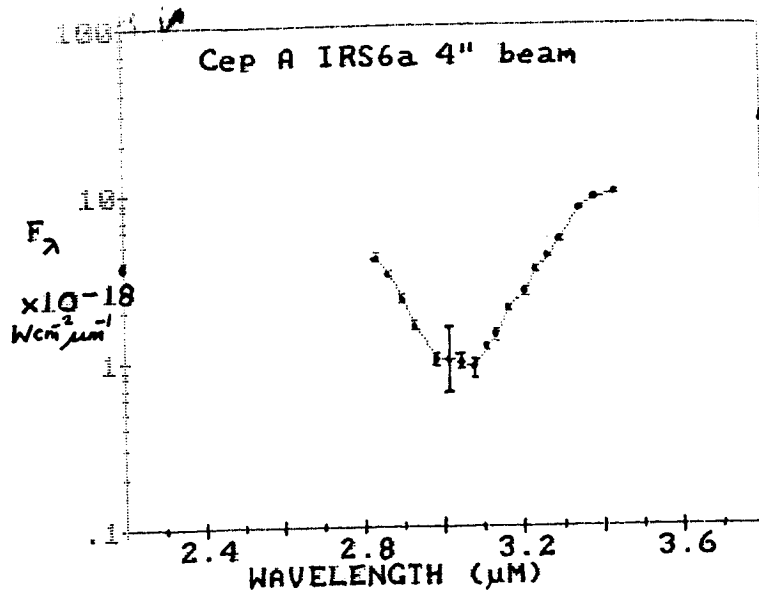
FIGURE 1 The 2.2-3.8 µm spectra of the infrared reflection nebula in Cep A (IRS6a) taken at the NASA IRTF. The feature at ~3.1 µm is generally attributed to water ice.

Differential Scattering Cross Section v. Wavelength
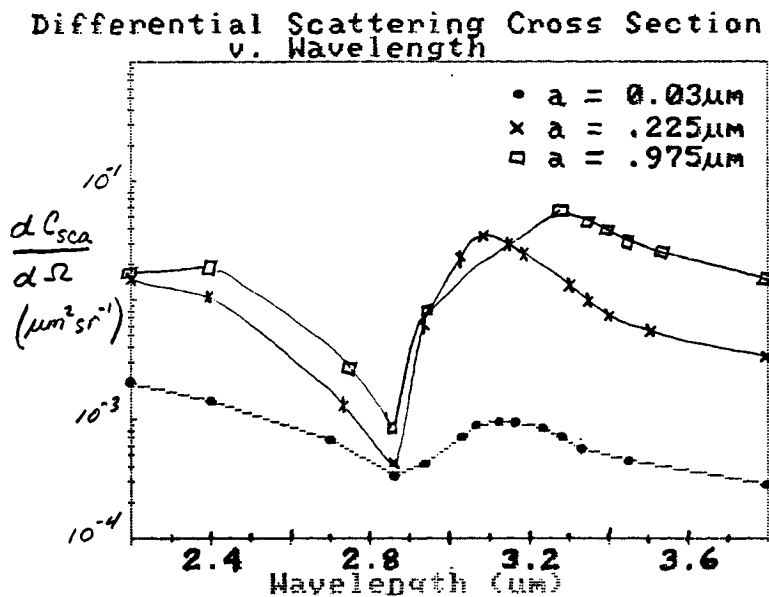
FIGURE 2 The differential scattering cross section, $dC_{sca}/d\Omega$, at a scattering angle of 60 degrees, for ice coated silicate grains as a function of wavelength. The grain size, a, includes both the core and mantle. The curves for 0.03 and 0.225 µm have been multiplied by factors of 1E6 and 1E2, respectively. Note that in scattering the ice band feature reaches a minimum at ~2.85 µm compared to ~3.1 µm in absorption.

132

Relationships Between Dust Grain Components
Responsible for Observed Interstellar
Extinction and Polarization

Geoffrey C. Clayton
Washburn Observatory, University of Wisconsin

I. Introduction

Twelve years after Gehrels (1974) published the first observations of interstellar polarization at ultraviolet wavelengths, no further observations have been reported. In contrast, the ultraviolet extinction properties of interstellar dust have been well observed. Although all extinction curves show the same basic shape, significant variations from the "average" curve are common (Massa, Savage, and Fitzpatrick 1983; Witt, Bohlin, and Stecher 1984). In particular, the amount of extinction measured in the visible (E(B-V)), at the 2200 A feature (E(Bump)), and in the far-ultraviolet (E(1550-V)) are only vaguely correlated indicating that at least 3 fairly independent populations of grains contribute to the overall extinction curve.

With the exception of Gehrel's observations toward two stars, observations of interstellar polarization have been confined to visible and infrared wavelengths. Are the grain populations responsible for ultraviolet extinction aware that the third population is aligned by the Galactic magnetic field? Meyer and Savage (1981) found only a weak correlation between λ_{max}, the wavelength at which maximum polarization occurs, and a measure of ultraviolet extinction, (E(1550-3300)/E(B-V), for 91 stars.

A search of the literature was made for polarimetric observations of the 1415 stars included in the extinction catalogue derived from Astronomical Netherlands Satellite (ANS) data (Savage t al. 1985). It was found that about 900 of the stars had at least one unfiltered polarimetric observation, p(%). In addition, 150 stars had calculated values of λ_{max}.

II. Results

a). λ_{max}

This parameter is usually considered to be related to the mean size of the population of aligned grains (Savage and Mathis 1979; Mathis 1985). The weak correlation found by Meyer and Savage (1981) is also found here

in the larger sample. Larger values of λ_{max} have generally weaker far-ultraviolet extinction as measured by E(1550-V)/E(B-V). However, if λ_{max} is plotted against E(1550-3300)/E(Bump) removing the dependence on visible extinction, the correlation virtually disappears. Therefore, changes in the visible extinction reflected in E(B-V) may be responsible for the correlation found by Meyer and Savage.

b) p/E(B-V)

This parameter is a measure of grain alignment efficiency and uniformity of the Galactic magnetic field. It is also a measure of extinction by unaligned grains which contribute to E(B-V) but not to p. The maximum value observed in the Galaxy is 9 %/mag. A weak relationship is found between E(Bump)/E(B-V) and p/E(B-V). As can be seen in Figure 1, stars with very weak bumps have small values of p/E(B-V). Perhaps along these lines of sight the fraction of unaligned grains contributing to E(B-V) is large compared to the aligned grains and the grains producing the bump.

Figure 1
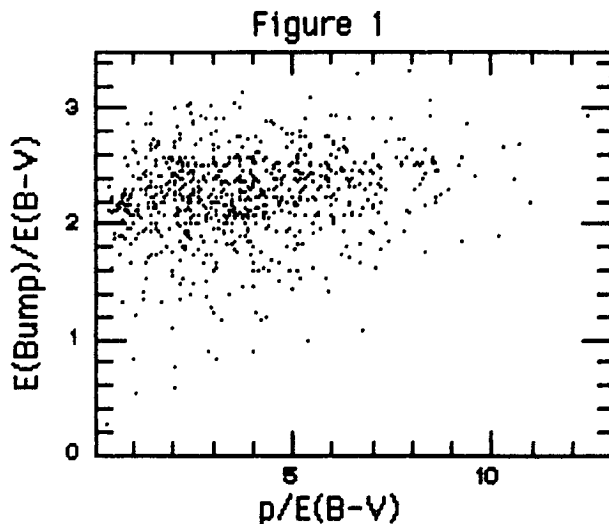
References

Gehrels, T. 1974, A.J., 79, 450.
Massa, D., Savage, B.D., and Fitzpatrick, E.L. 1983, Ap.J., 266, 662.
Mathis, J.S. 1985, Ap.J. submitted.
Meyer, D.M., and Savage, B.D. 1981, Ap.J., 248, 545.
Savage, B.D., and Mathis, J.S. 1979, A.R.A.A., 17, 73.
Savage et al. 1985, Ap.J. Suppl., 59, 397.
Witt, A.N., Bohlin, R.C., and Stecher, T.P. 1985, Ap.J., 279, 698.

Depletions And Extinction Curves For Lines Of Sight Through The Outer Edges Of Truly Dense Molecular Clouds

Charles L. Joseph

Princeton Observatory

Observations of a few moderately reddened $(0.3 < E(B-V) < 0.6)$ lines of sight through the outer edges of truly dense molecular clouds, not only show the overall depletions in these clouds to be as much as 0.5 (dex) greater than in comparably reddened diffuse clouds, but reveal a possible tendency for certain species to deplete preferentially (Joseph *et al*. 1986). For example, the Cr/Fe and the Mn/Fe abundance ratios both appear to be substantially less ($\sim$0.6 dex) for lines of sight with large abundances (log N $\gtrsim$ 13.0) of cyanogen (CN). Chromium and manganese may be good discriminators between the condensation (Field 1974) and the accretion (Snow 1975) models, since both elements are expected to deplete less rapidly than Fe in the condensation model and more rapidly than iron in the accretion model. Similarly, depletions of certain species in the densest portions of the molecular lines of sight (inferred from abundances of neutral atoms) appear to be enhanced by more than 1.0 (dex) over those found for the entire sightline (Joseph *et al*. in prep.). Since the lines of sight observed so far are believed (on the bases of CN data) to have large spatial densities, the observed depletion pattern for these sightlines may represent the best observational evidence of dust-gas interactions, leading to density-dependent depletion.

Manganese is perhaps the best indicator of this new depletion mechanism, even though the three absorption lines of Mn II used in this study have similar wavelengths and oscillator strengths and usually are all close to being saturated. Mn is depleted only slightly (typically 0.8 in the log less than iron) in both diffuse interstellar clouds (Jenkins *et al*. 1986) and in the less dense regions of the ρ Ophiuchi Dense Cloud (Snow and Jenkins 1980). On the other hand, the depletion of manganese is systematically closer to the values found for iron in molecular lines of sight and in sightlines well into the Ophiuchi cloud. The depletion of Mn actually is measured to be larger than Fe in the line of sight to HD 21483, having the largest amount of CN (log N = 13.5) in the present study.

The above results suggest that the preferential depletion of certain species should be readily observable in diffuse clouds, if each species accretes with its own time constant and if dust-gas interaction is a dominant depletion mechanism. Although numerous authors have cited a correlation between spatial densities and the amount of overall depletion as evidence of interstellar accretion, a careful examination of the element-to-element depletion from one line of sight to another contradicts this claim (e.g. Snow and Jenkins 1980, Joseph, Snow and Morrow 1985). In addition, with one exception, Snow (1984) found abundance ratios in the dense cores of diffuse clouds to be similar to the cloud as a whole. If density enhancements do exist and if density-dependent depletion occurs in the diffuse interstellar medium, then differences in the depletion ratio of various elements should be observed between high and low density diffuse clouds as well as between

the cloud cores and the whole sightline as they are for the molecular lines of sight observed by Joseph *et al.*

Most of these molecular lines of sight exhibit anomalously high far-UV extinction with weak to normal strength 2200 A bumps superimposed on the underlying extinction. In contrast, shock models (Seab and Shull 1983) predict the extinction to be stronger than normal in both the far UV and the 2200 A spectral regions. The type of extinction curve observed in the molecular clouds is predicted from a simple model of grain accretion where modest amounts of new material have been mantled onto a standard (Mathis, Rumpl, Nordsieck 1977) grain size distribution (Joseph *et al.* 1986). While, calculations show that an accretion of an additional 20% by mass onto the grains should be sufficient to produce these extinction curve anomalies, only volatile elements still have sufficient gaseous phase abundance to be able to alter the grain size distribution. Ice mantling is possible, however, since it is observed frequently for lines of sight well into dense molecular clouds (Joyce and Simon 1982) and thick mantles have been inferred for a similar nearby line of sight to HD 29647 (Goebel 1983).

It is worth emphasizing that these results should be considered to be tentative until additional molecular lines of sight can be observed at high spectral resolution. Each line of sight requires large amount of observing time in order to obtain the multiple spectral images necessary to provide a sufficient signal-to-noise ratio.

Field, G.B. 1974, *Ap.J.*, 187, 453.
Goebel, J.H. 1983, *Ap.J.Letters*, 268, L41.
Jenkins, E.B., Savage, B.D., and Spitzer, L. 1986, *Ap.J.*, 301, 355.
Joseph, C.L., Snow, T.P., and Morrow, C. 1985, *Ap.J.*, 296, 213.
Joseph, C.L., Snow, T.P., Seab, C.G., Crutcher, R.M. 1986, *Ap.J.*, *in press*.
Joyce, and Simon, 1982, *Ap.J.*, 260, 604.
Mathis, J.S., Rumpl, W., and Nordsieck, K. H. 1977, *Ap.J.*, 217, 425.
Seab, C.G., and Shull, J.M. 1983, *Ap.J.*, 275, 652.
Snow, T.P. 1975, *Ap.J.Letters*, 202, L87.
Snow, T.P. and Jenkins E.B. 1980, *Ap.J.*, 241, 161.

THE SHAPES OF THE CIRCUMSTELLAR "SILICATE" FEATURES

Irene R. Little-Marenin (AFGL and Wellesley C.)
Stephan D. Price (AFGL)

Around oxygen-rich stars we find that the spectra of most long-period variables (LPV) show an excess infrared emission which is attributed to circumstellar silicate dust grains. These grains produce emission features at about 10 and 18 μm due to bending and stretching modes of SiO respectively. It has been known (Forrest, Gillett and Stein 1975) that the spectral energy distribution of the 10 μm emission shows variations from star to star. With the availability of many IRAS Low Resolution Spectra (LRS) in the 8-22 μm region of M stars, we can now study the 10 μm feature to determine its uniformity (or lack thereof). For this analysis we assume that the 8-22 μm emission from these stars is produced by a) the stellar photosphere, b) a continuum emission from the dust grains and c) a strongly wavelength dependent dust grain emission term. By representing the first two terms with blackbody energy distributions and subtracting them from the observed spectrum, we are left with a remaining strongly wavelength dependent emission feature which we call the excess silicate or 10 μm emission.
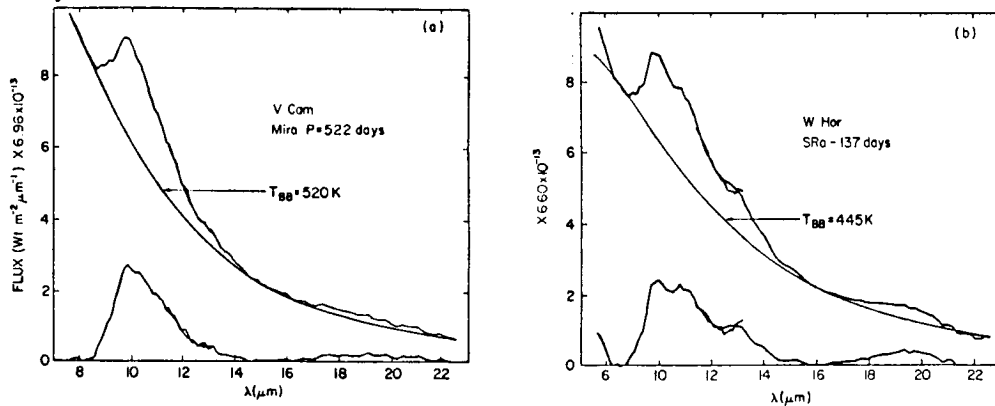

Fig. 1. Two M star LRS spectra (V Cam and W Hor) are plotted together with black body energy distributions fitted to either side of the emission feature. The 10 μm excess (observed - local black body continuum) is plotted above the wavelength axis. The difference in the shape of the excess between the two stars is obvious.

The excess silicate emissions from about 130 LPVs can be divided into three groups characterized by similiar spectral shapes. All three shapes are shown in Figure 2. The average silicate feature of semiregular (SRa,b,c) and irregular (Lb) variables is shown as a solid line. This feature extends from 8.4 to ~14.5 μm with a peak at 10 ± 0.05 μm. The FWHM is 2.1 ± 0.15 μm but the feature is asymmetric with the ratio of the widths of the short wavelength (rising) branch compared to the long wavelength (falling) branch of 0.6:1.5 at half intensity. The rising branch shows only minor variations in wavelength from star to star whereas the wavelength at the FWHM point of the falling branch varies by ±0.15 μm. The average silicate excess of Mira variables is shown as a dashed line in Figure 2. The average feature extends from 8 to 14.5 μm with a peak at 9.75 μm and a FWHM of 2.3 um. The feature is asymmetric but on the average has a less

steeply rising branch than the other LPVs giving a ratio of the rising width to the falling width of 0.75:1.5 at half intensity. However, the spectral shape of the silicate emission feature among the Miras shows much greater variation from star to star than that of the other LPVs. The shape of the emission from Miras ranges from one identical to the SRs and Lbs to a much broader one, extending from <8 μm (the limit of the LRS detectors) to ~14.5 μm with a corresponding shift in peak emission from 10 to 9.6 μm and an increase in the FWHM from 2.1 to 2.4 μm. The long wavelength edge of the feature appears to vary very little among these Miras. Hence the difference in spectral shape between the Miras and the other LPVs is primarily due to the fact that in Miras the rising branch varies in wavelengths accompanied by a shift in the peak emission to shorter wavelengths. This shift to shorter wavelength correlates with the strength of the silicate excess. In general the greater the strength of the feature the shorter the wavelength of the rising branch. Unlike the results of DeGioia-Eastwood et al (1981), we find that the strength correlates only very weakly with period. This corroborates the conclusion reached by Vardya, De Jong and Willems (1981). At a given period the excess can vary by a factor of 4. The 18 μm emission feature is very similiar in both types of profiles and extends from about 15 to >22 μm. Both these ~10 μm and 18 μm features have been attributed to silicates.

The most interesting 10 μm emission occurs in stars which tend to show weak excesses but includes a few stars which have excesses comparable in strength to the stars with the other types of features (see Fig. 1a and 1b). There are relatively few stars in this group, but they constitute almost half of the stars with weak emission irrespective of their variability type. The feature has three components (dotted line Figure 2) with peaks at 10, 11 and 13.1 μm. The 10 μm peak is strongest in M stars and agrees in wavelength with the silicate peak of the SRs but it is narrower. The intensities of the 11 and 13.1 μm peaks vary greatly being at times quite weak. These stars show an emission excess at long wavelength which is sigificantly different from the 18 μm emission. It appears to extend from about 16 to 22 μm with a peak at about 19.5 μm. If the 3 component feature is also due to silicates is not yet known. The peak at 8 μm seen in Figure 2 appears to be an artifact of our method of analysis. It disappears if photospheric temperatures are used to fit the shortest wavelengths of the LRS. This research is supported in part by a University Resident Research Fellowship from the Air Force Office of Scientific Research to the Air Force Geophysics Laboratory.
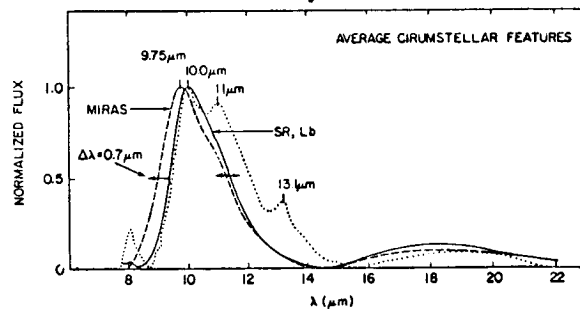

Fig 2. The three types of 10 μm excess.

REFERENCES

DeGioia-Eastwood, K., Hackwell, J.A., Grasdalen, G.L., and Gehrz, R.D. 1981, Ap.J., 245, L75.
Forrest, W.J., Gillett, F.C., and Stein, W.A. 1975, Ap.J., 175, 423.
Vardya, M.S., De Jong, T., and Willems, F.J. 1986, Ap.J., 304, L29.

The Ultraviolet Extinction in M-supergiant Circumstellar Envelopes

Richard H. Buss Jr. and Theodore P. Snow Jr.

Using *IUE* archival low-dispersion spectra, we have derived ultraviolet spectral extinctions in the circumstellar envelopes of two M supergiants: HD 60414 and HD 213310. The observed stellar systems belong to a class of widely-separated spectroscopic binaries that are called *VV Cephei* stars. These systems usually contain an early M supergiant and a hot companion B star that lies within the stellar wind of the M star. The ultraviolet radiation of the hot stars has allowed us to obtain ultraviolet spectral extinction curves for two different M supergiant envelopes: M0 Ib (HD 213310) and M2 Iab pe (HD 60414).

We first classified the hot stars with the *IUE* Low-Dispersion Spectral Atlas (Heck *et al.* 1984). By non-quantitative comparison, we found gB3 as the ultraviolet spectral type for HD 213310 and s-B3pe as the ultraviolet spectral type for HD 60414. It is interesting that the hot component of HD 213310 has been classified as a B8 V star (Hoffleit 1982) and that the hot component of HD 60414 has been tentatively classified as a B2 V star (Jasheck 1963). Though the the ultraviolet classification system and the MK system do not directly correspond, the discrepancies between the luminosity types for the same star indicate that the luminosity-sensitive ultraviolet lines better characterize the luminosity class for B stars in *VV Cephei* systems.

We calculated the total extinction by dividing the reddened fluxes with unreddened comparison fluxes of similar stars (g B2.5 for HD 213310 and a normalized s+B3 for HD 60414) from the reference atlas. After subtracting the interstellar extinctions (Seaton 1979), which we estimated from the E(B - V) reddening of nearby stars [E(ism) $\approx$ 0.12 toward HD 213310 and E(ism) $\approx$ 0.22 toward HD 60414], we normalized the resultant circumstellar extinctions (solid lines in the accompanying figures) to the interstellar extinction (crosses in the figures) at about 3.5 inverse microns.

Not only is the 2175 Å extinction bump absent in the circumstellar extinctions but also the far-ultraviolet extinction rise is absent. We interpret the rather flat, ultraviolet extinction curves as signatures of a population of non-carbonaceous, oxygen-rich grains that have diameters larger than the longest observed wavelength. Hence, the similarity of flat extinction in both the α Sco circumstellar envelope (Snow *et al.* 1986) and in these two *VV Cephei* systems, which contain primary and secondary stars that differ from each other's counterparts, indicates that the spectral subtypes of the stars do not greatly influence the composition and sizes of the nascent grains around M supergiants; all of the circumstellar grains appear to be large and non-carbonaceous.

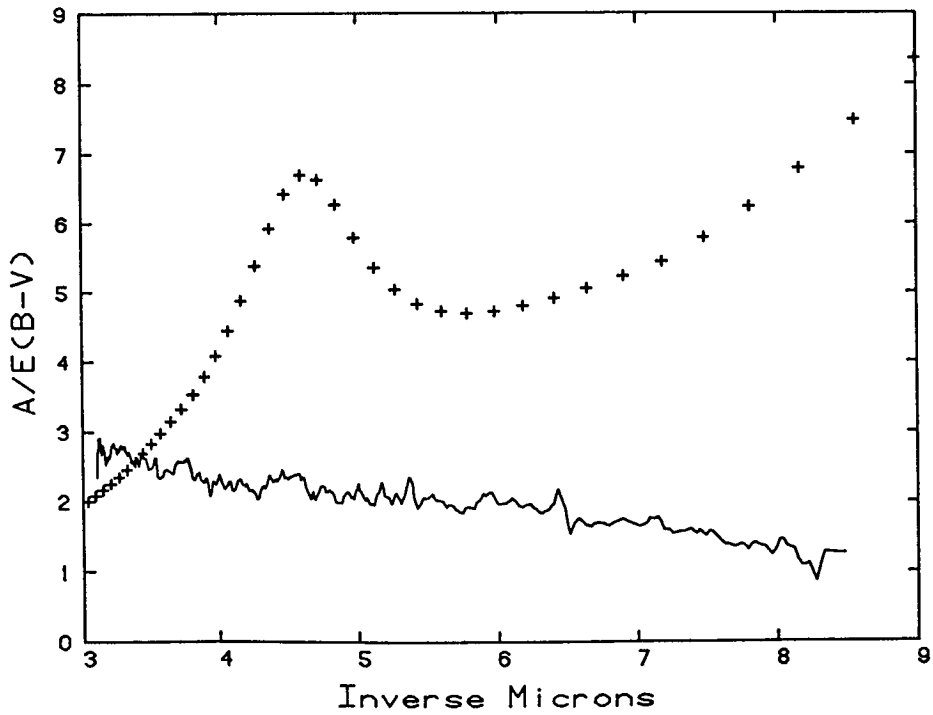## References

Heck, A., Egret, D., Jaschek, M., and Jaschek, C. 1984, *ESA* SP-1052.
Hoffleit, D., and Jaschek, C. 1982, *The Bright Star Catalog* 4th ed., Yale University Observatory.
Jaschek, C. and Jaschek, M. 1963, *P. A. S. P.*, **75**, 509.
Seaton, M. J. 1979, *M. N. R. A. S.*, **187**, 73P.
Snow, T. P., Buss, R. B., Gilra, D. P., and Swings, J. P. 1986, in preparation.

HD 213310
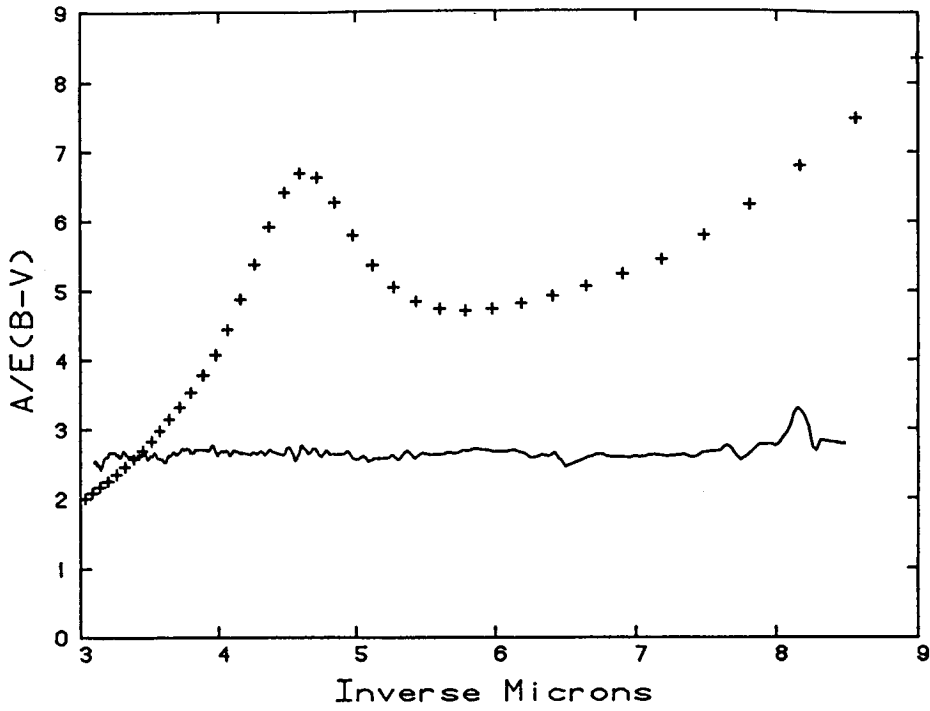
HD 60414

SPECTRAL CHARACTERISTICS OF DUST IN CARBON-RICH OBJECTS

R. F. Silverberg, H. Moseley, and W. Glaccum[1]
NASA/Goddard Space Flight Center

ABSTRACT

Some carbon-rich objects exhibit a strong broad emission feature beginning at $\lambda \sim 24\mu m$ and extending to $\lambda > 30\mu m$. We present a 20-65μm spectrum of the carbon star IRC+10216 and 30-55μm spectra of three carbon-rich planetary nebulae, IC 418, NGC 6572, and BD+30°3639 in Figs. 1 and 2. The 30-55μm observations were made with a six-channel spectrophotometer with $\sim$ 3.5μm spectral resolution, while the IRC+10216 spectrum was obtained using a two band 20-65μm 24-channel spectrometer with 3% resolution. The strong emission feature around 30μm is seen clearly in IRC+10216, IC 418 and NGC 6572. The decline at $\lambda > 40\mu m$ is particularly steep in these objects, while BD+30°3639 has a very flat spectrum in this spectral region.

It is remarkable to note that 22% of IC 418's far infrared ($\lambda > 10\mu m$) flux is emitted in this feature if a reasonable underlying continuum is removed. This fact puts stringent limits on our identification of this feature as thermal emission from dust. The short wavelength edge of the feature fits very well with that of MgS (Fig. 3), but the long wavelength emissivity in the laboratory spectrum is greater than in IC 418 or IRC+10216. This may be due to differences in grain structure between the laboratory dust and the nebular dust. The spectral match of amorphous MgS to the excess IC 418 and IRC+10216 emission is much better at long wavelengths than MgS in the cubic crystalline form.

The grains responsible for this feature must intercept at least as much ultraviolet and visible stellar and nebular radiation as is radiated in the infrared. This requires a rather large absorption cross section for these grains. We make the conjecture that the large infrared cross section can be produced by a thin ($<$ 0.1μm) coating on existing SiC grains. This model can serve to increase the MgS ultraviolet absorption cross section as well as the infrared emission efficiency with an acceptable amount of MgS.

The MgS feature is seen in some but not all carbon stars and carbon-rich planetary nebulae. In general, objects having the MgS feature also exhibit the SiC feature, while objects with the narrow lines (e.g. NGC 7027, BD+30°3639) do not have the far infrared feature. Following Barlow, we suggest that this variation is related to the C/O ratio. If C/O is only somewhat greater than unity, Si, which is about 10% as abundant as carbon, can occupy much of the excess carbon forming SiC, leaving the Mg and S to form MgS. If C/O $\gg$ 1, much of the S will be bound up in the stable gas molecule CS at the time of dust condensation. Therefore, MgS formation is inhibited by the reduction in available S and amorphous carbon or graphite grains would dominate the dust population rather than SiC.
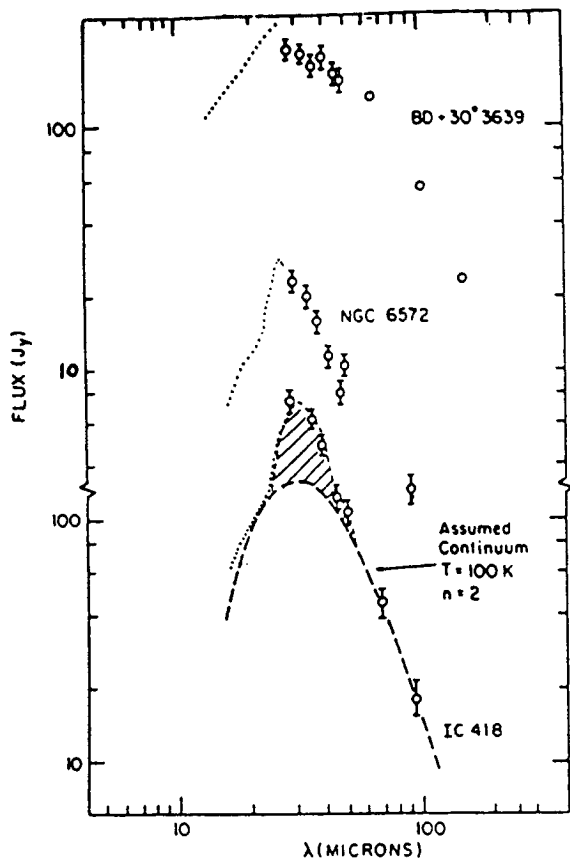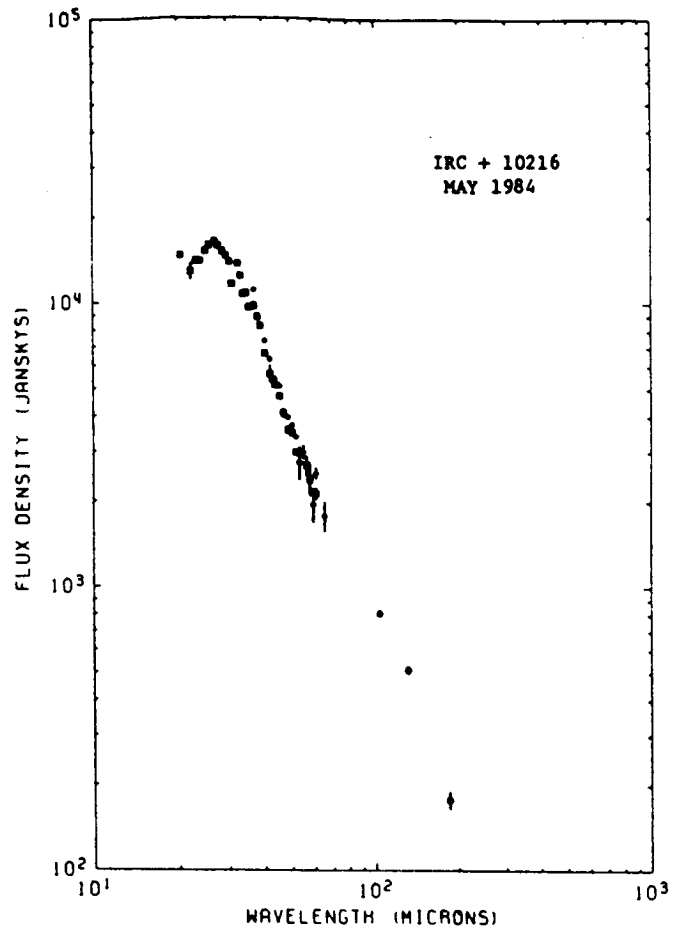
Figure 1

Figure 2

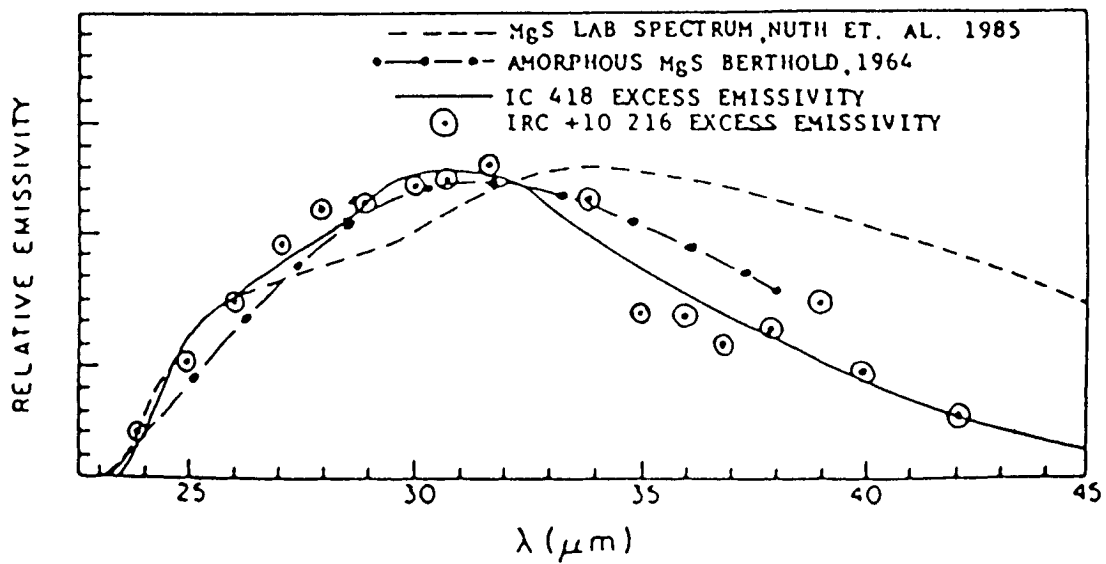Figure 3

The Organic Component of Interstellar Grains

W.A. Schutte and J.M. Greenberg
University of Leiden
The Netherlands

The 3.4 μm absorption feature observed in the spectrum of a number of Galactic Center sources indicates the presence of organic molecules in the interstellar medium. It is ascribed to the C-H stretch vibration of tetrahedrally bonded carbon (carbon which has only single bonds with other carbon atoms). These sources are thought to be principally obscured by the diffuse interstellar medium, as no molecular clouds have been observed in the direction of the G.C.. Fig. 1 shows the I.R. spectrum of the G.C. source IRS 7 (Butchart et al. 1986). Apart from the 3.4 μm feature two other absorptions are present: a broad feature centered at 2.98 μm and a rather shallow feature at 3.28 μm. The last feature can be ascribed to the C-H stretch vibration of trigonally bonded carbon. (carbon that has one double bond with another carbon atom). Laboratory experiments showed that the water band of a dirty ice mixture of composition $H_2O: CO:NH_3:O_2 = 20:14:8:20$ matches the 2.98 μm feature very well (fig. 1). This band possibly originates in intervening molecular clouds along the long line of sight towards the G.C.

From the observed features due to the interstellar organic material we can make an estimate of its composition and abundance. From $W_\lambda(3.28)/W_\lambda(3.4) = 0.11$ for IRS 7 we find a ratio of the number of C-H groups of tetrahedrally to those of trigonally bonded carbon $n(C_{te}-H)/n(C_{tr}-H) = 1.5$. The number of tetrahedral C-H bonds per carbon atom is given by:

$$\frac{n(C_{te}-H)}{n(C)} = \frac{W_\lambda(3.4)/A_\lambda(C_{te}-H)}{\alpha.\beta\ \tau(10).[C]}$$

where $W_\lambda(3.4)$ equals the equivalent width of the 3.4 μm feature, A_λ is the integrated intensity of the trigonal C-H stretch vibration $= 0.45 \times 10^{-20} cm^2$ μm (Francis 1950, 1951), α is $A(V)/\tau(10) = 18.5$ (Roche and Aitken 1984), β is $N(H)/A(V) = 1.9 \times 10^{21} cm^{-2} mag^{-1}$ and [C], the cosmic abundance of carbon $= 3.7 \times 10^{-4}$. $\tau(10)$, the depth of the silicate absorption towards the G.C. was taken equal to 3.6 (Becklin et al. 1978). We find $n(C_{te}-H)/n(C) = 0.26$. Taking into account the relative abundances of the different organic groups it follows that the organic material contains about 35 % of the cosmically available carbon.

The broadness of the 3.4 μm feature indicates a solid implying that the organic material indeed is a component of the grains. Gaseous species would exhibit a number of sharply peaked absorptions.

Duley and Williams (1986) proposed on the basis of observations of the depletion of argon and carbon in diffuse clouds (Duley 1985) that direct accretion of elemental carbon forming a hydrocarbon mantle around preexisting silicate cores is the production source of the organic material. However, the ratio of elemental hydrogen to elemental carbon in normal diffuse clouds is about equal to $n(H)/n(C) = 10^3$ (see e.g. Morton 1974), and therefore surface reactions between carbon and hydrogen would transform all accreting carbon into CH_4 (d'Hendecourt 1985), which would be desorbed in diffuse clouds circumstances (Draine and Salpeter 1979). Alternatively, it has been shown that photoprocessing of dirty ice mantles accreting on grains in molecular clouds form organic refractory grain mantles in sufficient abundance to explain the amount observed (Schutte and Greenberg 1986).
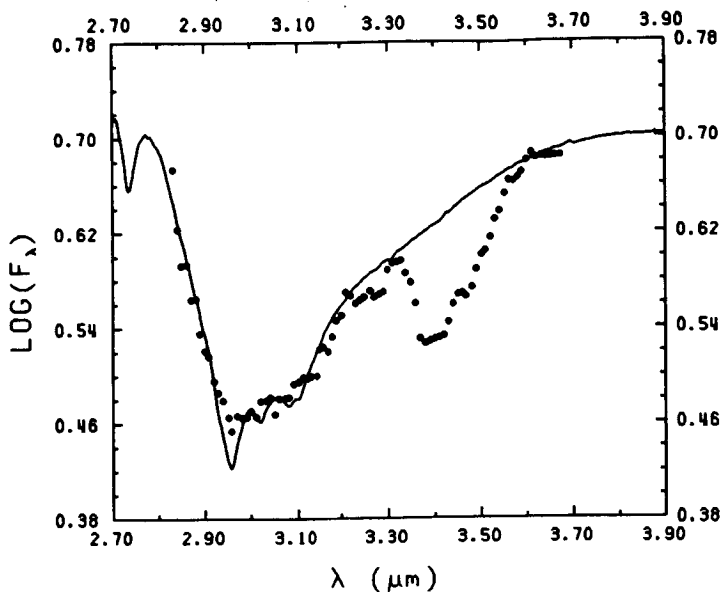
Fig 1. The I.R. spectrum of the G.C source IRS 7 compared with the H_2O absorption at 2.98 μm of an ice mixture of composition $H_2O:CO:NH_3:O_2 = 20:14:8:20$

In the diffuse medium, this organic mantle could be transformed into a hydrocarbon type material trough further photoprocessing by the interstellar radiation field eliminating the oxygen from the material and simultaneous hydrogenization by the interstellar atomic hydrogen.

References:

Allamandola, L.J., Tielens, A.G.G.M., and Barker, J.R. 1985, Ap.J.(Letters), 290, L25.

Becklin, E.E., Mathews, K., Neugebauer, G., and Werner, M.W. 1978, 220, 831.

Butchart, I., McFadzean, A.D., Whittet, D.C.B., Geballe, T.R., and Greenberg, J.M. 1986, Astr.Ap.(Letters), 154, L5.

Draine, B.T., and Salpeter, E.E. 1979, Ap.J., 231, 438.

Duley, W.W. 1985, Ap.J., 297, 296

Duley, W.W., and Williams, D.A. 1986, M.N.R.A.S., 219, 859.

Francis, S.A. 1950, J. Chem. Phys., 18, 861.

Francis, S.A. 1951, J. Chem. Phys., 19, 942.

d'Hendecourt, L.B. 1985, Astr. Ap., 152, 130.

Morton, D.C. 1975, Ap.J., 197, 85.

Roche, P.F., and Aitken, D.K. 1984, M.N.R.A.S., 208, 481.

Schutte, W.A., and Greenberg, J.M. 1986, Proc. of the IRAS conference "Light on Dark Matter".

Measuring Interstellar Grains from the Haloes of Binary X-ray Sources

Y. Xu and R. McCray (Univ. Colo. - JILA)

Coherent forward scattering of X-rays by interstellar grains creates a halo around the X-ray image of a compact source. The fractional halo brightness at 2 keV is typically of order 10% for moderately reddened galactic sources. The angular brightness distribution of the halo, which extends over several arcminutes, indicates the size distribution of the grains, and the spectrum of the halo indicates the composition of the grains. The halo will persist for several hours after the point source vanishes during an eclipse of a binary source; this provides a way to avoid systematic errors in measuring halo brightness due to an extended point response function of the X-ray telescope. Indeed, it is possible to infer the size distribution and composition of the grains without an imaging X-ray telescope by observing the time-dependence of the halo spectrum during eclipse.

IV. INTERSTELLAR CHEMISTRY AND ELEMENTAL ABUNDANCES

A. Interstellar Chemistry

MOLECULAR CATASTROPHES AND THE FORMATION OF CIRCUMSTELLAR DUST

Robert E. Stencel
Center for Astrophysics and Space Astronomy
University of Colorado, Boulder

Interstellar dust grains are presumed in part to have their origins in the outer atmospheres of red giant and supergiant stars because, despite the efficiency of shock destruction of grains in the ISM, meteoritic samples examined on Earth possess isotopic signatures that are consistent with nucleosynthetic origin in the interior of evolved stars (Clayton 1985). Among the four leading explanations for mass loss from such objects (thermally driven winds, magnetically driven winds, pulsation and radiation pressure on dust grains), there is ample evidence that once dust grains form near red giants and supergiants, radiation pressure is sufficient to drive them to infinity (Jura 1984). The problem of the formation of such dust is a classic one (Salpeter 1974) which requires understanding the combined roles of radiative transfer, gas dynamics and chemical reactions. Virtually all published studies have only attacked portions of the combined problem.

One key deficiency in previous efforts to understand the formation of circumstellar dust has been in using radiative equilibrium assumptions concerning the nature of the atmosphere underlying the circumstellar envelope (CSE). Contrary to the assertion of Jennings and Dyck (1972), based solely on optical Ca II K line emission, that chromospheres are 'quenched' in the presence of dust, recent ultraviolet and microwave analyses (Carpenter et al. 1985; Stencel et al. 1986; Hjellming and Newell 1983) have shown the chromospheres of dusty red supergiant stars to be persistent, and, unlike the solar chromosphere, can fill the entire volume out to the base of the CSE (several stellar radii). I suggest that this extended chromosphere is prone to instabilities which ultimately result in the formation of dust grains. Such instabilities are analogous to that known for the warm and cold phase of the ISM (cf. Lepp et al. 1985).

Compared to the ISM, the higher density atmospheres of stars (10^6 to 10^{12} cm^{-3}) occupy regions in a temperature-density plane for which molecular formation is required. Simple molecules like CO, SiO, H2O and OH are unique in that they have relatively high binding energies (11, 8, 5 and 4 eV), absorb well in the UV and radiate efficiently in the IR, and thus act as effective coolants. In high gravity stars like the Sun, the conditions in the upper photosphere tend to associate C and O. When this happens, the radiative cooling due to CO strongly cools the surroundings, leading to the formation of additional CO molecules which further enhance the cooling until complete CO saturation is achieved (a runaway process dubbed the "molecular catastrophe" by

Kneer 1983 and Muchmore 1986). In the Sun, there is a striking difference between the brightness temperatures in the 2.3 micron CO band, and atomic features of the upper photosphere. It is this strong temperature sensitivity of molecular opacity which I propose can operate to ultimately lead to the formation of dust at the base of CSE in red supergiant stars.

VLBI observations of the M4Ie supergiant VX Sgr by Chapman and Cohen (1986) and Lane (1984) are instructive in this context: the SiO masers lie closest to the stellar photosphere (at 1-2 radii), the OH and H2O masers occur farther out (tens and hundreds of radii). Localized CO catastrophes in the stellar photosphere give rise to pressure perturbations which result in SiO formation catastrophes in the extended chromosphere of the star. The formation of SiO in excited states prompts the observed maser emission, and subsequent chemistry anneals the SiO into clusters and associations like olivine (Mg,Fe)2SiO4 (Woolf and Nye 1969; Donn and Nuth 1985), which is removed from the star by radiation pressure. The OH and H2O masers result from their formation catastrophes at lower temperatures and densities in the outer chromosphere/CSE where conditions associated with their lower binding energy phase change take place.

The molecular catastrophe description for the conversion of chromospheric gas into molecular masers and circumstellar dust holds promise for a coherent expanation of the formation of these entities and the process of mass loss from cool, high luminosity objects. We will report elsewhere on quantitative simulations of this scenario, in collaboration with David Muchmore and Joseph Nuth, incorporating a full treatment of gas dynamics, radiative transfer and chemical reactions. This work has been supported by CASA at the University of Colorado, for which the author is grateful.

REFERENCES:
Carpenter, K., Brown, A. and Stencel, R. 1985 Ap.J. 289, 676.
Chapman, J. and Cohen, M. 1986 MNRAS in press.
Clayton, D. 1985 in Interrelationships Among Circumstellar, Interstellar and Interplanetary Dust, NASA Conf. Publ. 2403.
Donn, B. and Nuth, J. 1985 Ap.J. 288, 187.
Hjellming, R. and Newell, R. 1983 263, L85.
Jennings, M. and Dyck, H. 1972 Ap.J. 177, 427.
Jura, M. 1984 Ap.J. 286, 630.
Kneer, F. 1983 A&A 128, 311.
Lane, A. 1984 in VLBI and Compact Radio Sources, eds. Fanti et al. (Dordrecht; Reidel), p. 329.
Lepp, S., McCray, R., Shull, J.M., Woods, T. and Kallman, T. 1985 Ap.J. 288, 58.
Muchmore, D. 1986 A&A 155, 172.
Salpeter, E. 1974 Ap.J. 193, 585.
Stencel, R., Carpenter, K. and Hagen, W. 1986 Ap.J. 308 in press.
Woolf, N. and Ney, E. 1969 Ap.J. 155, L183.

TRANSLUCENT MOLECULAR CLOUDS:
THEORY AND OBSERVATIONS

Ewine F. van Dishoeck
Center for Astrophysics, Cambridge Ma 02138

and

John H. Black
Steward Observatory, Tucson, Az 85721

The study of interstellar clouds has traditionally been concerned with two different classes of clouds. Diffuse clouds, which have a total visual extinction $A_V \leq 2$ mag, have been observed through absorption lines of atoms and molecules at optical and ultraviolet wavelengths in the spectra of background stars. Photoprocesses, such as photodissociation and photoionization of the molecules and atoms, play an important role in the structure and chemistry of these clouds, and the fractional ionization is consequently high. Molecular clouds, which typically have $A_V > 10$ mag and much larger molecular column densities, have been studied by emission lines of molecules at centimeter and millimeter wavelengths. Because of the large extinction, photoprocesses are generally thought to be negligible inside molecular clouds, and the inferred electron abundances are much lower. Only few studies exist of clouds with $A_V \simeq 2$–10 mag, which bridge the gap between the diffuse and molecular clouds (Crutcher 1985). With the improved sensitivity of detectors in the red part of the spectrum, these clouds are amenable to study not only by radio techniques, but also through optical absorption line observations, provided that a suitable background star can be found. We will denote these clouds as "translucent molecular clouds".

On the observational side, few suitable stars behind molecular clouds have been identified. We have therefore performed a limited survey of interstellar lines toward highly–reddened stars ($V \simeq 5 - 10$ mag) in the southern sky, using the ESO 1.4 m CAT telescope with a Reticon detector, and the Cerro Tololo 4 m telescope equipped with a GEC CCD detector. Because of the reduced extinction at longer wavelengths, we searched primarily for molecules with transitions in the red part of the spectrum such as C_2 and CN. For some lines–of–sight for which C_2 was detected, the 4300 Å line of CH was also observed. Absorption lines of interstellar C_2 around 8750 Å were detected in the spectra of about one–fourth of the 36 observed stars. The inferred C_2 column densities range between 10^{13} and 10^{14} cm^{-2}, and are up to an order of magnitude larger than those found for diffuse clouds. The observed column densities of CH correlate very well with those of C_2 over this range. In contrast, the measured column densities of CN vary by orders of magnitude between the various regions, and they do not correlate with those of C_2 and CH. The observed rotational population distribution of C_2 also provides information about the physical conditions in the clouds (van Dishoeck and Black 1982). Densities n_H varying between 500 and 1500 cm^{-3}, and temperatures T ranging between 15 and 60 K were inferred.

Models of translucent molecular clouds have been constructed along the lines described by van Dishoeck and Black (1986) for diffuse clouds. The models compute accurately the fractions of atomic and molecular hydrogen as functions of depth into the clouds, as well as the excitation of H_2 by ultraviolet pumping. They also incorporate a detailed treatment of the photodissociation processes of the molecules (cf. van Dishoeck 1986), which play an important role in the chemistry up to depths of about 3 mag. In particular, the models include an accurate calculation of the depth dependence of the CO photodissociation, by using the most recent experimental

TABLE 1

Calculated column densities (in cm^{-2}) of various atoms and molecules
in models with increasing total visual extinction[a]

Nr.	A_V^{tot}	T (K)	n_H (cm^{-3})	I_{UV}^b	H_2	H	CO	C	C^+	CH	C_2	CN	OH	HD
1 ...	0.8	40	500	2	5.0(20)	2.6(20)	3(14)	3(15)	2(17)	3(13)	2(13)	3(12)	4(13)	1(15)
2 ...	1.5	20	500	2	1.0(21)	3.1(20)	3(15)	2(16)	4(17)	8(13)	5(13)	1(13)	1(14)	9(15)
3 ...	2.2	20	500	2	1.5(21)	6.3(20)	4(16)	7(16)	6(17)	2(14)	2(14)	5(13)	3(14)	3(16)
4 ...	3.0	15	700	1	2.2(21)	3.2(20)	2(17)	3(16)	2(17)	2(14)	1(14)	1(14)	2(15)	6(16)
5 ...	3.0	50	1500	12	2.0(21)	8.3(20)	1(16)	5(16)	4(17)	1(14)	1(14)	2(13)	2(14)	3(16)

[a] All models have oxygen and nitrogen depletion factors $\delta_O = \delta_N = 0.5$. Models 1–3 have a carbon depletion factor $\delta_C = 0.4$, whereas Models 4–5 have $\delta_C = 0.2$. A cosmic ray ionization rate $\zeta_0 = 5 \times 10^{-17}$ s^{-1} is employed throughout.

[b] Scaling factor for the strength of the ultraviolet interstellar radiation field relative to the average radiation field given by Draine (1978).

information on the predissociating lines of CO. Table 1 shows the results of the calculations for a series of cloud models with increasing total H_2 column density and extinction. The first model is representative of a typical diffuse cloud such as the cloud toward ζ Per. Model 4 has the physical conditions that are thought to prevail in the cloud in front of the star HD 29647, whereas Model 5 may be appropriate to describe the HD 147889 cloud. Table 1 clearly demonstrates the large increase (by several orders of magnitude) of the CO and C column densities relative to that of C^+ in the thicker clouds. The computed CH and C_2 column densities agree well with the observed values. The processes leading to the formation of the CN molecule are still not well understood. Further observations of translucent molecular clouds through ultraviolet absorption line observations and radio emission line measurements will be very fruitful.

REFERENCES:

Crutcher, R.M. 1985, *Ap. J.*, **288**, 604.

Draine, B.T. 1978, *Ap. J. Suppl.*, **36**, 595.

van Dishoeck, E.F. 1986, in IAU Symposium 120, *Astrochemistry*, eds. M.S. Vardya and S.P. Tarafdar (Dordrecht, Reidel), in press.

van Dishoeck, E.F. and Black, J.H. 1982, *Ap. J.*, **258**, 533.

van Dishoeck, E.F. and Black, J.H. 1986, *Ap. J. Suppl.*, in press.

DO LARGE RATE COEFFICIENTS FOR ION-POLAR NEUTRAL REACTIONS HAVE A SERIOUS EFFECT ON CHEMICAL MODELS OF DENSE CLOUDS?

Eric Herbst
Department of Physics, Duke University
Durham, NC 27706

and

Chun Ming Leung
Department of Physics, Rensselaer Polytechnic Institute
Troy, NY 12180-3590

Adams, Smith, and Clary (1985) have recently argued that rate coefficients for ion-polar neutral gas phase reactions occurring at interstellar cloud temperatures (<100 K) are considerably larger than the canonical Langevin value. While their conclusion is based primarily on the theoretical work of Clary (1985), a variety of previous theoretical treatments (see, e.g., Bates 1982) support this view. Herbst (1986) has noted, however, that all of these treatments consider the long-range attractive ion-dipole potential only and ignore possible short-range repulsive effects. If the long-range theories are correct, rate coefficients as large as 1x10(-07) cc/sec (two orders of magnitude greater than the Langevin value) can be expected at a temperature of 10 K. Although there is as yet little experimental evidence concerning the reliability of the calculated rates at temperatures below 100 K, it is important to determine the effect of such large rate coefficients on gas phase chemical models of dense interstellar clouds.

In order to incorporate large ion-polar neutral rate coefficients into existing gas phase reaction networks, it is necessary to utilize simplified theoretical treatments because of the significant number of rate coefficients needed. We (Herbst and Leung 1986a) have used two simple theoretical treatments - the "locked dipole" approach of Moran and Hamill (1963) for linear polar neutrals and the "trajectory scaling" approach of Su and Chesnavich (1982) for non-linear polar neutrals. The former approach is suitable for linear species because in the interstellar medium these are rotationally relaxed to a large extent and the incoming charged reactants can "lock" their dipoles into the lowest energy configuration. The latter approach is a better approximation for non-linear neutral species, in which rotational relaxation is normally less severe and the incoming charged reactants are not as effective at "locking" the dipoles. The treatments are in reasonable agreement with more detailed long-range theories and predict an inverse square root dependence on kinetic temperature for the rate coefficient. Compared with the "locked dipole" method, the "trajectory scaling" approach results in rate coefficients smaller by a factor of approximately 2.5.

The calculated large rate coefficients have been incorporated into the gas phase chemical model of Herbst and Leung (1986b) which contains 206 chemical species and 1958 reactions, and is pseudo time-dependent in the sense that physical conditions are assumed to remain constant as the chemistry evolves from given initial conditions. The changes found from previous results are less than dramatic. In our previous work (Herbst and

Leung 1986b; Leung, Herbst, and Huebner 1984) it was found that the calculated abundances of complex species peak at times earlier than that required for steady state to be achieved. This feature is preserved in the present calculation. In general, however, stable polar neutral species show decreases in their calculated abundances at both "early" times, when peak abundances are achieved, and at steady state of up to one order of magnitude. Most neutral atoms, stable nonpolar species, reactive neutral species (radicals), and some molecular ions deviate from this trend and show abundances that are unchanged from previous results or that actually increase. In addition, the use of the more rapid rates speeds up the chemistry of stable polar neutrals such as HC_3N resulting in the achievement of peak abundances at earlier times than in previous calculations. All of these changes are found to be stronger in our models of dark clouds, where the temperature is typically 10 K, than in our models of warmer sources such as OMC-1.

The decreases in calculated abundances of stable polar species are often coupled with increases in the calculated abundances of protonated ions of these species, as originally noted for CS and HCS+ by Millar et al. (1985). These authors showed via a small reaction network that the observed value of the abundance ratio HCS+/CS in both TMC-1 and Sgr B2 can only be accounted for if the rapid ion-polar neutral rates are utilized. Their results are in reasonable but not perfect agreement with our detailed model results. Our new results also show a considerable enhancement in the HCNH+/HCN ratio, which may explain the recent observation of HCNH+ (Ziurys and Turner 1985). Despite the sensitivity of these ion/neutral abundance ratios to the size of ion-polar neutral rate coefficients, we find that overall the agreement between model results and observation is not changed appreciably by adoption of the larger rate coefficients.

REFERENCES

Adams, N. G., Smith, D., and Clary, D. C. 1985, Ap. J. (Letters), **296**, L31.
Bates, D. R. 1982, Proc. R. Soc. Lond., **A 384**, 289.
Clary, D. C. 1985, Mol. Phys., **54**, 605.
Herbst, E. 1986, Ap. J., in press.
Herbst, E. and Leung, C. M. 1986a, submitted to Ap. J.
———————————————————1986b, M. N. R. A. S., in press.
Leung, C. M., Herbst, E., and Huebner, W. F. 1984, Ap. J. Suppl., **56**, 231.
Millar, T. J., Adams, N. G., Smith, D., and Clary, D. C. 1985, M. N. R. A. S., **216**, 1025.
Moran, T. F. and Hamill, W. H. 1963, J. Chem. Phys., **39**, 1413.
Su, T. and Chesnavich, W. J. 1982, J. Chem. Phys, **76**, 5183.
Ziurys, L. M. and Turner, B. E. 1985, IAU Symposium #120 on Astrochemistry held in Goa, India (Dordrecht: Reidel, to be published).

STUDIES OF INTERSTELLAR VIBRATIONALLY-EXCITED MOLECULES

L.M. Ziurys, R.L. Snell, and N.R. Erickson
Five College Radio Astronomy Observatory
University of Massachusetts

Several molecules thus far have been detected in the ISM in vibrationally-excited states, including H_2, SiO, HC_3N, and CH_3CN (e.g. Goldsmith, et al. 1985). In order for vibrational-excitation to occur, these species must be present in unusually hot and dense gas and/or where strong infrared radiation is present. Vibrationally-excited molecules thus serve as useful probes of the physical conditions near star-forming regions and in the circumstellar envelopes of late-type stars. They also trace material where "shock" or "high temperature" chemistry may be occurring (i.e., gas that is sufficiently hot such that activation energy barriers in chemical reactions are overcome, allowing otherwise inaccessible reaction pathways to take place). Even more fundamentally, molecules in an excited vibrational state are subject to a different reaction potential surface than in the ground state, and unique reaction pathways may become available as vibrational-excitation occurs.

Unfortunately, past studies of vibrationally-excited molecules in the ISM have been somewhat incomplete. Either they have involved measurements of rotation vibration transitions, done in the IR where sensitivity is limited; else, they have been concerned with microwave/mm-wave observations of rotational lines of relatively low-excitation bending modes of large polyatomic molecules such as CH_3CN. Such molecules are not very abundant and thus lines origining in excited states are weak and difficult to study.

In order to do a more thorough investigation of vibrational excitation in the ISM, we have done studies of several mm-wave transitions originating in excited vibrational modes of HCN, an abundant interstellar molecule. Vibrationally-excited HCN was recently detected toward Orion-KL and IRC+10216, using the NRAO 12 meter antenna (Ziurys and Turner 1986). The J=3-2 rotational transitions were detected in the molecule's lowest vibrational state, the bending mode, which is split into two separate levels, $(0,1^{1c},0)$ and $(0,1^{1d},0)$ states, due to ℓ-type doubling. This bending mode lies 1025K above ground state, with an Einstein A coefficient of 3.6 s^{-1}. The J=3-2 line of $(0,2^0,0)$ mode of HCN, which lies 2050K above ground state, was also observed toward IRC+10216, and subsequently in Orion-KL (Turner and Ziurys, private communication). Toward KL, these initial measurements suggested that vibrationally-excited HCN arises from the "hot core", being excited by 14 μm IR flux from IRc2 with a vibrational temperature of $T_{vib} \sim 150$-200K. In addition, these observations implied that the column density of HCN in this region was $>10^{18}$ cm^{-2}, thus making the abundance of HCN greatest in the "hot core" as compared with all other gas components in KL. Analysis of the vibrationally-excited HCN lines toward IRC+10216 indicated an r^{-2} spatial dependence of this species' abundance in the envelope, inconsistent with the "freeze-out" model of circumstellar chemistry.

Further measurements of vibrationally-excited HCN have been done using the FCRAO 14 meter telescope, which include the observations of the (0,1,0) and (0,2,0) modes towards Orion-KL, via their J=3-2 transitions at 265-267 GHz (Ziurys, Snell, and Erickson 1986). The spectrum of the J=3-2 line in Orion of the $(0,1^{1d},0)$ mode of HCN, taken with the FCRAO telescope, is shown in Figure 1. A map was subsequently made of this line, shown in Figure 2, which indicates that emission from vibrationally-excited HCN arises from a region probably smaller than the FCRAO telescope's 20 arcsec beam. Such a distribution is consistent with the species' emission arising from the "hot core". As the figure shows, however, there might be some E-W elongation of vibrationally-excited HCN. A map of the ground state J=3-2 HCN line was done as well with the FCRAO 14 meter, and is also shown in Figure 2. As evident from the map, the ground state line shows a completely different spatial

distribution from that of the vibrationally-excited emission, being far more extended and showing pronounced N-S elongation along the Orion ridge. Analysis of the two excited modes of HCN, along with the ground state $HC^{15}N$ line (Johansson, et al. 1984), indicates a vibrational temperature of 290 K for HCN; this value is close to that derived for vibrationally-excited HC_3N from Hat Creek interferometer measurements by Plambeck (1986), who found $T_{vib} = 265 \pm 35$ K. Such a vibrational temperature is consistent with infrared excitation of the vibrational modes of HCN by 7 an 14 μm radiation from IRc2.

References:
Goldsmith, P.F., Krotkov, R., and Snell, R.L. 1985, Ap.J., 299, 405.
Johansson, et al. 1984, Astr. Ap., 130, 227.
Plambeck, R.L. 1986, private communication.
Ziurys, L.M., and Turner, B.E. 1986, Ap.J., 300, L19.
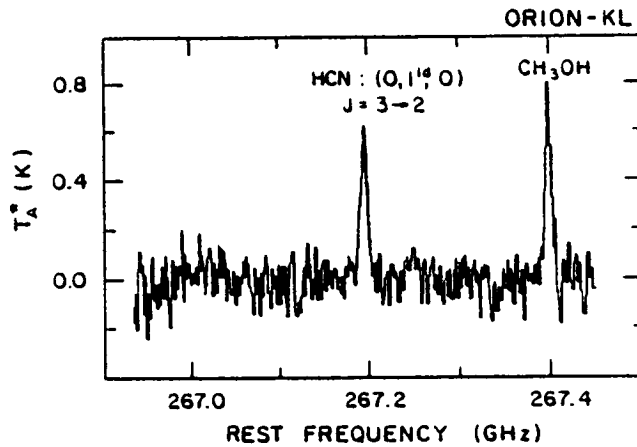Ziurys, L.M., Snell, R.L., and Erickson, N.R. 1986, in preparation.

Figure 1: The J=3-2 transition of the $(0,1^{1d},0)$ bending mode of vibrationally-excited HCN, observed towards Orion-KL with the FCRAO 14 meter telescope at 267 GHz.
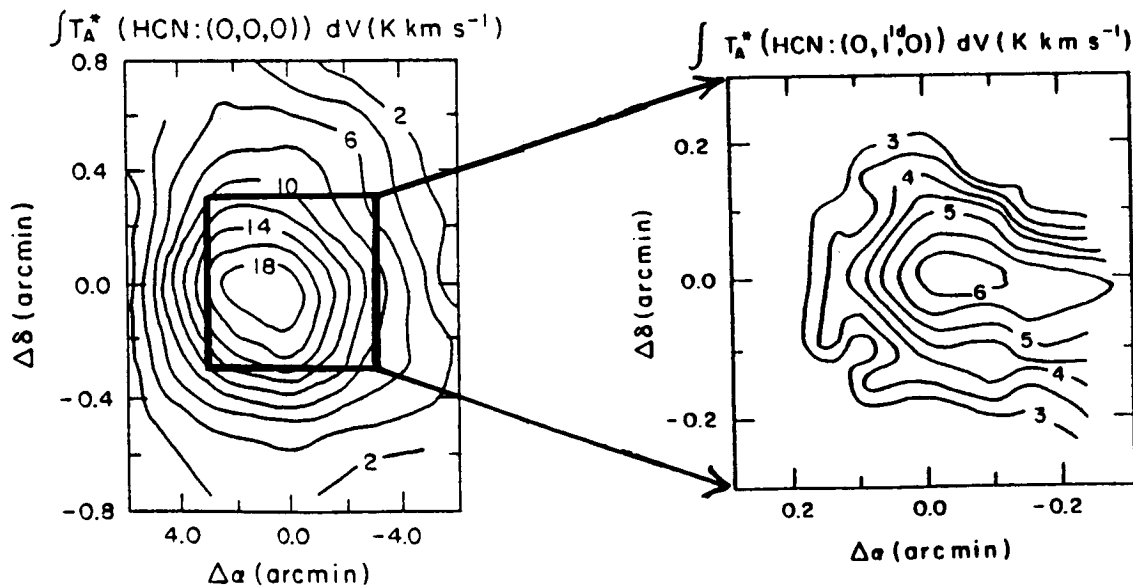

Figure 2: Maps of the integrated intensity of the J=3-2 lines of ground state and vibrationally-excited HCN, showing that they have different spatial distributions. The excited state emission probably arises from a source $\lesssim 20''$ in size.

MULTI-LEVEL STUDY OF C_3H_2: THE FIRST INTERSTELLAR HYDROCARBON RING

S. C. Madden, W. M. Irvine
Five College Radio Astronomy Observatory
University of Massachusetts

and

H. E. Matthews, L. W. Avery
Hezberg Institute of Astrophysics
National Reserch Council of Canada

Cyclic species in the interstellar medium have been searched for almost since the first detection of interstellar polyatomic molecules. It has been suggested that the relative abundance of rings might be related to the importance of reactions on grain surfaces as compared with that in the gas phase. Previous searches for rings, however, have only included stable closed shell molecules, and have not reached very low abundance limits. In contrast, the newly detected interstellar hydrocarbon ring, cyclopropenylidene (C_3H_2), is a di-radical, three-membered ring and was demonstrated by Matthews and Irvine (Ap. J. (Letters) $\underline{298}$, L61 1985) to be widespread throughout the Galaxy, originating in a variety of sources with a wide range of temperature and density. Since the serendipitious discovery of the easily detected ortho ground state transition, ($1_{10} \rightarrow 1_{01}$), followed by its identification by Thaddeus, Vrtikek, and Gottlieb (Ap. J. (Letters), $\underline{299}$, L63, 1985), we have made systematic Galactic surveys of several transitions and have concentrated in depth on the nearby dark dust cloud, TMC-1, which has shown an unusually high propensity toward C_3H_2. The fact that TMC-1 is also a dominant source of the carbon chain molecules, especially cyanopolyynes, leads to the speculation that the formation of this ring molecule may have some possible relationship to production of carbon chains.

We have detected 11 different C_3H_2 rotational transitions; 9 of them which have been studied in TMC-1 are shown in Figure 1. The $1_{10} \rightarrow 1_{01}$ and $2_{20} \rightarrow 2_{11}$ transitions were observed with the 43 m NRAO telescope, while the remaining transitions were detected with the 14 m antenna of the Five College Radio Observatory (FCRAO). The lines detected in TMC-1 have energies above the ground state ranging from 0.9 to 17.1 K and consist of both ortho and para species. Limited maps were made along the ridge for several of the transitions. Fortunately, we were able to map the HC_3N $J = 2 \rightarrow 1$ transition simultaneously with the C_3H_2 $1_{10} \rightarrow 1_{01}$ line and therefore can compare the distribution of this ring with a carbon chain in TMC-1. C_3H_2 is distributed along a narrow ($< 2'$) ridge with a SE - NW extension which is slightly more extended than the HC_3N $J = 2 \rightarrow 1$. Gaussian fits gives a FWHP extension of 8.5 for C_3H_2 while HC_3N has a FWHP of $7'$. Our data show variations of the two velocity components along the ridge as a function of transition. Most of the transitions show a peak at the position of strongest HC_3N emission while the $2_{21} \rightarrow 1_{10}$ transition shows a peak at the NH_3 position. The $3_{30} \rightarrow 2_{21}$ transition, which lies 17.1 K above the ground state, shows a weak, very narrow ($\sim.28$ km s^{-1}) component which seems to be sampling only one of the cloud components, perhaps indicating density variations throughout the source. The most surprising result was the detection of the $2_{20} \rightarrow 2_{11}$ transition in absorption against the 2.7 K background in TMC-1. Some results in other sources will also be presented.

C_3H_2 Detections in TMC-1

Figure 1: Ortho(left) and para(right) species of C_3H_2 detected in TMC-1 arranged in order of increasing energy above the ground state (bottom to top).

EFFECTS OF STELLAR OUTFLOWS ON INTERSTELLAR SULFUR OXIDE CHEMISTRY
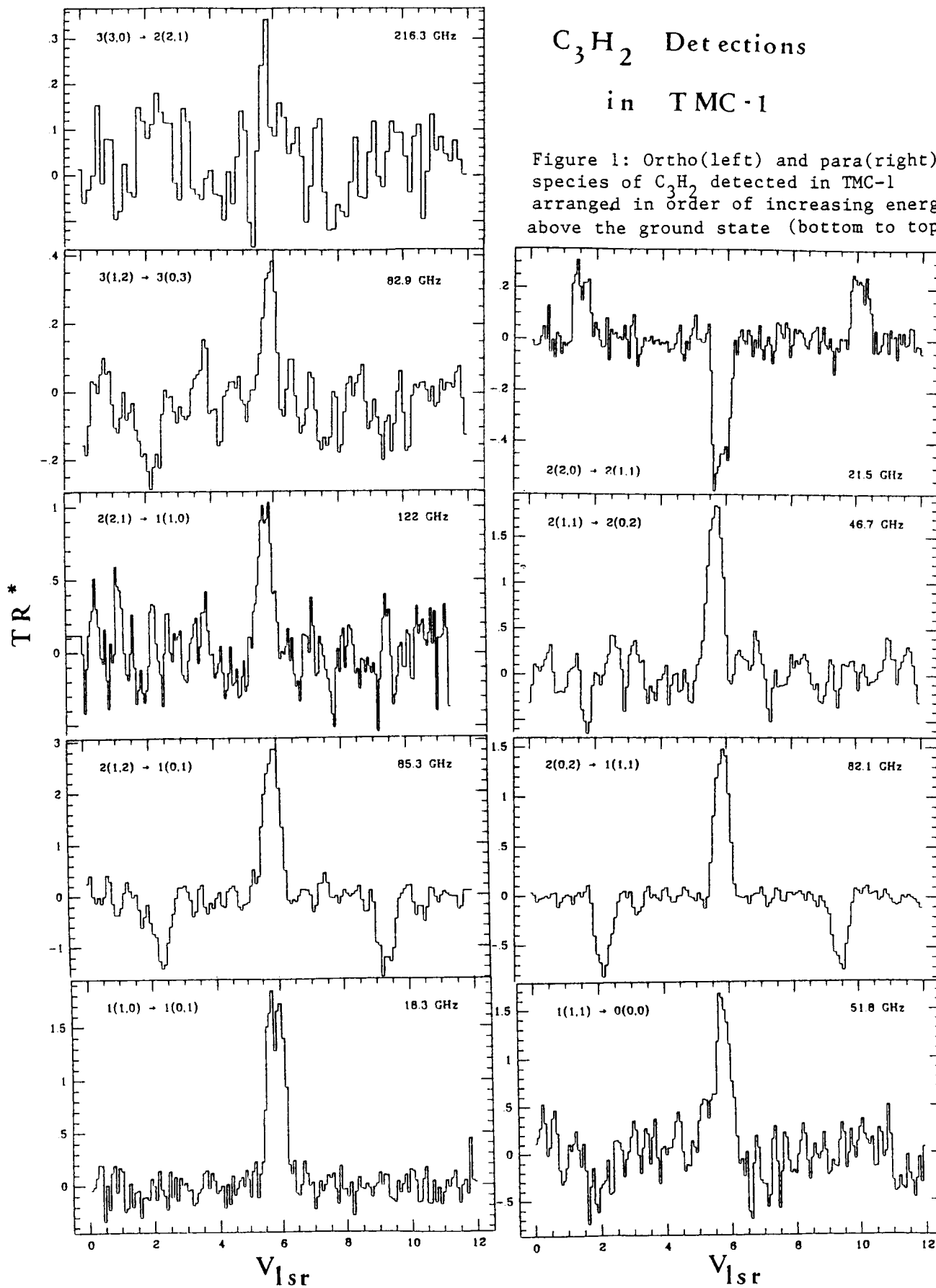
W. J. Welch(UC), S. Vogel(Caltech), S. Terebey(HAO),

J. Dreher(MIT), J. Jackson(UC), and J. Carlstrom(UC)

Interferometer Maps with 2"-6" resolution of a number of regions with active star formation (Orion A, W49, W51, SGRB2) show that the distribution of the molecule SO is very compact around stellar outflow sources. Both SO and SO_2 have been studied near three outflows, OrionA/IRc2 and two sources in W49. The two molecules have similar distributions and abundances. More than 95% of the emission comes from regions whose extents are only .05 to .2 pc., being larger around the more energetic sources. Their spectra are broad, 30 km/sec or more, suggesting that the oxide production is associated with the flows. The outflows are identified by water masers and by extended bipolar flows in SiO. Maps in other molecules, such as HCO^+ and CS, which have similar collisional excitation requirements, have much greater spatial extent. Thus it appears that the SO and SO_2 abundances are truly compact and are closely associated with the outflows. There are (at least) two obvious questions. (1) How does the outflow produce the SO and SO_2 and why in roughly equal proportions? (2) Why is it that these oxides do not diffuse into the rest of the clouds? Note that in the bulk of the clouds sulfur appears to be largely in the form of CS.

IV. INTERSTELLAR CHEMISTRY AND ELEMENTAL ABUNDANCES

B. Elemental Abundances

Interstellar Absorption Lines in the Spectrum of Sigma Sco
Using Copernicus Observations

M. Marsha Allen and Theodore P. Snow
Center for Astrophysics and Space Astronomy (CASA)
University of Colorado, Campus Box 391
Boulder, Colorado 80309

Since the launch of Copernicus in 1972, studies have been made of the depletion of gas-phase elements onto dust grains. A few stars have been studied in detail (Morton 1974, 1975, 1978; York and Kinahan 1979; York 1983; Snow 1976, 1977), resulting in a "standard" depletion pattern which has since been used for comparison. Recent developments, however, have suggested that this "standard" pattern may need to be re-examined. It has been recognized in the last few years that the curve-of-growth ambiguities in the saturated lines may be more serious than previously thought (e.g. de Boer 1979) with lines arising from low velocity dispersion gas being masked by broader lines from relatively higher velocity dispersions. Some weak, semi-forbidden lines have been detected recently which may be able to resolve some of the ambiguities. Studies of single elements have shown that depletion of carbon (Hobbs, York, Oegerle 1982) and oxygen (de Boer 1979) are much smaller than previously determined.

The high-resolution ultraviolet spectral scans of σ Sco (and three other stars; π Sco, δ Sco and ϑ Car) were originally made in 1973, but have only recently been analyzed. All these stars are bright (V 3.0) and moderately reddened. All four stars will be analyzed in detail, but σ Sco is the first one completed.

The data has broad coverage of ions, making these stars excellent candidates for determination of accurate depletions. We are using a profile-fitting analysis rather than curves-of-growth in order to determine separate abundances and depletions in components separated by several km/sec (the program and analysis procedure are described by Vidal-Madjar et al. 1977, by Snow and Meyers 1979 and by Meyers et al. 1985) In σ Sco three separate velocity components have been used for some lines. Two of the components were identified in high-resolution Na I (Hobbs 1969) at about -15 km/sec and -5 km/sec. However, in fitting S II (1250 Å , 1253 Å , 1259 Å), a third component was need at about -25 km/sec (out of range of Hobbs' data) (figure 1).

Sigma Sco in the the area of the ρ Oph cloud complex, a region which has been studied extensively. Meyers et al (1985) may have found a weak shock front in this area (velocity of about 10 km/sec). By studying this and other lines of sight in detail, we can get more information about the densities and temperatures related to weak shocks, in addition to increasing the number of stars with detailed depletion patterns.

References

de Boer, K. 1979, ApJ, 229, 132
Hobbs, L.M. 1969, ApJ, 157, 135
Hobbs, L.M., York, D.G., Oegerle, W.R. 1982, ApJ (Letters), 252, L21
Meyers, K.A., Snow, T.P., Federman, S.R., Breger, M. 1985, ApJ, 288,148
Morton, D.C. 1974, ApJ (Letters), 193, L35
Morton, D.C. 1975, ApJ, 197, 85
Morton, D.C. 1978, ApJ, 222, 863
Snow, T.P. 1976, ApJ, 204, 759
Snow, T.P. 1977, ApJ, 216, 724
Snow, T.P., Meyers, K.A. 1979, ApJ, 229, 545
Vidal-Madjar, A., Laurent, C., Bonnet, R., York, D.G. 1977, ApJ, 211,91
York, D.G. 1983, ApJ, 264, 172
York, D.G., Kinahan, B. 1979, ApJ, 228, 127

Fig 1: S II 1259.518 in σ Sco, decomposed into three components.
(solid line is observation, dotted lines are calculated Voigt profiles)
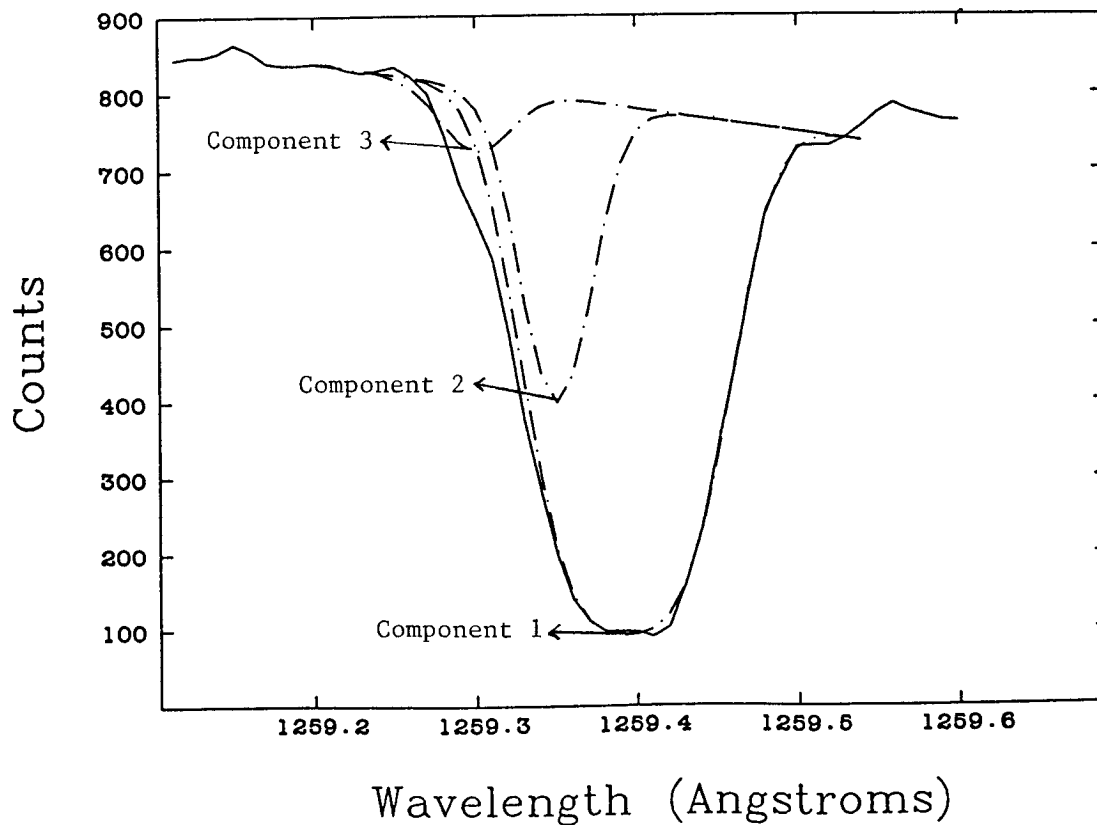
THE ABUNDANCE OF INTERSTELLAR SULPHUR AND ZINC
IN HIGH DENSITY SIGHT-LINES

A. W. Harris
Rutherford Appleton Laboratory
Chilton, Oxfordshire, U. K.

and

J. M. Mas Hesse
Dept. de Astrofisica, Universidad Complutense
Madrid, Spain

On the basis of early absorption line studies of individual lines of sight with the Copernicus satellite, chlorine, sulphur and zinc were classed together as elements which showed little or no depletion, relative to hydrogen, in the interstellar medium. The abundances of other less volatile elements, such as Fe and Mg were found to vary widely from one sight-line to another with gas-phase abundances in some cases being orders of magnitude below their solar counterparts. This depletion of elements from the interstellar gas is attributed to the existence of interstellar dust grains which contain a substantial fraction of the total mass of certain elements. Elements which show little or no depletion from the gas-phase are useful as tracers of metallicity or, alternatively, as a means of estimating hydrogen column densities, since their gas-phase abundances represent their true abundances in the interstellar medium. Recent work based on data from Copernicus and IUE has shown that in general depletion correlates well with the mean volume density of hydrogen, $\bar{n}(H)$, along a sight-line, while correlations with hydrogen column density, $N(H)$, are generally much weaker (Harris et al, 1984). Indeed, the large-scale survey of Harris and Bromage (1984) has revealed, contrary to expectation, that even the volatile element chlorine is depleted by factors of 5 or more in certain sight-lines and the depletion increases markedly with increasing $\bar{n}(H)$. The conclusion of Blake et al (1985) that the under-abundance of HCl in the Orion Molecular Cloud implies that Cl is depleted by up to a factor of 30 in this dense region is in excellent agreement with the density dependent behaviour of Cl depletion in diffuse clouds discovered by Harris and Bromage. Spitzer (1985) has shown that an idealized model of interstellar gas distribution consisting of a warm, uniformly distributed component and two types of cloud component offers a direct explanation for the "preference" of elements to deplete according to $\bar{n}(H)$.

Here we report on detailed studies of the depletion/ density behaviour of two other volatile elements which were previously considered to be virtually undepleted, S and Zn, using equivalent width data from both Copernicus and IUE observations. The results provide further evidence that the established dependence of depletion on $\bar{n}(H)$ extends to volatile elements and show that their use as tracers of metallicity, or for estimating hydrogen column densities, may lead to large errors in sight-lines through dense regions (with $\bar{n}(H) \gtrsim 10 \text{ cm}^{-3}$). It now appears that such elements may take part in the surface chemistry of grains and be important constituents of grain mantle material, although they probably do not contribute significantly to the

bulk mass of grains. Due to the very similar atomic masses and ionization potentials of sulphur and phosphorous, the thermal velocity distributions of the singly ionized species of these elements in interstellar clouds should be very similar. However, a comparison of Doppler widths (b-values) derived for SII and PII in the same sight-lines from the Bohlin et al (1983) Copernicus equivalent width measurements has revealed an unexpected systematic discrepancy of a factor of ~ 1.7. This discrepancy indicates that the normally adopted oscillator strengths of the PII $\lambda \lambda$ 1153 and 1302 Å lines may require revision.

Full details of the work described here are given in Harris and Mas Hesse (1986 a,b).

References

Blake, G. A., Keene, J., and Phillips, T. G. 1985, Ap. J., 295, 501.
Bohlin, R. C., Hill, J. K., Jenkins, E. B., Savage, B. D., Snow, T. P.,
     Spitzer, L. and York, D. G. 1983, Ap. J. Suppl., 51, 277.
Harris, A. W., and Bromage, G. E. 1984, M.N.R.A.S., 208, 941.
Harris, A. W., Gry, C., and Bromage, G. E. 1984, Ap. J., 284, 157.
Harris, A. W., and Mas Hesse, J. M. 1986a, M.N.R.A.S., 220, 271.
Harris, A. W., and Mas Hesse, J. M. 1986b, Ap. J., 308, Sept. 1, in press.
Spitzer, L. 1985, Ap. J., 290, L21.

IUE/IRAS STUDIES OF METAL ABUNDANCES AND INFRARED CIRRUS

Michael E. Van Steenberg and J. Michael Shull

Center for Astrophysics and Space Astronomy
and Joint Institute for Laboratory Astrophysics
University of Colorado and National Bureau of Standards

This paper reports on a survey of interstellar densities, abundances, and cloud structure in the Galaxy, using the IUE and IRAS satellites. We discuss heavy element depletions and their correlations with mean density, reddening, and galactic location. We also report on interesting correlations between the Fe/Si abundance ratio and the infrared diffuse cirrus, which may provide information on the history and formation of grains in the galactic halo.

From high-resolution (0.1 Å) IUE spectra we derive interstellar H I, Si II, and Fe II column densities toward 260 early-type stars by fitting the measured equivalent widths to single-component curves of growth. The IUE column densities of Fe II agree to 0.1 (dex), on average, with those derived by Copernicus (Jenkins, Savage, and Spitzer 1986) for 45 lines of sight in common. The good agreement depends critically on using consistent oscillator strengths and measuring the weak Fe II $\lambda 2260$ line to fix the curve of growth. Without this line, IUE data systematically overestimates the doppler parameter (b) and underestimates the Fe II column density by 0.2 - 0.8 (dex), owing to the presence of high-velocity components in the wings of strong lines. The abundances of Fe, Si, and other refractory elements are enhanced in these components by shock processing of grains.
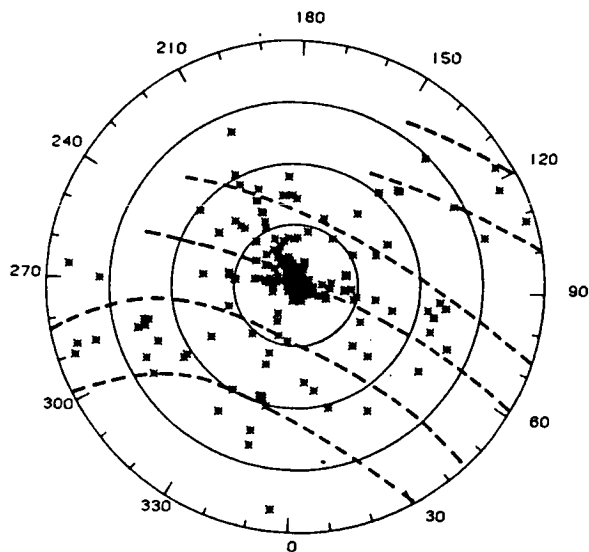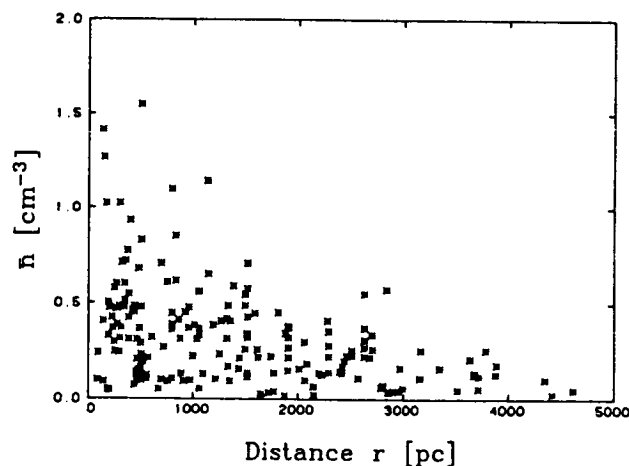

Figure 1

Figure 2

Figure 1 shows the 220 target stars in the statistical survey (B2.5 and earlier). The circular rings are 1 kpc apart and the dashed lines illustrate approximate locations of the spiral arms. Figure 2 shows the mean line-of-sight hydrogen density, $\bar{n}$ = N(H I)/r, towards these stars. The distribution of $\bar{n}$ suggests an intercloud medium of density ~0.1 cm^{-3}. The survey averages are $\langle \bar{n} \rangle$ = 0.55 cm^{-3} and $\langle N(H\ I)/E(B-V) \rangle$ = 5.2×10^{21} cm^{-2} mag^{-1}. The vertical scale heights of H I, Si II, and Fe II are 144 ± 80 pc, 168 ± 90 pc, and 268 ± 100 pc, respectively.

Figure 3 shows the correlation of Si and Fe depletions with $\bar{n}$. This pattern is consistent with in-cloud depletion or with enhanced shock processing in low density regions. These and other data suggest that the intercloud medium contains a smoothly distributed component, of about 0.1 cm^{-3} density, in which heavy element depletions are considerably less than in the cloud cores.
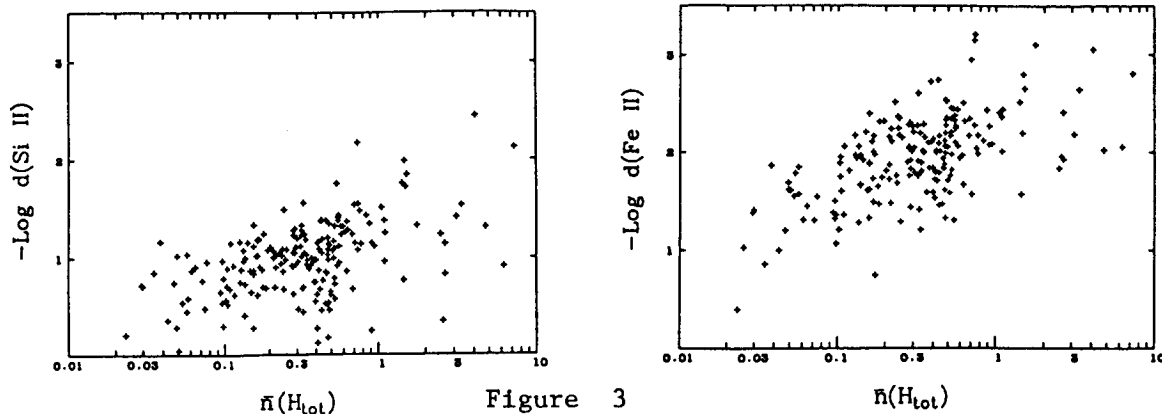

Figure 3

The Fe/Si ratio increases with galactic latitude (Fig. 4). The means are $\langle Fe/Si \rangle$ = 0.12 in the disk (b < 20°) and 0.22 in the halo (b > 20°). This difference may result either from Fe-production from Type I supernovae in the halo or from differential shock destruction of iron-containing grains.
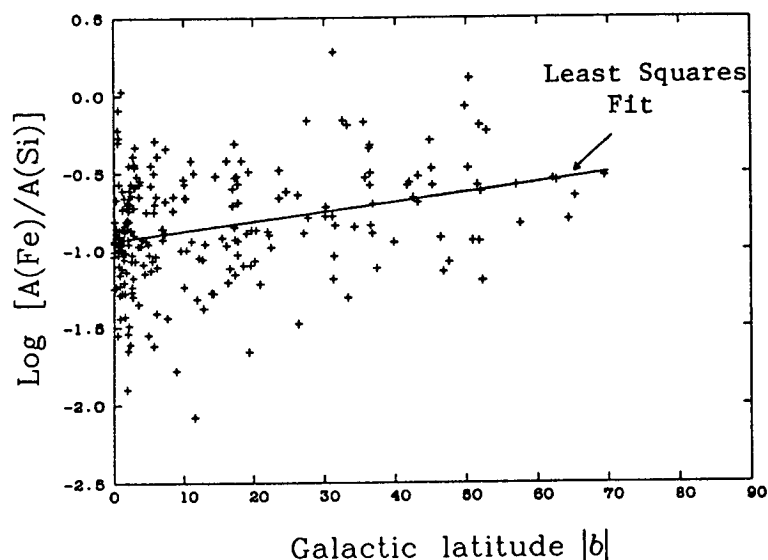
Fig. 4

Surprisingly, the Fe/Si ratio goes in the opposite sense with infrared diffuse cirrus, even for stars in the halo. We find increased Fe depletion and decreased Si depletion in lines of sight containing substantial 100 μm cirrus. Thus, although Fe/Si is generally higher in the halo, the ratio declines with increasing cirrus flux. The origin of this correlation is unknown. Several suggestions are:

(1) The grains in cirrus clouds are formed iron-rich and silicate-poor, because of the halo metal environment or seed-grain characteristics.

(2) The relative shock destruction of iron and silicate grains differ in the cirrus cloud and intercloud regions in the halo because of different shock propagation (speeds, ambient densities, shell sizes).

V. THE ROLE OF THE MAGNETIC FIELD IN THE ISM

FRAGMENTED MOLECULAR COMPLEXES: THE ROLE OF THE MAGNETIC FIELD IN FEEDING INTERNAL SUPERSONIC MOTIONS

Falgarone E.[1,2], Puget J.L.[1,2], Pérault M.[1,2]

[1] Observatoire de Paris-Meudon, France
[2] Ecole Normale Supérieure, Paris, France

A hierarchical structure for molecular complexes (mean density $\sim 10 cm^{-3}$, mass larger than a few $10^5 M_\odot$) in their "cold" phase i.e. preceeding the formation of massive stars, has been derived from extensive large scale $^{13}CO(J=1-0)$ observations: the mass is found to be distributed into virialized clouds which fill only a very low fraction ($\sim 10^{-2}$) of the volume of the complex and are supported against gravity by internal supersonic motions.

We have found an efficient mechanism to transfer kinetic energy from the orbital motions of the clouds to their internal random motions. The large perturbations of the magnetic field induced at the cloud boundaries by their interactions with their neighbours generate systems of hydromagnetic waves trapped inside the clouds. The magnetic field lines being closely coupled to the gas at the densities which prevail in the bulk of the clouds volume (a few $100 cm^{-3}$), internal velocity dispersion is thus generated.

Although our approach relies on an analytical solution obtained when shear only is considered, the interesting conclusions are:
  i) the computed internal velocity dispersion of the clouds is comparable to the values deduced from the observed linewidths,
  ii) the energy pumping rate allows the internal velocity dispersion to be fed over several 10^7 years, an order of magnitude longer than the dissipation timescale of the supersonic motions.

The observational part of this work is published in Pérault et al. (Astron. Astrophys. 152,371), the other is in press in the same journal.

ON THE INTERPRETATION OF THE $B - \rho$ RELATION IN INTERSTELLAR CLOUDS

Arieh Königl
Department of Astronomy and Astrophysics
The University of Chicago

Troland and Heiles (1986) have recently presented an updated compilation of observational data concerning the relationship between the interstellar magnetic-field strength B and the gas density ρ (or, equivalently, the particle density n). One of the main findings of their survey was that B remains constant (at a value of $\sim 5\,\mu G$) over the density range $0.1 - \sim 100\ cm^{-3}$ and shows evidence for increase only at higher densities. They compared this result with theoretical predictions based on the Parker-instability scenario for the formation and evolution of interstellar clouds in the presence of the galactic magnetic field. In this picture (reviewed, e.g., by Mouschovias 1985), low-density gas is driven by the magnetic Rayleigh-Taylor instability into magnetic "valleys," where it accumulates into denser concentrations. The gas initially flows along the magnetic field lines and there is little increase of the field strength with density; B only starts to rise when n becomes large enough for self-gravity to begin competing with the magnetic stresses. For a cloud mass of $\sim 10^3\ M_\odot$ and the measured background field strength, the critical density for contraction is $\sim 75\ cm^{-3}$. Troland and Heiles therefore concluded that this scenario is basically consistent with the observations.

Why should, however, the cloud mass M in the expression for the critical density n_{crit} be $\sim 10^3\ M_\odot$? In fact, since $n_{crit} \propto B^{1.5} M^{-0.5}$, why doesn't the total mass in the magnetic "valleys," which is of the order of $10^5 - 10^6\ M_\odot$, cause the field strength to start increasing already at much lower densities? The relevant mass scale for the estimate of n_{crit} is not specified in the theoretical models considered by Troland and Heiles and must be determined with the help of additional physical input. In fact, the question of the appropriate mass only enters because the relevant observable quantity is n. By using simple balance-of-forces arguments or the virial theorem, one can readily see that B is directly related not to the density but rather to the *column density*, or, equivalently, to the surface mass density Σ. Thus, for example, in order for a cold, spheroidal cloud in virial equilibrium to contract, the surface density must satisfy $\Sigma > \epsilon B/\sqrt{G}$, where G is the gravitational constant and ϵ is a geometry-dependent factor $\gtrsim 0.1$ (Strittmatter 1966).

In order to determine the behavior of the gas that accumulates in the magnetic-field "valleys," one must consider the equilibrium configurations of the gas-field system that are reached at the conclusion of the Parker instability. Mouschovias (1974) has constructed explicit solutions to this problem for the case where the gravitational field is dominated by the background galaxy. However, in the present case it is the self-gravity of the inflowing gas that is most relevant. Elmegreen (1982a,b) has carried out a linear analysis of the Parker instability in a self- gravitating gas, drawing useful conclusions about the formation of large-scale cloud complexes. However, his results do not extend to the late stages of the evolution that are of interest here. The influence of self-gravity in the last phase of the Parker instability is a difficult problem that has not yet been addressed in the literature. Here I illustrate, in a very simplified manner, one possible aspect of the final configuration that could be relevant to the observed $B - \rho$ relation.

In a simple representation of the Parker instability (e.g., Blitz and Shu 1980), the galactic magnetic field is pictured as lying originally in the plane of the galaxy and being "frozen" into an isothermal gas layer whose initial scale height normal to the galactic plane is H_i. If the galactic gravitational acceleration g is taken to be a constant ($\sim 3 \times 10^{-9}$ cm s^{-2}) and the thermal, magnetic, and cosmic-ray contributions to the pressure are approximately equal, then $H_i \approx 3 C_i^2 / g$ (where C_i is the isothermal speed of sound in the initial state) and the critical wavelength along the field for the onset of the instability is $\lambda_{P,crit} \approx 1.2 \pi H_i$. The mass that ultimately gathers in the magnetic "valleys" is assumed to come from a region of volume $\sim 2 H_i \times 2 H_i \times \lambda_{P,crit}$ and can be estimated by multiplying this volume by the initial midplane density ρ_i.

In order to consider the effect of self-gravity on the magnetic-field strength in the final configuration, we adopt the following idealized picture. We approximate the field as lying in the plane of the galaxy and having a constant magnitude equal to its initial midplane value B_i. We further assume that the accumulated gas is in the form of a uniform, self-gravitating, isothermal disk of area $2 H_i \times 2 H_i$ and scale height (along the field) $H_f \approx (C_f^2 / 2 \pi G \rho_f)^{1/2}$ (where C_f is the isothermal sound speed in the final configuration and ρ_f is the midplane density in the disk). The surface density of the disk is given by $\Sigma \approx 2 H_f \rho_f$ and is equal to $\sim \lambda_{P,crit} \rho_i$. To evaluate the Jeans-stability of this configuration, we adopt the results of the infinite-slab fragmentation analysis of Nakano and Nakamura (1978). According to this analysis, the disk will fragment only if $\Sigma > B_i / 2 \pi G^{1/2}$ (consistent with the above-mentioned virial-equilibrium results) and if the wavelength *in the plane of the disk* exceeds $\lambda_{J,crit} \approx 2 \pi H_f (1 - B_i / 2 \pi G^{1/2} \Sigma)^{-1}$. Now, the first condition is marginally satisfied for representative galactic parameters ($\rho_i \approx 3 \times 10^{-24}$ g cm^{-3}, $C_i \approx 7$ km s^{-1}, $B_i \approx 5 \mu G$), and so is also the self-consistency requirement that the gravitational acceleration due to the disk be $\gtrsim g$. However, the second condition is *not* satisfied for these parameters so long as $C_f \approx C_i$ because $\lambda_{J,crit}$ then exceeds the assumed diameter ($\sim 2 H_i$) of the disk. This inequality is only strengthened if one considers the effect of the finite size of the disk on the above condition, and it holds also if one substitutes the wavelength of maximum growth for the marginal-stability wavelength in the preceding discussion. Physically, the disk does not fragment in this case because its diameter remains smaller than the relevant "magnetic" Jeans length.

In view of the highly simplified nature of the foregoing arguments and the marginal values obtained in the numerical estimates, it is unclear whether one can draw any firm conclusions from the above result. However, if the Jeans-length effect is at all applicable, then this offers a possible clue to the interpretation of the observed constancy of B for $n \lesssim 100$ cm^{-3}. In this picture, the field strength can only start increasing after C_f has dropped sufficiently below C_i for $\lambda_{J,crit}$ to be less than $2 H_i$. Such a reduction in C_f could be the result of a thermal instability that might develop in the gathering H I gas; in fact, an instability of this type could produce a phase transition (cf. Field, Goldsmith, and Habing 1969) that would raise the particle density in the disk to ~ 100 cm^{-3} and would thus fix the value of n at which B starts to increase. Thermal instabilities might, therefore, trigger the formation of dense interstellar clouds even though they could not by themselves give rise to the observed large-scale condensations (cf. Mouschovias 1978). Other possible implications of this scenario (e.g., to the interpretation of "turbulence" in interstellar clouds) could also be explored; however, one should first verify the validity of the basic idea by calculating self-consistently the effects of self-gravity on the evolution and the end states of the Parker instability.

References

Blitz, L., and Shu, F.H. 1980, *Ap. J.*, **238**, 148.

Elmegreen, B. G. 1982a, *Ap. J.*, **253**, 634.

---------------. 1982b, *Ap. J.*, **253**, 655.

Field, G. B., Goldsmith, W., and Habing, H. J. 1969, *Ap. J. (Letters)*, **155**, L149.

Mouschovias, T. Ch. 1974, *Ap. J.*, **192**, 37.

---------------. 1978, in *Protostars and Planets*, ed. T. Gehrels
   (Tucson: University of Arizona Press), p. 209.

---------------. 1985, *Astr. Ap.*, **142**, 41.

Nakano, T., and Nakamura, T. 1978, *Publ. Astr. Soc. Japan*, **30**, 671.

Strittmatter, P. A. 1966, *M.N.R.A.S.*, **132**, 359.

Troland, T. H., and Heiles, C. 1986, *Ap. J.*, **301**, 339.

MAGNETIC FIELDS IN MOLECULAR CLOUD CORES:

LIMITS ON FIELD STRENGTHS AND LINEWIDTHS

Alyssa A. Goodman

Harvard-Smithsonian Center for Astrophysics

Summary: *Preliminary observations by others indicate that the magnetic field strength in dense molecular cloud cores is on the order of 30 μG, much closer to the background field strength than to the flux-freezing prediction for this density. This result implies that some process must exist to decrease the magnetic field strength in these regions to much less than its flux-frozen value, e.g. ambipolar diffusion. At these moderate field strengths, magnetohydrodynamic waves in the cores provide a good explanation of observed supra-thermal molecular linewidths.*

ABSTRACT

Magnetohydrodynamic waves may be the source of the supra-thermal molecular linewidths observed in molecular cloud cores. If so, a substantial fraction of the non-thermal portion of the linewidth is the result of magnetohydrodynamic turbulence, which gives rise to the shear Alfvèn waves in the cloud core (Zweibel and Josafatsson 1983).

New data on core properties (Myers and Benson 1983; Benson and Myers 1983; Myers 1983,1984,1985; Myers, Goodman and Benson 1986) enable us to place limits on the field strength in a region if one assumes that the linewidth observed is comparable to the Alfvèn speed in that same region. Energy considerations give further constraints on field strength. All techniques of estimation used in this paper, as well as available direct (Zeeman-splitting) observations (Troland and Heiles 1986; Heiles and Stevens 1986) indicate field strengths substantially weaker than a 'flux-frozen' value.

Assuming an energy source exists to maintain dynamical turbulence, the field strengths required to sustain MHD turbulence and waves are an order of magnitude weaker than field strengths calculated using a flux-freezing analysis. In the flux-freezing scenario $(B/B_o) \approx (n/n_o)^k$, where n and B are the local density and magnetic field strength, respectively, n_o and B_o are ambient values, and $1/3 \leq k \leq 1/2$. If we consider a generalized cloud core with density $n = 10^{4.4}$ cm^{-3} in a medium with ambient density $n_o = 100$ cm^{-3} and magnetic field $B_o = 20$ μG, flux-freezing predicts $B \approx 200$ μG. (See Table I.) If, however, we make the order-of-magnitude assumption that the non-thermal portion of the observed linewidth, Δv_{nt}, is approximtely equal to the Alfvèn speed, v_A, we calculate $B \approx 33$ μG.

We have also considered the energy balance in cloud cores, in order to estimate the field strength from another point of view. Pressure balance gives values similar to $B_{v_A = \Delta v_{nt}}$, as one would expect, owing to the similarity of the equations involved. (See Table I.) And, the magnetic pressure for $B \approx 30$ μG is either comparable to or less than the gravitational pressure in these cores, wheras the magnetic pressure for $B \approx 200$ μG is far too great to permit gravitational collapse.

This idea—that flux-freezing is unlikely in dense star-forming molecular cloud cores—almost certainly means that ambipolar diffusion is important in these regions (Shu 1983, Mestel 1985). At core densities, and higher, only the (increasingly small) ionized component of the plasma is coupled

to the field lines, and the neutral particles may stream through relatively easily, potentially leading to the formation of a star.

The field strengths required to explain linewidths with MHD turbulence and waves, and those for stars to be able to form are self-consistent. Important remaining considerations are: [1] what could be an appropriate energy source for the Alfvèn waves; [2] what is the lifetime of the waves, given a finite energy source; and [3] what is the field strength, observationally?

TABLE 1: COMPARISON OF MAGNETIC FIELD STRENGTHS [1]

$B_{flux-freezing}$ (k=1/3)	124 μG [2]
$B_{flux-freezing}$ (k=1/2)	317 μG
$B_{Zeemansplitting}$	50 μG $\geq 3\sigma$ [3]
$B_{equalpressure}$	36 μG [4]
$B_{virialequilibrium}$	57 μG [5]
$B_{v_A=\Delta v_{nt}}$	33 μG [6]

Notes: [1] for a "mean" cloud where log(n) = 4.40; FWHM linewidth = 0.32 km s^{-1}; T = 11K; radius = 0.12 pc (Myers and Benson 1983) [2] (B/20 μG) = (n/100 cm^{-3})^k [3] probably an underestimate due to beam-dilution effects; value from Heiles and Stevens (1985) [4] $B^2/8\pi = \rho\sigma_{nt}^2 + \rho kT/\mu$ (σ_{nt} = non-thermal portion of linewidth) [5] virial equilibrium for a spherical cloud [6] $v_A = \Delta v = B/(4\pi\rho)^{1/2}$ (will automatically be of order $B_{equalpressure}$)

REFERENCES

Benson, P.J. and Myers, P.C. 1983, *Ap. J.*, **270**, 589.

Heiles, C. and Stevens, M. 1986, *Ap. J.*, **301**, 331.

Mestel, L. 1985, in *Protostars and Planets II*, eds. D.C. Black and M. Shapley Matthews (Tuscon: University of Arizona Press), p. 320.

Myers, P.C. 1983, *Ap. J.*, **270**, 105.

_____. 1984, IAU meeting Invited Review, Toulouse, France, in Springer-Verlag *Lecture Notes in Physics*.

_____. 1985, in *Protostars and Planets II*, eds. D.C. Black and M. Shapley Matthews (Tuscon: University of Arizona Press), p. 81.

Myers, P.C. and Benson, P.J. 1983, *Ap. J.*, **266**, 309.

Myers, P.C., Goodman, A.A. and Benson, P.J. 1986, in progress.

Shu, F. 1983, *Ap. J.*, **273**, 202.

Troland, T.H. and Heiles, C. 1986, *Ap. J.*, **301**, 339.

Zweibel, E.G. and Josafatsson, K. 1983, *Ap. J.*, **270**, 511.

MODELS FOR APPLICATION OF RADIATION BOUNDARY CONDITION FOR MHD WAVES IN COLLAPSE CALCULATIONS

C. T. Vanajakshi
NASA-Ames Research Center, CA 94035

E. H. Scott
Computer Sciences Corporation
NASA-Goddard Space Flight Center, MD 20771

and

David C. Black
NASA Headquarters, Washington, D. C. 20546

The problem of reflection of magnetohydrodynamic (MHD) waves at the boundary of a numerical grid has to be resolved in order to obtain reliable results for the end state of the (isothermal) collapse of a rotating, magnetic protostellar cloud. The only attempt made so far (Dorfi 1982) to resolve the reflection problem made use of an approach similar to the work of Bayliss (1982), where the Navier-Stokes equation for a magnetic, conducting fluid was linearized near the boundary while the density of the external medium was kept constant and the resulting restricted set of equations were solved. While this approach is better than assuming zero magnetic field in the external medium (which causes the energy to flow back similar to a wave along a string tied at the ends) the assumption of small fluctuations, which is necessary to linearize the equations, breaks down when the magnetic braking is efficient and causes large amplitude alfven waves. Since the goal of investigating magnetic braking in collapse simulations is to see if the transport of angular momentum via alfven waves is large enough to solve the 'angular momentum problem' an approximation that artificially suppresses large amplitudes in the MHD waves can be self-defeating.

For this reason, four alternate methods of handling reflected waves where no assumptions are made regarding the amplitudes of the waves have been investigated. In order to study this problem (of reflection) without interference from other effects these methods were tried on two simpler cases:

(1) The analytical case of a perpendicular rotator by Mouschovias and Paleologou (1979) where the magnetic braking of a rigid disk with a radial magnetic field was followed.

(2) A simpler model of this disk in which a 'spike' in the field is generated at a specific time in an otherwise quiescent configuration and the propogation of the wave thus generated and its reflection are followed.

The basic models for the four methods are as follows:

Method 1: The rate of change of Δ B (where ΔB is the change in magnetic energy) with respect to distance is calculated near the boundary. Using this quantity and the distance between the last two grids ΔB in the last grid is computed at each time step. Then this change in magnetic energy is partitioned along the three directions using

the ration $(\Delta B)_{h}$: $(\Delta B)_{\phi}$: $(\Delta B)_{z}$ in the previous grid. The directions of the components $(+)$ are also echoed from those in the previous grid. This method works for long wavelength alfven waves. When the wavelength is comparable to grid size this approach may become invalid.

Method 2: The fluxes $\dfrac{\delta B^2}{4\pi}(\bar{v}_a + \bar{v})$ where $\bar{v}_a$ is the alfven velocity and $\bar{v}$ the

material velocity are matched between the two grids that border the boundary.

Method 3: This method uses transformations to diagonalize the equations of motion. For the component in the direction of reflection the amplitude of the incoming waves is set to zero. The other components are solved in the normal fashion.

Method 4: This method uses a damping term in the Navier-Stokes equation at the boundary.

$$\rho \frac{d\bar{v}}{dt} = - \nabla p + \rho g - \frac{B}{4\pi} \times (\nabla \times B) + \eta \, \nabla^2 \, \bar{v}$$

This damping term can absorb the energy and suppress the reflection.

Results of these studies will be presented.

REFERENCES: Bayliss, A. 1982, J. Comp. Phys.,48,182.
Dorfi, E. 1982, Astr. Ap.,114,151
Mouschovias, T. Ch. and Paleologou, E. V., 1979, Ap.J.,230,204
Thompson, K. W. 1986 In press.

MAGNETIC BRAKING IN WEAKLY IONIZED CIRCUMSTELLAR DISKS

Arieh Königl
Department of Astronomy and Astrophysics
The University of Chicago

Recent observations of disk-like mass distributions around newly formed stars have provided evidence for rapid rotation on scales $\lesssim 0.1\,\mathrm{pc}$ with specific angular momenta much higher than typical stellar values. A likely mechanism for the extraction of angular momentum from these regions is magnetic braking by means of Alfvén waves that propagate into the lower-density ambient medium. However, because of the relatively high particle densities ($\gtrsim 10^5\,\mathrm{cm}^{-3}$) and the correspondingly low implied ionization fractions in these apparent disks, their constituent ions and neutrals need not be well coupled to each other and could develop large relative drift velocities. For this reason, previous treatments of magnetic braking that assumed perfect coupling between ions and neutrals have to be modified in this case. In particular, one has to take into account both the *azimuthal* drift that develops because only the ions are directly coupled to the magnetic field and the *radial* drift (or *ambipolar diffusion*) which leads to a redistribution (and leakage) of the magnetic flux. This contribution describes the results of a preliminary analysis of these effects.

The effect of the azimuthal drift is studied with the help of a simple model problem of a two-component disk that is threaded by a uniform magnetic field parallel to the rotation axis. An exact analytic solution for the magnetic braking of the disk is obtained under the assumption that both the ionized and the neutral disk components rotate rigidly and have the same initial angular velocity. In the limit of a low ionization fraction, the neutral disk component is found to brake with an e-folding time given by $\tau_{b,n} = (1+\delta)\tau_{\|,n}$, where $\tau_{\|,n}$ is the nominal braking time of the neutrals due to Alfvén-wave propagation along the field lines. The parameter δ measures the strength of the azimuthal coupling between the ions and the neutrals, and is given by $\delta \equiv \tau_{ni}/\tau_{\|,n}$, where τ_{ni} is the slow-down time of a neutral due to collisions with ions. In the limit $\delta \ll 1$ (*strong coupling*), the angular velocities of the two disk components are nearly equal at all times, whereas in the $\delta \gg 1$ limit (*weak coupling*) the ion angular velocity rapidly declines to a fraction δ^{-1} of the neutral angular velocity. This difference in the rotation velocities is potentially detectable by high-resolution observations of molecular-line tracers such as HCO^+ and HCN. It is shown that equilibrium configurations of self-gravitating disks necessarily correspond to the strong-coupling regime, but that low-mass disks that are formed in the gravitational field of a central star can, in principle, have a large value of δ.

The results of the azimuthal-drift analysis are incorporated into another model problem that focuses on the effect of the radial drift. Through a set of numerical calculations, it is demonstrated that the relative importance of ambipolar diffusion in the braking process is determined by the parameter $\epsilon \equiv \tau_d/\tau_{b,n}$, where τ_d is the characteristic ambipolar-diffusion time. It is argued that the radial ion-neutral drift is unlikely to interfere strongly

with magnetic braking in contracting, self-gravitating disks because the latter must satisfy $\epsilon \gg 1$ so long as the external-to-internal density ratio is not very small ($\gtrsim 10^{-3}$). By contrast, it is shown that in circumstellar disks with negligible self-gravity, ambipolar-diffusion effects could influence the braking process even for relatively large density ratios.

As expected, ambipolar diffusion is found to reduce the efficiency of magnetic braking by decreasing the flux-to-mass ratio in the disk and thereby increasing $\eta_{\parallel,n}$. The initial effect of diffusion in the weak-coupling limit could, nevertheless, be to accelerate the braking process by inducing a contraction that increases the density in the disk and thereby reduces τ_{ni}. (Radial contraction induced by the loss of centrifugal support may, in turn, serve as a catalyst for ambipolar diffusion.) However, flux leakage should cause the disk to evolve towards the strong-coupling regime where the only effect of diffusion would be to slow down the braking process. Several additional aspects of the disk evolution are discussed, and the need for more extensive numerical calculations is emphasized.

VI.   COMETS AS PROBES OF THE ISM

COMET P/HALLEY 1910, 1986: An Objective-Prism Study.
U. Carsenty (ASU), E.S. Bus (Lowell), S. Wyckoff (ASU),
B. Lutz (Lowell)

Comets are the most distant voyagers of the solar system, sampling regions that are essentially "interstellar" in nature. Unlike the larger planets they have undergone only little, if any, metamorphosis over the history of the solar system, and can therefore provide information on the physical and chemical state of the primordial solar nebula. The tiny cometary nucleus, the dirty snowball of frozen gases mixed with dust, becomes active following its interaction with the solar radiation field and wind. The results are the extended gaseous coma and the long double tail (plasma & dust), features that kept humankind fascinated throughout the ages. The physical processes involved are: sublimation, photo excitation (fluorescent scattering), photo dissociation, photo ionization, dissociative recombination, etc... The observed cometary spectrum is a superposition of molecular emission bands, atomic emission lines, and reflected (by dust) solar continuum.

V. M. Slipher of the Lowell Obs. collected a large amount of spectroscopic data during the 1910 apparition of Halley's comet. We selected 3 of his post-perihelion objective-prism plates (Table 1), digitized them and subjected them to modern digital data reduction procedures. Some of the important steps in our analysis where: 1) Density to intensity conversion for which we used 1910 slit spectra of Fe-arc lamp on similar plates (Sigma) and derived an "average" characteristic curve; 2) Flux calibration using the fact that during the period June 2-7 1910 P/Halley was very close (angular distance) to the bright star Alpha Sex (A0III, V=4.49), and the spectra of both star and comet were recorded on the same plates. We assumed that the flux distribution of Alpha Sex is similar to that of the standard star 58 Aql (A0III) and derived a sensitivity curve for the system; 3) Atmospheric extinction using the standard curve for the Lowell Obs.; 4) Solar continuum subtraction using the standard solar spectrum binned to our spectral resolution.

In Fig. 1 we present an example of a flux-calibrated spectrum of the coma (integrated over 87,000km) before the subtraction of solar continuum. All the "classical" features, e.g. molecular emission bands, are present and display the typical band head structure. In objective-prism spectroscopy (no aperture) the observed emission regions are considerably larger than the projected scale lengths for photo dissociation of the various species. If we assume that the coma is optically thin, the total number of emitting molecules (N) is given by:

$$N = \frac{4\pi F}{g} \Delta^2 r^2$$

where F $[ergs/cm^2/sec]$ is the observed flux in a particular band, Δ [AU] is the distance comet – earth, r [AU] is the distance comet – sun, and g [ergs/molecule/sec] is the fluorescence efficiency at 1 AU. Traditionally, instead of the coma abundance for a given species, what is given is the production rate (Q) of the species, which under steady state condition is related to N by:

$$Q = \frac{N}{\tau}$$

where τ [sec] is the lifetime of the species. Our results for both N and Q are presented in Table 2. These results are, to our knowledge, the first quantitative physical values from the 1910 apparition of comet P/Halley. It is yet too early to compare the 1910 results with new 1986 results. However, we present here some preliminary results.

Our 1986 objective-prism plates (Fig. 2) were obtained on January 12.13 and 13.13 1986 using the Burrell Schmidt (Kitt Peak) with the 10 prism. We used IIIaJ and IIIaF plates with spectral coverage of 3700Å to 5000Å and 3700Å to 7000Å, respectively. We are still in the midst of the data reduction and analysis.

Table 1. The 1910 Data

Plates	: Sigma
Plate Scale	: 1050"/mm or 21"/pix
Spectral range	: 3700Å – 4950Å
Linear dispersion	: 1.237 Å/pix at λ3885 and 2.945 Å/pix at λ4735
Dates (UT)	: June 2.25, 3.264, 6.267
Delta (AU)	: 0.53 0.57 0.685
r (AU)	: 1.062 1.07 1.12

Table 2. The 1910 Results

Emission bands	CN(λ3883)	C$_2$(λ4737)	C$_3$(λ4050)	CH(λ4315)
g [ergs/mole/sec]	3.23(-13)	2.59(-13)	1.03(-13)	9.2 (-13)
Column Density [molecules/m^2]	1.3 (15)	0.8 (15)	5.5 (13)	1.0 (13)
N [molecules]	3 (32)	2 (32)	2.5 (30)	4.5 (29)
τ [10^5 sec]	2.1-6.3	0.7-2.1	0.35-1.05	0.07-0.21
Q [mole/sec]	0.5-1.4(27)	0.9-2.8(27)	2.4-7.1(25)	2.1-6.4(25)

Note: exponents of ten are in parenthesis

Fig.2. Objective-prism spectrum of comet P/Halley 1986
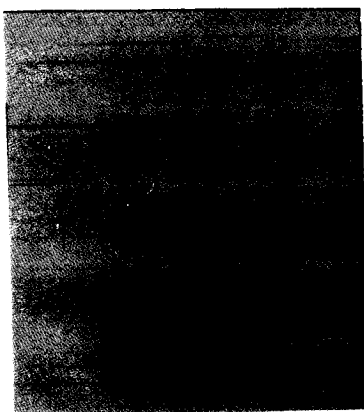
Fig.1. Flux-calibrated coma spectrum of comet P/Halley 1910

AUTHOR INDEX

1. Report No. NASA TM 88342	2. Government Accession No.	3. Recipient's Catalog No.
4. Title and Subtitle SUMMER SCHOOL ON INTERSTELLAR PROCESSES: ABSTRACTS OF CONTRIBUTED PAPERS		5. Report Date October 1986
		6. Performing Organization Code
7. Author(s) D. J. Hollenbach and Harley A. Thronson, Jr. (University of Wyoming, Laramie, Wyoming)		8. Performing Organization Report No. A-86393
		10. Work Unit No.
9. Performing Organization Name and Address Ames Research Center Moffett Field, CA 94035		11. Contract or Grant No.
		13. Type of Report and Period Covered Technical Memorandum
12. Sponsoring Agency Name and Address National Aeronautics and Space Administration Washington, DC 20546		14. Sponsoring Agency Code 188-48-52

16. Abstract

The Summer School on Interstellar Processes was held on July 3-7, 1986 to discuss the current understanding of the interstellar medium and to analyze the basic physical processes underlying interstellar phenomena. Extended abstracts of the contributed papers given at the meeting are presented here.

Many of the papers concerned the local structure and kinematics of the interstellar medium and focused on such objects as star forming regions, molecular clouds, HII regions, reflection nebulae, planetary nebulae, supernova remnants and shock waves. Other papers studied the galactic-scale structure of the interstellar medium either in the Milky Way or in external galaxies. Some emphasis was given to recent observations of interstellar grains and polycyclic aromatic hydrocarbons. Contributions were also made in the areas of interstellar chemistry, elemental abundances, the role of the magnetic field, and comets as probes of the interstellar medium.

17. Key Words (Suggested by Author(s)) Interstellar medium Radio astronomy Infrared astronomy Submillimeter astronomy	18. Distribution Statement Unclassified – Unlimited Subject category – 90
19. Security Classif. (of this report) Unclassified	20. Security Classif. (of this page) Unclassified

19. Security Classif. (of this report)	20. Security Classif. (of this page)	21. No. of Pages	22. Price*
Unclassified	Unclassified	205	A10